Università degli Studi di Milano-Bicocca
Dipartimento di Biotecnologie e Bioscienze
Dottorato di ricerca in Tecnologie Convergenti per i Sistemi
Biomolecolari - XXXIV Ciclo

Metabolism and signaling crosstalk regulate nutrients perception and mitochondrial respiration in eukaryotic model systems

Candidate: Riccardo Milanesi
Supervisor: Prof. Paola Coccetti

Anno Accademico 2020-2021

Department of Biotechnology e Bioscience

PhD program in Convergent technology for biomolecular systems

XXXIV Cycle

Metabolism and signalling crosstalk regulate nutrients perception and mitochondrial respiration in eukaryotic model systems

Candidate: Milanesi Riccardo

Registration number: 780328

Tutor: Piatti Simonettta

Supervisor: Coccetti Paola

Coordinator: Branduardi Paola

ACADEMIC YEAR 2020/2021

List of Contents

Prologue

The present thesis is the result of the work done at the University of Milano-Bicocca under the supervision of Prof. Paola Coccetti, supplemented with part of the results obtained during my external stay at the Novo Nordisk Center for Biosustainability in Copenhagen. The readers will notice that the content of this thesis is focused on the study of metabolism from different perspective and working with different model organisms. This is the result of a path that brought me from the study of S-adenosylmethionine role in the regulation of eukaryotic metabolism, to the investigation of the molecular mechanism governing Snf1/AMPK pathway in *Saccharomyces cerevisiae*; from the use of yeast as model organism for aging and neurodegeneration, to the engineering of *Pseudomonas putida* for the overproduction of S-adenosylmethionine.

The results obtained in these different projects are presented in five independent chapters provided with detailed introductions and discussions. Hence, the aim of the following thesis outline is to touch upon each of them and provide the *fil rouge* connecting all the different chapters.

Outline

The achievement of biological robustness

The Achievement of Biological Robustness

From a general point of view, the reasons and aims of doing science can be traced down to few essential aspects: understand phenomenon, providing reliable models of interpretation, and use these models for the development of new technologies to solve society's problems. This is far from being a victory of technology over fundamental science since every new device of solution is based on fundamental discoveries. In turn, any new application of the knowledge acquired highlights limitations and gaps, stimulating curiosity and laying the foundations for novel research branches.

Bringing these speculations down to biology, this branch of science contributed for the last two centuries in improving the quality of life, allowing for the treatment of diseases and developing biobased solutions for the production of goods. All these achievements have been allowed by a great improvement in the understanding of living organism, that has been obtained for many years through the study of the single components of the biological systems.

Anyway, in the last decades arose the awareness that a living organism is not just the sum of its parts, but rather the synergistic interaction among them. This observation paved the way towards the definition of system biology as new research field and, this holistic approach, it is still the most advanced paradigm for the study of living organism [1].

The core property of every system is the robustness, or rather the ability to withstand external (changes in the environment) and internal (I.e., stressors damage and mutations) perturbations maintaining the general properties of the system [2]. Even if this concept was formulated for the study of engineering systems, it perfectly applies also to biological ones, allowing to

define what make a system a robust one. This holistic paradigm, combined with the study of the molecular mechanism governing cellular processes, provide the knowledge necessary to describe the emergent properties of a biological system [2].

The first source of robustness is the redundancy. The presence of genes and the expression of proteins with overlapping functions is extremely widespread in all the biological reign, providing backup copies of key elements and increasing the probability to withstand the mutation of essential components [2]. A more complex level of redundancy is the one regarding entire biological circuits that can complement one another under specific conditions. Circuits also contribute to the robustness of the system thanks to specific properties of their architecture. For example, evolution seems to preferentially select modular design in which components contributing to a specific function are grouped and organized to work independently from the rest of the system. This prevents the malfunctioning of a circuit to spread over the entire system, buffering the effects of a negative phenomenon [2].

These modules often also present a tight regulation of their activity, thanks to well defined control strategies, such as feedback and feedforward circuits, allowing for the repression or the activation of specific function.

This is pivotal for the dynamic regulation of the circuits, allowing for the integration of different signals and the coordination of between circuits active simultaneously [2]. Most of these control circuits are organized in a bow-tie architecture in which several independent stimuli are perceived by different pathways that, organized in modules, converge their signals on highly conserved core processes. This allows for the integration of the components of the system and give rise to the its general behavior as an

emergent property [2]. Finally, robust circuits are often designed to return or move to a specific state after every perturbation of their functioning. These states are defined as basins of attraction and play central roles in different biological processes such as the transitions in the different stage of cell cycle, the return to off state of signal transduction pathways and even the arising of pathological state [2].

Whether these are the characteristics that make a system robust, the robustness is achieved in practice through the dynamic adaptation to extra and intracellular conditions. To achieve this, systems must constantly monitor the environment perceiving variation in the concentrations of nutrient and presence of toxic compounds. Receptors and signal transduction pathways have been studied for decades depicting the mechanism responsible for the perception of nutrients and growth factors [3,4]. Nevertheless, an increasing amount of evidence suggest that signal transduction is inherently connected also to intracellular metabolism through the interaction between metabolites and proteins of the signal transduction pathways [5,6].

Prompted by these observations, I decided to open this thesis with a chapter focused on reviewing the known molecular mechanism connecting signaling pathways with the central metabolism of eukaryotic organisms.

As highlighted in the chapter 1, all the eukaryotes present conserved pathway for the sensing of carbon and nitrogen sources responsible for the coordination among cell growth and the nutritional status of the cells [3,4]. These pathways are centered on the conserved kinase PKA, Snf1/AMPK/SnRK1 and TORC1 complexes and the chapter systematically describe the protein-metabolite interactions (PMIs) known to affect their activation. This work of literature review highlighted that the metabolites

belonging to the upper glycolysis strongly influence PKA and Snf1/AMPK/SnRK1 activation state in yeast and mammalian and plants cells [5–7]. In the meanwhile, components of the TORC1 pathway result to be the center of interaction for the sensing of amino acids availability [8–11].

Interestingly, were found evidence supporting the role of central metabolites in the regulation of the mitochondrial retrograde response (RTG) in yeast and calcium signaling in yeast and mammalian cells [12,13]. This highlights that PMIs play an important role in the signaling-metabolism coordination also for pathways not directly involved in the regulation of metabolism.

This work also highlighted knowledge gaps in the understanding of the molecular mechanism connecting cellular metabolism with signal transduction. For example, the molecular details of glutamine perception by TORC1 complex in yeast or which glucose 1-phosphate, glucose 6-phosphate and trehalose 6-phosphate regulation of SnRK1 activity in plants must be further investigated [14,15].

Interestingly, it also pointed out the need of an exhaustive comprehension of the crosstalk between Snf1/AMPK and Ras/PKA pathways, as well as glucose regulation of Snf1/AMPK activity in yeast. In chapter 2, I present results demonstrating that Snf1/AMPK and Ras/PKA pathway are independently controlled by glucose metabolism to which are respectively connected through glucose 6-phosphate and fructose 1,6-bisphosphate synthesis. Decoupling glucose transport rate from glucose availability, we also showed that Snf1/AMPK activation state is controlled by glucose transport rate and not by glucose availability. Eventually, we provided evidence suggesting that glucose 6-phosphate may directly interact with

Snf1 complex enhancing the exposure of the phosphorylated regulatory threonine (T210) to phosphatases.

This experimental work allowed us to extend the comprehension of the mechanisms by which signaling pathways responsive to glucose coordinate their activation state. Coherently with the bow-tie architecture of signaling, the crosstalk between Snf1/AMPK and Ras/PKA take place at the level of their downstream effectors, while the two kinases are independently responsive to different stimuli.

With a parallelism, the effect of nutrients and environmental condition on the fate of a microorganism can resemble the effect that environment and lifestyle can have on the long-term health of human beings. In these terms, eukaryotic microorganism like yeast or simple pluricellular organism such as *Drosophila melanogaster* or *Caenorhabditis elegans* can serve as model organism for the study of the aging process.

An aging system is characterized by specific disfunction that compromise its overall robustness. Genomic instability, mitochondrial disfunction, deregulated nutrient sensing, loss of proteostasis and epigenetic regulation are some of the most frequent hallmarks of an aging cell [16].

An aging organism can be seen as a system in which the accumulation of damages and the deregulation of processes are gradually compromising its robustness. Genetic definitively contributes to the rate of aging anyway, several evidence suggest that the environment and lifestyle can strongly impact on the aging perspective of an organism.

Dietary regimes like calory restriction or the consumption of functional food enriched with anti-aging molecules can extend the healthy lifespan of an organism [17]. Chapter 3 presents the results obtained during a collaborative study aimed to the evaluation of the properties of *Vigna*

unguicolata (a bean originating from Africa and nowadays cultivated also in the Mediterranean areas) as functional food ameliorating aging and neurodegeneration.

In this study, several organism models were employed showing that bean extracts extend the life span of *Saccharomyces cerevisiae*, *Drosophila melanogaster*, *Caenorhabditis elegans* and mammalian cells. This effect results to be additive to calory restriction, opening to the development of dietary regimes restricted in calories and containing the beans to maximize their beneficial effect. Indeed, the use of yeast and Drosophila enable to identify the Snf1/AMPK pathway as the one involved in the beneficial effect of the extracts, coherently with its activation in low energy condition and its well-known anti-aging function [18].

Interestingly, the bean extract also showed neuroprotective properties reducing the in vitro aggregation of α-synuclein, its membrane localization in yeast and neuroblastoma cells and decreased the age-related degeneration of cephalic dopaminergic neurons in *Caenorhabditis elegans*.

The biological robustness can become detrimental when the malfunctioning of one or more of its components drive the emergence of pathologies. This is the case of cancer, in which several processes escape their physiological controls and determine new harmful conditions for the organism. In these cases, the mechanism meant to guarantee the robustness of healthy cells enhance tumor robustness against therapy [2]. This, often result in the necessity to tackle malignancies with combined strategies to impair different key process of tumor cells.

A promising approach for the development of such treatment is to make use of negative genetic interactions by which the inactivation of a gene product become detrimental only in a background mutated in the interacting

gene/process [19]. From this point of view, *S. cerevisiae* is a well-suited model organism that allow for the identification of such interactions thank to the extensive knowledge of its genetic and to its similarity with mammalian cells, both in terms of metabolic network and regulatory strategies.

In chapter 4, these concepts are applied to the investigation of new putative approaches for the treatment of hepatocellular carcinoma (HCC). Indeed, a preliminary study we showed the coupling of *SNF1* deletion with methionine supplementation rewires yeast metabolism partially reverting the Crabtree effect (the aerobic fermentation of glucose), increasing the content of S-adenosylmethionine and reducing cellular proliferation [20]. Being methionine and S-adenosylmethionine metabolism mainly active in the liver [21], we investigated whether AMKP inhibition coupled with a high methionine dosage can ameliorate the phenotype of hepatocellular carcinoma cell lines. We observed that these conditions induce a metabolic rewiring characterized by a higher activity of the TCA cycle and a higher amount of ATP derived from respiration. Furthermore, the reduction of the Warburg phenotype, was associated with a reduction of the aggressiveness (growth rate, ability to migrate and to form colonies) in the hepatocellular carcinoma cell lines HepG2 and Huh7. Hence, these results open to the development of a dietary-pharmacological combined treatment for the hepatocellular carcinoma, the second leading cause for death of cancer.

System robustness can be a double-edged sword also in the engineering of biological system for biotechnological purposes. Robustness can determine better performance in production processes, but it can also represents a hurdle for the rewiring of metabolism towards the production of a molecule of interest.

Hence, the aim of metabolic engineering and synthetic biology is to design engineered pathway integrated with the native metabolism of the host, making use of the Design-Build-Test-Learn framework [22]. The concepts are applied in last chapter of this thesis in which is the advancement in the engineer of the environmental bacteria *Pseudomonas putida* for the overproduction of S-adenosylmethionine (SAM).

P. putida is gaining interest as a promising host for biotechnological applications. The ability to grow on refractive carbon sources (i.e., aromatic compounds), the high resistance to redox stress and the increasing number of engineering techniques are paving the way for the use of P. putida as microbial chassis [23].

In the meanwhile, S-adenosylmethionine is an important fine chemical used in the treatment of alcoholism and depression [24] and for the synthesis of melatonin, antibiotics and flavonoids [25–27].

Because of its high energetic cost, SAM synthesis is tightly controlled both transcriptionally and post-translationally [28,29]. To achieve the overproduction of this molecule, we designed a feedback-free inducible pathway to duplicate SAM production pathways in P. putida. The design also implies the coupling of this additional pathway to the TCA cycle exploiting the conversion of succinyl-CoA into succinate catalyzed in the first step of methionine synthesis.

In implementing this design, we had to face with the robustness of P. putida central carbon metabolism investigating possible anaplerotic reaction replenishing succinate synthesis. This allowed us to gain useful details on the regulation of the TCA metabolism in *P. putida* and highlighted that information acquire in enterobacteria *E. coli* are not always translatable to other type of bacteria.

In conclusion, this outline shows that different biological questions can have a common interpretation when organisms are seen as dynamic systems selected to withstand perturbations. This perspective can significatively help the development of new approaches to biological problems providing new tools and concepts to understand and innovate.

Chapter 1

Protein metabolite interactions enable metabolism to signaling crosstalk

From: Milanesi et al., Biomolecules 2020

Protein Metabolite Interactions enable Metabolism to Signalling crosstalk

Introduction

As highlighted in the outline, the robustness of a biological system is defined as the ability to maintain its principal functionalities regardless of external and internal variations [2]. The concept of robustness could be applied at systems of different order of magnitude. This property generally arises from a specific architecture of the

systems itself, that may be a cell, a metabolic pathway, a microbial community or a multicellular organism [1]. Robust systems are typically organized with a bow-tie architecture, where a lot of input signals converge on a limited number of elements, from which a large number of outputs emerge [30].

Metabolic and signalling networks show such an organization, with several metabolites and signals that converge on the central metabolism or on a limited number of signalling pathways [30].

A key aspect of every robust system is the ability to monitor the environmental conditions and adapt its functions to perturbations [31]. For example, from a system biology point of view, it is common

to see the maximization of growth as the objective function of a cell. To do so, metabolism, growth and cell cycle progression must be coordinated and finely tuned to fully exploit the available nutrients [32,33].

This requires a precise crosstalk between metabolism, signal transduction pathways and cell cycle progression. Therefore, some molecular events should connect given metabolic reactions with signal transduction cascades, to coherently integrate a given flux distribution with the activity of

regulatory proteins, such as the kinases upstream to signalling pathways. However, recent publications support the idea that we still need more data to understand the role of specific metabolites in controlling proteins activity at a systems level [34,35].

Since the beginning of the omics era, emergent technologies have focused on the qualitative and quantitative analysis of chemically homogeneous groups of molecules, giving rise to transcriptomics, proteomics and metabolomics. Nevertheless, the interpretation of the data acquired with these approaches is not always straightforward since the functioning of a biological system emerges by the interactions between chemically different molecules.

The molecular interaction between proteins and DNA has been systematically investigated for many years. On the contrary, the systematic study of the interaction between proteins and metabolites (PMI, protein-metabolite interaction) has started to be explored only very recently. Although recent reports suggest an important role of PMIs in the regulation of signalling [5,6] most publications still focus on the effect of the metabolites belonging to glycolysis and TCA cycle on the activity of the enzymes of the same pathways [34–36]. Therefore, a systematic analysis of the interaction between molecules of the central carbon metabolism and the proteins that compose the signal transduction network is still largely missing.

Here we review the known PMIs taking place between signal transduction pathways component and metabolites belonging to the central metabolism, focusing on the output that these interactions have on the activity of the key cellular pathways.

The Biochemistry of the Protein-Metabolite Interaction (PMI)

From a biochemical point of view, the output of a protein-metabolite interaction is a variation in the protein activity due to a conformational change associated with the binding of a small molecule.

NMR and single-molecule spectroscopy studies revealed that proteins can undergo conformational changes both when bound and unbound to a small molecule, as a consequence of thermally activated exchanges between the higher and the lowest energy conformations [37,38]. This means that folded proteins in their basal conformation can sample the energy landscape moving towards relatively higher energy states, that are the one proposed to bind the ligands [39,40]. Because of this, an allosteric regulation due to the binding of a small molecule on its target can be explained by two different models: conformational selection and induced fit [41,42].

According to the conformational selection model, a protein complex spontaneously undergoes a conformational change moving from a basal state to an excited one, characterized by a higher energy and, for this reason, less abundant [42]. In this mechanism, the ligand binding takes place after the conformational change and results in the stabilization of the excited conformation, therefore leading to the enrichment of the bound molecular species [43,44]. On the contrary, in the induced fit model, ligand binding takes place with the basal conformation of the target before any conformational change, this results in an intermediate bound complex still in the initial conformation and characterized by a higher energy. The relaxation of this structure is achieved through the fitting of the target to the bound molecule, as recalled by the definition of this mechanism [41,45].

From a technological point of view, a deep understanding of the control mechanism of a given protein may be an important insight to rationally

design drugs to target it. Alongside classical drugs that target the active site of a protein, nowadays research is focusing also on the development of molecules that may act as allosteric effectors [46,47]. A possible way to exploit conformational selection is to develop molecules that bind to a protein in a high energy conformation and stabilize it, shifting the equilibrium away from the active conformation [46,48].

To achieve this aim, the detailed biochemistry of the regulation of the target must be understood, also considering possible allosteric interactions and conformational changes.

The Main Pathways of Nutrient Sensing and Cellular Signalling

Cell growth and progression through the cell cycle must be coordinated, as already reported, with the availability of nutrients [33,49,50]. In eukaryotic organisms, such as yeasts and mammals, but also in plants, the most important nutrients are carbon and nitrogen sources, whose availability represents a positive signal for cellular proliferation. The perception of these nutrients relies mainly on three different signalling pathways centred on three widely conserved protein kinases: PKA, AMPK and TORC1 complexes [4,51]. The activation of such pathways takes place through a molecular interaction between nutrients (more often a derived molecule) and a receptor. This gives rise to a transcriptional and post-translational response, that results in the regulation of genes and proteins required for protein translation, cell cycle progression and response to nutritional stress [52,53]. Mitochondrial dysfunction is signalled to the nucleus through the retrograde response pathway (RTG), which controls the expression of genes required for respiration and consumption of alternative carbon sources [54]. In addition, the release of cytoplasmic calcium from stores, which allows a

huge variety of functions, from muscular contraction to neuronal activities in multicellular organisms, is a highly controlled mechanism.

A relevant part of the crosstalk between signal transduction and metabolism is known to take place at the plasma membrane, where nutrients perception elicits signal transduction resulting in the modification of gene expression and in the post-translational modification of key metabolic enzymes [55]. Some examples are the perception of glucose by Snf3 and Rgt2 in *Saccharomyces cerevisiae* and the perception of amino acids, ammonium, sulphate and phosphate through transceptors in the same organism (see [32,56] for a detailed description of these phenomena). Despite this, the aim of this review is to highlight the mechanism by which intracellular primary metabolites affect the activity of signalling pathways in different eukaryotic species, going beyond the classic description of signalling control on metabolism. All the pathways cited before are controlled by protein-metabolite interactions and will be extensively discussed in the present review. Interestingly, the involvement of PMIs in the control of mitochondrial retrograde response (RTG) and calcium signalling testifies how this mechanism can be considered a general feature in cell signalling and is not limited only to signalling pathways related with metabolism [54].
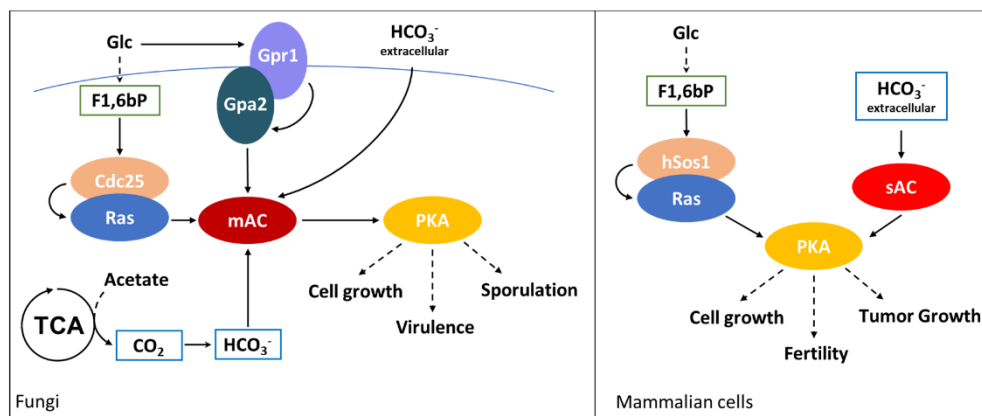
Protein-Metabolite Interactions Controlling the Ras/PKA Pathway

Glucose is the preferred carbon source for many organisms, but also for many healthy and unhealthy mammalian cell types. In the budding yeast *Saccharomyces cerevisiae*, glucose availability activates the cAMP mediated Ras/PKA pathway through extracellular and intracellular mechanisms [57]. The extracellular system relies on the G-protein coupled receptor Gpr1, which, once bound to glucose, interacts with Gpa2, the α-subunit of a

heterotrimeric G-protein complex. This interaction promotes Gpa1 loading with GTP and its release from the complex [58]. In parallel, intracellular perception of glucose is mediated by the monomeric GTP-binding protein Ras, product of *RAS1* and *RAS2* genes, that in the presence of glucose exchanges GDP with GTP in a reaction catalysed by the GEF (Guanine Nucleotide Exchange Factor) Cdc25 [59,60].

The two different mechanisms for Ras/PKA activation converge on the adenylate cyclase (AC) Cyr1, whose catalytic activity is triggered by the interaction with Ras2 and Gpa2, resulting in a strong increase of intracellular cAMP concentration. Interestingly, the Gpr1/Gpa2 pathway requires Ras pre-activation of Cyr1, with the result that the perception of extracellular glucose is subordinated to its actual consumption into glycolysis [61]. Glucose-mediated increase in cAMP concentration results in PKA activation

Figure 1. Ras/PKA modulation by PMIs. F1,6bP (green boxes) activates Ras both in yeasts and in mammals, interacting with Cdc25 and hSos1, respectively. Extracellular bicarbonate (blue boxes) interacts with yeast adenylate cyclase, activating virulence promoting processes, such as filamentous growth in *C. albicans* and encapsulation in *C. neoformans*. In mammalian cells, bicarbonate activates soluble adenylate cyclase (sAC) enabling the competence of spermatozoa. Moreover, this interaction promotes cellular growth in oncogenic Ras-driven tumors. In *S. cerevisiae*, acetate oxidation to CO2 through the TCA cycle induces sporulation of diploid cells grown in medium containing only this carbon source. Continuous arrows indicate direct activations, dashed lines indicate indirect processes.

thanks to the binding of the second messenger cAMP to Bcy1, the inhibiting subunit of PKA, inducing its dissociation from the catalytic subunits (Tpk1,2,3) [62]. Active PKA promotes fermentative growth by stimulating glycolytic flux. Accordingly, it represses processes associated with slow growth, such as mitochondrial respiration, stress responses and carbohydrate storage [32,55].

The Ras/PKA pathway is strongly influenced by the interactions between its components and metabolites that coordinate the activation state of the kinase with the metabolic state of the cell. In fact, as shown in Figure 1, cAMP synthesis is responsive to glucose transport into the cell and its phosphorylation to glucose-6-phosphate (G6P), while it has been discovered that fructose-1,6-biphosphate (F1,6bP) is the glycolytic metabolite that actually controls Ras activity (Figure 1) [5,63].

Evidence of this regulation has been obtained starting from the observation that yeast hexokinases (Hxk1 and Hxk2) are negatively controlled by G6P conversion into trehalose by Tps1 [64]. *TPS1* deleted cells show a higher glycolytic flux and a stronger increase in Ras activation, with a higher amount of Ras-GTP than the wild type [5]. This phenotype is reverted in cells deleted in the phosphofructokinases (*PFK1* and *PFK2*) and completely impaired in the production of F1,6bP[65]. In addition, Ras activation positively correlates with F1,6bP concentration in permeabilized spheroplasts, while F1,6bP binds to the complex formed by the catalytic domain of hSOS (the human homolog of Cdc25) and H-RAS, one of the human isoforms of Ras (Figure 1) [5]. This interaction has been proposed to take place at the interface between Cdc25 and Ras while point mutations of Cdc25 residues involved in the binding of Ras impair F1,6bP activation of the latter [5]. These results strongly suggest that the glycolytic flux is connected to the PKA

pathway by a molecular interaction between F1,6bP and the Ras/Cdc25 complex, which results in the activation of the G-protein and in the increase of cAMP concentration (Figure 1) [5]. Furthermore, this allosteric regulation is coherent with the proposed role of F1,6bP as glycolytic flux-sensor. In fact, F1,6bP concentration positively correlates with sugar uptake rate and is associated with yeast fermentative metabolism [66]. Since the Ras/PKA pathway responds to glucose availability and supports fermentation, its regulation by F1,6bP looks perfectly coherent with this function and gives mechanistic insights of how F1,6bP level could correlates with glycolytic flux and ethanol production. Remarkably, as shown in Figure 1, F1,6bP have been clearly demonstrated to bind with hSos1, the mammalian Cdc25 homologue, suggesting that F1,6bP control on the Ras/PKA pathway is also conserved in higher eukaryotes [5]. As described above, cAMP production by adenylate cyclase (AC) plays a central role in the activation of PKA. Prokaryotes and vertebrates present two classes of AC, distinguished in transmembrane (tmAC) and soluble (sAC) adenylate cyclases (as indicated also in Figure 1) [67]. tmACs represent the "classical" adenylate cyclases responsive to G-protein coupled receptors, while sACs are activated by bicarbonate ions that induces a strong increase in their catalytic activity [68,69]. Crystallographic analysis of human and of *Spirulina platensis* sACs revealed similar structures and a conserved interaction with bicarbonate ions [70,71]. *S. platensis* sAC presents two different ATP binding sites, while a bicarbonate specific binding site is still undiscovered due to the difficulties in sAC co-crystallization with this ion [70]. On the contrary, in human sAC one of the putative ATP binding sites is reported to bind with bicarbonate ions too [71].

Despite this difference, bicarbonate interaction induces a conformational change in both these enzymes. For *S. platensis* sAC this causes to the closure

of the active site and the exit of ATP pyrophosphate group, leading to the onset of catalysis [70]. In mammals, sAC is prevalently expressed in testis. Bicarbonate stimulation of sAC has been reported to be pivotal in the activation of processes involved in fertility and, indeed, its deletion results in sterile mice [72]. In addition, sAC is also expressed in other organs, such as in kidney and in the choroid plexus, and its function has been recently linked to the oncogenic Ras-dependent activation of pro-tumoral macropinocytosis [68,73].
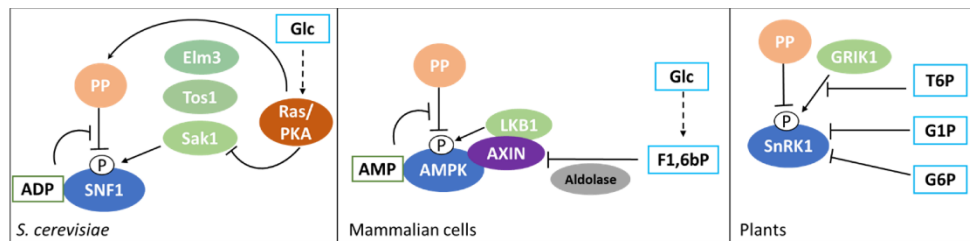
This process has been reported to support cancer growth, gaining amino acids from the degradation of extracellular proteins [74]. Interestingly, the onset of this process does not require the activity of the tmAC, but that of the sAC, which is stimulated by the bicarbonate imported from the extracellular matrix by SLC4A7 transporter. In such a way, the metabolism of cancer cells expressing an oncogenic Ras result to relate with the

extracellular acidification, coupling pH homeostasis and metabolic adaptation of mutant Ras-driven tumours (as schematically shown in the right part of Figure 1) [73].

Phylogenetic studies revealed the existence of four different classes of AC and eukaryotes have been reported to express only class III AC. Both transmembrane and soluble mammalian AC belong to this class but, strikingly, no soluble ACs have been found in *S. cerevisiae*, *Caenorhabditis elegans*, *Drosophila melanogaster* and plants [75]. Despite this, classical ACs from *Candida albicans* and *Cryptococcus neoformans* has been shown to be activated by bicarbonate, promoting virulence associated processes such as filamentous growth and encapsulation (see the left part of Figure 1) [76,77]. This highlights that given the differences between the ACs expressed by mammals and yeasts, these enzymes can be valuable therapeutic targets

for the treatment of Candida and *C. neoformans* infections.

Of note, bicarbonate activation of AC is also physiologically relevant for sporulation of diploid cells of *S. cerevisiae*. During this process, the Ras/PKA pathway needs to be finely tuned since low PKA activity is required to trigger meiosis and cAMP level oscillates during this process [78]. An environmental condition that triggers sporulation is the availability of acetate as sole carbon source. In particular, as schematized in Figure 1, acetate-dependent sporulation is triggered by bicarbonate ions produced by acetate oxidation in the TCA cycle and CO_2 hydration by the carbonic anhydrase (Figure 1) [79]. Bicarbonate interacts with the adenylate cyclase Cyr1 and the mutation of one of the lysine involved in the interaction (Cyr1^{K1712A}) results in the loss of the modulation of the sporulation efficiency by acetate concentrations. The same phenotype is observed in Ras and PKA depleted cells and

demonstrates that acetate modulation of sporulation passes through the Ras/PKA pathway and the modulation of Cyr1 activity, due to acetate oxidation and bicarbonate production [78].

All these results suggest that despite yeasts do not express soluble adenylate cyclase, bicarbonate control of AC activity is conserved in bacteria, fungi and mammals, with fungi canonical ACs being controlled both by G-proteins and bicarbonate ions, as indicated in Figure 1.

Figure 2. SNF1/AMPK/SnRK1 modulation by nucleotides (green boxes) and glucose metabolites (light blue boxes) in different species. ADP and AMP inhibit dephosphorylation of the regulatory Thr, in yeast and in mammalian cells, respectively. Glucose metabolites inhibit phosphorylation, although the specific mechanism is different in the different species. Additionally, AMPK is also controlled by glycogen through its binding with the Carbon Binding Module (CBS). See text for details. Continuous arrows indicate direct activations, dashed lines indicate indirect processes

Protein-Metabolite Interactions Controlling SNF1/AMPK/SnRK1 Pathway

As described above, glucose represents a positive signal for cell growth through the Ras/PKA pathway. Its presence is associated with a good nutritional condition which ensures enough carbon and energy to grow and proliferate [32]. However, since nutrient availability is only one of the parameters that could influence the energy balance, all eukaryotic systems have evolved signalling pathways able to monitor the global energetic status of the cell. These pathways are centred on the protein kinases Snf1, AMPK and SnRK1, depending on the organism (yeast, mammals or plants), as better explained below [80–82].

These kinases operate as heterotrimeric complexes composed of a catalytic subunit α and two regulatory subunits, β and γ. SNF1/AMPK/SnRK1 complexes are active in low energy conditions and are tightly connected to cellular metabolism. The key event in their regulation is the phosphorylation of the catalytic subunit on a functionally conserved threonine (T210 in yeast, T172 in humans and T175 in plants) which activates these kinases that I turn switch off energy-expensive processes [80–82].

In *S. cerevisiae*, Snf1 protein kinase was discovered in a genetic screening of mutants unable to grow on non-fermentable carbon sources [83]. Because of this, the SNF1 complex has been generally recognized as being active in low glucose conditions or in the presence of alternative carbon sources such as ethanol, glycerol and galactose. In these conditions, SNF1 activity is pivotal to rewire the yeast metabolism and to sustain cell growth with the induction of fatty acid oxidation, mitochondrial respiration and gluconeogenesis [53]. Despite this, recent reports suggest the involvement of SNF1 in the control of metabolism also under glucose repression [20,84]. While the Snf1 upstream kinases, Sak1, Tos3 and Elm1 are constitutively active (with Sak1 being the primary upstream kinase), the phosphatase activity of Reg1/Glc7 is strongly induced by availability of glucose [85]. Reg1-Glc7 PP1 plays the major role, also Ptc1 protein phosphatase 2C and Sit4 type 2A-related phosphatase were shown to contribute to glucose-regulated dephosphorylation of SNF1 [86,87].

A decrease in the ATP-to-ADP intracellular ratio is representative of a perturbation of the energy homeostasis and SNF1 activation state is controlled by a protein-metabolite interaction with ADP. As presented in Figure 2, the result of this interaction is the protection of the regulatory loop from phosphatase activity, with a resulting higher phosphorylation level of the threonine 210 [88]. Despite this clear evidence, the ADP-dependent protection of Snf1 phosphorylation is still controversial. At first, the protective effect was attributed to ADP binding with the Bateman (CBS) domains of the γ regulatory subunit [88], but later, an alternative model was proposed, according to which the direct binding of ADP in the catalytic site of the α subunit could promote phosphatase resistance [89]. In addition, some data shown that SNF1 activity negatively correlates with glucose

availability and glucose-6-phosphate synthesis, but the molecular mechanism through which glucose represses SNF1 is not fully understood.

It has been reported that glucose strongly increases PP1 and PP2A phosphatases activity in a PKA- dependent manner, while Sak1, the major Snf1 upstream kinase, is phosphorylated by PKA (Figure 2) [85,90]. Moreover, SNF1 complex has been reported to influence PKA pathway by phosphorylating Cyr1 [91]. These findings suggest that Snf1 phosphorylation may be linked to glycolysis through the Ras/PKA pathway and that these kinases may be connected by a feed-back mechanism.

A different hypothesis is based on the observation that Reg1/Glc7 can dephosphorylate its target Mig1 also in low glucose conditions, suggesting that PP1 basal activity may also be sufficient to inactivate Snf1. Therefore, glucose inhibition may take place through a change in the exposure of T210, regardless the activity level of the phosphatase [92].

The SNF1 homolog AMPK plays a well conserved role in mammalian cells and, as for yeast Snf1, its activity is controlled by the phosphorylation on a regulatory Thr, T172, by the upstream kinases LKB1 and CaMKK2 [93,94]. AMPK activation reflects an energetic stress of the cell and coherently induces a downregulation of anabolism and the activation of catabolic processes, such as β-oxidation of fatty acids and mitochondrial respiration [95,96].

AMPK is activated by energy depletion sensed as a decrease in the ATP-to-AMP ratio and thanks to AMP-dependent protection of AMPK complex from phosphatase activity (Figure 2) [97,98]. It was reported that AMP interacts with the γ regulatory subunit of AMPK, similarly to what was shown for ADP on yeast SNF1 complex (Figure 2) [88,99]. The γ regulatory subunit presents four different Bateman (CBS) domains, each characterized by an AMP

binding site and it has been shown that the weaker site mediates AMP control of AMPK, resulting in the protection from phosphatases and in the increase of the catalytic activity of the complex [98].

Interestingly, the full-length crystal structure of active AMPK shows a closed conformation in which T172 exposure to phosphatases is reduced. On the contrary, the crystal structure of unphosphorylated and inactive AMPK presents a higher exposure of T172 to the medium [100]. Strikingly, point mutations in the auto-inhibition domain of the catalytic subunit involved in the interaction with the AMP-binding site 3, abolish the AMP-induced protection from phosphatases and the increase of the catalytic activity [100,101].

Additionally, to this mechanism connecting AMPK to energy balance, it has been reported a connection between AMPK and F1,6bP, independently from the ATP-to-AMP ratio [6]. Glucose starvation has been demonstrated to increase the affinity of myristoylated AMPK for the scaffold protein AXIN, that fosters AMPK-LKB1 interaction, thus promoting AMPK phosphorylation (Figure 2) [102]. This takes place on the late lysosome membrane, where a protein complex composed of Ragulator (late endosomal adaptor, MAP and mTOR activator 1 and 5) and the V-ATPase alternatively recruits mTOR, in high energy conditions, or AMPK, in low energy conditions, playing an important role in the switch from anabolism to catabolism and vice versa [103]. Remarkably, F1,6bP promotes the dissociation of the AXIN/LKB1/AMPK complex and cells lacking phosphofructokinase show a high phosphorylation of AMPK also in presence of glucose [6]. Moreover, aldolases triple knockdown causes AMPK activation regardless glucose concentration, strongly suggesting that F1,6bP effect on AMPK could be mediated by the interaction with these glycolytic enzymes (Figure 2).

Aldolase split F1,6bP into glyceraldehyde-3-phosphate (G3P) and dihydroxyacetone-phosphate (DHAP) and F1,6bP binding to aldolase catalytic site is followed by a conformational change of the protein and the formation of a covalent bound between the substrate and the enzyme [104]. Strikingly, ALDOA-K230A point mutant, being impaired in its catalytic activity, prevents F1,6bP inhibition of AMPK and AXIN/LKB1/AMPK complex dissociation [6].

These results indicate that AMPK phosphorylation is directly controlled by glucose availability, which is sensed through changes in F1,6bP concentration, in a mechanism mediated by aldolases.

This is the first clear demonstration of a regulation of AMPK activity that takes place before and independently from any variation of the energetic status of the cell, directly connecting its activity to glucose metabolism and glycolytic flux [6].

AMPK activity is also linked to glucose metabolism through the interaction with glycogen. AMPK β subunits present a glycogen binding domain (GBD), also known as carbohydrate binding module (CBM), and its interaction with glycogen have been reported to affect AMPK activity. Single α1-6 branched glycogen molecules have been proved to act as allosteric inhibitors of AMPK, reducing its catalytic activity and preventing its phosphorylation by upstream kinases, without influencing AMPK dephosphorylation by upstream phosphatase PP2Cα and PP1 [105]. Such a control clearly suggests that AMPK, besides the perception of AMP/ATP ratio, can also monitor energy availability through the amount of reserve carbohydrates [105].

Interestingly, this feature of AMPK seems not to be conserved in yeast and plants. Yeast's Snf1 complex β subunits Gal83 and Sip2 present a functional GBD that is involved in the control of Snf1 activity, but not through the

binding of glycogen [106]. While in plants, the different CBD isoforms do not show the ability to bind glycogen [107].

As concerns plants, energy homeostasis is maintained by the SnRK1 complex, the homolog of SNF1 and AMPK. Energy depleting conditions could affect photosynthesis, mitochondrial respiration or carbon allocation and activate SnRK1 that downregulates anabolic processes and promotes catabolism [81]. As mentioned, also SnRK1 activity is controlled by a phosphorylation event regarding the T175 in the activation loop, and the active form of SnRK1 is represented by the canonical heterotrimeric complex composed of an α catalytic subunit and two regulatory subunits, β and γ [108].

SnRK1 phosphorylation relies on the activity of the upstream kinases GRIK1 and GRIK2, but also on a strong auto-phosphorylation activity and the overexpression of SnRK1 α subunit is sufficient to increase the catalytic activity of the complex [109]. These observations suggest that the SnRK1 complex is constitutively active, while it is repressed under energy abundance conditions.

This control strategy is opposite to those of SNF1 and AMPK complexes, but is coherent with the general feature of plant cells signalling of preferring downregulations rather than activations [110].

We have described that yeast *SNF1* and mammalian AMPK are controlled by two different stimuli, one regarding the general energetic status of the cell and the other responsive to glucose metabolism. Despite the structural similarities with SNF1 and AMPK, SnRK1 does not respond to changes in AMP or ADP concentration, coherently with the fact that βγ Bateman (CBS) domains present mutations in the residues involved in the binding of

adenosyl-nucleotides [107,111]. On the contrary, the effect of glucose on SNF1/AMPK/SnRK1 pathway is well conserved also in plants [7].

As depicted in Figure 2, trehalose-6-phosphate (T6P), glucose-6-phosphate (G6P) and glucose-1-phosphate (G1P) can directly bind and inhibit SnRK1 [7,15]. The availability of trehalose and sucrose signal a good nutritional state of the plant and therefore the possibility to switch on anabolic processes and growth. T6P has been reported to reduce SnRK1 catalytic activity as a non-competitive inhibitor, without affecting enzyme affinity to ATP. Furthermore, G1P influences SnRK1 enzymatic activity following the same mechanism and the combination of T6P and G1P have a synergistic effect on SnRK1, opening to the hypothesis that these metabolites could bind at two different sites. On the contrary, G6P is known to inhibits ATP binding to the catalytic domain and has a cumulative effect when combined with T6P [15].

Eventually, SnRK1 inhibition by T6P was recently reported to depend on T6P binding to KIN10, the catalytic subunit of SnRK1, affecting its interaction with the upstream kinase GRIK1, therefore reducing SnRK1 phosphorylation and enzymatic activity [112].

According to the presented evidence, we can conclude that energy homeostasis in eukaryotic cells is maintained through protein-metabolite interactions in which key metabolites transduce information to a protein-based control system, whose function is to downregulate anabolic processes and to promote catabolism.

Protein-Metabolite Interactions Controlling TOR Activity in Yeast and Mammalian Cells

Amino acids are among the nutrients that most influence the growth of eukaryotic cells. While glucose ensures energy and carbon availability, amino acids are directly connected to protein and nucleotide synthesis.

TOR pathway is deputed to amino acids perception in all eukaryotes and its activation represents a positive signal for cellular growth. Active TOR promotes anabolic processes such as protein, lipid and nucleotide synthesis and represses autophagy [113].

As for carbon, also nitrogen sources show a precise hierarchy in their preferred consumptions. In mammalian cells, mTORC1 is preferentially activated by leucine and arginine, while glutamine is the main activator of TORC1 complex in yeast [8,52].

Amino acid sufficiency represents an essential input for TOR activation and its sensing largely relies on RAG-GTPase complexes. Amino acids stimulate the loading with GTP of mammalian RagA/B and of Gtr1 in yeast. Meanwhile,
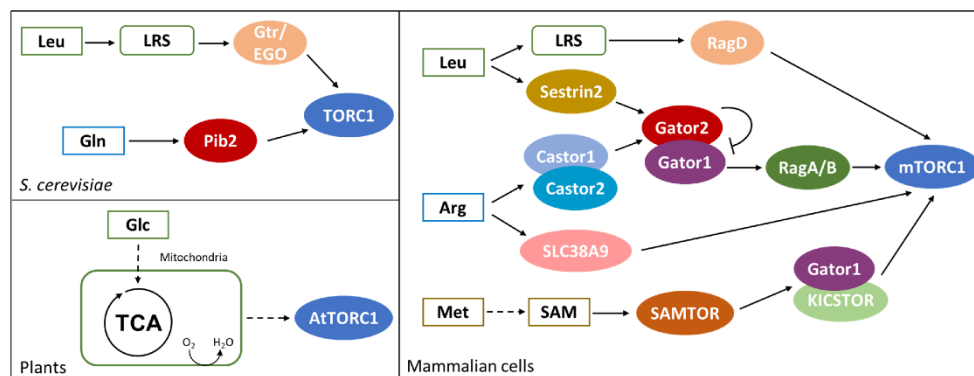
Figure 3. TOR modulation in yeast and in mammalian cells. Both in *S. cerevisiae* and in mammalian cells, leucine activates TOR through Leu-tRNA-synthase (green boxes). In addition, Gln in yeast (blue box), Arg and Met in mammalian cells (purple and orange boxes, respectively) were shown to activate TOR. Contrary to yeast and mammals, in plant cells TOR activity is controlled by glucose oxidation and mitochondrial metabolism. See text for details.

amino acids promote the loading of RagC/D and Gtr2 with GDP, promoting TOR activation [114,115].

Amino acids perception requires their transport into the cell and protein-metabolite interactions between key amino acids and regulator proteins upstream of TOR. As shown in the left part of Figure 3, in *S. cerevisiae*, glutamine and leucine activate TORC1 through Pib2 and Gtr/Ego pathways, respectively [14,115]. *PIB2* genetically interacts with *GTR1* and their double deletion leads to synthetic lethality. Moreover, the suppression of Pib2 expression in a *gtr1Δ* background completely abolishes TORC1 activation, suggesting that amino acid sufficiency in yeast is exclusively sensed through these protein complexes [14,116].

PIB2 deletion is reported to impair glutamine activation of TORC1 (Figure 3). Pib2 coprecipitates with TORC1 under amino acids sufficiency and glutamine is reported to enhance Pib2-TORC1 interaction in vitro in a dose-responsive manner. However, *in vitro* experiments failed to identify a direct interaction between glutamine and purified Pib2 protein, while glutamine interacts with Pib2 when incubated with cell extracts suggesting that the binding may be indirect and mediated by another Pib2 interactor [14].

The Ego complex (Ego1, Ego2, Ego3) is known to tether the Grt1/Gtr2 GTPase to the vacuole and amino acids, mainly leucine, stimulate Gtr1 loading with GTP and of Gtr2 with GDP, activating the complex [117]. In yeast, TORC1 constitutively localizes at the vacuole, forming punctate structures under amino acid starvation and diffusing all over the membrane in presence of key amino acids. Active Gtr1/Gtr2 complex strongly interacts with TORC1 and induces its activation [115,118]. As represented in Figure 3, leucine perception by the Gtr/Ego pathway relies on the leucyl-tRNA synthetase (LRS), encoded by *CDC60* [119]. This tRNA synthase presents

both an aminoacyl-tRNA-synthetase activity and a proofreading one, functional to the control of the loading with the proper amino acid [120]. Leucine is the most abundant amino acid in proteins and its tRNA synthetase is the most expressed in yeast cells [121,122]. These observations provide a rationale for TORC1 activation by leucine, even though it is not the preferred nitrogen source in yeast. Cdc60 has been reported to interact with Gtr1 in the presence of leucine and treatment with the leucyl-tRNA-synthetase inhibitor 1,3-dihydro-1-hydroxy-2,1-benzoxaborole (DHBB) downregulates TORC1 activity [119]. Since DHBB is known to form an adduct at the proofreading site of the enzyme, trapping it in the uncharged state, it is likely that leucine starvation may affect Cdc60-Gtr1 interaction due to an increase of mischarged tRNALeu and the activation of the proofreading activity [123,124]. Eventually, Cdc60 dissociation from Gtr1 may expose it to the interaction with a yet unknown GAP, causing GTP hydrolysis and the inactivation of the complex, leading to downregulation of TORC1 activity [119].

Pib2 and Gtr1/Gtr2 form distinct complexes with TORC1 and independently modulate its activity. Pib2, as Tor1, localizes in puncta on the vacuole under starvation and diffuses all over the vacuole membrane under amino acids sufficiency. Despite the independent functions of Pib2 and Gtr1, a strain deleted in GTR1 shows an accumulation of both Tor1 and Pib2 puncta even in presence of amino acids, suggesting that Pib2 localization may be controlled by the Gtr1/2 complex [14].

These observations underline the fact that despite some clear evidence, further studies are required to understand the fine tuning of these two different control mechanisms in *S. cerevisiae*.

In mammalian cells, mTOR activity is controlled by both amino acid sufficiency (in particular by leucine, arginine and methionine, as shown in the right part of Figure 3) and growth factors [125,126]. Under amino acid sufficiency, the Gtr1 ortholog RagA/B is loaded with GTP and dimerizes with the Gtr2 ortholog RagC/D charged with GDP. RAG GTPases constitutively localize on the lysosome membrane and amino acids induce their interaction with the Ego ortholog Ragulator, while their interaction with Raptor recruits mTORC1 at the lysosome [127,128]. Once localized at the lysosome, mTORC1 is activated through the interaction with the GTPase RHEB, which is controlled by growth factors through the AKT pathway [126,129]. Therefore, mTORC1 is activated only when nutritional and environmental conditions are advantageous and cellular growth is both feasible and allowed. As represented in Figure 3, the function of leucyl-tRNA-synthetase (LRS) in mediating leucine perception is conserved also in mammalian cells [130]. Leucine other amino acids availability induces LRS localization at the lysosome membrane, where it interacts with Raptor and mTORC1 complexes. Both LRS knockdown and point mutation of the leucine binding site result in a reduced activation of mTORC1 upon leucine supplementation, demonstrating that leucine availability is perceived through its binding with LRS. Leucine availability also induces the interaction of LRS with RagD, inducing the hydrolysis of GTP to GDP and the activation of mTORC1 [130]. Nevertheless, LRS depletion does not totally impair mTORC1 activation since leucine availability in mammalian cells is also perceived through Sestrin2 (see Figure 3), a monomeric protein sharing common folding with the carboxymucolactone decarboxylase (CMD) protein family.

The C-terminal domain of Sestrin2 presents a binding pocket specific for leucine, with residues Glu451 and Arg390 interacting with leucine amine and

carboxylic group, respectively. The hydrophobic base of the pocket excludes charged and polar amino acids, while large hydrophobic residues are excluded by steric clash and small one cannot form stable interactions. In addition, a lid structure completely covers leucine within the binding pocket and stabilizes the protein structure [9].

Sestrin2 is known to interact with Gator2, the inhibitor of Gator1, a protein complex acting as GAP of RagA/B. During amino acid starvation, Sestrin2 recruits Gator2 presumably promoting RagA/B GTPase activity and therefore mTORC1 inactivation. On the contrary, during amino acid sufficiency, Gator2 inhibits Gator1, promoting the loading of RagA/B with GTP and mTORC1 activation [131,132]. Leucine is reported to bind to Sestrin2 and affects Sestrin2-Gator2 interaction, while a Sestrin2 mutant impaired in the binding with Gator2 fails to activate mTORC1 in the presence of leucine [130].

Eventually, HEK-293T cells expressing a Sestrin2 mutant with a reduce affinity for leucine show a dose-response activation of mTORC1 shifted towards a higher concentration of amino acids, clearly demonstrating that leucine-dependent activation of mTORC1 requires leucine binding to Sestrin2 [9].

As indicated in Figure 3, arginine is another amino acid known to directly affect mTORC1 activity and, also its perception, is centred on the protein Gator2 [10,125]. Amino acid starvation induces Gator2 interaction with Castor1 and Castor2, two homolog proteins presenting four small molecule binding domains (ACT) each. These proteins can combine into homo- and hetero-complexes, and their dimerization is necessary for their interaction conformation of a glycine-rich loop and therefore allowing for ACT2-ACT4 interaction [10]. I280A point mutation of Castor1 is reported to impair arginine binding with the protein, resulting in a constitutive interaction with

Gator2. Crystallographic analysis revealed that arginine binds Castor1 at the interface between ACT2 and ACT4, presumably arranging the with Gator2. Crystallographic analysis revealed that arginine binds Castor1 at the interface between ACT2 and ACT4, presumably arranging the Gator2 and in the inactivation of mTORC1, even in the presence of arginine [10,133]. According to these results, arginine availability activates mTORC1 through the inhibition of Gator1 by Gator2, that may be released from Castor1 due to a conformational change in Castor1 altering the exposure of key residues required for its interaction with Gator2 [133].

Interestingly, the ACT domains of Castor1 structurally resemble the allosteric regulatory domain of bacterial aspartate kinase (AK), which is known to be sensitive to leucine. Since AK is absent in metazoan and Castor1 is present only in this lineage, it is likely that arginine perception evolved starting form an already existing module, i.e., prokaryotic aspartate kinases [116]. Following this line of evidence, arginine perception could be relevant also in yeast, through the aspartate kinase Hom3. In fact, Hom3 has been reported to genetically interact with component of the EGO complex and its deletion increases rapamycin sensitivity, suggesting the involvement of Hom3 in arginine perception in yeast [134,135].

In mammalian cells, arginine perception relies also on the lysosomal transmembrane protein SLC38A9 (Figure 3). It has been reported that SLC38A9 interacts with Ragulator complex and with a RagB mutant that mimics a constitutive binding with GDP [136]. Moreover, its deletion affects mTORC1 activation by arginine availability. Since SLC38A9 presents a transport activity specific for amino acids and with a preference for arginine, it may link mTORC1 activity with arginine concentration within the lysosome [136].

Interestingly, a recent report suggests that arginine perception by Castor1 and SLC38A9 occur through independent mechanisms and the residual activation of mTORC1 in cells lacking Castor1 and SLC38A9 suggests the existence of additional controls on the pathway [10].

As indicated in Figure 3, TOR pathway in mammalian is also influenced by methionine availability conversation into S-Adenosylmethionine (SAM) [11]. Furthermore, SAM level can be influenced also by folate, betaine and vitamin B12, suggesting that also these molecules could indirectly influence mTORC1 activity. Methionine perception in mammalian cells depends on a PMI between its activated form SAM, and SAMTOR, a protein presenting a class I Rossmann fold methyltransferase domain able to bind SAM [11]. This mechanism is conserved in *D. melanogaster*, which presents a SAMTOR homolog dSamtor, but not in *S. cerevisiae*, in which methionine availability is perceived through PP2A methylation and not through PMIs [137].

Differently from Sestrin2 and Castor complexes, SAMTOR negatively regulates mTORC1 interacting with Gator1 and KICSTOR, suggesting that Gator1 is inactive when bound to SAMTOR. Hence, the binding of SAM to SAMTOR results in the disruption of the SAMTOR-Gator1-KICSTOR complex, releasing Gator1 and activating mTORC1 [11].

The TOR pathway is quite conserved also in plants, even if its regulation by PMIs is much less clear. *Arabidopsis thaliana* genome encodes for functional homologs of TOR (AtTOR) and two TOR-interactors: LST8 (AtLST8-1 and AtLST8-2) and RAPTOR (AtRAPTOR1A and AtRAPTOR1B). On the contrary, no TORC2 homolog has been identified [138]. It was shown that glucose and sucrose (but not other sugars such as fructose, xylose and galactose) stimulate root growth and meristem activation in a TOR-dependent manner [139]. Glucose activation of TOR pathway is prevented by 2-deoxy-glucose

and by the inhibitors of the electron transport chain, indicating that glucose must be oxidised to activate TOR (Figure 3) [139].

In addition, it has been recently reported that nicotinamide (vitamin B3) affects ATP level and inhibits glucose-TOR signalling, regulating the circadian clock, meristem activation and root growth [140].

Although the precise molecular mechanism of glucose activation is still unknown, this study suggests a link between the energetic status of the cell and TOR activity. This leads to the hypothesis that TOR activation by glucose may be mediated by the kinase SnRK1, which phosphorylates RAPTOR as AMPK does in mammalian cells, where this phosphorylation has an inhibitory effect [141,142].

A second hypothesis is that glucose signals could be required for TORC1 dimerization [138]. In mammalian cells, the glucose/energy sensitive Tel2-Tti1-Tti2 (TTT)- RUVBL1/2 complex (which has orthologous genes in plants) is required for TORC1 dimerization and translocation to the lysosome membrane [143]. The assembly of the TTT-RUVBL1/2 complex and its interaction with TOR requires the activity of RUVBL1/2, which is repressed by respiration inhibition, therefore indirectly linking respiration and TOR activation.

In plants, TOR signalling also responds to sulphur availability and sulphur deficiency causes TOR inhibition, due to a reduction of the levels of glucose, maltose, sucrose and TCA cycle intermediates, suggesting that sulphur shortage is sensed through the same glucose-TOR signalling described above [144].

Finally, although the major TOR activators in yeast and mammals are amino acids, no amino acid sensors have been discovered in plant genomes.
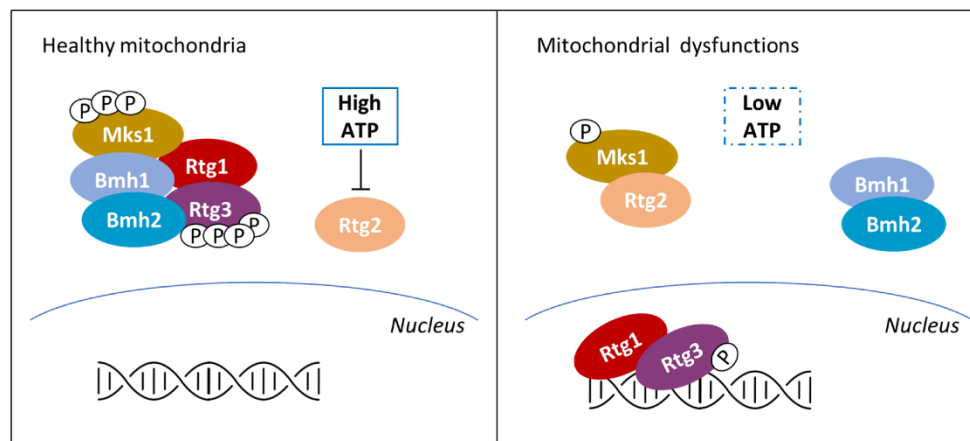
Indeed, it was shown that TOR activity cannot be stimulates by amino acid cocktail [139]. Nevertheless, it was recently reported that mutants accumulating branched chain amino acids (BCAA) present a higher TOR activity and an altered organization of actin cytoskeleton and endomembrane [145]. This evidence suggests that also in plant cells, amino acids somehow involved in the regulation of TOR pathway.

Yeast Mitochondrial Retrograde Response Is Influenced by Protein-Metabolite Interactions

Classically defined as the powerhouse of the cell, it is now clear that mitochondria functions go beyond energy production and that mitochondrial health critically define cell fate [146–148]. In mammals, yeast and plants, mitochondrial dysfunctions activate retrograde response pathways (RTGs), eliciting the transcription of nuclear genes with the aim of coping with the perturbation. In yeasts, RTG is known to be triggered by the shift on non-fermentable carbon sources and leads to the expression of genes involved in respiration and consumption of carbon sources alternative to glucose, but it is also involved in multi-drug resistance [149–151]. As reported in Figure 4, among the different stimuli activating the RTG pathway in yeast there is the drop in ATP concentration [54]. On the contrary, in mammals and in plants, mitochondrial dysfunctions are signalled to the nucleus mainly by the alteration of mitochondrial membrane potential, followed by a strong increase in cytoplasmic calcium without involving PMIs (see [152,153], for further details). ATP control of RTG pathway in yeast is based on a PMI. In cells presenting healthy mitochondria (see the left part of Figure 4), the Mks1-Bmh1/2 complex

prevents Rtg3 dephosphorylation and therefore its migration into the nucleus. Mitochondria dysfunctions (right part of Figure 4) induce partial dephosphorylation of the transcription factor Rtg3 and its nuclear localization in complex with Rtg1 [154]. The onset of the signalling is centred around Rtg2 that, under mitochondrial stress, binds Mks1 and promotes Rtg1-Rtg3 translocation into the nucleus [155]. Rtg2 is known to present an N-terminal ATP-binding domain like the Hsp70/sugar kinase/actin protein superfamily, whose activity results to be pivotal for the onset of RTG [139]. It has been reported that ATP strongly impairs Rtg2 interaction with Mks1 at physiological concentrations, while a non-hydrolysable ATP homologue (adenosine 50-(β,γ- imido) triphosphate) has no effect on Rgt2-Mks1 interaction [12].

This suggest that ATP must be hydrolysed to induce Mks1 dissociation from Rgt2; yet ATP interaction with the ATP-binding domain of Rtg2 has not been

Figure 4. Regulation of the mitochondrial retrograde response in *S. cerevisiae*. In yeast cells presenting healthy mitochondria, Rtg1-Rtg3 complex is recruited to the cytosol by the Mks1-Bmh1/2 complex, with both Rtg3 and Mks1 hyper-phosphorylated. The interaction between Rgt2 and Mks1 is inhibited by ATP interaction with Rtg2 or with other components of the complex. Mitochondrial dysfunction causes a drop in ATP concentration (indicated by the dotted box), leading to Rtg2-Mks1 interaction and hypo-phosphorylated Rtg3 and Mks1. As a consequence, the nuclear localization of the Rtg1-Rtg3 complex induces the expression of RTG genes.

proved, leaving open the possibility of an indirect sensing of the ATP availability.

Strikingly, the role of ATP in controlling Mks1 activity is also reported in other yeasts, such as *Kluveromyces lactis* and *Kluveromyces waltii*, suggesting the conservation of this control mechanism among Fungi [12].

In conclusion, despite Snf1 conserved role in monitoring the energetic status of the cell, recent evidence suggests that Snf1 and RTG pathways can independently respond to ATP depletion in yeast [143].

Protein-Metabolite Interactions Controlling Calcium Release

Transient changes in the concentration of intracellular calcium are important regulators of cellular signalling in human cells. The increase of intracellular calcium can be due either to Ca^{2+} entry from the extracellular space through L-type Ca^{2+} channels and to Ca^{2+} release form the endoplasmic/sarcoplasmic reticulum (ER/SR).

Two major calcium channels exist on the ER/SR, one dependent on calcium ions, the other controlled by inositol-3-phosphate (IP3). The so-called calcium-induced calcium release (CICR) is mediated by Ryanodine receptors (RyRs), homotetrameric channels, which are normally closed when the cytosolic calcium concentration is low (100–200 nM), while they are open when calcium increases up to low micromolar concentrations [156]. The other pathway of calcium release is activated by IP3 binding to IP3 receptors. Hormones, growth factors and neurotransmitters can stimulate the formation of IP3 through activation of G-protein-coupled receptors (GPCR) or tyrosine kinase associated receptors, which are associated with phospholipase C (PLC). PLC catalyses the formation of diacylglycerol (DAG) and IP3 from phosphatidyl inositol-4,5-bisphosphate, and IP3 stimulates IP3
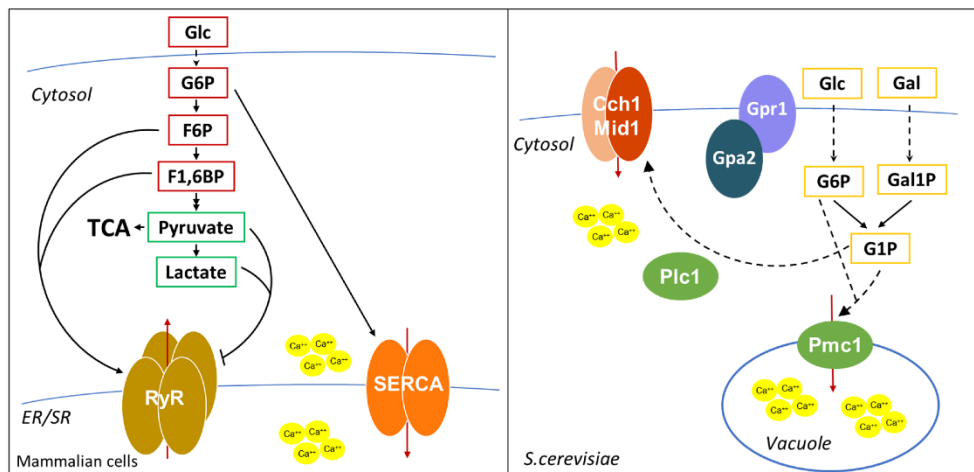
receptors, inducing calcium release form the endoplasmic reticulum, characterized by brief calcium transients, that can be repeated to give oscillations [157]. Instead, calcium uptake from the cytosol back into the ER/SR relies on the activity of the SERCA (sarcoendoplasmic reticulum Ca^{2+}-ATPase) pump, whose function is essential to guarantee calcium homeostasis. Calcium signalling pathway controls several different processes, among which muscle contraction, neuronal functions, gene expression, metabolism, secretion, fertilization and proliferation, while defects in this pathway are associated with a wide range of pathological conditions [157].

Cyclic ADP-ribose (cADPR) is a cyclic metabolite of NAD^+, synthesized by ADP-ribosyl cyclase, and is the main known regulator of calcium release. It induces calcium release from the SR via RyRs [158–161], it directly binds to SERCA and stimulates calcium sequestration in the SR [162–164] and can also regulate calcium influx from the environment, activating the calcium influx channel TRPM2, at the cell surface [165].

As shown in Figure 5, calcium levels are also controlled by glycolysis. More than 30 years ago, it was shown that in pancreatic islets glucose-6-phosphate increased the ATP-dependent calcium content in the ER [166]. The same effect of G6P on SERCA activity was shown in other tissues [13,167], and G6P import in the ER was suggested to be required for calcium sequestration [167].

In addition, in cardiac myocytes, glycolysis is required for excitation-contraction coupling, regulating SR Ca^{2+} release and Ca^{2+} sequestration by

Figure 5. Overview of the effect of glycolytic intermediates on calcium accumulation into the cytoplasm. Metabolites of the upper part of glycolysis (red boxes) are reported to positively influence the activity of RyR channels and SERCA pump, regulating the oscillation of calcium concentration into the cytosol. On the contrary, metabolites of the lower part of glycolysis (green boxes) negatively regulate calcium release from ER/SR through RyR channels. In *S. cerevisiae* (dotted box) calcium import by the plasma membrane calcium channel is regulated by glucose and galactose availability through their conversion into G6P and G1P.

SERCA [168,169]. Interestingly, it was shown that F6P and F1,6BP directly stimulate the open probability of RyRs, while pyruvate and lactate inhibit RyRs activity [168], suggesting that glycolysis modulates calcium release through multiple metabolites.

Calcium regulation in yeast is quite different from that in human cells. The main calcium storage organelle in yeast is the vacuole, a large organelle resembling animal lysosome, which contains more than 90% of calcium of the cell. Calcium is imported from the cytosol by the vacuolar Ca^{2+}/ATPase Pmc1 and by the H^+/Ca^{2+} antiporter Vcx1 [170–172], while Ca^{2+} efflux out of the vacuole is mediated by Yvc1 [173]. A minor, exchangeable pool of calcium is located in the ER and Golgi apparatus, where proper calcium levels are maintained by the Ca^{2+}/ATPases Spf1 and Pmr1, important for the regulation of protein folding and processing of proteins that transit through

the secretory pathway [174]. Yeasts also have a calcium channel on the plasma membrane, composed by Cch1 and Mid1, responsive to intracellular Ca^{2+} storage [172]. Although *S. cerevisiae* does not have an IP3 receptor, it was shown that IP3 generation by Plc1 activation is involved in the calcium increase after glucose addition to starved cells [175].

In yeast, calcium signals are generated during mating, upon environmental stresses (such as osmotic and alkaline stress, ER stress, oxidative stress, heat shock), after glucose addition to starved cells and during mitosis [170]. Calcium shortage was reported to affect cell cycle, cell growth, metabolism and protein folding [176].

Interestingly, as in mammalian cells, glucose metabolites were shown to modulate calcium levels also in *S. cerevisiae*. Glucose or galactose addition to starved cells leads to a transient calcium increase due to the opening of plasma membrane calcium channels and requires hexose transport and phosphorylation [177], but also the Gpr1/Gpa2 complex and the phospholipase C Plc1 [175,178].

Interestingly, cells lacking Pmg2, the major isoform of phosphoglucomutase that catalyses the interconversion of G1P and G6P, present higher G1P levels when grown in galactose and show higher intracellular calcium levels [179], due to elevated Pmc1-dependent vacuolar Ca^{2+} uptake and reduced ER/Golgi Ca^{2+} accumulation [180]. Strikingly, deletion of the phosphofructokinase Pfk2 in a *pgm2Δ* strain restores the balance between G1P and G6P and restores Ca^{2+} concentration to a level comparable to that of wild type cells [181]. These data suggest that the ratio between G1P and G6P, rather than the level of each single metabolite, regulates intracellular calcium levels. However, the molecular mechanism of this regulation in still unknown, since neither G6P nor G1P are able to directly stimulate Ca^{2+}

transport into the vacuole [181]. An indirect mechanism may involve the Snf3 pathway, which was shown to sense G6P levels [169] or the Gpr1/Gpa2 pathway, which has already been implicated in the calcium increase after glucose readdiction to starved cells [178].

Concluding remarks

It is evident that metabolism has a strong impact on cell signalling and that the interactions between key metabolites and proteins have crucial roles in the cellular response to specific environmental and metabolic conditions. As schematically represented in Figure 6, several metabolites of the central metabolism directly participate in the regulation of different signalling pathways. Metabolites of the glycolysis modulate the SNF1/AMPK/SnRK1 pathway, as well as the PKA pathway and the calcium release mechanism. Molecules belonging to the TCA cycle regulate the retrograde response in yeast and the Ras/PKA pathway. Finally, key amino acids control the TORC1 pathway, through multiple mechanisms.

However, all the mechanisms reviewed here have been discovered in hypothesis-driven studies and large-scale analyses exploring protein-metabolite interactions, as well as their structural and physiological consequences on regulatory proteins, are still needed. One obvious problem is that metabolites mostly interact with metabolic enzymes, while only a small fraction is involved in interactions with signalling proteins to perform regulatory functions [182]. In addition, PMI investigation is hindered by technical problems since different approaches are needed to study molecules with different chemical properties [34]. Several methodologies for the analysis of the interaction between proteins and small molecule have been developed in recent years (see [34] for a detailed description);
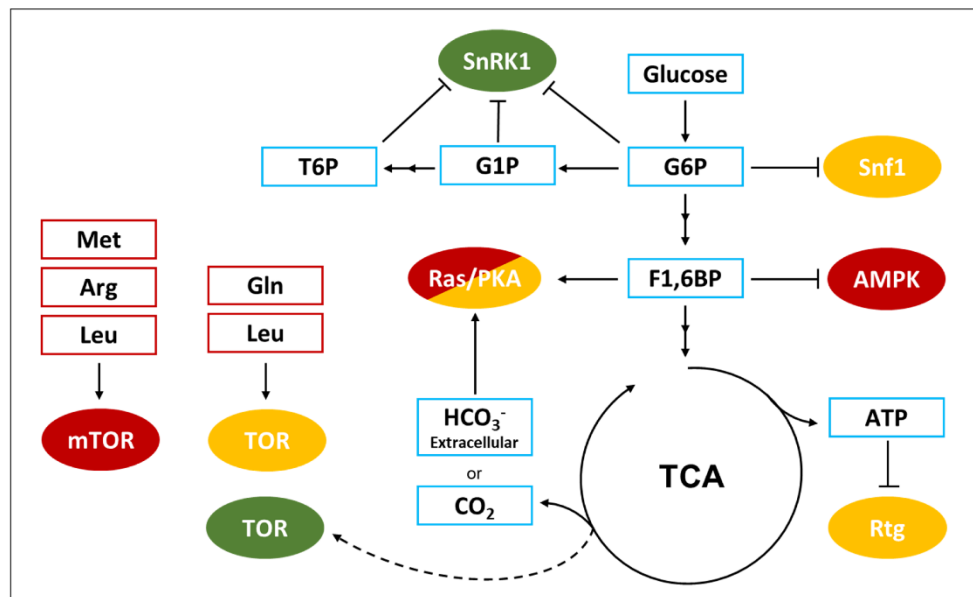
Figure 6. Overview of the Protein-metabolite interactions connecting metabolism and signal transduction pathways in different species. The central carbon metabolism influences the activity of Ras/PKA and SNF1/AMPK/SnRK1 pathways, but also the mitochondrial retrograde response, in yeast, mammals and plants (shown respectively in yellow, red and green). The availability of specific amino acids controls the activity of TOR pathway both in yeast and in mammals, while in plants its activity is influenced by mitochondrial respirations.

however, their application has mainly been focused on the interaction between metabolites and metabolic enzymes. The dynamical nature of PMIs, the high number of interactions involving metabolic enzymes, the necessity of validating the binding *in vitro* and their effect *in vivo* exacerbate, if possible, the difficulties of the study of PMIs at large scale when focused on regulatory proteins.

Nevertheless, the information acquired from such studies would represents significant progress for the comprehension of biological systems. For instance, a systematic analysis of in vivo PMIs in *S. cerevisiae* directed against non-polar small molecules revealed that 20% of protein kinases interact with hydrophobic metabolites [183]. Additionally, system level analysis on yeast

cells shifted from glucose to ethanol revealed the requirement of the 14-3-3 protein Bmh1 for yeast growth on ethanol [163]. These examples suggest that our comprehension of the crosstalk between metabolism and cell signalling is still poor, and that the allosteric modulation of regulatory proteins by PMIs could be a common mechanism by which cell signalling is dynamically connected to metabolism.

Chapter 2

Glucose metabolism controls the activity of Snf1/AMPK protein kinase

From: Milanesi et al., Int. J. Mol. Sci. 2021

Glucose metabolism controls the activity of Snf1/AMPK protein kinase

Introduction

As extensively described in the previous chapter, living organism must adapt to challenging environments, coping with stresses and monitoring the availability of nutrients. For microbial cells, the success of this adaptation is represented by the ability to grow, such that the maximization of the growth rate is usually taken as the objective function of a cell [184]. To this aim, the fine-tuning of several cellular processes is pivotal for the coordination of metabolism, cell cycle, and growth. In this process, the crosstalk between different signalling pathways is necessary to successfully coordinate cell functions, as highlighted by the widespread bow-tie architecture of signal transduction pathways [1].

The budding yeast *Saccharomyces cerevisiae* is a powerful model for studying fundamental aspects of eukaryotic cell biology, especially connected to signal transduction and metabolism, thanks to the high degree of conservation of several key cellular processes between yeast and mammalian cells [185]. Yeast metabolism is characterized by the preference of aerobic fermentation of glucose, similarly to Warburg-positive transformed cells, while glucose availability is perceived by Snf3/Rgt2 and Gpr1/Gpa2 systems, activates the Ras/PKA pathway, and suppresses the Snf1/AMPK pathway, as described in the previous part [32]. This results in the promotion of glucose fermentation and cell growth, while stress tolerance, mitochondrial respiration, and the consumption of alternative carbon sources to glucose are repressed [51]. On the other hand, low

glucose concentration is associated with the repression of the Ras/PKA pathway and the activation of Snf1/AMPK, leading to the induction of genes associated with respiration, β-oxidation, and the upregulation of stress tolerance [80].

Among the genes controlled by glucose availability, there are those required for glucose transport. *S. cerevisiae* possesses at least 20 different glucose transporters, all sharing a common structure with 12 transmembrane regions, and characterized by different affinity and capacity for glucose transport [32]. Yeast specialization for glucose consumption is highlighted also by its ability to dynamically adapt the expression pattern of glucose transporters according to the extracellular glucose concentration. High titration leads to the expression of low-affinity and high-capacity transporters (such as Hxt1 and Hxt3), allowing for a massive intake flux. Whereas a decrease in glucose concentration leads to the expression of high-affinity and low-capacity transporters (such as Hxt7, Htx6 and Gal2), succeeding in the passive import of glucose even at low millimolar concentrations [32].

PKA and Snf1/AMPK opposite activations suggest the existence of a thick crosstalk between these two pathways. Snf1/AMPK phosphorylates and inhibits Cyr1, the adenylate cyclase upstream of the PKA pathway [91]. On the other hand, PKA is known to phosphorylate and inactivate Sak1, the major activator kinase of Snf1/AMPK [90]. This feedback mechanism by which according to nutritional conditions, PKA inactivates Snf1/AMPK, and vice versa, allows yeast cells to avoid transcriptional inconsistencies undermining cellular homeostasis. Anyway, the molecular mechanism underlying this crosstalk is still missing [186]. Besides glucose, yeast cells can selectively consume different carbon sources through respiration or

fermentation. It has been shown that sugar uptake rate defines the manner of their consumption, going beyond the classical model by which yeast's metabolic fate is controlled by glucose concentration in the growth medium [66]. Moreover, fructose-1,6-bisphosphate (F1,6BP) concentration has been reported to correlate with sugar transport rate, mirroring the glycolytic flux and potentially acting as a flux sensor [66,187]. As mentioned in Chapters 1, F1,6BP has been reported to interact with Cdc25—the guanine nucleotide exchange factor upstream of Ras—inducing the activation of the Ras/PKA pathway (Figure 1, Chapter 1) [5,188]. This interaction connects PKA with the function of F1,6BP as a reporter of the glycolytic flux, suggesting a molecular regulatory role of the flux-sensing mechanism. Strikingly, the Ras/PKA pathway is also responsible for the activation of Reg1/Glc7—the phosphatase complex upstream of Snf1/AMPK—thus leaving open the hypothesis that Snf1/AMPK activation state may be indirectly linked to glucose metabolism through F1,6BP synthesis and PKA activation.

In keeping with this hypothesis, mammalian AMPK has been recently proven to be controlled by F1,6BP, which induces the release of AMPK from the AXIN/LKB1/AMPK complex (Figure 1, Chapter 1) [6]. In this process, signal transduction from glycolysis to AMPK is mediated by F1,6BP's interaction with aldolase, whose activity is essential for F1,6BP-dependent control of the AMPK activation state [6]. However, the *S. cerevisiae* ortholog of the AXIN/LKB1/AMPK complex has not been identified, suggesting a different coordination between glycolysis and Snf1/AMPK activity.

In the present work, we investigate whether the connection between Snf1/AMPK and glycolytic metabolism is indirectly mediated by the Ras/PKA pathway, trying to fill the knowledge gap regarding Ras/PKA and Snf1/AMPK crosstalk in *S. cerevisiae* (Figure 1 and 2, Chapter 1).

Interestingly, we demonstrate that glucose-6-phosphate (G6P), and not F1,6BP, is involved in the control of the Snf1/AMPK phosphorylation state. We also report that the Ras/PKA pathway is dispensable for the inhibition of Snf1/AMPK upon glucose replenishment. Therefore, we propose that the glycolytic flux is independently perceived by the two signalling pathways (i.e., Snf1/AMPK and Ras/PKA) through interactions with different glycolytic metabolites (i.e., G6P and F1,6BP). This model is coherent with the bow-tie architecture of cell signalling, while the information conveyed by Snf1/AMPK and Ras/PKA pathways that integrate at the level of downstream effectors.

Glucose Inhibition of Snf1/AMPK Is Independent from the Ras/PKA Pathway

As described before, the Snf1/AMPK activation state is controlled by phosphorylation of the regulatory residue Thr210—a substrate of both the upstream kinases (Sak1, Tos3, and Elm1) and the Reg1/Glc7 phosphatase (Figure 2) [85,189]. Glucose availability promotes Snf1-T210 dephosphorylation, while growth on non-fermentable carbon sources is associated with a high level of Snf1/AMPK phosphorylation. As already reported, PKA phosphorylates Sak1, inducing a mild reduction in Snf1/AMPK phosphorylation [90]. While, according to another report, the activity of Snf1/AMPK upstream kinases is not influenced by glucose availability [92]. In addition, Reg1/Glc7 phosphatase is activated by glucose in a Ras/PKA-dependent manner [85]. Taken together, all these observations prompted us to better investigate the involvement of the Ras/PKA pathway in the control of the phosphorylation state of Snf1/AMPK. Since the Ras/PKA pathway is linked to glycolysis by F1,6BP physical interaction with Cdc25 (Figure 1) [5], we first asked whether Snf1/AMPK phosphorylation may be

indirectly influenced by this interaction. To address this issue, we carried out shift-up experiments, growing yeast cells until exponential phase in ethanol (condition in which Snf1/AMPK is highly phosphorylated) and adding glucose at the final concentration of 2% (inducing a rapid dephosphorylation of Snf1/AMPK). Snf1/AMPK phosphorylation rapidly decreased in the wild-type strain, becoming barely detectable 5 min after the addition of glucose (Figure 7A). The same behaviour was observed in the CDC25^{T1490P} mutant, known to prevent F1,6BP-dependent activation of Ras [5] (Figure 7A). To further dissect the involvement of the Ras/PKA pathway, we decided to test the effect of the lack of the Ras2 protein on Snf1/AMPK dephosphorylation. We carried out a shift-up experiment in a *ras2Δ* strain and, as in the CDC25^{T1490P} strain (Figure 7A), we observed the complete dephosphorylation of Snf1/AMPK after 5 min from the shift-up (Figure 7B). This ruled out the possibility that Snf1/AMPK could indirectly perceive the availability of glucose through F1,6BP stimulation of the Ras/PKA pathway.

As reported previously, Ras/PKA activity is pivotal for glucose induction of PP1 and PP2A phosphatases [85]. Glucose-dependent Snf1/AMPK dephosphorylation in the *ras2Δ* strain shown in Figure 7B could either depend on residual Ras activity due to the presence of Ras1, still able to activate the PKA pathway [190], or be completely independent from the PKA-dependent phosphatase activation.

To discern between these two possibilities, we carried out shift-up experiments in the *tpk1Δtpk2Δtpk3Δyak1Δ* strain, which completely lacks PKA activity. We confirmed that no defect in Snf1/AMPK dephosphorylation was observed also in this background (Figure 7C), thus excluding any involvement of PKA activity in Snf1/AMPK inactivation upon glucose replenishment.
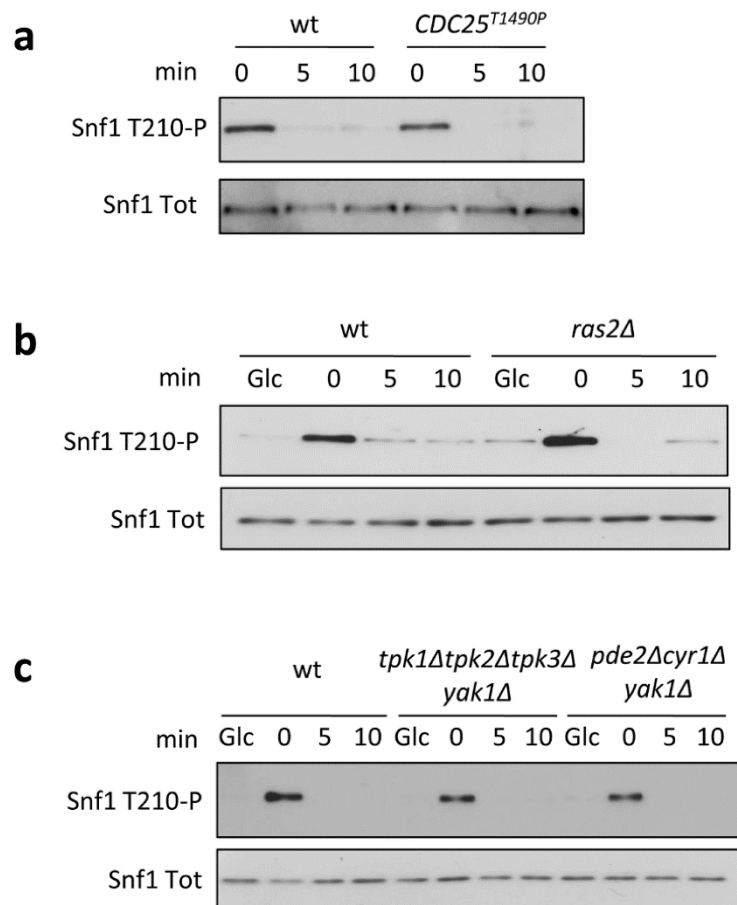
Figure 7. Snf1-T210 phosphorylation is independent from the Ras/PKA pathway. (A–C) Shift-up experiments in (A) wild-type and CDC25T1490P strains, (B) ras2Δ strain, and (C) strains lacking PKA activity (*tpk1Δtpk2Δtpk3Δyak1Δ* and *pde1Δcyr1Δyak1Δ*). One representative Western blot analysis using anti-pAMPK antibody (to detect Snf1-T210 phosphorylation) and anti-His antibody (to detect total Snf1) is shown.

Along with the glycolytic flux, PKA perceives extracellular glucose availability through the Gpr1/Gpa2 system, integrating nutritional signals and modulating cell fate via cAMP synthesis and PKA activation [32]. Hence, we cannot exclude that PKA activation triggered by extracellular glucose could influence the Snf1/AMPK phosphorylation state.

To rule this out, we performed a shift-up experiment in the *pde1Δcyr1Δyak1Δ* strain, in which *CYR1* deletion prevents both intracellular and extracellular stimulation of PKA activity. Remarkably, as in the control strain, Snf1/AMPK was completely dephosphorylated after the shift-up (Figure 7C), supporting a model by which its phosphorylation state is controlled by glucose independently from the Ras/PKA pathway; both in terms of intracellular and extracellular perception of glucose.

Snf1/AMPK Phosphorylation Is Correlated with Glucose Transport Rate

Snf1/AMPK phosphorylation has always been correlated with glucose availability. A high glucose concentration is associated with low phosphorylation of Snf1/AMPK, while high phosphorylation of Snf1/AMPK is a feature of cells grown in low glucose concentrations (lower than 0.05%) [191]. Moreover, different glucose concentrations are associated with alternative metabolic states of yeast cells. High glucose concentration supports fermentation, while a low one induces a respiratory metabolism. Recently, yeast metabolism has been correlated with sugar transport rate, which is associated with fermentation in a high glucose flux and mitochondrial respiration in a low one [66]. Considering this change of paradigm from glucose concentration to its flux rate, we also asked whether Snf1/AMPK phosphorylation state could be controlled by glucose transport rate rather than glucose concentration in the medium.

To address this issue, we used yeast strains expressing only one type of hexose transporter under the control of a constitutive promoter. The high-capacity low-affinity Hxt1, the high-affinity low-capacity Hxt7, or the chimeric transporter Tm6* (composed of the N-terminal of Hxt1 and the C-terminal of Hxt7) have been expressed in three independent yeast strains [192].
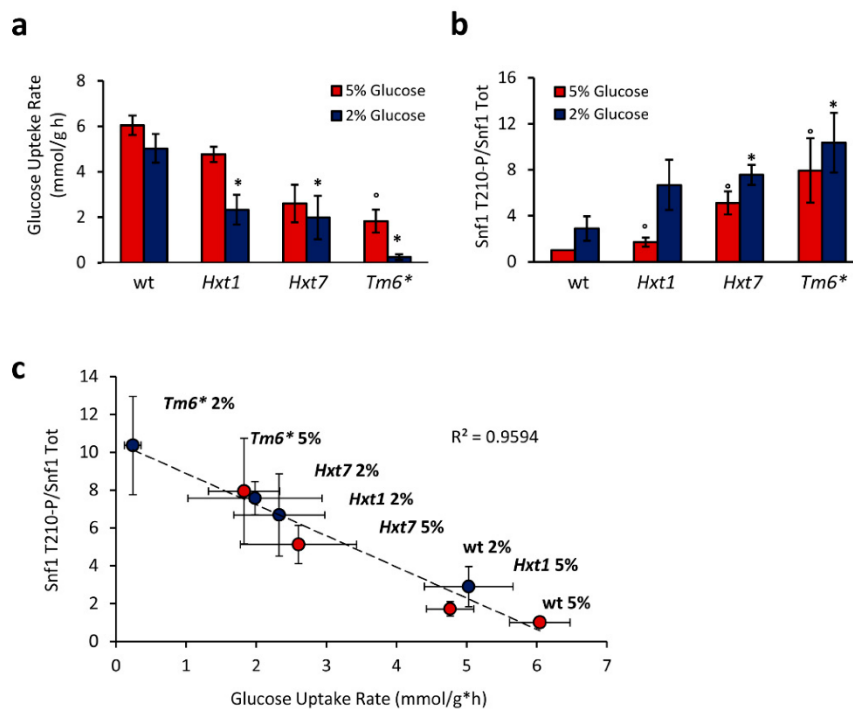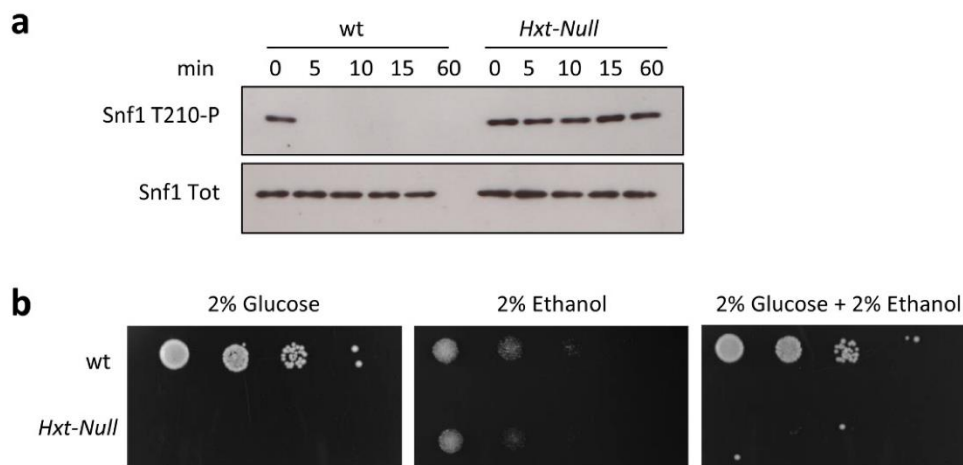

Figure 8. Snf1-T210 phosphorylation correlates with glucose transport rate. (a) Glucose uptake rate and (b) Snf1-T210 phosphorylation level measured in 2% and 5% glucose media of yeast strains expressing only Hxt1, Hxt7, or the chimeric transporter Tm6*, under a constitutive, non-glucose-responsive promoter. Mean ± standard deviation is shown (n = 3 for each). * $p < 0.05$ relative to wt in 2% glucose; ° $p < 0.05$ relative to wt in 5% glucose (t-test). (c) Linear correlation between Snf1 phosphorylation and glucose uptake rate shown in (a, b).

As previously reported, these strains exhibited a reduction in glucose consumption rate, with the Tm6*-expressing strain showing the lowest transport rate in both 2% and 5% glucose-containing media [193] (Figure 8A).

Interestingly, these strains also presented altered phosphorylation of Snf1/AMPK. In fact, all the mutants showed an increased level of Snf1-T210 phosphorylation, in both 2% and 5% glucose media (conditions in which wild-type cells present a fermentative metabolism and a very low Snf1-T210 phosphorylation; Figure 8B). Hence, altering the expression of glucose transporters, we managed to uncouple glucose transport rate from glucose concentration in the medium, observing complete independence of Snf1/AMPK phosphorylation from glucose concentration (Figure 8B). On the contrary, we found an inverse correlation between Snf1/AMPK phosphorylation state and glucose consumption rate (Figure 8C), demonstrating that Snf1/AMPK activation state is not statically controlled by glucose availability, but dynamically regulated by transport flux.

To confirm that Snf1/AMPK activation depends on glucose transport, we carried out shift-up experiments using a strain deleted in all of the hexose transporters (Hxt-Null) and unable to grow on glucose due to its inability to import glucose from the medium [194]. The addition of glucose to ethanol-grown cells induced rapid and almost complete dephosphorylation of Snf1/AMPK in the wild-type strain (Figure 9A). Conversely, in the Hxt-Null mutant, Snf1/AMPK phosphorylation remained high after the addition of glucose without any significant decrease until 60 min (Figure 9A), demonstrating that if glucose import is prevented, Snf1/AMPK dephosphorylation is completely impaired. The fact that glucose does not affect Snf1/AMPK phosphorylation in the Hxt-Null strain (Figure 9A) implies

Figure 9. Snf1-T210 dephosphorylation requires glucose transport. (a, b) Shift-up experiments in wild-type and Hxt-Null strains. Cells were harvested after 0, 5, 10, 15, and 60 min of glucose supplementation; anti-pAMPK antibody (to detect Snf1-T210 phosphorylation) and anti-His antibody (to detect total Snf1/AMPK) were used; one representative immunoblot is shown. (b) Wild-type and Hxt-Null strains were equalized, spotted at 10-fold serial dilutions, and grown on synthetic complete plates containing 2% glucose, 2% ethanol, or 2% glucose and 2% ethanol as carbon sources.

that the perception of extracellular glucose is not involved in the regulation of Snf1/AMPK activity. This is also consistent

with the unaffected dephosphorylation of Snf1/AMPK in the *pde1Δcyr1Δyak1Δ* strain (Figure 7C), where the sensing of extracellular glucose no longer impinges on the Ras/PKA pathway [91].

Once active, Snf1/AMPK is known to alter the transcription and the activity of metabolic genes and enzymes counteracting glucose catabolite repression [53]. In agreement with a previous report, and despite the high level of phosphorylation of Snf1/AMPK, the Hxt-Null strain was unable to grow when glucose and ethanol were mixed as carbon sources (Figure 9B) [193] Furthermore, our attempt to isolate Hxt-Null mutants able to consume ethanol in the presence of glucose failed. These indicate that glucose catabolite repression predominates over the consumption of alternative

carbon sources to glucose, even when the Snf1/AMPK regulatory mechanism is impaired.

G6P and Not F1,6BP Influences Snf1/AMPK Phosphorylation

The dependency of Snf1/AMPK phosphorylation on glucose transport rate (Figure 8) is consistent with the existence of a flux-sensing mechanism that coordinates cell signalling with glycolytic rate. F1,6BP concentration has been proposed to be the core of this mechanism, being proportional to the glycolytic flux [187]. In addition, in mammalian cells, F1,6BP controls the stability of the AXIN/LKB1/AMPK complex, thus regulating AMPK-T172 phosphorylation [6]. As shown above, we excluded any indirect effect of F1,6BP on the Snf1/AMPK phosphorylation state mediated by the Ras/PKA pathway (Figure 7). Because of this, we wondered whether F1,6BP may affect the Snf1/AMPK activation state through other mechanisms.

To address this issue, we carried out shift-up experiments in a yeast strain in which both genes encoding for phosphofructokinase (*PFK1* and *PFK2*) were deleted to prevent the synthesis of F1,6BP from glucose [65] (Figure 10A).

Surprisingly, the *pfk1Δpfk2Δ* strain presented rapid and almost complete dephosphorylation of Snf1/AMPK upon the addition of glucose, as did the control strain (Figure 10B).

Yeast strains of the CEN.PK background have been proven to carry a point mutation in the *CYR1* gene, known to influence yeast metabolism upon the deletion of glycolytic genes [195]. To completely exclude side effects due to this mutation, we also conducted shift-up experiments in the W303 and CEN.PK JT4 backgrounds, bearing the wild-type *CYR1* gene [195]. Remarkably, in both the backgrounds, we observed complete dephosphorylation of Snf1/AMPK without phosphofructokinase activity and
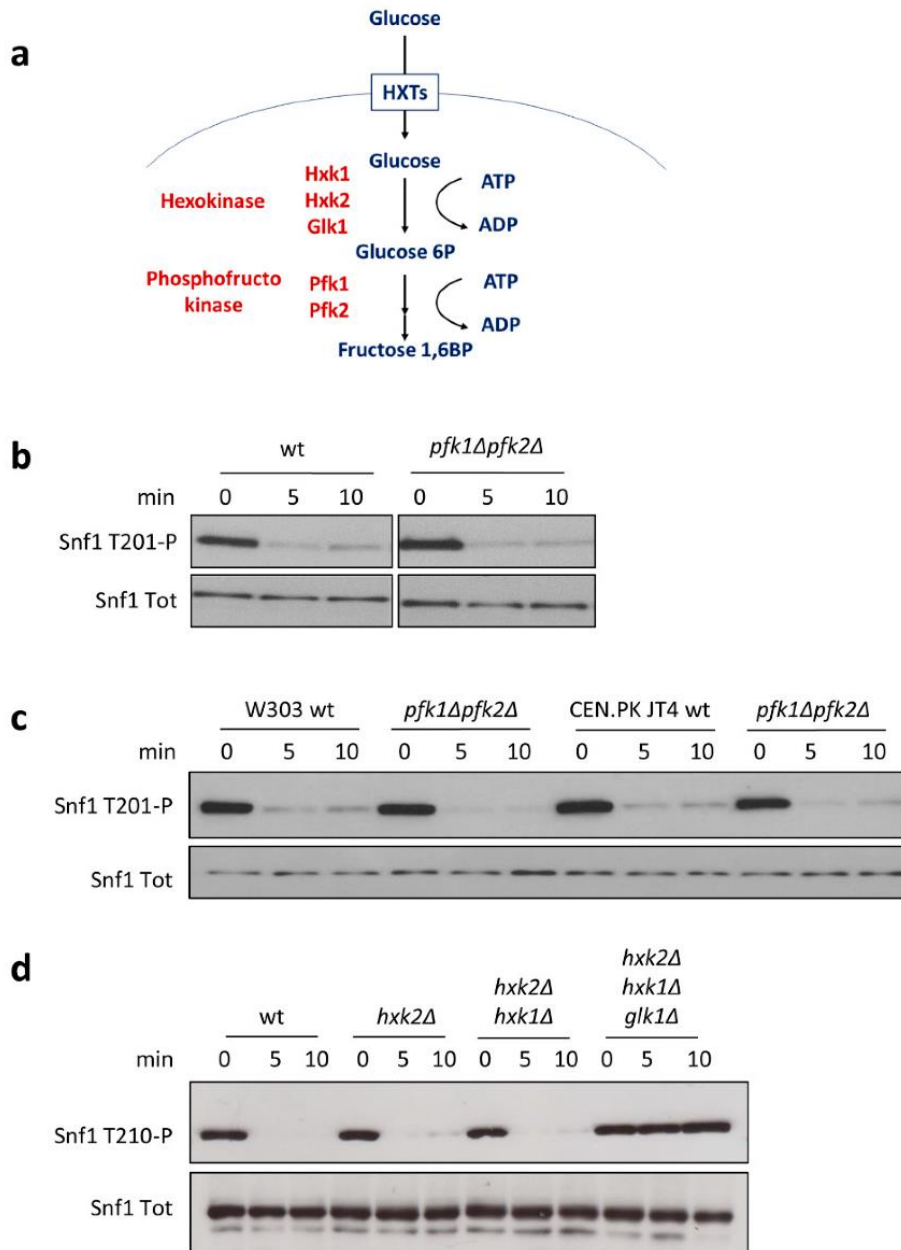
Figure 10. Snf1-T210 phosphorylation depends on G6P. (a) Schematic representation of the upper part of glycolysis in yeast. (b) Shift-up experiments in the *pfk1Δpfk2Δ* strain, with the two genes coding for phosphofructokinase deleted. (c) Shift-up experiments in *pfk1Δpfk2Δ* mutants in W303 and CEN.PK JT4 backgrounds. (d) Shift-up experiments in strains with one or more genes coding for hexokinases deleted. Anti-pAMPK antibody (to detect Snf1-T210 phosphorylation) and anti-His antibody (to detect total Snf1) were used. One representative immunoblot is shown.

upon the addition of glucose (Figure 10C), indicating that F1,6BP is not involved in the control of the activation state of Snf1/AMPK.

Thus, despite the inverse correlation between Snf1/AMPK phosphorylation and glucose uptake rate (Figure 8C), we failed to show a correlation between F1,6BP synthesis and Snf1/AMPK activation (Figure 10B, C).

Next, we investigated the role of hexokinases (Hxk1, Hxk2, and Glk1), given that glucose-6-phosphate (G6P) synthesis was already suggested to influence Snf1/AMPK phosphorylation state [51]. Among yeast hexokinases, Hxk2 represents the catalytically dominant form, which also has a regulatory function involved in the maintenance of glucose repression [196]. Nevertheless, Snf1/AMPK dephosphorylation in the *hkx2Δ* strain still responded to the addition of glucose, suggesting that Hxk2's regulatory function is not involved in the control of Snf1/AMPK activation (Figure 10D). Similarly to *hxk2Δ* cells, the double-deleted *hxk1Δhxk2Δ* strain also showed rapid dephosphorylation of Snf1/AMPK upon the addition of glucose (Figure 10D), while only the triple-mutant *hxk1Δhxk2Δglk1Δ*, completely lacking hexokinase activity, resulted in a loss of Snf1/AMPK dephosphorylation (Figure 10D).

Altogether, these data strongly indicate that G6P is the glycolytic intermediate that connects Snf1/AMPK phosphorylation with glucose metabolism.

Concluding remarks

AMPK is a master regulator of glucose and lipid metabolism and in higher eukaryotes it plays crucial roles in several diseases, such as cancer, obesity, diabetes and cancer [197]. Hypothalamic AMPK plays a critical role in whole-body energy homeostasis, mediating the effects of hormones and nutrients

on food intake, energy expenditure, and metabolism of peripheral organs [198–200]. Indeed, AMPK activity is regulated by several compounds other than glucose, such as α-lipoic acid, leptin, insulin, ghrelin, cytokines, as well as natural compounds such as resveratrol, curcumin, epigallocatechin 3-gallate, and many others [201–203]. Among these, α-lipoic acid—a cofactor of mitochondrial enzymes with antioxidant capacity—was shown to decrease AMPK activity in the hypothalamus, leading to anti-obesity effects in different organisms [204]. On the other hand, α-lipoic acid was shown to increase AMPK activation in β-cells and in the liver in eukaryotic systems [205].

Although AMPK modulation is much more complex in mammals, the use of model organisms to elucidate fundamental aspects of its regulation is a valuable tool to understand its activity in vivo. In particular, *Saccharomyces cerevisiae* biochemistry and genetics are extremely useful to study the crosstalk between different signalling pathways, as exemplified by this work. *S. cerevisiae* has evolved its metabolism to optimally consume glucose across a wide range of concentrations. This is achieved through a complex signalling network specialized in the sensing of glucose availability and in the dynamic adaptation of cellular metabolism [51]. The Ras/PKA pathway is strongly activated by glucose availability, and its function enhances cellular proliferation as well as glucose fermentation. PKA is also known to enhance the glycolytic flux, stimulating the pyruvate kinase Cdc19 and the 6-phosphofructo2-kinase (Pfk26) through phosphorylation, triggering a positive feedback loop in which glucose availability stimulates glycolysis and simultaneously inhibits gluconeogenesis (Figure 11) [55].

Meanwhile, a glucose concentration higher than 0.05% represses Snf1-T210

phosphorylation, preventing the expression of genes involved in mitochondrial respiration, oxidation of fatty acids, and the consumption of alternative carbon sources to glucose [80]. Of note, PKA is also known to positively regulate the activity of the phosphatase Reg1/Glc7, responsible for Snf1/AMPK inactivation (Figure 11) [85].

In the present work, we investigate the connection between Snf1/AMPK and Ras/PKA pathways during the onset of glucose catabolite repression (i.e., during a nutritional shift from ethanol to glucose). Our results clearly show that glucose induction of Snf1/AMPK dephosphorylation is completely independent of Ras/PKA activity, despite the dominant role of Ras/PKA in regulating yeast glucose metabolism (Figure 7).
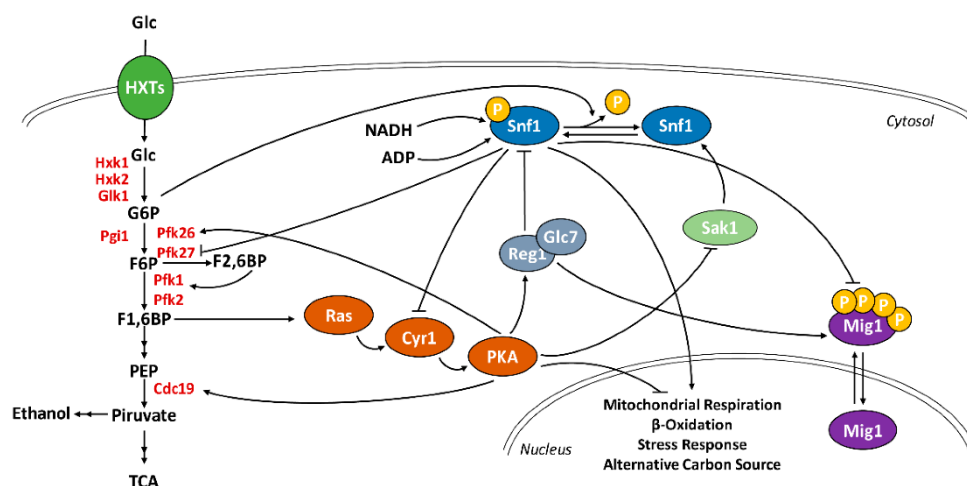
Figure 11. Schematic representation of the interactions between the glycolysis, Ras/PKA, and Snf1/AMPK pathways. F1,6BP synthesis influences Ras/PKA activity which, in turn, phosphorylates Pfk26 and Cdc19, stimulating the glycolytic flux. G6P promotes Snf1/AMPK dephosphorylation, thus inhibiting the kinase. NADH and ADP interact with Snf1/AMPK, giving rise to an interaction hub for the monitoring of cellular metabolism. Active PKA stimulates Reg1/Glc7 and reduces Sak1 activity, without influencing the Snf1/AMPK phosphorylation state, during a nutritional shift-up. In turn, phosphorylated Snf1/AMPK inhibits Cyr1 and Pfk27 activity and prevents Mig1 nuclear translocation. As a final result, PKA and Snf1/AMPK alternatively regulate the expression of genes involved in mitochondrial metabolism, stress response, and alternative carbon metabolism.

Signal transduction pathways are known to be organized with a bow-tie architecture in which several signals are independently perceived by different signalling molecules and converge on a limited number of downstream effectors [2].

Thus, the Ras/PKA and Snf1/AMPK pathways result to be independently and alternatively influenced by glycolysis during a nutritional shift-up, while their signals can integrate on downstream effectors (Figure 11). This concept is exemplified by the result shown in Figure 9; even if, Snf1/AMPK is highly phosphorylated in the Hxt-Null strain but, cells robustly persist in the preference of glucose as carbon source, suggesting that glucose fermentation still predominates over Snf1/AMPK stimulation of ethanol consumption.

Glucose control of Snf1-T210 phosphorylation has long been considered to be dependent on glucose concentration in the growth medium [191]. To maximize glucose consumption, yeast cells have evolved a signal transduction pathway controlling the expression of glucose transporters, in accordance with the availability of this nutrient. This regulation results in the matching of high glucose concentrations with the expression of the high-capacity transporters, whereas high-affinity transporters are expressed when the glucose concentration is low. Thus, in *S. cerevisiae* glucose uptake rate is inherently dependent on glucose availability [32].

Working with yeast strains constitutively expressing only one glucose transporter (either Hxt1, Hxt7, or Tm6*), we managed to decouple glucose transport rate from the availability of glucose. This allowed us to depict an inverse correlation between Snf1-T210 phosphorylation state and glucose transport rate, clearly showing that the activity of this kinase is dynamically regulated by glucose transport flux (Figure 8). Our results are also in

agreement with previously reported microfluidic experiments, which proved an altered nuclear localization of Mig1 in the Hxt1-only and Hxt7-only strains [40]. Mig1 is a transcriptional repressor preventing the expression of genes involved in alternative carbon metabolism. An active Snf1/AMPK massively phosphorylates Mig1, promoting its Msn5-mediated export from the nucleus [206]. Therefore, the altered Mig1 localization in strains with a modified glucose transport indicates that glucose uptake rate influences the entire Snf1/AMPK pathway, from the activation state of the kinase to its downstream key metabolic effectors.

As described in the Chapter 1, protein–metabolite interactions (PMIs) are molecular events pivotal for the coordination between cellular metabolism and signal transduction [188]. F1,6BP is one of the most influential metabolites, controlling Ras/PKA activation in yeast and mammals, and AMPK phosphorylation state in mammalian cells (Figure 2) [5,6]. Moreover, other phosphorylated sugars such as G6P, G1P, and T6P inhibit SnRK1 (the plant ortholog of AMPK) (Figure 2, Chapter 1) [7,15], suggesting that the role of sugar phosphates in the regulation of the AMPK kinases is evolutionary conserved.

In keeping with that, our data show that G6P regulates Snf1/AMPK phosphorylation. Mutant strains completely lacking glucose transporters or hexokinases are unresponsive to the addition of glucose (Figure 9A and Figure 10D). However, we cannot clearly state whether this interaction is direct or mediated, since we failed in measuring the interaction between G6P and the Snf1/AMPK complex through isothermal calorimetry analysis (Figure 12). The issues faced in the measurement of a putative interaction between Snf1/AMPK and G6P may depend on several factors. In the first place, the dissolution of phosphorylated sugars can release heat that

interfere with the ITC signal [207]. Secondly, the Snf1/AMPK protein complex used for the analysis could have presented two putative

A

B
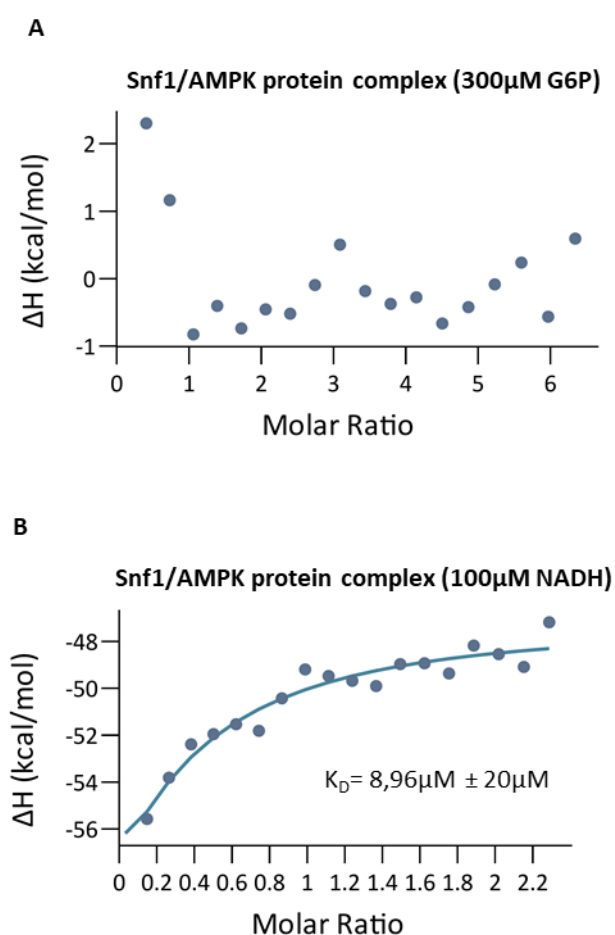
Figure 12. Titration curves for the interaction between Snf1/AMPK protein complex and (A) 300 μM G6P or (B) 100μM NADH. Isothermal calorimetry (ITC) assays have been performed loading a Snf1/AMPK protein complex (9 μM) purified from yeast cells shifted in low glucose condition. (A) Titration with 300μM G6P shows a negligible variation of enthalpy suggesting the absence of an interaction between Snf1/AMPK complex and G6P in these experimental conditions. (B) Titration with 100μM NADH was used as positive control. The experiment shows a variation of enthalpy compatible with a molecular interaction between Snf1/AMPK protein complex and NADH. Despite the wide interval of confidence, the dissociation constant (K_D) reported here agrees with the K_D measured in a competition binding assay, confirming the quality of our Snf1 purification [65].

configuration, one responsive and one refractive to the interaction, decreasing the sensitivity of the analysis [100].

Since Gal83 GBD was previously reported to be required for the glucose-dependent dephosphorylation of Snf1 [208], we further explored the possibility of a direct interaction by considering the carbohydrate-binding properties of the Snf1/AMPK β-subunits. We performed a docking analysis with several sugar phosphates on the isolated glycogen-binding domain (GBD) of Sip2 (from PDB ID: 2qlv) or Gal83 (modelled by homology, based on Sip2-GBD). Unfortunately, we failed to detect a binding pocket with a high affinity for G6P on the isolated GBD (data not shown).

Therefore, we considered the hypothesis that G6P act on GBD when bound on the active complex. The conformation of the active complex in yeast is not available, but several structures of the active mammalian AMPK were resolved where the carbon-binding motif (CBM) of the β-subunit was docked on the active kinase domain, generating a pocket that can bind to several activators [98,100]. We attempted the construction of a homology model for the yeast GBD in the same conformation, but it was evident that whereas the kinase pocket facing CBM is conserved from mammalian to yeast, neither the GBD from Sip2 nor from Gal83 share the characteristics of the mammalian homolog interface (Figure 13). This raises doubts about where the catalytic subunit localizes in the complete yeast structure and how its position affect those of the GBD and α-hook (Figure 13).

Figure 13. (A) Representation of yeast Snf1 (left; PDB ID:2qlv) and human AMPK (right; PDB ID: 4cfe) complexes. The surface of the proteins is shown with homologous subunits in the same colours. In the truncated crystal of Snf1 both the alpha-hook and the GBD (or CBM) are localized in completely different position compared to AMPK structure. Caption continues in the next page.

Figure 13. (B, C) Yeast β-subunits do not share the interface to AMPK kinase domain identified in mammalian homologs. Sequences of the indicated proteins were aligned with Clustal Omega. The blue boxes highlight the residues involved in the interface between the CBM of the β-subunit (A) and the AMPK kinase domain (B) in rat AMPK structure (PDB ID:4qfg).

The only other structure available in yeast was obtained with the truncated C-terminal portion of Snf1 and shows the Sip2-GBD docked on a completely different site, bound to Snf4 (Figure 13) [209]. This is not compatible with the position of the kinase domain in the active complex, as characterized for mammalian AMPK complexes.

Nevertheless, making use of this truncated structure we could identify three potential binding pockets for G6P (Figure 14A). All the pockets localized in proximity or in correspondence of the GBD, whose presence is pivotal for glucose induced dephosphorylation of Snf1/AMPK [210]. The physiological role for these pockets is supported by the observation that point mutations of residues in their proximity (and at the interface between the β and γ subunits) (Figure 14B) resulted in a higher phosphorylation of Snf1/AMPK in glucose grown cells [208,211]. Anyway, it is still unclear whether the conformation used for the docking (lacking the catalytic subunit) represents an alternative structure of Snf1 complex, possibly reflecting the inactive conformation of Snf1, and therefore if the identified binding pockets are physiological and actually play a role in the regulation of Snf1/AMPK activity. In order to further investigate the role of G6P in the dephosphorylation Snf1/AMPK, we also carried out in vitro dephosphorylation assays on Snf1/AMPK complex purified from yeast cells [88]. The addition of the commercial PP2Cα phosphatase induced a stronger dephosphorylation of Snf1-T210 when G6P was present in the reaction mix (Figure 14C). Importantly, we ruled out that 1mM or 0.5mM G6P could affect the activity

of PP2Cα in our experimental conditions (Figure 14D), while we observed an effect of G1P, F1,6BP and trehalose-6 phosphate when added at 0.5mM in the reaction mix (Figure 14D). This made difficult for us to check the effect of these sugars on the *in vitro* dephosphorylation of Snf1/AMPK and prevented us to rule out any involvement of G1P in the regulation of Snf1. Mammalian AMPK complex has been demonstrated present two different conformations with the regulatory threonine more exposed to the solvent in the inactive state [100]. This prompted us to think that the higher dephosphorylation rate of Snf1/AMPK in presence of G6P could be due to a conformational change of the complex resulting in a higher accessibility of T210 (Figure 14C). These observations combined with the *in vivo* data support a regulatory mechanism of Snf1/AMPK phosphorylation dependent on the availability/synthesis of G6P.

However, we failed in demonstrating a clear dose-effect response for Snf1/AMPK dephosphorylation in presence of 0.5 mM and 1 mM G6P (Figure 14C).

The simplest interpretation of the results shown in figure 14C is that our experimental setup (an *in vitro* dephosphorylation followed by a western blot) it is not sensible enough to state whether G6P directly influence Snf1-T210 accessibility to phosphatases. This and the lack of the demonstration of a direct interaction between Snf1 complex and G6P (Figure 12A) impede us from clearly stating the molecular mechanism connecting G6P synthesis and Snf1/AMPK dephosphorylation in yeast cells. On the contrary, it is clear that metabolites of the upper part of glycolysis actively influence the signalling pathways that regulate glucose metabolism in yeast, mammals, and plants (Figure 1 and Figure 2) [5–7,15]. In particular, this work highlights
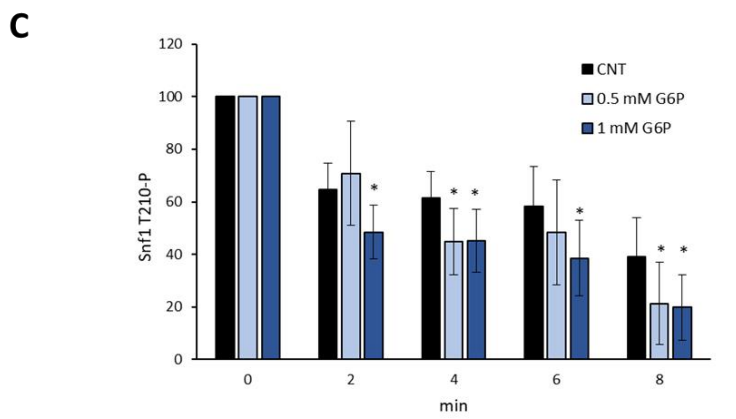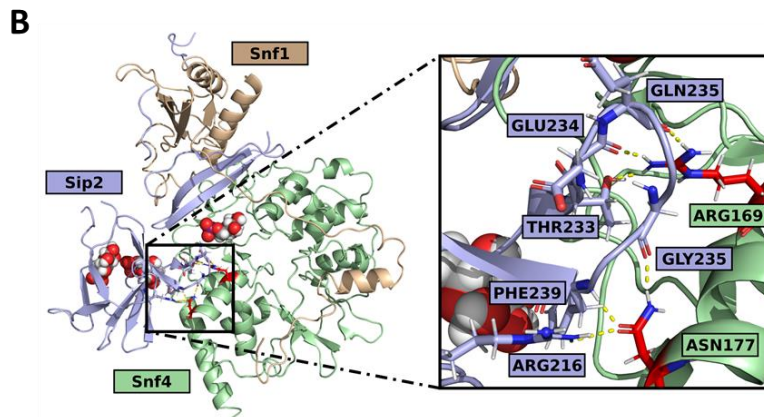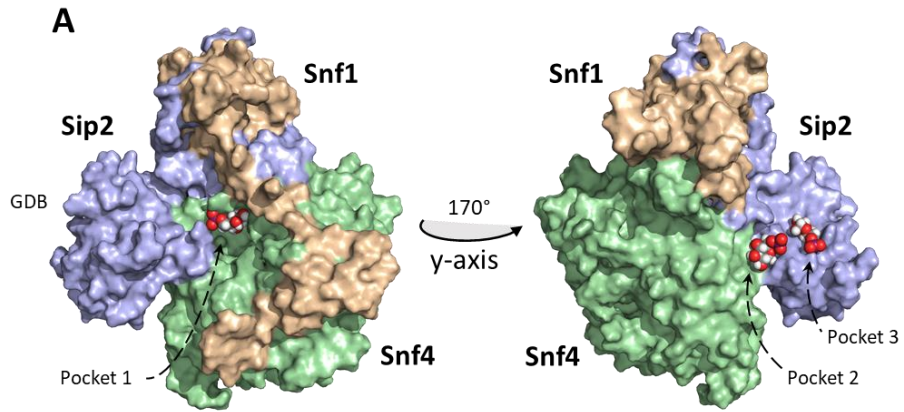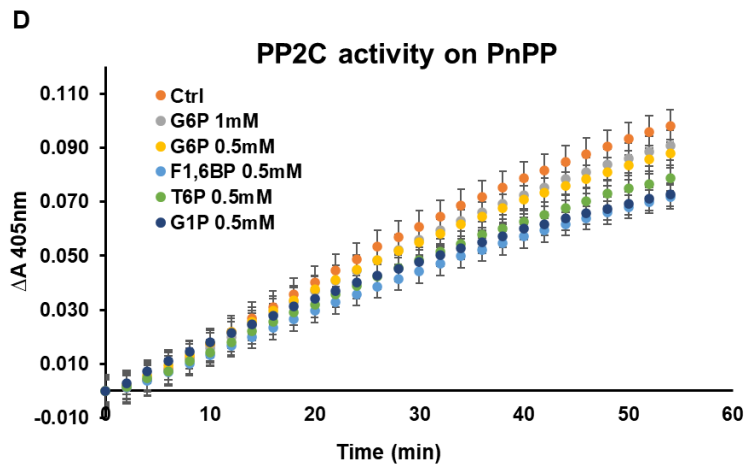
Figure 14. (A) G6P has been docked on the regulatory subunit of Snf1/AMPK complex (PDB ID: 2qlv). Snf1 is shown in yellow, Sip2 in blue and Snf4 in green. It is possible to identify three different binding pockets: one at the interface between Snf4 and the GBD of Sip2 and two only involving the GBD of Sip2. (B) Zoom in of the interface region between Snf4 and Sip2. Residues influencing Snf1-T210 phosphorylation (if mutated) are highlighted. (C) Dephosphorylation assay on Snf1/AMPK complex in presence of 0.5mM and 1mM G6P. Phosphorylation level were detected through western blot with anti-phosphorylated T210 after the assay. The phosphorylation level is normalized for each condition on the phosphorylation level before the onset of the reaction. *In vitro* assay of PP2C activity on para-nitrophenyl phosphate (PnPP) in presence of several phosphorylated sugars: glucose 6 phosphate (G6P), fructose 1,6 bisphosphate (F1,6BP), trehalose 6 phosphate (G6P) and glucose 1 phosphate (G1P).

that yeast Snf1/AMPK undergoes a similar regulation, with G6P being the molecule connecting the Snf1/AMPK phosphorylation state with glycolytic flux. indeed, this enables the monitoring of glucose metabolism and the coordination of fermentative and respiratory metabolism. In addition, through the interaction with ADP [88] (Figure 11), Snf1/AMPK senses the energetic status of the cell and regulates catabolic and anabolic processes to achieve energy homeostasis.

In conclusion, our observations, alongside previously reported interactions, underline the role of Snf1/AMPK as a central hub for the tuning of cellular metabolism through protein–metabolite interactions [188].

Chapter 3

Saccharomyces cerevisiae as model organism for the study of aging and neurodegeneration

From: Tripodi et al., Aging 2020

Saccharomyces cerevisiae as model organism for the study of aging and neurodegeneration

Introduction

Nutrients and their metabolites control energy balance, enzymatic activities and genome stability throughout the lifecycle. It is an unequivocal statement that nutritional deficiency as well as excess contribute to the aging process. Dietary restriction is known as the most effective longevity intervention ranging from yeast to primates [212–216]. Several results have suggested new roles of key nutrients in the protection against aging and age-related disorders [216,217]. Thus, there is an increasing interest in nutrition as a way both to prevent diseases and to reach healthy aging.

Much of the current knowledge on the molecular mechanisms of aging comes from lifespan studies on short-lived model organisms, such as the budding yeast *Saccharomyces cerevisiae*, *Drosophila melanogaster* and *Caenorhabditis elegans* [218]. Specifically, AMPK (AMP-activated protein kinase), IGF (insulin-like growth factor) and TORC1 (target of rapamycin kinase complex 1) signalling pathways play key functions in regulating aging [219–221].

Neurodegenerative diseases, characterized by aberrant aggregates of the presynaptic protein α-synuclein, are collectively referred to as synucleinopathies, the second most common group of neurodegenerative diseases [222–224]. One of the most common synucleinopathies is Parkinson's disease (PD) and autosomal dominant forms of PD have been linked to mutations in α-synuclein. In PD patients, neurodegeneration is found predominantly in dopaminergic neurons. Despite the advances in the study of these pathologies, the detailed molecular mechanism of neuronal

degeneration is still largely unknown. Several studies underline the relevant role of cellular models for a better understanding of the molecular regulation of human pathologies [225]. As such, budding yeast has been extensively employed in models of synucleinopathies [226–229]. In addition, an age-related degeneration of dopaminergic neurons has been shown in wild-type *C. elegans* [230]. Interestingly, neuronal and dendritic loss are accelerated and more severe when human α-synuclein is expressed in dopaminergic neurons in *C. elegans* [231].

Vigna unguiculata (L.) Walp. or cowpea is the most relevant Vigna species for human food. It is cultivated in tropical and subtropical zones of the world, including Africa, Asia, Latin America and also in some Mediterranean countries [232]. Cowpea seeds are a good source of proteins, which mainly consist of globulins (vicilins or 7S globulins) and, to a lesser extent, albumins, glutelins and prolamins [233]. From a nutritional point of view, there is a high ratio of essential-to-non-essential amino acids, which is over 50%, suggesting the potential capacity of cowpea to cover human nutritional requirements [234,235]. Moreover, bioactive peptides with antioxidant activity are successfully obtained from enzymatic proteolysis of cowpea proteins, indicating also its potentiality as a functional food [233]. In comparison with other legumes, cowpea has a low-fat content with high level of unsaturated fatty acids and is also characterized by a high proportion of carbohydrates (mainly dietary fibres and resistant starch) [233]. Apart from the relevant source of essential macronutrients, cowpea also constitutes an interesting source of micronutrients [236].

All these features, together with the presence of minerals (calcium, iron and zinc) and phytochemicals, such as phenolic compounds, are attracting the

attention of consumers and researchers, also because of its beneficial properties for health, including anti-diabetic, anti-cancer, anti-hyperlipidemic, anti-inflammatory and anti-hypertensive properties [237]. The aim of the present work is to investigate whether *V. unguiculata* also has anti-aging and neuroprotective effects, exploiting different model organisms to address complementary aspects. We show that an aqueous extract from *V. unguiculata* beans increases lifespan in yeast cells, being dependent on Snf1/AMPK (sucrose-non-fermenting/AMP-activated protein kinase) and Ras/PKA (Rat sarcoma/protein kinase A) pathways. Its pro-longevity feature is also confirmed on the multicellular organism *D. melanogaster*, which is consistent with the increased expression of AMPK-dependent genes associated with fly lifespan extension. Cowpea extract is able to significantly reduce the aggregation of α-synuclein in vitro and to attenuate its toxicity both in yeast and neuroblastoma cells. Remarkably, in a nematode model expressing human α-synuclein, the age-dependent degeneration of the dopaminergic neurons is strongly reduced under chronic treatments with *V. unguiculata* extract.

Vigna unguiculata extract extends lifespan in yeast cells

Considering the nutritional properties and positive effects for health of *Vigna unguiculata* [237], we investigated the composition of aqueous bean extracts from *V. unguiculata* in comparison with those obtained from *Cajanus cajan L.* and *Phaseolus vulgaris L.*, originating from the Arusha area in Tanzania. *V. unguiculata* extract was characterized by a higher starch
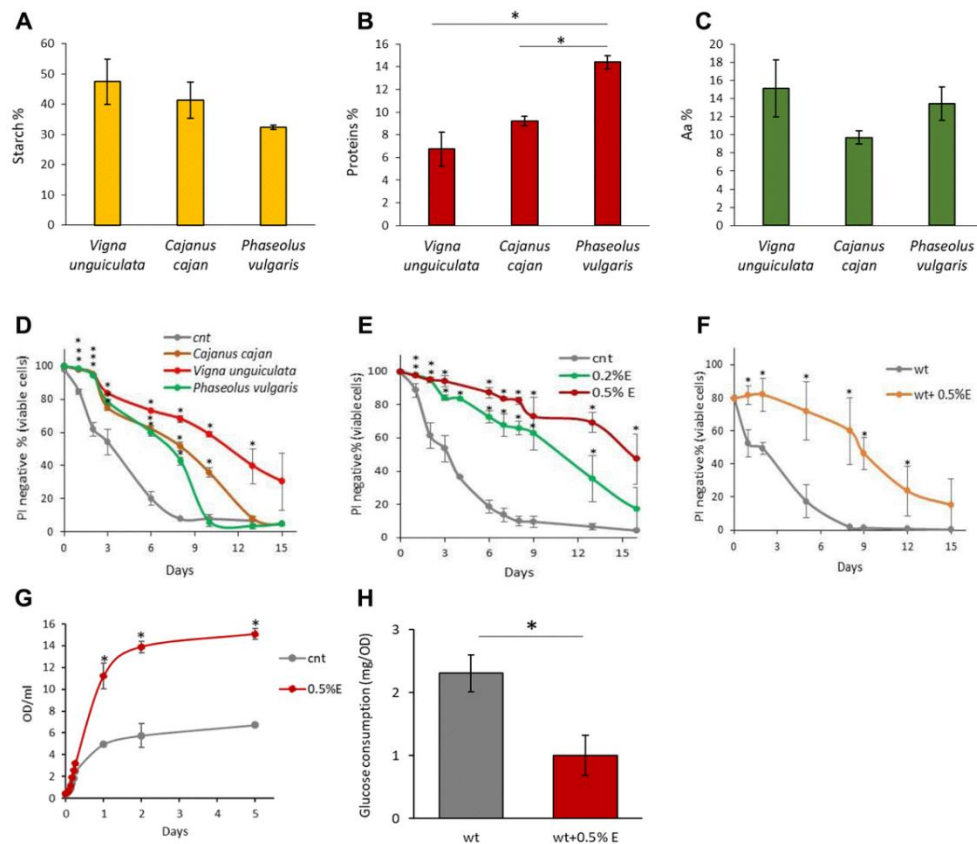
Figure 15. Chemical properties of bean extracts. (A) Starch content, (B) protein content and (C) amino acid content in *V. unguiculata*, *C. cajan* and *P. vulgaris* extracts. *p<0.05. (D) CLS of yeast cells grown in the absence or presence of 0.2% *V. unguiculata, C. cajan and P. vulgaris* extracts. *p<0.05 relative to control cells. (E) CLS of yeast cells grown in SD medium containing 2% glucose in the absence or presence of 0.2% or 0.5*% V. unguiculata* extract, added in exponential phase of growth. *p<0.05 relative to control cells. (F) CLS of yeast cells grown in SD medium containing 2% glucose in the absence or presence of 0.5% *V. unguiculata* extract, added to cells in stationary phase (and not in exponential phase, as in the other experiments). *p<0.05 relative to control cells. (G) Growth curves of yeast cells grown in SD medium containing 2% glucose in the absence or presence of 0.5% extract *V. unguiculata*. *p<0.05 relative to control cells. (H) Glucose consumption (mg/OD) of yeast cells grown in SD medium in the absence or presence of 0.5% *V. unguiculata* extract, measured on growth media sampled at multiple time points during exponential phase of growth (0.2-2.5 OD/ml). *p<0.05 relative to control cells.

	Phaseolus vulgaris	*Cajanus cajan*	*Vigna unguiculata*
aa and bases			
glycine	1.00	1.07	2.66
L-leucine	1.00	0.49	2.90
L-threonine	1.00	0.00	10.74
L-alanine	1.00	0.80	2.72
L-proline	1.00	34.35	3.94
L-asparagine	1.00	0.63	52.44
L-aspartic acid	1.00	1.55	1.05
hypoxanthine	absent	absent	present
D-pyroglutamic acid	1.00	3.93	3.17
methylthiouracil	1.00	1.11	2.40
glycolysis/fermentation and TCA			
citric acid	1.00	1.90	2.25
malic acid	1.00	0.11	0.17
lactic acid	1.00	0.98	4.60
fatty acids			
glycerol	1.00	0.71	3.28
linolealidic acid	1.00	5.33	8.41
linolenic acid	1.000	0.162	2.663
stearic acid	1.000	0.968	1.342
palmitic acid	1.000	0.779	1.209
other organic acids			
D-pipecolic acid	1.00	0.78	absent
2-pentenedioic acid	1.00	1.34	1.14
2-thiobarbituric acid	1.00	0.66	0.29
L-dihydroorotic acid	1.00	0.62	0.84
glycolic acid	1.00	1.13	1.01
D-pipecoli acid	1.00	0.69	0.00
hydracrylic acid	1.00	6.98	1.05
butenoic acid	1.00	2.46	9.71
2-pyrrolidinone-5-carboxylic acid	1.00	1.18	0.43
others			
methyl-amino acetate	1.000	0.013	0.218
acetamide	1.000	0.577	18.533
triazol-3-amine	1.000	0.910	2.026
maltol	1.000	1.291	1.125
2-mercaptophenol	1.000	1.108	1.276
urea	1.000	very low	3.444

Table 1. Metabolite content in extracts *of P. vulgaris, C. cajan* and *V. unguiculata*, analysed by GC/MS. Relative amounts of each metabolite are referred to *Phaseolus vulgaris* content, which was set to 1

amount and less proteins compared to the extracts obtained from the other pulses, while the percentage of total amino acids was comparable among species (Figure 15A–C). We also confirmed that cowpea seeds are a good source of amino acids (included the essential ones), as well as of unsaturated fatty acids (more abundant in comparison with the other two beans),

confirming its nutritionally desirable features (Tables 1, 2) [233]. To explore if these differences could have an impact on the longevity of yeast cells, exponentially growing cells were treated with 0.2% of the extracts from *V. unguiculata*, *C. cajan* or *P. vulgaris* beans and chronological lifespan was monitored by measuring the viability of the cultures throughout time.

Analytes	Target ion (m/z)
glycine	246
L-leucine	200
L-threonine	404
L-alanine	232
L-proline	184
L-asparagine	417
L-aspartic acid	418
hypoxanthine	307
D-pyroglutamic acid	300
methylthiouracil	313
Citric acid	459
Malic acid	419
DL-glyceraldehyde	115
Lactic acid	261
glycerol	377
Linolealidic acid	337
Linolenic acid	335
Stearic acid	341
Palmitic acid	313
D-pipecolic acid	186
2-pentendioic acid	315
2-thiobarbituric acid	429
L-dihydroorotic acid	443
Glycoli acid	247
2-pipecoli acid	186
Hydroacrylic acid	261
Butenoic acid	289
2-butenoic acid	273
2-pyrrolidinone-5-carboxylic acid	186
Methyl-amino-acetate	146
acetamide	116
Triazol-3-amine	213
maltol	183
2-mercaptophenol	297
urea	231

Table 2. Identified analytes by GC/MS and target ion used to measure the peak area.

| lifespan (days)		
wt strain	mean	maximal
cnt (no extract)	3.05 ± 0.42	9.46 ± 1.47
0.2% *P. vulgaris*	6.42 ± 0.12	11.72 ± 0.05
0.2% *C. cajan*	7.74 ± 0.30	13.53 ± 0.32
0.2% *V. unguiculata*	9.55 ± 0.49	18.55 ± 0.64
0.5% *V. unguiculata*	16.03 ± 3.01	>20

Table 3. Mean and maximal lifespan of wt cells grown in the presence of the indicated extracts.

All the extracts increased longevity of yeast cells, with the highest response given by the presence of *V. unguiculata* one, with a mean lifespan increasing from 3 days to about 9.5 days (Figure 15D, Table 1). Considering these results, we decided to continue our analysis by using only the cowpea extract.

A strong dose-response effect on yeast longevity was observed by increasing the concentration of *V. unguiculata* extract in the culture (from 0.2% to 0.5%), since it was able to extend the mean lifespan up to 16 days at the higher concentration (Figure 15E, Table 3).

This anti-aging properties were evident also when the extract was added to "aged" cells, i.e., after they had already entered the stationary phase (Figure 15F). Remarkably, cowpea extract not originating from Arusha maintained the same effect, letting us to suppose that the origin of the beans has no relevant impact on its anti-aging features (data not shown).

Cell growth was then monitored in the presence of the highest concentration of the extract. Although the growth rate in the presence of 0.5% extract showed only a minor increase in exponential phase, the final biomass of the population was more than doubled in comparison with the
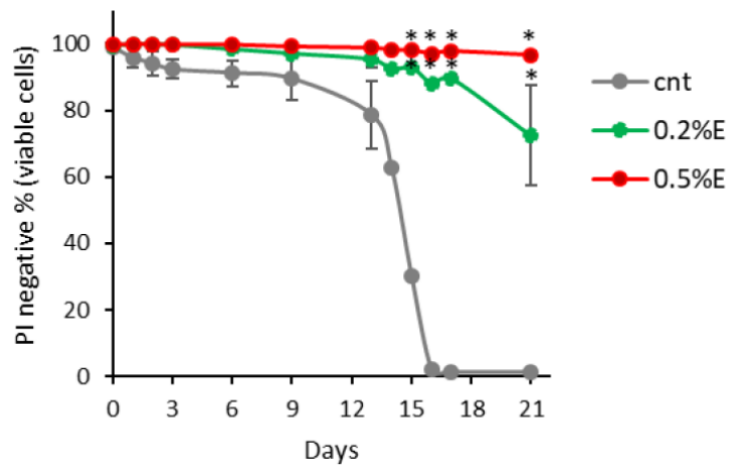
Figure 16. CLS of yeast wt cells grown in SD medium containing 0.5% glucose in the absence or presence of 0.2% or 0.5% extract of *Vigna unguiculata*. *p<0.05 relative to control cells.

control (Figure 15G). On the other hand, the consumption of glucose in the media during the exponential phase of growth was strongly reduced (more than 50%), suggesting that the presence of either starch or proteins induced a decrease of glucose uptake from the medium (Figure 15H). However, the lower glucose consumption in the presence of the extract has no effect on the experimental determination of CLS, which starts after carbon source exhaustion.

Importantly, the anti-aging effect of the extract was synergistic with caloric restriction, one of the most effective non-genetic interventions known to promote lifespan extension in several model organisms (Figure 16) [220]. Overall, the data presented indicate that cowpea aqueous extract extends chronological aging in yeast cells.
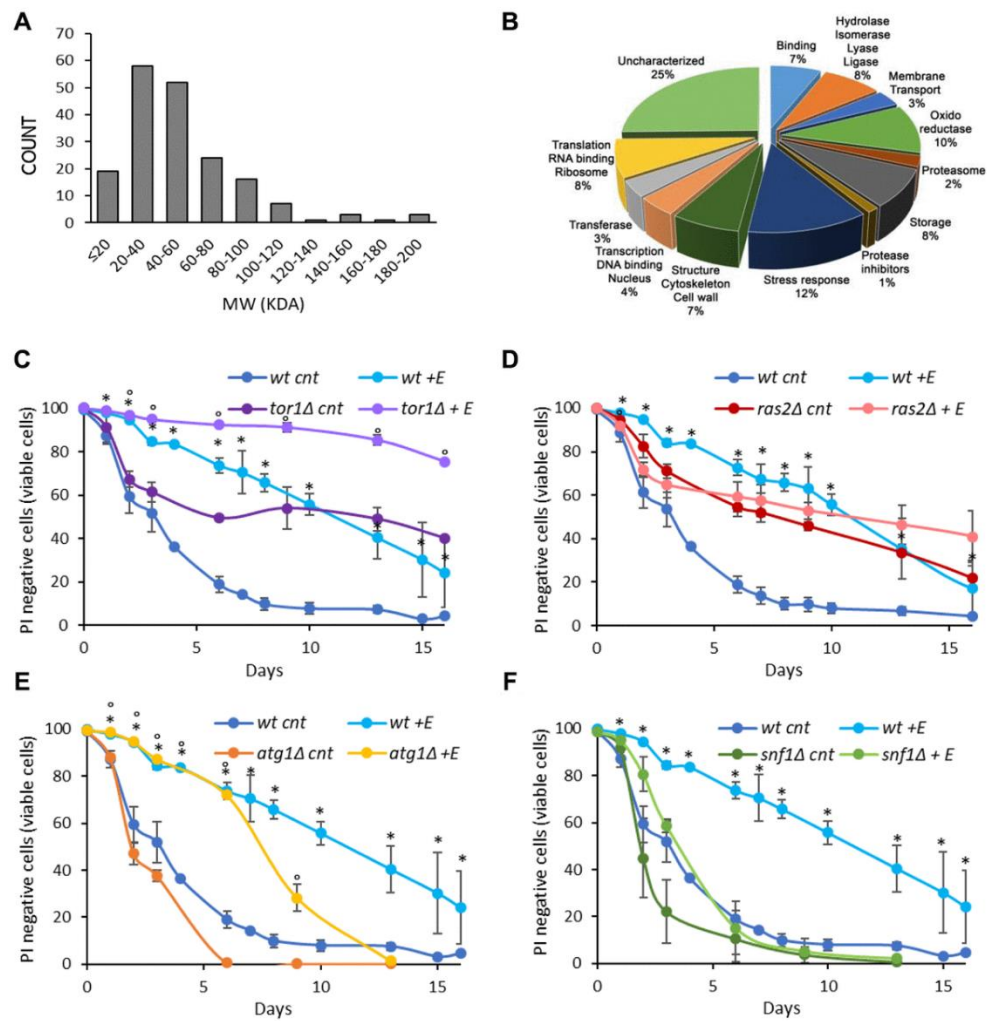
Figure 17. Cowpea extract extends yeast lifespan. (A, B) Analysis of V. unguiculata extract by mass spectrometry using a shotgun proteomic approach to identify all the proteins present in the sample. (A) MW distribution and (B) classification of the proteins identified. The data have been deposited to the ProteomeXchange Consortium via the PRIDE partner repository with the dataset identifier PXD017716. (C–F) CLS of wt and (C) tor1Δ, (D) ras2Δ, (E) atg1Δ, (F) snf1Δ cells, grown in SD medium containing 2% glucose in the absence or presence of 0.2% V. unguiculata extract. *p<0.05 relative to untreated wt cells, °p<0.05 relative to untreated mutant cells. Curves of wt untreated cells and treated with the extract were repeated in C–F.

	lifespan (days)			
	mean		maximal	
strain	cnt	0.2% E	cnt	0.2% E
wt	3.05 ± 0.42	9.55 ± 0.49	9.46 ± 1.47	18.55 ± 0.64
ras2Δ	7.48 ± 0.40	10.48 ± 4.98	18.95 ± 1.34	>20
tor1Δ	5.87 ± 0.23	>20	18.5 ± 0.14	>20
atg1Δ	2.22 ± 0.10	7.35 ± 0.21	4.95 ± 0.21	11.45 ± 0.78
snf1Δ	2.0 ± 0.42	3.35 ± 0.21	4.8 ± 2.40	7.2 ± 1.56

Table 4. Mean and maximal lifespan of mutant strains grown in the presence of 0.2% **V. unguiculata** extract. Data of wt cells were repeated for clarity.

To increase our knowledge on the composition of *V. unguiculata* extract we performed a proteomic analysis. We identified 174 proteins with a molecular weight ranging from 200 to less than 20 kDa, of which 10% are oxidoreductase, 12% are stress response proteins while 25% are still uncharacterized (Figure 17A, 17B).

The signalling pathways connected to longevity regulation are well known in yeast. Among them, the Snf1/AMPK (sucrose-non fermenting/AMP-activated protein kinase) and the autophagic pathways are anti-aging pathways, while the Ras2/PKA (Rat sarcoma/protein kinase A) and the TORC1 (target of rapamycin complex 1) pathways are pro-aging ones [80,218,219]. To identify through which of them the cowpea extracts extended yeast chronological lifespan, we tested its effect on mutants bearing deletion in one of the aforementioned pathways (*snf1Δ, atg1Δ, ras2Δ, tor1Δ*) (Figure 17C–F, Table 4). The anti-aging effect of 0.2% cowpea extract was still evident in *tor1Δ* and *atg1Δ* strains (Figure 17C, 17E, Table 4), while it was strongly reduced in *ras2Δ* and *snf1Δ* mutants (Figure 17D, 17F, Table 4), indicating that the Ras/PKA and the Snf1/AMPK pathways are involved in mediating the anti-aging effect of cowpea extract in yeast cells.
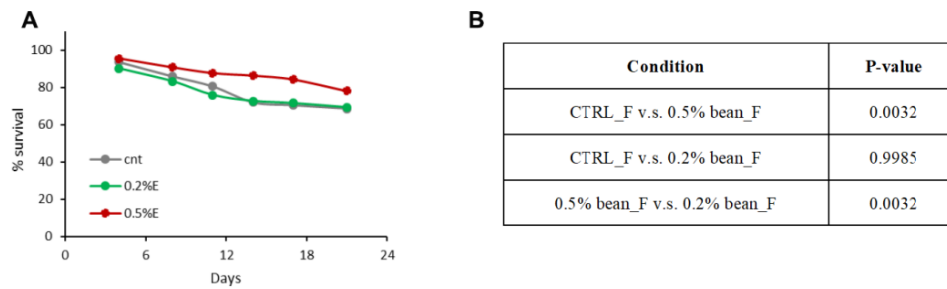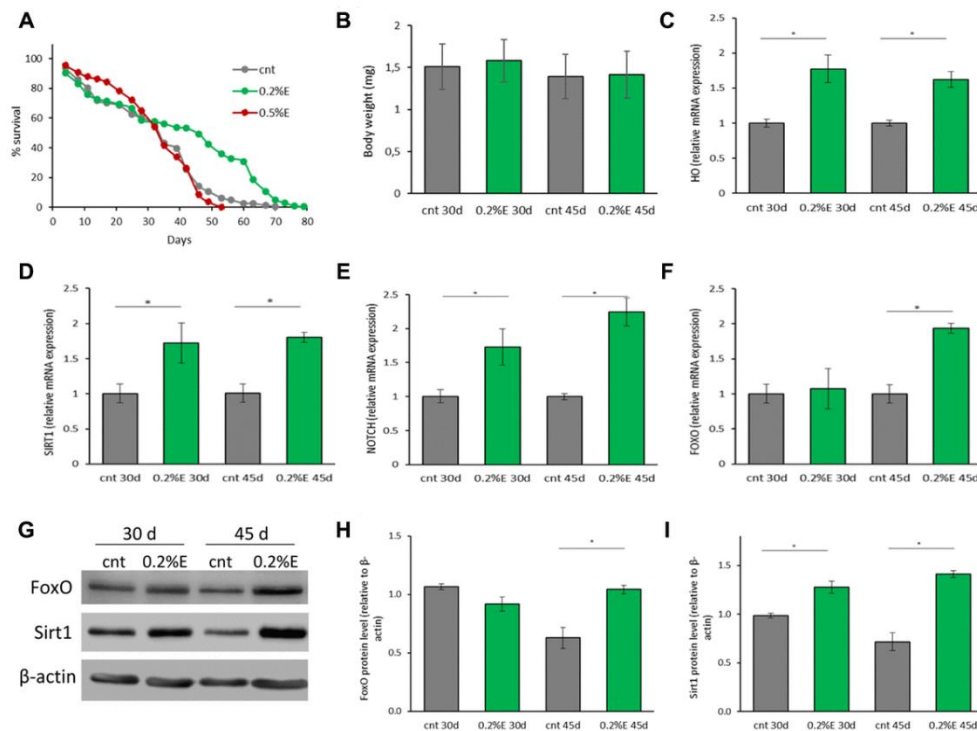
Figure 18. Survivorship of adult female *D. melanogaster*. (A) Flies have been supplemented with 0.2 and 0.5% cowpea extract lifelong. Data are presented as percentage survival of flies as function of time (in days). (B) Analysis of the survivorship data with log-rank test using the online application for the survival analysis of life-span assays OASIS.

Vigna unguiculata extract supplementation extends lifespan in *Drosophila melanogaster*

To investigate the pro-longevity effect of the cowpea extract also in a multicellular organism, female Canton S flies were lifelong supplemented with 0.2% or 0.5% *V. unguiculata* extract. A significant marked increase in mean lifespan was observed in flies supplemented with 0.2% bean extract in respect to controls (40.09±1.08 days vs 31.82±0.86 days; 25.99% increase), while mean lifespan of flies supplemented with 0.5% bean extract was comparable to that of control flies (Figure 18A). These data are only partially in agreement with the results obtained in yeast cells, where the 0.5% cowpea supplementation was more effective than the 0.2% one. Nevertheless, considering only the survivorship data obtained after a 3 weeks supplementation, a higher survival of flies supplemented with 0.5% in respect to both 0.2% supplement and control was observed (Figure 19A, B).

To verify whether the increase of the mean lifespan in the presence of 0.2% extract was due to bean extract supplementation itself and not to CR

induced by bean extract off-flavour, the body weights of flies were recorded at 30 and 45 days. No differences in fly body weights were observed, suggesting an equal food uptake in control and supplemented groups (Figure 18B). To gain molecular insights for the positive effect of 0.2% cowpea extract supplementation on *D. melanogaster* lifespan, the expression of genes involved in preserving cellular homeostasis and longevity was investigated. Flies were supplemented with cowpea extract for 30 or 45 days and the expression of genes involved in aging-related signalling pathways

Figure 19. Cowpea extract extends *D. melanogaster* lifespan. (A) Survivorship of adult female *D. melanogaster*. Flies were supplemented with 0.2% and 0.5% bean extract lifelong. (B) Body weights of *D. melanogaster* supplemented with 0.2% bean extract. Flies were supplemented with 0.2% bean extract for 30 or 45 days. (C–F) Expression of genes related to longevity and oxidative stress. Flies were supplemented with 0.2% cowpea extract for 30 or 45 days. Total RNA was isolated and the mRNA levels of HO (C), SIRT1 (D), NOTCH (E), FOXO (F) were quantified using RT-PCR. (G) Western analysis using anti-FoxO and anti-Sirt1 antibodies on proteins extracts from flies supplemented with 0.2% cowpea extract for 30 or 45 days. (H–I) Densitometric analysis of FoxO and Sirt1 proteins. *p<0.05 with respect to the corresponding controls.

(SIRT1-sirtuin1-, FOXO-Forkhead box O- and NOTCH) and antioxidant defence systems (HO-heme oxygenase and TRXR-thioredoxin reductase) were measured (Figure 19C–19F). Oxidative stress has been recognized to play a key role in aging [238] and according to the oxidative stress theory of aging speculates that the functional losses typical of elderly are associated with the accumulation of structural impairments caused by the oxidative damage to macromolecules [239]. HO expression was significantly up regulated by cowpea extract supplementation after both 30 and 45 days (Figure 3C), while TRXR was not influenced at all (data not shown), suggesting that *V. unguiculata* extract partially modulates the endogenous antioxidant defence system.

SIRT1, a member of the class III NAD$^+$-dependent histone deacetylases (HDACs) has been implicated in the extension of longevity in *D. melanogaster* [240]. SIRT1 expression was significantly up regulated in flies supplemented with cowpea extract after both 30 and 45 days (Figure 19D). Remarkably, also NOTCH expression increased at both time points (Figure 19E), in accordance with findings showing that SIRT1 is a positive modulator of NOTCH [241]. FOXO is a fundamental transcriptional regulator of the insulin pathway modulating growth and proliferation and its increase has been associated with extension of life lifespan [242]. Although FOXO expression after 30 days of supplementation with *V. unguiculata* was the same as in control flies, cowpea extract triggered a significant upregulation of FOXO expression at 45 days (Figure 19F). In agreement with the gene expression, the level of FoxO and Sirt1 proteins increased in flies supplemented with cowpea extract (Figure 19G–I).

Thus, the aging-related signalling pathways of SIRT1, FOXO and NOTCH are involved in mediating the effect of cowpea extract in fruit flies.

***Vigna unguiculata* extract reduces both α-synuclein toxicity and aggregation in vitro**

Extensive literature report the fibrillation-inhibiting effects of plant extracts, including those consumed as part of a healthy diet [243,244] and others found in traditional medicine [245–248].

α-Synuclein is a presynaptic protein associated with the pathophysiology of synucleinopathies, including Parkinson's disease [222–224], and budding yeast has been extensively employed in models of synucleinopathies [226]. Thus, the effect of *V. unguiculata* extract on the longevity of yeast cells over-expressing the human α-synuclein [249] was evaluated. Interestingly, the addition of cowpea extract to exponentially growing cells strongly reduced the toxic effects of α-synuclein with a significant marked increase in mean lifespan (11.19 ± 2.18 days vs 2.22 ± 0.31 days; 404% increase) (Figure 20A, Table 5).

| | lifespan (days) | | | |
| | mean | | maximal | |
strain	cnt	0.5% E	cnt	0.5% E
[pYX242]	9.96 ± 0.49	13.3 ± 1.13	>15	>15
[pYX242-SNCA]	2.22 ± 0.31	11.19 ± 2.18	14.21 ± 1.06	>15

Table 5. Mean and maximal lifespan of yeast cells bearing pYX242 empty vector or pYX242-SNCA plasmid grown in the absence or presence of 0.5% V. unguiculata extract.
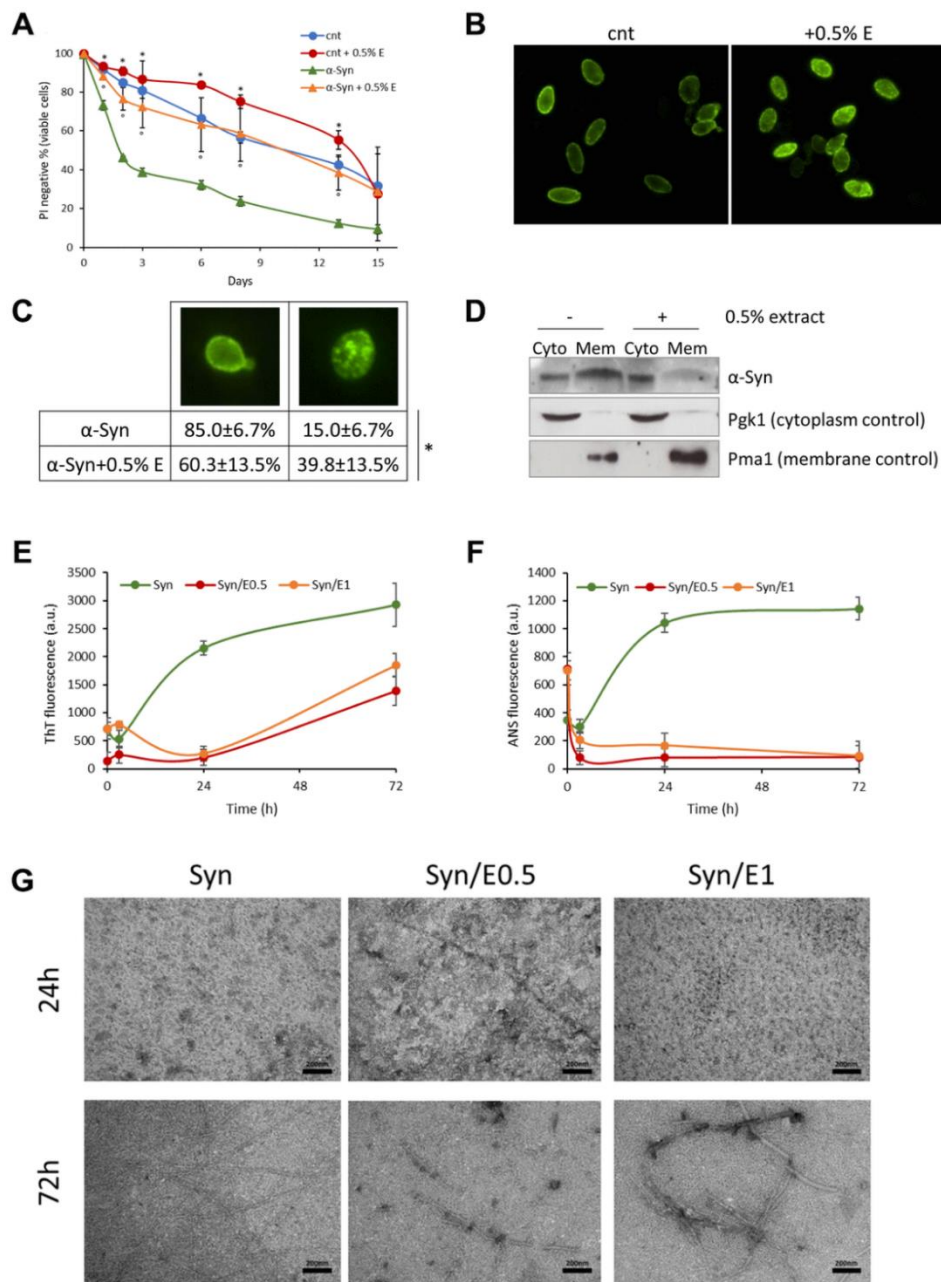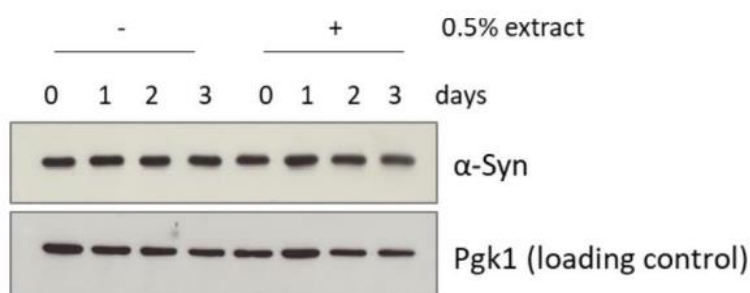
Figure 20. (D) Western analysis using anti-α-synuclein antibody on cytolpasmic and membrane fractions isolated from wt [pYX242-SNCA] cells after 1-day treatment with 0.5% V. unguiculata extract. Pgk1 was used as cytoplasmic marker, Pma1 as membrane marker. (E, F) α-synuclein aggregation process followed by ThT fluorescence (E) and ANS binding (F) assays. (G) TEM pictures taken from α-synuclein aggregation mixture after 24 h and 72 h of incubation in the absence or in the presence of cowpea extract at molar ratio protein:extract 1:0.5 (E0.5) and 1:1 (E1); scale bars are shown.

Figure 20. Cowpea extract reduces α-synuclein toxicity and aggregation. (A) CLS of yeast cells bearing pYX242 empty vector or pYX242-SNCA plasmid grown in SD medium containing 2% glucose in the absence or presence of 0.5% V. unguiculata extract. *$p<0.05$ relative to untreated cells bearing the empty vector, °$p<0.05$ relative to untreated α-synuclein expressing cells. (B, C) Immunofluorescence showing localization of α-synuclein in cells untreated or treated for 1 day with 0.5% V. unguiculata extract. The percentage of cells with α-synuclein localized in the cellular membrane is shown in (C). *$p<0.05$. Caption continues in the next page.

Although α-synuclein protein was still present 3 days after the treatment (Figure 21), it was less localized to the plasma membrane, as shown by immunofluorescence analysis (Figure 20B, 20C) and cell fractionation (Figure 20D). These data suggest that a different localization of α-synuclein, rather than its protein clearance, could be responsible for the reduced toxicity in the presence of the bean extract. The process of α-synuclein fibrillation was then investigated in vitro at two different concentrations of cowpea extract. The increase of ThT and ANS fluorescence emission intensity was used to quantify fibrils formation and conformational change of the protein with or without cowpea extract (Figure 20E, 20F). The presence of *V. unguiculata* extract led to a significant concentration-independent decrease of ThT fluorescence in the α-synuclein aggregation solution, with an increase of the lag time and a decrease of both β-sheet growth rate and final equilibrium levels (Figure 20E).

In agreement with a nucleation-dependent polymerization model, α-synuclein exhibited a sigmoidal binding without cowpea extract (Figure 20E). This evidence suggests that *V. unguiculata* extract significantly altered the amyloid aggregation pattern of α-synuclein. Moreover, the ANS binding fluorescence data indicate that the cowpea extract might increase the formation of α-synuclein species with minor solvent exposure of

Figure 21. α-synuclein level is unchanged but it is differently localized in the presence of cowpea extract in yeast cells. Western blot analysis is using anti-synuclein antibody in wt [pYX242-SNCA] cells after 5h, 1 day, 2 days, 3 days treatment with 0.5% V. unguiculata extract. Pgk1 was used as loading control.

hydrophobic clusters, or it might decrease the binding of ANS to α-synuclein surfaces (Figure 20F). The morphology of α-synuclein aggregates was also studied by TEM analysis. After 24 h of aggregation, the protein, either alone or in the presence of cowpea extract, existed as globular micelle-like and prefibrillar assemblies (Figure 20G). After 72 h of aggregation in the absence of the extract, α-synuclein samples were mostly mature fibrils. Remarkably, the presence of cowpea extract enriched the samples with short fibrils covered by densely packed globular clusters (Figure 20G). Overall, these findings are consistent with an inhibitory effect of *V. unguiculata* extract on the formation of amyloid fibrils.

It has been reported that cytotoxicity of amyloidogenic species largely depends on their biophysical surface properties, which influences their reactivity with the cellular plasma membrane [250–252].

To assess α-synuclein toxicity, we performed MTT assays on the human neuroblastoma SH-SY5Y cell line exposed for 48 h to extracellular α-synuclein aggregates pre-formed in vitro in the absence or in the presence of cowpea extract. Coherently, α-synuclein obtained without extract

supplementation exhibited the highest cytotoxicity: oligomers (OI) and fibrils (Fib) showed about 70% and 50% viability, respectively (Figure 22A). In cells incubated

with α-synuclein aggregates formed in the presence of the extract, toxicity was reduced and cell viability was about 83% with oligomers (OI/E0.5) and 86% with fibrils (Fib/E0.5) increasing up to 100% and 95% at the highest concentration of the extract (Figure 22A). Accordingly, ROS level significantly decreased in cells exposed to oligomers and fibrils formed in the presence of cowpea extract (Figure 22B).

These data suggest that in the presence of *V. unguiculata* extract, α-synuclein aggregation is redirected into non-toxic aggregate species.

To further explore the potential mechanism for the protective effect of the cowpea extract, the interaction of α-synuclein aggregates with the plasma membrane of neuroblastoma cells was monitored by confocal microscopy.

As previously reported [251,252], a large number of α-synuclein oligomers or fibrils (stained in red) were bound to the cell membrane (stained in green) (Figure 22C). When cells were exposed to α-synuclein aggregates formed in the presence of cowpea extracts, the binding of both oligomers and fibrils to the cellular membranes was drastically reduced (Figure 22C).

 In conclusion, these data show that the presence of cowpea extract during α-synuclein aggregation decreases the ability of the resulting aggregates to bind the plasma membrane and to raise ROS production and cytotoxicity.
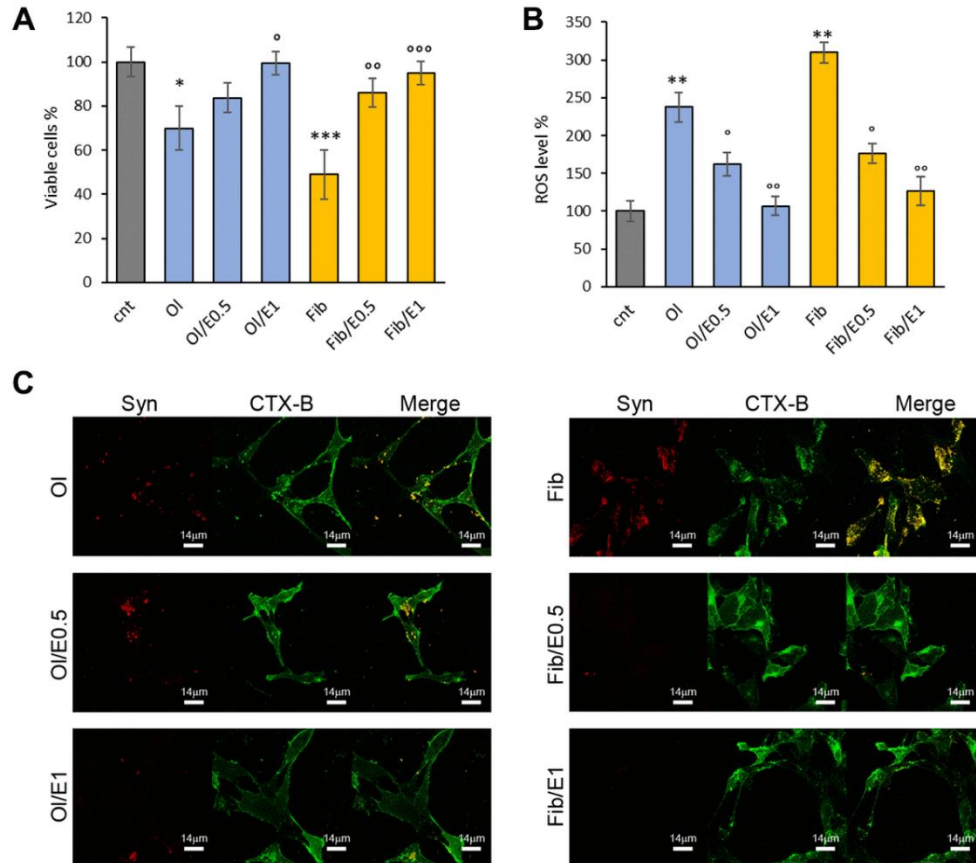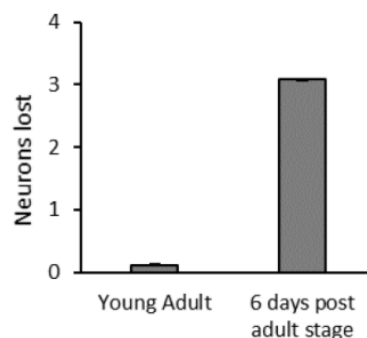
Figure 22. *V. unguiculata* extract reduces α-synuclein toxicity in neuroblastoma cells. (A, B) SH-SY5Y cells were grown for 48 h in the absence (cnt) or presence of 5 μM α-synuclein solution obtained after 24 h (oligomers, Ol) and 72 h (fibrills, Fib) of aggregation, without or with extract at molar ratio protein:extract 1:0.5 (E0.5) and 1:1 (E1). (A) Cell viability assessed by MTT assay and (B) ROS level evaluated by DCFDA fluorescence intensity assays. *p<0.05; **p<0.01; ***p<0.001 vs untreated cells. °p<0.05; °°p<0.01 vs treated cells with α-synuclein aggregates oligomeric (Ol) and fibrillar (Fib) grown without extract. (C) Z-projection of SH-SY5Y cell images by α-synuclein immunostaining (red) and CTX-B plasma membrane staining (green). Scale bars are shown.

Vigna unguiculata **extract reduces α-synuclein induced neurodegeneration in** *Caenorhabditis elegans*

To evaluate the neuroprotective effects of cowpea extract on a multicellular organism, we turned to the nematode *C. elegans*. The expression of human α-synuclein in *C. elegans* causes the age-dependent degeneration and death of the four cephalic dopaminergic neurons (CEP), a phenotype which can be easily scored using a red fluorescent marker expressed only in those neurons [253].

Consistent with previous reports, we observed an age-related decline in the number of fluorescent dopaminergic neurons expressing human α-synuclein (Figure 23). Thus, we investigated the effects of *V. unguiculata* extract both at 0.2% and 0.5%, in 6-day adult animals (Figure 24A, 24B). While in mock treated animals a mean of 3 out of 4 CEP neurons died, in animals exposed to *V. unguiculata* extracts there was a partial rescue of neurodegeneration, with 2 neurons dying in 0.2% extract and only 1 in 0.5%.

Figure 23. α-synuclein causes age-related dopaminergic neurons lost in *C. elegans*. Number of nonvisible CEP dopaminergic neurons in human α-synuclein expressing strain. In a wild type strain four CEP neurons expressing DsRed are always visible (not shown). In young adults almost no neurodegeneration is visible, while 6 days after adult stage a mean of 3 neurons is lost (p<0.0001 Mann Whitney nonparametric test). Error bars represent the SEM for two independent experiments. The number of young adult animals scored is 100, while after 6 days post adult stage is 91.
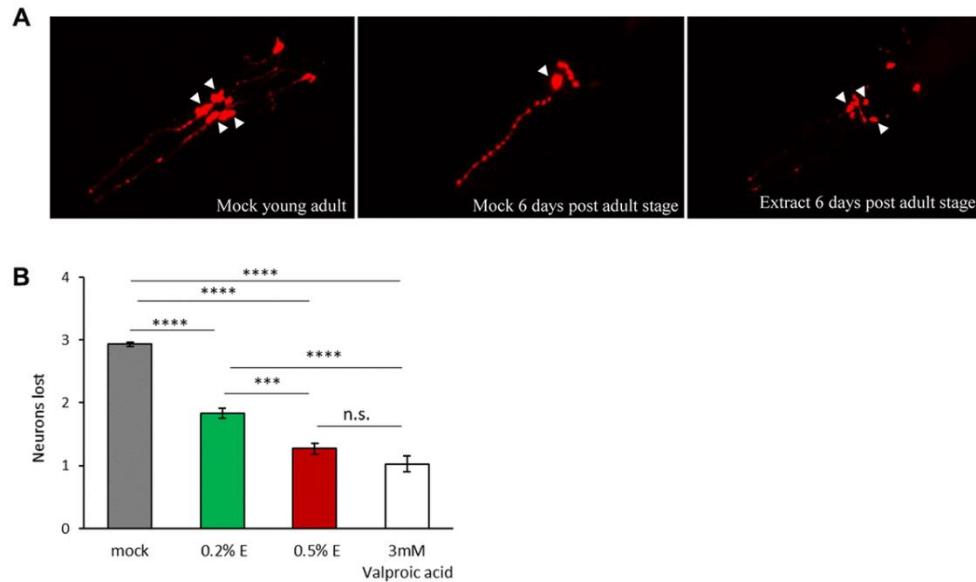
Figure 24. *V. unguiculata* extract is neuroprotective in a dose-dependent manner in a *C. elegans* model of α-synuclein toxicity. (A) The four CEP neurons (indicated by arrowheads), expressing DsRed and human α-synuclein, are viable and with a wild type morphology in young adult animals cultivated in mock conditions (left panel); only one neuron is visible and viable after 6 days from adult stage cultivated in mock conditions (central panel); 0.5% V. unguiculata extract partially rescued the neurodegeneration after 6 days from adult stage (right panel). Anterior is to the left. (B) Quantification of dopaminergic neuron loss in human α-synuclein expressing animals grown with 0.2% and 0.5% of V. unguiculata extract. ***p<0.001, ****p<0.0001. The number of animals scored with mock is 95, with 0.2% extract is 103, with 0.5% extract is 94 and with 3 mM valproic acid 92.

A similar effect was observed in animals treated with 3 mM valproic acid (positive control) [254].

Our results indicate that *V. unguiculata* extract protects CEP dopaminergic neurons from degeneration in a *C. elegans* model of α-synuclein toxicity, in a dose-dependent manner.

Concluding remarks

Cowpea is considered as a source of health-promoting compounds, with a low fat and high protein content, as well as dietary fibres, phenolic compounds and minerals. Consumption of cowpea is associated with reduced risk of gastrointestinal disorders, cardiovascular diseases, hypercholesterolemia, obesity, diabetes and several types of cancer [255]. We now add new important health benefits of cowpea beans, i.e. their anti-aging and neuroprotective effects. Indeed, we show that *V. unguiculata* extract extends lifespan, in two different eukaryotic models, such as budding yeast and fruit flies (Figures 15, 19). The extension of longevity requires Snf1/AMPK pathway in yeast (Figure 17F) and induces the upregulation of two downstream proteins of the AMPK pathway, such as FOXO and SIRT1 in *Drosophila* (Figure 19) [256–258]. Strikingly, it has been reported that AMPK and SIRT1 are downregulated with aging and their pharmacological activation is necessary to increase longevity [216].

The anti-senescence properties of cowpea extract are strongly additive with caloric restriction (Figure 16), the most effective non-genetic intervention delaying senescence [259], suggesting that *V. unguiculata* beans could display their best effect in terms of aging delay in a proper dietary regimen. The strong neuroprotective features of cowpea extract are conserved in evolutionary distant eukaryotic systems. Indeed, *V. unguiculata* extract decreases α-synuclein toxicity in both yeast and neuroblastoma cells, as well as in a *C. elegans* PD model by partially rescuing the degeneration of cephalic dopaminergic neurons (Figure 24).

The anti-aggregation properties of cowpea on α-synuclein is clearly evident (Figure 20E–G). Along similar lines, the extract decreases the localization of synuclein to cell membrane both in the yeast model, in which α-synuclein is

intracellularly expressed (Figure 20A–D), and in neuroblastoma cells, where α-synuclein is added to the medium (Figure 5), also in keeping with the minor solvent exposure of hydrophobic clusters detected by ANS on amyloid assemblies (Figure 20F). These results suggest that *V. unguiculata* extract decreases the neurotoxicity caused by the intracellular accumulation

of α-synuclein aggregates and the cellular damage induced by oligomeric aggregates interacting with the cell membrane by displacing the toxic protein from the lipidic bilayer. Our data are in accordance with recent results showing that inhibition of α-synuclein binding to membranes reduces the toxicity of the protein both in worms and in mice [260,261].

The aqueous extract of cowpea beans contains starch, amino acids, as well as several different proteins and peptides (Figures 15A–C, 17A, 17B), while it is probably very poor in phenolic compounds. Although abundance of starch and proteins is generally considered negative from an aging point of view [220], the protection against senescence and neurodegeneration might be the result of a synergistic effect of different elements. Indeed, the nutrient combination of the extract rather than a single component might be responsible for the metabolic reprogramming, which leads to the longevity phenotype.

Although the identity of the active components in the extract remains to be investigated, the extraction process strongly mimics the way in which these beans are consumed. Therefore, the anti-aging and neuro-protecting compounds are likely to be conserved during the cooking process. Remarkably, it has been reported that cooking legumes in water increases the insoluble fibre content, protein quality and digestibility, although with a reduction of the content of vitamins and minerals [255]. Therefore, the use of cowpea beans should be encouraged and eventually the identification of

the bioactive compounds could lead to the development of specific dietary supplements to support healthy aging and to delay neurodegeneration.

Any dietary intervention that has the potential of delaying the progression of age-related diseases could improve the quality of life of the aging population, also inducing an important impact on the economic implications of elderly on the society. Thus, *V. unguiculata* consumption in the global food chain is encouraging since our study suggests that cowpea beans supplementation can prevent age-related disorders.

Although data on bioactive compounds from cowpea are still poor, some reports indicate components like peptides may contribute to health benefits derived from cowpea [237]. Remarkably, several proteins identified by proteomic analysis are still uncharacterized (Figure 17A, 17B). We believe that additional work is necessary to discover the bioactive compounds in cowpea and their interactions to efficiently exploit them in foods, such as snacks and breakfast cereals by targeting benefits to immune function and health gut. Indeed, interesting data show that progression of PD has been frequently associated with dysbiosis of gut microbiota [262,263].

In conclusion, considering the role of functional food in the management of age-related diseases, we strongly support the intake of *V. unguiculata* beans to reduce senescence, neuroinflammation and the extent of neurodegeneration.

Chapter 4

S-Adenosyl-L-Methionine metabolism crosstalk with

Snf1/AMPK pathway

From: Tripodi et al., Cells 2020

S-Adenosyl-L-Methionine metabolism and Snf1/AMPK activity

Introduction

S-adenosylmethionine (SAM) was discovered by Giulio Cantoni 1953 as the biochemical donor of activated methyl groups [264]. Its synthesis requires methionine condensation with an ATP molecule and the formation of a covalent bond between methionine sulphur atom and ATP ribose. The reaction is thermodynamically driven by the elimination of ATP's phosphate and diphosphate groups in a reaction catalysed by S-adenosylmethionine synthetase [264]. In eukaryotes and prokaryotes SAM synthetases/methionine adenosyl-transferases (*SAM1* and *SAM2* in *S. cerevisiae*, *metK* in *E. coli* and *P. putida* and MAT1A and MAT2A in mammalian cells) are well conserved and their activity is essential for yeast and *E. coli* growth [265,266], while deficiency in Mat activity in humans lead to hypermethioninemia [267].

Target specific methyl transferases consume the 95% of SAM pool catalysing the methylation of proteins, DNA and small molecule, while the remaining 5% is consumed in the synthesis of polyamine [268]. Transmethylation reactions produce S-adenosylhomocystein (SAH) as a by-product that is then recycled into SAM through its conversion into homocysteine and therefore in methionine with the elimination of an adenosine molecule and the consumption of N^5-methyl-tetrahydrofolate [269]. In addition, bacteria can also recycle SAH into homocysteine removing an adenine molecule and producing S-ribosylhomocysteine as intermediate [270].

SAM concentration is tightly controlled in both eukaryote and prokaryote because of the energetic cost of its synthesis and to properly regulate methyl transferases activity. In yeast, both Sam1 and Sam2 activities are regulated

by a negative feedback loop depending on SAM concentration, while only *SAM2* transcription (which is known to increase during exponential growth) is mitigated by the presence of methionine in the media [266].

In human, the expression of adenosyl transferases differs for the tissues, with MAT1A being expressed only in liver cells and MAT2A in extrahepatic tissues and fetal liver [271]. Interestingly, SAM level post-transcriptionally control MAT2A abundance reducing its splicing efficiency due to a reduce binding with the N^6-adenosinemethyltransferase (METTL16) [272]. This regulation closely resembles the bacterial mechanism by which SAM-responsive riboswitches repress the expression of genes involved in methionine and SAM synthesis (see chapter 5 for details).

A recent publication connects Snf1/AMPK pathway with the metabolism of methionine and S-adenosyl-methionine (SAM) in *S. cerevisiae* [20]. Since the stimulation of SAM synthesis induces a higher phosphorylation of Snf1 [273], Tripodi and coworkers investigated the effect of methionine supplementation on yeast metabolism [20].

The addition of 0.1 g/L methionine to the growth media of the prototrophic background CENPK JT4 resulted in an increased activity of the kinase in the presence of methionine, while a *Δsnf1* strain showed a growth defect proportional to the methionine concentration in the media [20]. To characterize cellular physiology, the authors measured methionine and glucose uptake, as well as the main product of yeast fermentation, in the wild type and *Δsnf1* strain with and without methionine. Despite methionine uptake is comparable in the two strains, the author reported a decreased glucose uptake and secretion of ethanol, acetate and glycerol in the knockout strain and in presence of methionine, with an additive effect when

the activity of Snf1/AMPK was lost [20]. Interestingly, methionine supplementation induced a strong increase of the methylation potential (ratio between S-adenosylmethionine and S-adenosylhomocysteine concentrations) in the *Δsnf1* strain highlighting a role of Snf1/AMPK in the regulation of SAM metabolism in *S. cerevisiae* [20].

To further characterize this phenotype, the authors carried out omics analysis detecting strong differences in the proteomes of wild type and *Δsnf1* strains grown with and without methionine, such that principal component analysis (PCA) segregates each of these condition from the others. Through gene ontology (GO) enrichment, the authors identified processes related to oxidative metabolism, amino acids metabolism, transports and mitochondria related processes as those mainly affected by *SNF1* deletion, methionine supplementation and by the combination of the two conditions [20]. Hence, metabolomics confirmed the alteration of amino acids and glucose metabolisms in these conditions, suggesting that *SNF1* deletion combined with methionine supplementation alters yeast metabolism.

Eventually, the author proved this hypothesis with metabolic flux analysis (MFA) showing that *SNF1* deletion and methionine addition, both independently and synergistically, rewire yeast metabolism, increase pyruvate influx into mitochondria and partially revert the Crabtree effect stimulating mitochondrial respiration [20].

For decades, *S. cerevisiae* served as model organism for the study of the genetic, signal transduction, metabolism and cell cycle progression of eukaryotic cells, thanks to the strong conservation of these processes from yeast to mammals. Furthermore, yeast aerobic glucose fermentation into

ethanol (Crabtree effect) strongly resembles glucose fermentation into lactate in Warburg positive cancer cells, providing a model organism for the study of this phenotype.

Considered this, the strong growth defect of the *Δsnf1* strain supplemented with methionine and its metabolic rewiring, prompted us to investigate the crosstalk between AMPK pathway and SAM metabolism in cancer cells to investigate novel combined therapeutic opportunities.

Liver cancer is the second leading cause of cancer-related death worldwide. Hepatocellular carcinoma (HCC) is the most common form of primary liver cancer and is associated with chronic liver damage, which can be caused by viral infections, such as hepatitis B virus (HBV) and hepatitis C virus (HCV) infection or by alcoholic liver diseases and non-alcoholic steatohepatitis (NASH). Potentially curative treatments for very early/early stage HCC patients include surgical resection, liver transplantation and percutaneous ablation. At an advanced/late stage surgery is no longer applicable, and the currently available therapies are effective only in small groups of patients [274–276]. Very few therapeutic options, with unsatisfactory antitumor effects and toxicity, are nowadays available, thus, prognosis remains very poor. In 2007 Sorafenib was the first VEGFR TKI (vascular endothelial growth factor receptor (VEGFR)-tyrosine kinase inhibitor (TKI)) to be approved in advanced HCC, and it is used as standard treatment for patients who have no/mild cirrhosis. However, it gives a significant, but moderate improvement in median overall survival [277]. More recently, other drugs against HCC have been approved, such as Regorafenib, Lenvatinib, and Cabozantinib [277].

AMP-activated protein kinase (AMPK) is a heterotrimeric Ser/Thr protein

kinase, highly conserved from yeast to humans (Figure 2). It functions as a sensor of the cellular energy status: in response to metabolic stress AMPK is activated by phosphorylation on a conserved threonine residue (T172), resulting in the upregulation of adenosine triphosphate (ATP)-producing pathways (catabolism) and in the downregulation of ATP-consuming pathways (anabolism), in order to restore energy homeostasis [278]. Downregulation of AMPK in several tumour tissues has been associated with the loss of control in tumorigenesis, cell cycle progression, proliferation and survival, invasion and metastasis, cancer metabolism, and drug resistance. However, its role in carcinogenesis is still controversial, being now considered a double-edged sword that can have either pro-tumour or anti-tumour functions depending on cellular and metabolic demand [279]. The catalytic AMPK-α2 subunit is frequently under-expressed in human HCC cells and inactivation of AMPK promotes hepato-carcinogenesis [280]. It was also found that patients with cirrhosis that present low AMPK phosphorylation had a significant higher incidence of HCC than patients with high phospho-AMPK levels [281]. In addition, low phospho-AMPK staining is correlated with aggressive clinicopathologic features and poor prognosis in patients with HCC [282]. For these reasons, the activation of AMPK in patients with liver cancer has been proposed as a clinical target. Metformin, the widely used anti-diabetics drug, is the most commonly used activator of AMPK, with well-documented pharmacokinetic and safety profiles [283]. However, clinical evaluation of metformin effectiveness alone, or in combination with Sorafenib, has given no clear results yet [284]. Liver is the organ where 50% of methionine metabolism and where 85% of all transmethylation reactions take place [285]. Methionine is an essential amino-acid, particularly abundant in animal food and seafood, but also in nuts, seeds, and cereals,

while it is less abundant in fruits and vegetables [286]. In the liver, methionine is converted into S-adenosyl-methionine (SAM), an important cofactor for transmethylation reactions [287]. SAM is also involved in the trans-

sulphuration pathway, particularly active in the liver to give cysteine biosynthesis, the rate-limiting precursor for glutathione (GSH) synthesis. SAM is also required for the synthesis of polyamines, small positively charged molecules involved in transcription, translation, cell growth, and death [288].

Methionine restriction is associated with the increase of lifespan in different models (yeast, Drosophila, human fibroblasts, rodents [286]) and to the inhibition of cell growth in different cancer cells, such as sarcoma, melanoma, prostate carcinoma, colorectal cancer cells in vitro, as well as in animal models [289].

In general, a different regulation should be assumed in liver cancer cells, considering the peculiar role of the liver in both the synthesis and in the degradation of methionine. SAM is synthesized by methionine adenosyl-transferase (MAT), encoded by two genes (MAT1A and MAT2A). MAT1A is expressed in adult differentiated liver, while MAT2A is expressed in extrahepatic tissues and fetal liver. Liver carcinogenesis is associated to a switch between MAT1A and MAT2A, with a consequent less efficient methionine metabolism, that enhances the capacity of hepatocytes and hepatoma cells to utilize nutrients for anabolic processes to support growth [17]. In addition, MAT1A and GNMT (glycine N-methyltransferase) knockout mice, with respectively very low and very high SAM levels, spontaneously develop HCC, further supporting the crucial role of methionine-cycle homeostasis for this organ [285,290].

Strikingly, it was recently published that SAM supplementation inhibits liver cancer cell invasion in vitro [291] and decreases liver cancer formation in a mouse model [292]. Additionally, a quite old clinical trial on patients with alcoholic cirrhosis and less severe hepatic dysfunction demonstrated the beneficial role of SAM treatment, by increasing GSH levels and decreasing the probability of liver transplantation and death [293].

Thus, since methionine/SAM administration in liver seems to have an opposite role than in other cancer types, more studies are necessary to support a therapeutic role of methionine or SAM supplementation in patients.

Here, we investigate the effect of methionine supplementation in liver cancer cells in vitro, to explore the possibility that alterations in methionine dietary consumption could help treatment of liver cancer.

High Methionine and Compound C Induce Proteomic Changes

As reported in the preliminary results section of this chapter, methionine activates Snf1/AMPK and increases mitochondrial metabolism and respiration in the model organism *Saccharomyces cerevisiae*, especially in cells lacking Snf1/AMPK activity [33].

To investigate whether this is a conserved mechanism triggered by methionine, we explored the effect of high methionine concentrations in liver cancer cells, in the presence or absence of Compound C, which mimics AMPK inhibition. We performed a proteomic analysis on HepG2 cells grown for 48 h (CTR), in the presence of Compound C (CTRCC), in the presence of
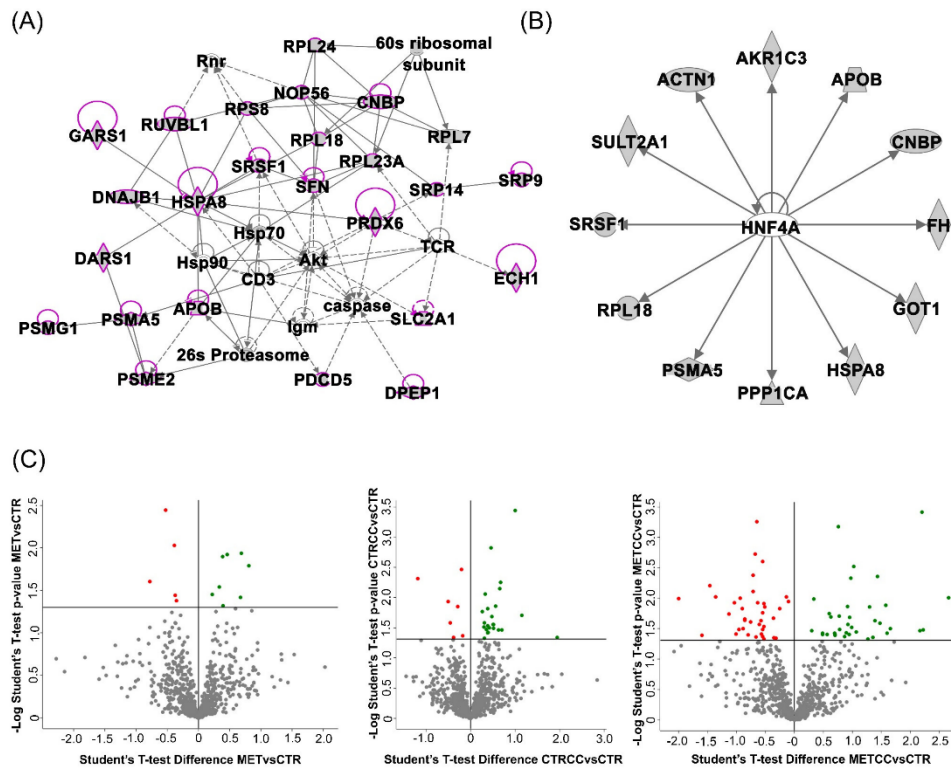
Figure 28. Bioinformatic analysis of the proteomic data of HepG2 cells grown for 48 h (CTR), in the presence of Compound C (CTRCC), high methionine (MET) and high methionine and Compound C (METCC). (A) Ingenuity® Pathway Analysis (IPA) analysis carried out on the 46 proteins common to all data sets, whose expression is statistically different, highlighted that 25 out of 46 proteins differentially expressed belong to a network classified as: cancer, protein synthesis, RNA damage and repair. These proteins are shown in magenta among all the proteins belonging to the pathway. Each protein is reported with the corresponding IPA symbol. (B) The upstream regulator analysis, based on prior knowledge of expected effects between transcriptional regulators and their target genes in IPA, shows hepatocyte nuclear factor 4 (HNF4A) (p-value 0.001) which target 12/46 of the proteins differentially expressed. (C) Volcano plots of the comparison MET versus CTR, METCC versus MET, CTRCC versus CTR. In green: proteins upregulated; in red: proteins downregulated; in grey: proteins that are not statistically different (Student's t-test p-value = 0.05).

high methionine (MET), and in double treated cells (METCC) by a quantitative shotgun label free strategy. The comparison of the four data sets by an ANOVA test (p-value 0.05) showed proteins exclusively expressed in each condition, as well as 717 proteins common to all data

sets, among which, 46 were statistically different. IPA analysis carried out on these proteins to find possible interactions highlighted that 25 out of 46 proteins differentially expressed belonged to a network classified as: cancer, protein synthesis, RNA damage and repair (Figure 28A). The

upstream regulator analysis, based on prior knowledge of expected effects between transcriptional regulators and their target genes in IPA, suggested that two transcription regulators were probably involved, hepatocyte nuclear factor 1 (HNF1A, p-value 0.0005) and hepatocyte nuclear factor 4 (HNF4A, p-value 0.001) (Figure 28B), which target 6/46 and 12/46 of the proteins differentially expressed, respectively. This result suggests that the presence of methionine and Compound C significantly affects transcription, in keeping with Wang and co-workers who reported an impact on methionine metabolism by HNF4A [294].

These proteins were further analysed to find possible enrichment in GO Biological Processes (Figure 29) and pathways (Figure 30), in the comparison between control and treatments with high methionine or/and Compound C. Differentially expressed proteins mainly belonged to the classes of metabolic processes, mitochondrion, and mitochondrial dysfunction, translation, RNA and protein processing and response to oxidative stress. As shown in Figure 29A and 29B, the expression of proteins related to oxidation-reduction events were altered, either up or downregulated, indicating a general impact on these processes in the
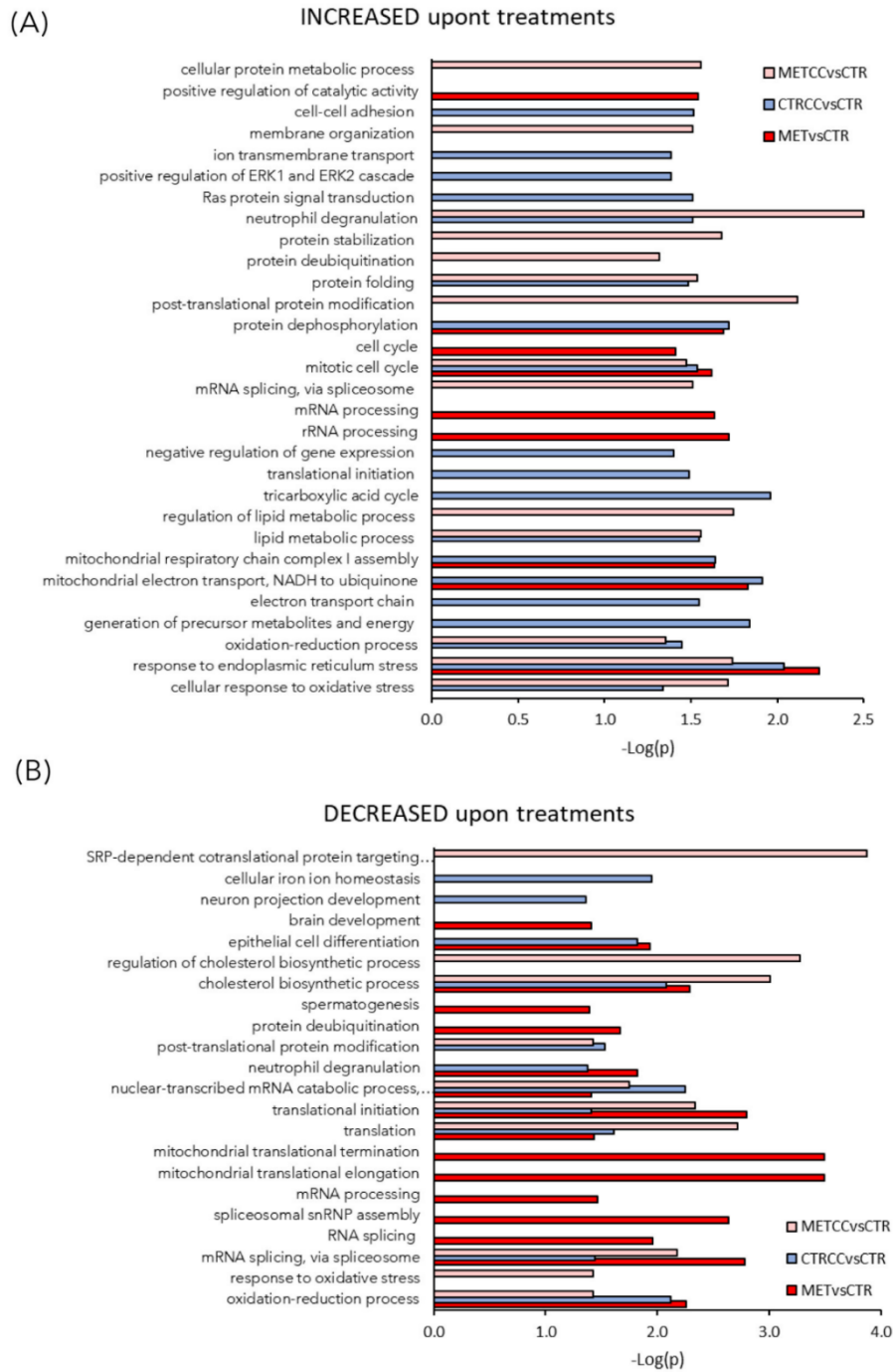
(A) INCREASED upont treatments

(B) DECREASED upon treatments

Figure 29. Caption in the next page.

Figure 29. High methionine and Compound C induce proteomic changes. (A–C) Functional analysis of the proteins differentially expressed in the comparison MET versus CTR, METCC versus MET, CTRCC versus CTR. Proteins were considered differentially expressed if they were present only in one condition or showed significant t-test difference (Student's t-test p value = 0.05). (A) GO Biological Processes increased in the three comparison (B) GO Biological Processes decreased in the three comparisons. Functional grouping was based

presence of methionine and/or Compound C compared to the control. Many proteins involved in mitochondrial respiratory chain were upregulated by the double treatment with high methionine and Compound C. In particular, high methionine induced an increase of proteins involved in the mitochondrial electron transport and in complex I assembly, while

| Canonical Pathways	METvsCTR	METCCvsCTR	CTRCCvsCTR
Mitochondrial Dysfunction	5.06	6.17	7.07
Oxidative Phosphorylation	2.40	4.14	5.39
TCA Cycle II (Eukaryotic)	0.69	2.26	2.81
Production of Nitric Oxide and Reactive Oxygen Species in Macrophages	2.39	2.19	2.37
NRF2-mediated Oxidative Stress Response	1.08	3.65	1.07
Sirtuin Signaling Pathway	3.41	5.34	5.77
EIF2 Signaling	4.47	5.37	4.45
Regulation of eIF4 and p70S6K Signaling	4.55	1.31	3.59
Protein Ubiquitination Pathway	1.76	5.31	0.72
HIPPO signaling	1.10	3.07	2.90
mTOR Signaling	3.75	0.95	2.18
Breast Cancer Regulation by Stathmin1	2.28	1.50	3.03
Clathrin-mediated Endocytosis Signaling	1.04	2.83	2.35
Integrin Signaling	1.54	1.44	2.94
Superpathway of Cholesterol Biosynthesis	1.94	2.20	1.93
FXR/RXR Activation	0.77	3.75	1.41
D-myo-inositol (3,4,5,6)-tetrakisphosphate Biosynthesis	2.08	0.88	2.89
D-myo-inositol (1,4,5,6)-Tetrakisphosphate Biosynthesis	2.08	0.88	2.89
ERK/MAPK Signaling	1.04	1.57	3.13
3-phosphoinositide Degradation	1.94	0.80	2.72

Figure 30. Bioinformatic analysis of the proteomic data on HepG2 cells grown for 48 h (CTR), in the presence of Compound C (CTRCC), high methionine (MET) and high methionine and Compound C (METCC). The analysis was carried out by IPA on the proteins differentially expressed among the comparison MET versus CTR, METCC versus CTR and CTRCC versus CTR. Proteins were considered differentially expressed if they were present only in one condition or showed significant t-test difference (Student's t-test p-value 0.05). Functional grouping was based on Fischer's exact test p value ≤ 0.05 and at least three counts. The colored bars are a visual representation of the corresponding –log p-value reported abreast.

Compound C treatment mainly increased the level of tricarboxylic acid (TCA) cycle and lipid metabolic processes (Figure 29A).
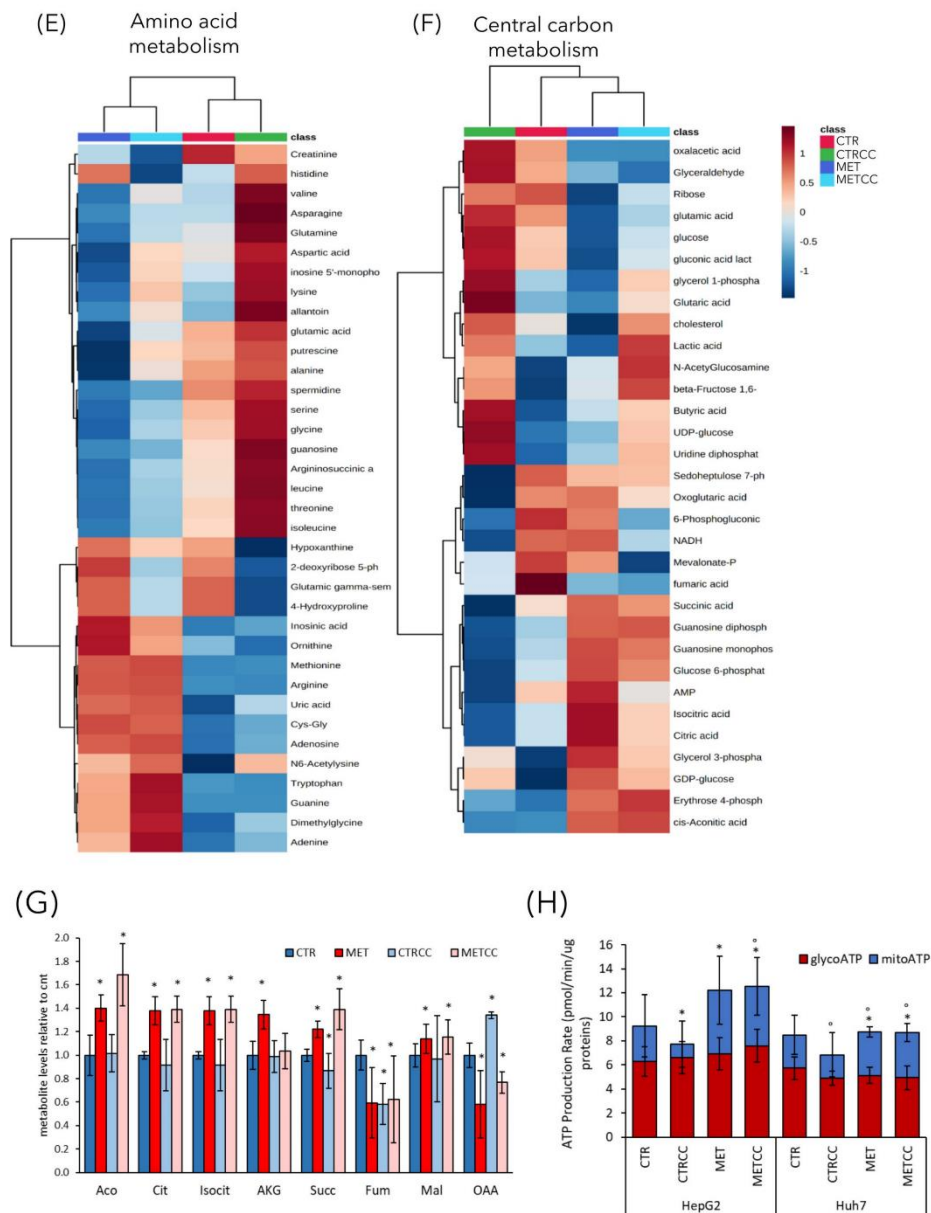
Methionine and Compound C presence upregulated proteins involved in the cellular response to oxidative stress, manly at the endoplasmic

reticulum level (Figure 29A, Figure 30), while Compound C alone induced the expression of proteins involved in membrane organization, transmembrane transport, and cell–cell adhesion (Figure 29A).

Interestingly, methionine and Compound C altered sirtuin signalling pathway (Figure 30). This pathway is a master regulator of several cellular processes and known to both extend lifespan and regulate spontaneous tumour development. It is well known that S-adenosyl-methionine, sirtuin, and mTOR pathway are strictly related [295]. In keeping with these data and with results reported above, the proteomic analysis suggested that mTOR signalling was altered mainly in response to increased methionine in the medium (Figure 30).

Among the processes more altered in HepG2 cells treated with methionine and Compound C, RNA processing and mitochondrial translation were downregulated mainly by methionine, while Compound C had more impact on general translation (Figure 29B). Overall, the double treatment with high methionine and Compound C induced a decrease in the level of ribosomal proteins RPS9, RPL23A, RPL34, mitochondrial ribosomal proteins MRPL37, MRPS18C, and translational initiation factors, such as EIF1 and EIF3M, as well as proteins of the SRP (signal-recognition-particle) co-translational process (SRP14, SSR3, SRP9), suggesting a general reduction of translation in this condition.
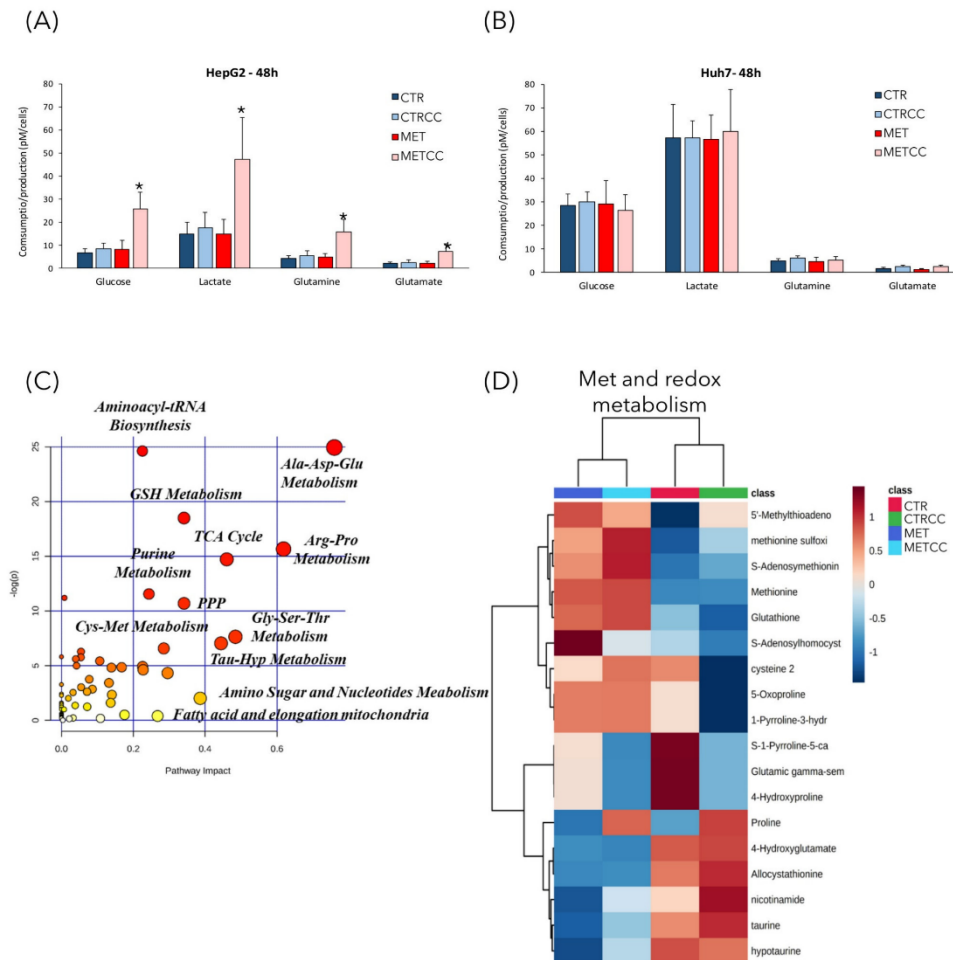
Figure 31. High methionine and Compound C affect cellular metabolism. (A, B) HepG2 (A) and Huh7 (B) cells were grown for 48 h in regular medium or in the presence of high methionine and/or Compound C. Media from three biological replicates were collected to measure glucose and glutamine consumption, lactate, and glutamate secretion. (C–F) HepG2 cells were grown for 48 h in regular medium (CTR), or in the presence of high methionine and/or Compound C. Metabolomics analysis was performed by GC/MS and LC/MS on five biological replicates, each analyzed in technical duplicate. (C) Metabolic pathways mostly affected in this analysis. The metabolic pathway analysis was performed using the MetaboAnalyst 4.0 tool. The metabolic pathways are represented as circles. Color intensity (white-to-red) and size of each circle reflects increasing statistical significance, based on the p-value [−log(P)] from the pathway enrichment analysis, and pathway impact value derived from the pathway topology analysis, respectively. (D–F) Hierarchical clustering heatmaps from one-way ANOVA analysis of differential metabolites belonging to (D) methionine and redox metabolism.

Figure 31. (E) amino acid metabolism, (F) central carbon metabolism. The heatmaps were obtained using the MetaboAnalyst 4.0 tool. The color code scale indicates the normalized metabolite abundance. (G) Histogram of the level of metabolites of the TCA cycle in the four conditions in HepG2 cells, measured in the metabolomics analysis. The level of each metabolite in the control was set to 1. * p < 0.05 compared to control. (H) Seahorse adenosine triphosphate (ATP) rate assay analysis in HepG2 and Huh7 cells, grown for 48 h in regular medium or in the presence of high methionine and/or Compound C. * p < 0.05 for mitoATP compared to control, p < 0.05 for glycoATP compared to control.

High Methionine and Compound C Induce a Metabolic Rewiring

Since methionine supplementation induced deep changes of proteins associated with cellular metabolism, we further investigated this feature by performing metabolomics analysis in cells grown with high methionine and/or Compound C. Extracellular metabolites were analysed by YSI biochemical analyser. In HepG2 cells, only the double treatment (high methionine and Compound C) showed an increase of glucose and glutamine consumption, with a proportional increase in lactate and glutamate secretion (Figure 31A). However, no changes in extracellular metabolites were observed in Huh7 cells in any condition. This difference could be due to the lower growth rate of Huh7 cells, or to their higher basal metabolism compared to HepG2 cells; indeed, their basal glucose uptake and their lactate secretion were three times higher than those of HepG2 cells (Figure 31A, B).

We then measured relative abundance of intracellular metabolites in HepG2 cells treated for 48 h with high methionine and/or Compound C, by an untargeted metabolomic GC/MS and LC/MS analysis. This analysis revealed a strong metabolic change due to high methionine, but also to Compound C addition (Figure 31C). The most affected pathways were those related to amino acids metabolism, like Cys-Met (as expected upon methionine supplementation), Ala-Asp-Glu, Arg-Pro, and Gly-Ser-Thr (Figure 31C), but also those related to aminoacyl-tRNA biosynthesis, coherently with the downregulation of translation associated proteins (Figure 29B). In addition, alterations in the pathways of glutathione metabolism (which is directly associated to methionine metabolism), of the sulphur-containing molecules taurine and hypotaurine, in the pathways of purine and nucleotide metabolism and of fatty acid metabolism were identified (Figure 31C). As

expected, methionine supplementation in the medium (either in the presence or absence of Compound C) increased the intracellular level of methionine, but also of its derived metabolites, such as S-adenosyl-methionine and S-adenosyl-homocysteine, which are part of the methionine cycle (Figure 31D). In addition, high methionine treatment induced an increase of cysteine, which can derive from homocysteine and serine, through conversion to cystathionine, and of glutathione, which is synthesized from Cys, Glu, and Gly. In high methionine condition there was also an increase of two direct methionine derivatives, the regulatory metabolite methylthioadenosine (MTA) and the toxic compound methionine sulfoxide (Figure 31D). Remarkably, the MTA level negatively correlates with growth potential in the liver [296,297]. In fact, it has been reported that MTA decreases after partial hepatectomy, when the replicative response of hepatocytes is higher, and MTA administration in vitro reduces liver cell growth [298]. Furthermore, MTA inhibits the synthesis of polyamines [296], whose level is correlated with proliferation and which were indeed decreased in high methionine condition (see spermidine and putrescine, Figure 31E). On the contrary, the MTA derivatives adenine and adenosine increased in high methionine condition (Figure 31E). High methionine also induced an increase of metabolites related to the urea cycle, such as arginine, ornithine, uric acid (Figure 31E), which was probably increased to convert excess nitrogen (given by the high methionine supplied in the medium) into urea.

High Methionine and Compound C Increase Mitochondrial Functionality

The metabolomics analysis revealed also that many metabolites of the TCA cycle were modulated by high methionine, with higher levels of cis-aconitate, citrate, isocitrate, α-ketoglutarate, succinate and malate and lower levels of fumarate and oxaloacetate compared to the control (Figure 31F, G).

Since the metabolomics and proteomics data suggested an increase of the TCA cycle, and in light of the preliminary results (Figure 26 and Figure 27), we measured the rate of ATP production from glycolysis and from mitochondrial respiration in HepG2 and Huh7 cells, through Agilent Seahorse technology (Figure 31H). Although the amount of ATP deriving from glycolysis was only slightly altered by treatments, cells grown in high methionine condition (with or without Compound C) produced a higher fraction of ATP through mitochondrial respiration (Figure 31H). The increase of mitochondrial-derived ATP was clearly evident in HepG2 cells and it was also confirmed, albeit with a lower increase, in Huh7 cells.

Since the phenotype of a biological system is the results interactions between several components [49], we decided to integrate the results from metabolomic and proteomic analysis, using the IPA and MetaboAnalyst software. This integration better highlighted that TCA cycle was one of the most affected processes in all three comparisons (MET versus CTR, CTRCC versus CTR, METCC versus CTR) (Figure 32A–C). However, as reported in Figure 31D, E, focusing on the first 10 more significant pathways in terms of enrichment (p-values) and topology (pathway impact) in the three comparisons, the integration analysis suggested that citrate and TCA cycle were more affected by the presence of Compound C than methionine, which, in turn, had a major impact on amino acid metabolism, especially of

those amino acids directly linked to the nitrogen cycle, such as Arg, Gln, and Glu. In keeping with the effect on TCA cycle, pyruvate metabolism and the synthesis and degradation of ketone bodies prevailed in the presence of Compound C if compared to the supplementation of methionine (Figure 32D, E).

Strikingly, the pentose phosphate pathway, Arg/Pro metabolism, glyoxylate, and dicarboxylate metabolism were altered only upon double treatment (Figure 32D). In addition, glutathione metabolism and metabolism of xenobiotics, which were affected by single treatments, were no more altered upon double treatment (Figure 32D).
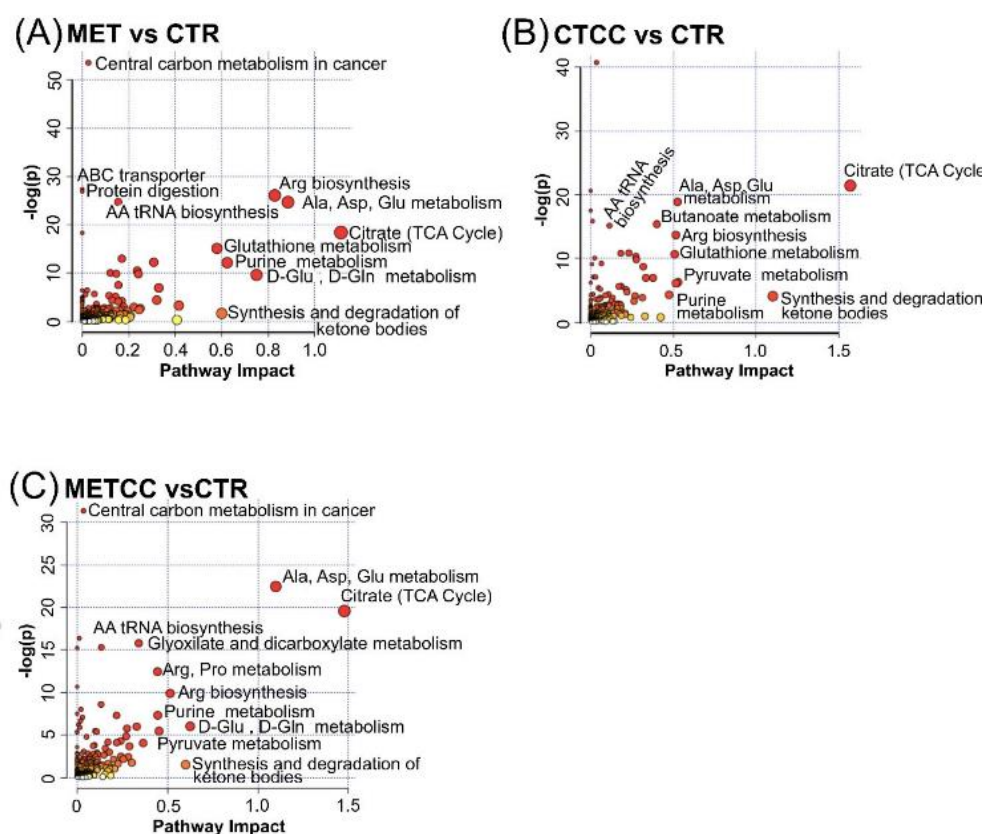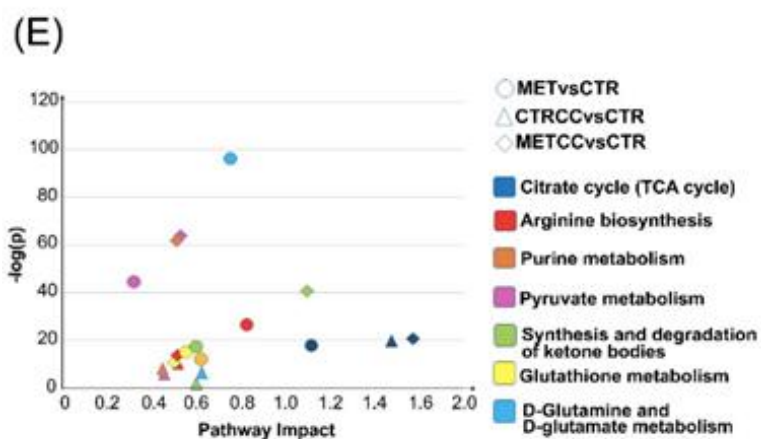

Figure 32. Caption in the next page

(D) **Pathways**

| Pathways	METvsCTR			CTRCCvsCTR			METCCvsCTR		
	Counts	Pathway Impact	-log(p)	Counts	Pathway Impact	-log(p)	Counts	Pathway Impact	-log(p)
Citrate cycle (TCA cycle)	9	1.1	18.4	10	1.6	21.4	10	1.5	19.6
Arginine biosynthesis	11	0.8	26.1	7	0.5	13.7	6	0.5	9.9
Purine metabolism	13	0.6	12.2	9	0.5	61.4	11	0.4	7.3
Pyruvate metabolism	4	0.3	44.5	5	0.5	62.9	5	0.5	5.5
Synthesis and degradation of ketone bodies	1	0.6	16.9	2	1.1	40.8	1	0.6	1.5
Glutathione metabolism	10	0.6	15.1	8	0.5	10.7			
D-Glutamine and D-Glutamate metabolism	4	0.8	96.5				3	0.6	6.0
Metabolism of xenobiotics by cytocrome P450	2	0.4	0.3	3	0.4	0.8			
Glycolysis or Gluconeogen	4	0.4	33.2						
Glycine, Serine, Threonine metabolism	6	0.3	69.7						
Alanine, Aspartate, Glutamate metabolism				10	0.5	18.9	12	1.1	22.5
Starch and sucrose metab				4	0.5	43.1			
Butanoate metabolism				9	0.4	15.4			
Pentose P pathway							4	0.4	4.1
Arginine and Proline metab							11	0.4	12.5
Glyoxylate and dicarboxylate metabolism							11	0.3	15.8

Figure 32. Integration of metabolomics and proteomics analysis. (A) Metabolic and proteomic pathways mostly affected in MET versus CTR. (B) Metabolic and Proteomic pathways mostly affected in CTRCC versus CTR. (C) Metabolic and Proteomic pathways mostly affected in METCC versus CTR. The scatter plots show a summary of the joint evidence from enrichment analysis (p-values) and topology analysis (pathway impact). Dots size and color (white to red) are proportional to the numbers of genes and compounds present in a pathway. (E) List of the 10 more significant pathways in each of the three comparisons. (E) Scatter plot of the common pathways among the list shown in (D).

123

These results indicate that the combination of Compound C and high methionine does not result in a simple synergistic effect of the single treatments, but rather leads to the emergence of new features in liver cancer cell metabolism.

High Methionine Activates AMPK and mTOR Pathways

Since methionine can activate Snf1/AMPK in budding yeast (Figure 26A), we then investigated methionine effect on AMPK activation state in liver cancer cells. AMPK showed a dose-dependent activation after 24 h in HepG2 cells (Figure 33A), detectable as increased phosphorylation on T172, as well as increased phosphorylation of Acc1-S79, the main target of AMPK, often used as reporter of its activity. As reported in chapter 1, AMPK activation is mainly due to an energy reduction [299], although it can also be activated without any ATP decrease (Figure 2) [300].

Since data presented above (Figure 31H) indicate that ATP level did not decrease, but rather increased after methionine treatment, we can speculate that AMPK activation was not a result of energy deficiency, but rather the effect of a reduced flux through glycolysis (Figure 31H). To better investigate AMPK activation, we performed time-course experiments in both HepG2 and Huh7 cell lines. A total of 1.5 g/L of methionine was added to cells growing in regular medium and phosphorylation of AMPK-T172 and of Acc1-S79 were detected by Western blot analysis (Figure 33B).
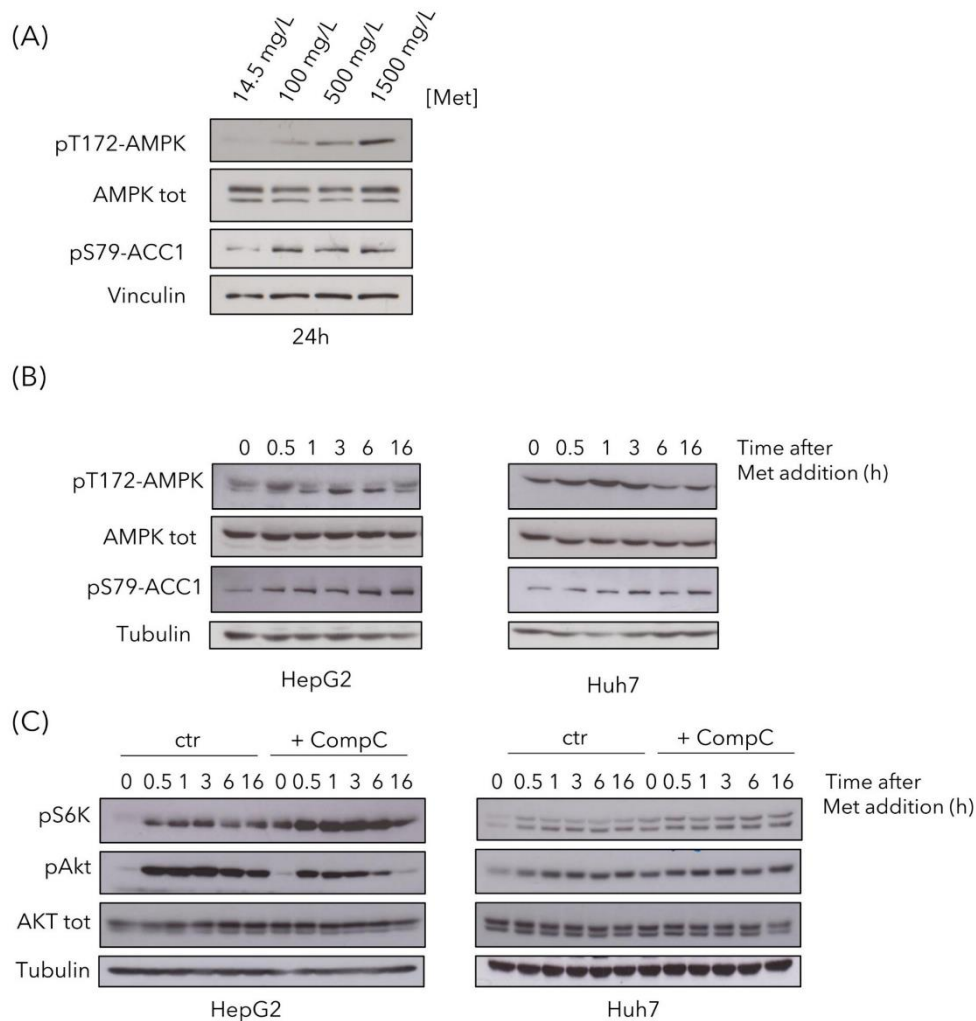
Figure 33. High methionine activates AMK-activated protein kinase (AMPK), mTOR and Akt pathways. (A) HepG2 were treated with methionine for 24 h and AMPK activation state was assayed by Western analysis, using the pT172-AMPK antibody (against pT172 in the activation loop) and using the anti-pS79-Acc1 antibody (against the target site of AMPK on Acc1). An anti-AMPK total antibody and an anti-vinculin antibody were used as controls. (B) HepG2 and Huh7cells were gown in control medium and 1.5 g/L methionine was added to the cultures at time 0. Samples were collected at the indicated time points to evaluate AMPK activation, using an anti-pT172-AMPK antibody and an anti-pS79-Acc1 antibody. An anti-AMPK total antibody and an anti-tubulin antibody were used as controls. (C) HepG2 and Huh7 cells were gown for 48 h in the absence or presence of Compound C. Then 1.5 g/L methionine was added to the cultures, and samples were collected at the indicated time points to evaluate mTOR activation, using anti-pS6K antibody and Akt activation using anti-pS473-Akt antibody. Anti-Akt total antibody and anti-tubulin antibody were used as controls.

AMPK phosphorylation, as well as the phosphorylation of its target Acc1, increased in both cell lines, with a peak at 0.5 h and 1 h after methionine addition, for HepG2 and Huh7 respectively (Figure 33B). Since amino acids can activate mTOR, the master regulator of cell growth (Figure 3) [301] and, since mTOR involvement was suggested by our proteomics analysis (Figure 30), we investigated the activation of the mTOR pathway. mTOR was activated in response to high methionine in the medium, as observed by increased pS6K phosphorylation (Figure 33C), in keeping with previously reported data [11], both in HepG2 and in Huh7 cells. Phosphorylation increased after 30-min treatment, remaining high until 16 h (Figure 33C). This increase was more evident in cells pre-treated with Compound C, in which the release of mTOR inhibition by AMPK resulted in a higher pS6K phosphorylation, both at time 0 and in response to high methionine (Figure 33C). High methionine also induced activation of the Akt pathway, involved in cell proliferation and survival [45], in both cell lines, although in HepG2 cells, it was less persistent over time when AMPK was inhibited (Figure 33C).

**High Methionine Reduces Cancer Associated Phenotypes**

Since in yeast cells, methionine induced a slow-down of growth rate, especially in cells lacking Snf1/AMPK activity [20]. The increase of methionine concentration in the medium (up to 1.5 g/L, versus 15 mg/L in regular medium) induced a slight slow-down of growth rate both in HepG2 and in Huh7 cell lines (Figure 34A, B). Inhibition of AMPK with Compound C slightly reduced growth rate in both cell lines, but drastically impaired growth when combined with high methionine in the medium (Figure 34A, B).

These results suggest that the effect of methionine on cellular proliferation is a conserved feature that deserves further investigation.

In addition to a higher proliferation, one of the most relevant features of cancer cells is their ability to migrate and to form colonies from single cells, to give metastasis. To analyse the effect of methionine on cell migration, we used Boyden chambers and migration of serum starved cells was assessed in the presence or absence of high methionine concentration and/or Compound C. Cell migration through the membrane of the transwell was significantly impaired in high methionine in both cell lines, even more when AMPK was inhibited (Figure 34C, D).

We then tested the ability of single cells to form colonies in the presence of high methionine and/or inhibition of AMPK. As shown in Figure 34E, F, colony formation was reduced by high methionine supplementation, especially in the presence of Compound C (Figure 34E, F).

Altogether, our results suggest that high methionine supplementation inhibits cancer associated phenotypes, especially in combination with AMPK inhibition.
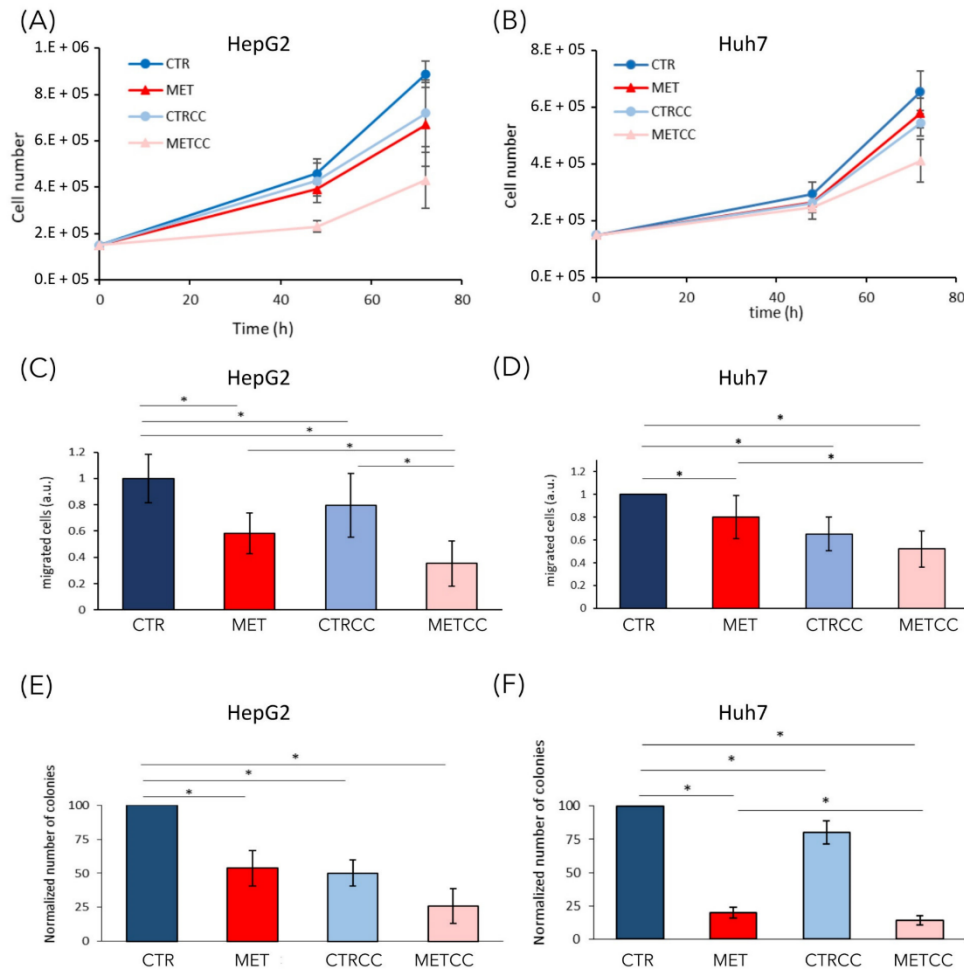
Figure 34. High methionine and Compound C inhibit cancer phenotypes. (A, B) Cell growth of (A) HepG2 and (B) Huh7 was monitored until 72 h in regular medium (CTR) or in the presence of 1.5 g/L methionine (MET) and/or Compound C to obtain partial AMPK inactivation (2 µM Compound C for HepG2 and 1.5 µM for Huh7). The experiments were performed at least in triplicate. (C, D) HepG2 or Huh7 were grown for 24 h in regular medium (CTR), or in the presence of high methionine and/or Compound C. Then they were starved for 24 h in the same medium without serum and migration was evaluated with a transwell assay for 24 h. (E, F) Colony formation assay of HepG2 or Huh7 grown in regular medium or in the presence of high methionine and/or Compound C. Experiments were performed in triplicate. * $p < 0.05$.

The Effect of High Methionine and Compound C is Specific for Liver Cancer Cells

Although Compound C has been extensively used to inhibit AMPK activity, it may also inhibit other kinases. To discern whether the effect of Compound C on growth inhibition in high methionine condition was specifically due to AMPK inhibition, we silenced the expression of AMPKα/α' subunits in HepG2 and Huh7 cells and tested their growth in the presence of high methionine in the medium (Figure 35A,B). We found that cells with siAMPKα/α' showed a reduced growth at 72 h in the presence of high methionine, thus, confirming that high methionine had a negative effect on growth when AMPK activity was low (either due to chemical inhibition or to reduction of the catalytic subunit). These data confirm that the effect of Compound C on growth rate was mediated by AMPK inhibition, and not by non-specific effects of the compound. Finally, to analyze whether the effect of high methionine and AMPK inhibition was specific for liver cancer cells or could be observed also on other cancer cell types, we performed the growth assay and the clonogenic assay on three cell lines deriving from different tumors: SW480 colorectal cancer cells, A549 lung cancer cells and MCF7 breast cancer cells. High methionine and/or Compound C had no effect on the growth of SW480 and A549 cells, while high methionine slightly reduced the growth of breast MCF7 cells also in combination with AMPK inhibition (Figure 35C). However, the ability of forming colonies from single cells was not impaired in none of the cell lines tested (Figure 35D), although in MCF7 cells high methionine induced the formation of smaller colonies (not shown). Thus, we can assume that the effect of this treatment on cancer associated phenotypes is specific for liver cancer cells.
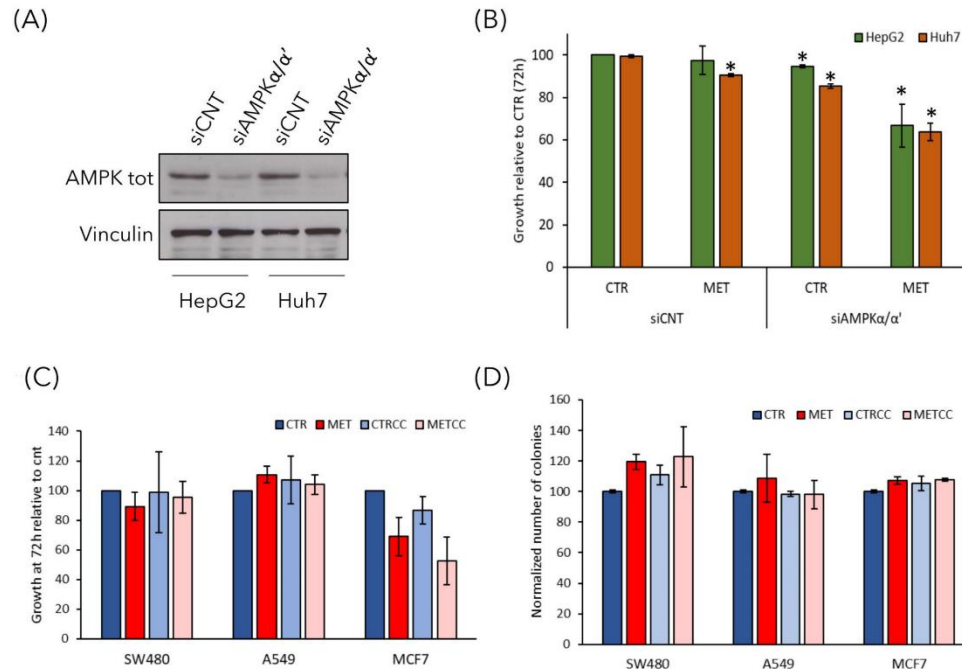
Figure 35. The effect of high methionine and AMPK inhibition is specific for liver cancer cells. (A, B) Gene knockdown for AMPKα/α' in HepG2 and Huh7 cells was achieved by siRNA. (A) The level of endogenous AMPKα/α' protein was detected by immunoblot by using anti-AMPK total antibody. anti-tubulin antibody was used as loading control. (B) Cell growth of HepG2 and Huh7 cells transfected with siCNT or siAMPKα/α' was monitored for 72 h in regular medium (CTR) or in the presence of 1.5 g/L methionine (MET). Cell growth is expressed as a ratio on the growth in control medium. * p < 0.05 compared with siCNT cells. (C) Cell growth of SW480 colorectal cancer cells, A549 lung cancer cells, and MCF7 breast cancer cells was monitored until 72 h in regular medium (CTR) or in the presence of 1.5 g/L methionine (MET) and/or 2 μM Compound C. Cell growth is expressed as a ratio on the growth in control medium. (D) Colony formation assay of SW480, A549, and MCF7 cells grown in regular medium (CTR) or in the presence of high methionine and/or 2 μM Compound C.

Concluding remarks

The role of methionine has been long investigated in many different fields [13]. Indeed, it is well known that methionine restriction extends lifespan in different model systems, from budding yeast to *Drosophila melanogaster*, *Caenorhabditis elegans*, and mammalian cells [302–305]. Methionine

restriction also affects the cardiovascular system [306] and bone development [307].

On the contrary, the relationship between methionine and human cancers progression is still very ambiguous, most probably because it is cancer specific. Different studies showed that methionine restriction delays cancer progression. This was reported for instance in colon and prostate cancer animal models [308,309], as well as in breast cancer in vitro and in vivo [310,311]. On the contrary, other reports indicate that methionine supplementation induces cell-cycle arrest and transcriptional alterations in breast and prostate cancer cells [312].

It was reported that S-adenosyl-methionine (SAM) supplementation inhibits liver cancer cell invasion in vitro [291], by inducing changes in the methylation state of DNA, that lead to downregulation of genes involved in growth and metastasis, already known to be upregulated in liver cancer cells. In addition, in a rat model of hepatocarcinogenesis [298], as well as in a mouse model for inflammation-mediated HCC [292], SAM administration exerted a chemopreventive effect on HCC development. However, although a short-term treatment with SAM showed positive effects in the mouse model, a long-term administration did not affect tumor growth and hepatocyte proliferation [292]. Here, we explored the combination of methionine administration (the precursor of SAM) and AMPK inhibition in vitro. AMPK is a dual role kinase, being either anti- or pro-tumorigenic depending on the context, on the stage of tumor development and on the cancer type [6]. We showed that, in liver cancer cells, high methionine concentration in the medium reduces cell growth inhibits colony formation and cell migration in two different liver cancer cell lines (Figure 34) and, remarkably, these phenotypes were increased when high methionine was

combined with AMPK inhibition (Figure 34 and Figure 35). This is perfectly in line with what we observed in budding yeast, where growth rate reduction due to methionine in the medium was largely dependent on the presence of an active Snf1/AMPK pathway [20]. Moreover, methionine induces an activation of Snf1/AMPK in *S. cerevisiae*, as we observe in liver cancer cells (Figure 33), highlighting that AMPK involvement in the response to methionine is a conserved feature in eukaryotic systems. An intriguing aspect of methionine response is the activation of the mTOR pathway (Figure 33), which is coherent with the reported effect of SAM (the first metabolite of methionine) on mTOR activation through SAM-sensor upstream of mTOR1 (SAMTOR) [11]. However, the intracellular level of most amino acids was downregulated in cells grown in high methionine (Figure 31), and this probably leads to the observed downregulation of proteins involved in translation and tRNA synthesis (Figure 28, Figure 29, Figure 31 and Figure 32) and to the reduction of growth rate (Figure 34). This condition—active mTOR with reduced translational capacity—reminds the condition of cycloheximide treatment, in which mTOR phosphorylates pS6K [313] although growth is impaired, thus, producing the effect of a counter circuit in the cell.

High methionine has also a strong effect on metabolome and proteome remodeling, as also reported in yeast cells [20], especially when combined with Compound C. In fact, reduction of intracellular amino acid levels and alterations in metabolites of the TCA cycle were found in both yeast and liver cancer cells. Interestingly, the observed increase of proteins and metabolites of the TCA cycle could be a direct consequence of methionine metabolism to homocysteine, which can be then converted to α-keto-butyrate and enter the mitochondria. However, in yeast cells, the effect of methionine on

mitochondrial functionality was much more evident, probably due to the fact that yeast cells have a fermentative metabolism in the presence of glucose. On the contrary, in human cells, which have a mixed respirative and fermentative metabolism, the effect on mitochondria better emerges by integrating metabolomics and proteomics data. These results, together with the reduction of polyamine levels (which are associated to growth rate), could explain at least in part the observed reduction of cancer phenotypes. Why does methionine metabolism have this anti-tumor role on liver cancer cell lines, contrary to other cancer cells? It should be noted that methionine metabolism in the liver is very peculiar, since the liver is the organ where most of the methionine is converted to S-adenosyl-methionine and where only the gene MAT1A is expressed. Therefore, most of the observed effects could be due to this liver-specific metabolism, although we cannot exclude the possibility that methionine could carry out also other functions more related to protein synthesis. In fact, Mato and Lu suggest that liver cancer cells, in contrast to normal non-proliferating, differentiated hepatocytes, tend to utilize methionine mainly for protein synthesis [295].

An interesting translational application of our results could be to directly increase methionine uptake through the diet, both in animal models and in human patients. Methionine should easily reach the liver, since it is the physiological organ where it is metabolized. It should have no side effect on normal hepatocytes, since SAM was shown to have negligible effects on primary untransformed liver cells [291]. Therefore, further investigations should explore the possibility that alterations in methionine dietary consumption, in combination with pharmacological treatments, could have clinically relevant outcomes in liver cancer patients.

Chapter 5

Engineering of S-Adenosyl-L-Methionine biosynthesis in Pseudomonas putida

Unpublished results

Engineering of S-Adenosyl-L-Methionine biosynthesis in Pseudomonas putida

Introduction

The aim of synthetic biology and metabolic engineering is to develop new processes for molecules of interest, exploiting the inherent versatility of Nature and in particular microbes. This idea arose from the necessity to reduce the ecological impact of classic petrochemical processes, but is nowadays moving also towards the production of new-to-nature compounds [314]. The economic and environmental sustainability of a process depends on several aspects: The type of feedstock, the supply chain, and the requirement of laborious downstream processes are only some of the factors that can determine the failure or the success of a biobased process [315].

A key aspect in the development of any bioproduction is the selection of a robust chassis able to cope with stresses. Indeed, the toxicity of substrates or by-products, harsh fermentation conditions, a high metabolic burden and several other stressors that can impair the efficiency of a cell factory and reduce yield, titer or productivity [316]. Among the most used hosts for engineering purposes, especially for proof-of-principal aims, the model organisms *S. cerevisiae* and *E.coli* can be found. This is mainly due to the deep understanding of their metabolism, genetics and availability of engineering tools. Nevertheless, in the last decade soil bacteria and in particular the Gram-negative bacteria *Pseudomonas putida* gained attention as a promising cell factory [317].

Environmental bacteria are constantly subjected to variation in the physicochemical condition, exposed to toxins and in competition with

predatory microbial species, because of this, they evolved a peculiar metabolic robustness and flexibility, as exemplified by *P. putida* ability to grow on broad range of carbon sources, including a variety of aromatic compounds [318].

P. putida's metabolism, as those of many other *Pseudomonads*, is characterized by a periplasmatic pathway for oxidation of sugars, including glucose. Glucose can be either directly phosphorylated to glucose-6-phosphate (G6P) or periplasmatic oxidized to gluconate and subsequently 2-ketogluconate, with a direct transfer of electrons on the electron transport chain and consequently ATP synthesis. Gluconate and 2-ketogluconate are then taken up into the cytosol and converted to 6-phosphogluconate (6PG) and converge into hexose assimilation pathways. Due to the lack of phosphofructokinase (Pfk) activity, *P.putida*'s glycolysis present a circular topology defined as the EDEMP (Entner-Doudoroff Embden-Meyerhof-Parnas) cycle. In this pathway, G6P can be converted either into glyceraldehyde 3 phosphate (G3P) and pyruvate through the Entner-Doudoroff pathways or metabolised through the pentose phosphate pathway (see Figure 38A for a schematic representation) [319]. The distribution of the flux through the pathways is dynamically adapted in function of the availability of nutrients and the growth phase [320], but its regulation is little understood. This peculiar glycolytic metabolism has been demonstrated to be the source of a high capability of NADPH production and partly explains *P. putida's* high resistance to redox stress [321]. Furthermore, the high availability of NADPH could be of particular interest for engineering purposes aiming to implant redox-expensive pathways.

These characteristics prompted different research groups to develop new technique to manipulate the genome of *P. putida* rapidly and precisely and

to expand the tool box for expression of heterologous genes. These achievements paved the way for the rational development of a *P. putida* chassis for synthetic biology and metabolic engineering purposes [317].

Nowadays paradigm for the engineering of microbial cell factory reflects a well-known paradigm of classical engineering and consists in four consecutive steps: design, build, test, and learn. The *Design-Built-Test-Learn* cycle (DBTLc) is the attempt to develop a cyclic rational workflow for the engineering of biological systems that goes beyond a "simple" trial and errors approach [22,322]. In the *Design* phase the microbial chassis and the fermentation conditions are chosen and the engineering strategy is developed: which and how much enzymatic activity must be obtained, which competing reactions must be knocked out and how to select for the engineered strain. In this first step, any available system-wide information represents a fundamental resource for the designing of a pathway coherently integrated into the metabolism of the host. In the *Build* phase the engineered strain is constructed taking advantage of the available synthetic biology tools, as defined in the *Design* step. The strain is then tested (*Test* step) for the desired biological function (e.g., yield, titer and productivity). In this step, omics analysis offers a general overview of the properties of the engineered system and can provide important information for the *Learn* phase. Here in the Learn phase, all available information from the previous steps (and cycles) is gathered and analysed, providing pivotal knowledge (e.g. enzymatic bottlenecks) for successive cycles of the DBTLc [22].

Despite the rational beyond this paradigm being robust and clear, metabolic engineers are still facing issues during its application: a complete run of the cycle generally takes from weeks to months, revealing the necessity for

further technological development to shorten the time-around of the cycle like the automation of the steps and for a more successful scale-up approaches [22,322].

Coupling SAM production with TCA cycle

During my external stay at the Novo Nordisk Foundation Centre for Biosustainability (NNF-CFB), I applied the *DBTLc* paradigm to the overproduction of S-adenosyl-L- methionine (SAM) in the microbial chassis *Pseudomonas putida*.

As highlighted in chapter 4, SAM is an essential metabolite involved in transmethylation reactions in all organisms. As we showed, unbalance in the production and consumption of SAM alters the metabolism of yeast and acts as a synergic factor for the treatment of hepatocellular carcinoma [20,323]. Moreover, SAM has a high pharmaceutical value, being used in the treatment of osteoarthritis and depression [24,324] and it is a valuable cofactor for the enzymatic production of antibiotics, flavours, fragrances and other fine chemicals (e.g. melatonin) [25–27]. Importantly, SAM is the only organic substrate involved in bio-halogenation reactions. The first fluorinating enzyme, fluorinase, was discovered in 2002 in Streptomyces cattleya, thanks to its ability to produce fluoroacetate and fluorothreonine as antibacterial compounds [325]. While fluorinases evolved probably to kill competing microorganism, their biochemical activity opens new biotechnological opportunities to develop biobased production of organofluorines.

This requires to face several bottlenecks: All known fluorinase exhibit poor catalytic activities, while fluoride, a substrate of the pathway, and fluorinated compounds, a product of the pathway, are highly toxic.
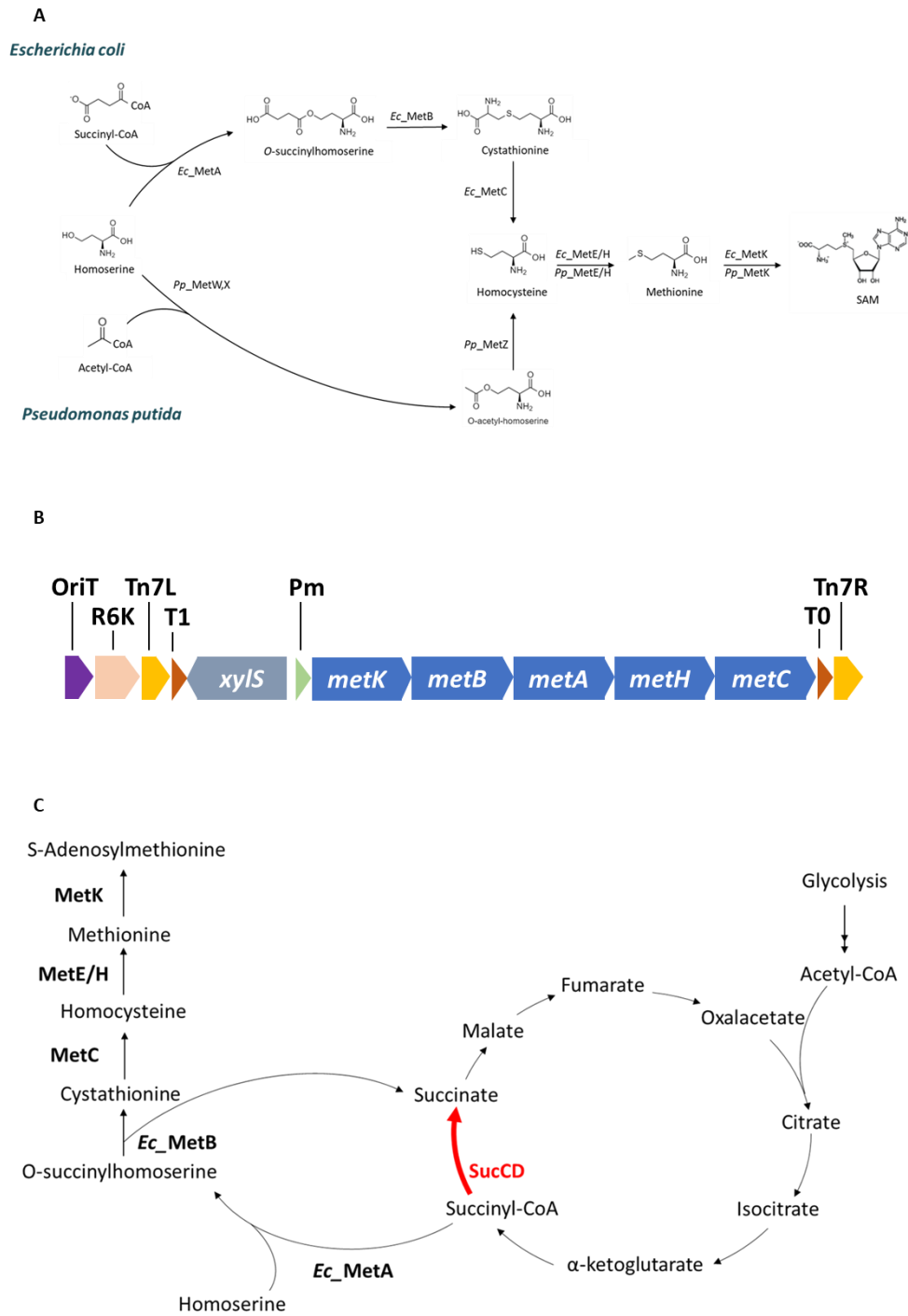
A

Escherichia coli

Pseudomonas putida

B

C

Figure 36. Caption in the next page

Figure 36. (A) Pathways for *de novo* synthesis of S-adenosyl methionine in *E. coli* and *P. putida.* They share conserved enzymatic activities last synthesis steps (*metE/H* and *metK*), while relying on different reactions in the first part of the pathways. (B) The artificial SAM synthesis operon on the plasmid pTn7-M. The integrative pTn7-M plasmid has been chosen as scaffold for the cloning of the genes for the synthesis of S-adenosyl-methionine. The construct carries also the gene encoding for the 3-methylbenzoate induced activator XylS and present one single XylS responsive promoter. (C) Schematic representation of the coupling between SAM engineered pathway and the TCA cycle. The gap in the TCA cycle at the level of succinyl-CoA conversion into succinate is bridged by MetA and MetB activities. Succinate is synthetized from O-succinylhomoserine with the consumption of homoserine and the production of cystathionine, further processed into S-Adenosylmethionine along the pathway.

Additionally, SAM concentration, the second substrate of the reaction, is tightly controlled and generally low in cells. Therefore, the aim of this project is to increase SAM production in *P. putida* in order to create a microbial chassis for the synthesis of SAM-derived compounds.

The engineering solution to fulfil this goal is based on the difference between de novo synthesis of SAM in *E. coli* and *P. putida*. The two pathways differ in the conversion of homoserine into homocysteine. In *E. coli*, MetA catalyses homoserine acylation consuming succinyl-CoA and producing succinylhomoserine. In *P. putida*, acetyl-CoA is the acyl donor in the conversion of homoserine into acetylhomoserine catalysed by MetX,W (Figure 36A) [265]. SAM de novo synthesis, being energetically expensive, is also highly transcriptionally and post-transcriptionally regulated. SAM responsive riboswitches repress *metE, metX, metA, metC* and *metB* [20]. While MetK and MetA are feed-back inhibited by their products and cobalamine represses the expression of metE [28,29,326].

To circumvent these regulations, we designed a synthetic operon in which *metA, metB, metC, metK* of *E. coli* and *metH* (encoding a cobalamin-dependent methionine synthase 50-times more active than MetE) of *P. putida* under the transcription control of the inducible regulator/promoter

pair *XylS/Pm*. These operon was cloned into the integrative cassette on the pTn7-M plasmid [327], with *metK* and *metA* carrying the mutations I304V and I296S, respectively to escape the negative feedback regulations (Figure 36B). Furthermore, all translational regulators (i.e., riboswitches) were replaced by synthetic parts.

This design allows for the genetic duplication of the SAM synthesis pathway in *P. putida* and opens the possibility to couple SAM synthesis to the TCA cycle: *metAB* production of succinate from succinyl-CoA can act as a bypass in a strain lacking *sucCD* and unable to complete the TCA cycle (Figure 36C). This will establish a conditional auxotrophy that will act as selective pressure against revertants, since the heterologous pathway is required to overcome the stall of the TCA cycle. Moreover, the high flux carried by the TCA cycle can drive a higher flux towards the production of SAM, possible increasing SAM titers.

According to the design, we deleted *sucC* and *sucD* in *P. putida* KT2440 by homologous recombination (Figure 36C) [327]. However, the *ΔsucCD* strain did not show any relevant growth defect on a variety of different carbon sources (data not shown), ruling out any possible coupling with the heterologous pathway. This lack of phenotype might be due to the existence of anaplerotic reactions able to replenish the TCA cycle with succinate. We therefore focused on *scpC* and *aceA*, responsible for succinate production from proprionate and isocitrate, respectively (Figure 37A). Interestingly, the *ΔsucCD ΔscpC ΔaceA* strain displayed a mild growth defect when grown in a 96-multiwell-plate in minimal medium (de Bont) supplemented with either 20 mM glucose, 26.6 mM citrate or 34 mM succinate (Figure 37B, 37D, 37E).
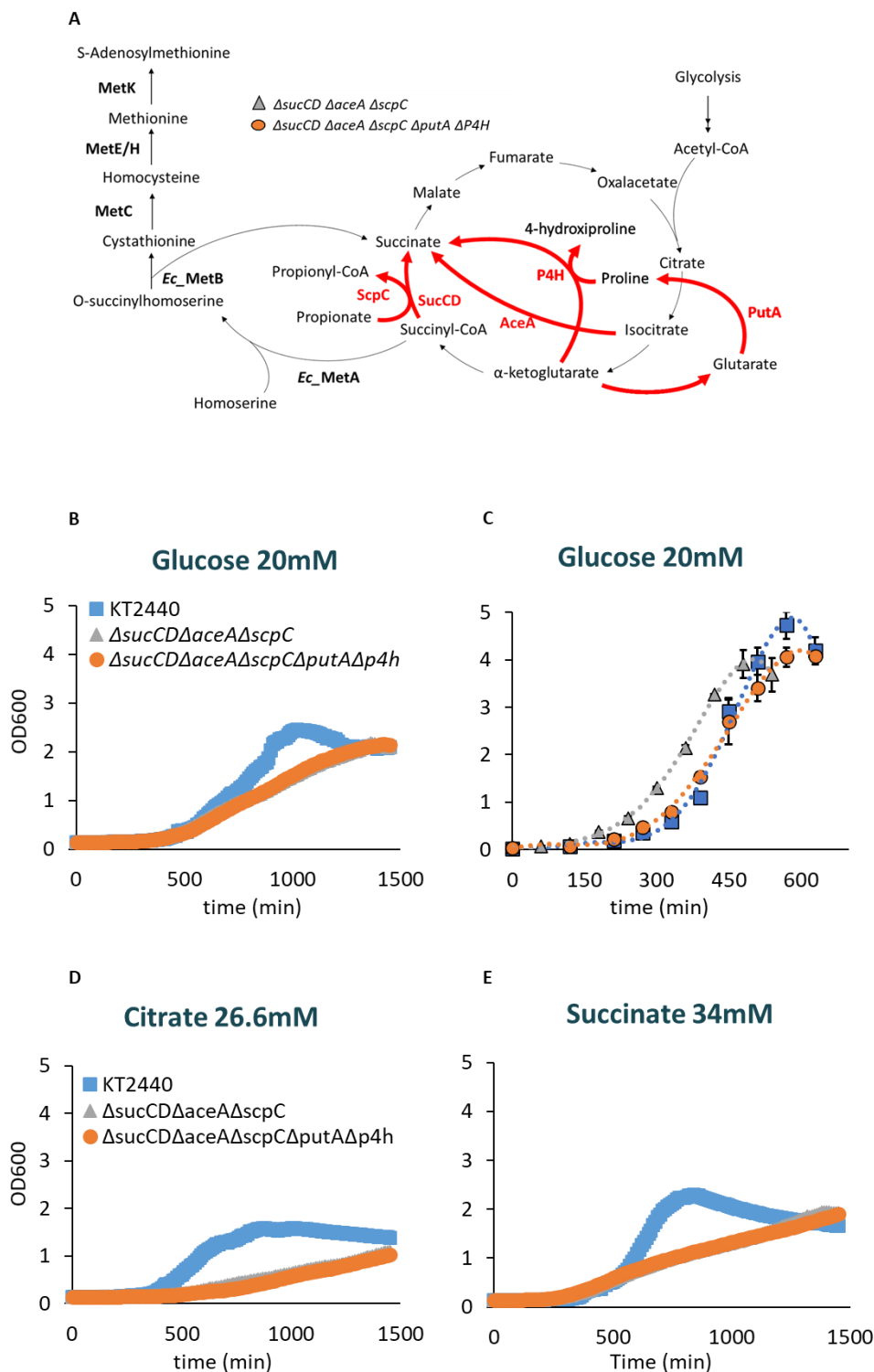
Figure 37. Caption in the next page

Figure 37. (A) Schematic representation of the coupling between SAM heterologous production pathway and the TCA cycle. Red arrows display the reactions (with corresponding enzymes) deleted to achieve a growth defect sufficient to establish a conditional auxotrophy. (B, D, E) Growth curves of wild type (KT2440), *ΔsucCD ΔscpC ΔaceA* and *ΔsucCD ΔscpC ΔaceA ΔputA ΔP4H* strains in 96 multiwell plates. Wild type is shown in blue, while *ΔsucCD ΔscpC ΔaceA* and *ΔsucCD ΔscpC ΔaceA ΔputA ΔP4H* are respectively shown in orange and grey (with the curve of the triple knockout overlapping with the quintuple one). The growth has been conducted in minimal de Bont medium supplemented with 20 mM glucose or 26.6 mM citrate or 34 mM succinate as carbon source. (B) Growth curve of wild type (KT2440), *ΔsucCD ΔscpC ΔaceA* and *ΔsucCD ΔscpC ΔaceA ΔputA ΔP4H* strains in flask. The concentration of the different carbon sources has been chosen equilibrating the available electron moles. Each condition has been assayed in triplicates.

Yet, this phenotype was not conserved when cells were grown in flask in presence of 20mM glucose (Figure 37C). Therefore, the phenotype is not sufficient to allow for the coupling.

In *E. coli*, the deletion of the α-ketoglutarate dehydrogenase *(ΔsucA)*, the isocitrate lyase *(ΔaceA)*, and the proline dehydrogenase (*putA*) completely impair cell growth [328]. This growth defect is abolished by the overexpression of the proline-4-hydroxilase/ α-ketoglutarate oxigenase, P4H, responsible for the synthesis of α-ketoglutarate from hydroxylated proline [328].

Following this line of evidence, we deleted *putA* and the P4H orthologue *PP_5159* in combination with *ΔsucCD ΔscpC ΔaceA* (Figure 37A). However, the *ΔsucCD ΔscpC ΔaceA ΔputA ΔP4H* did not show any additional growth defect when compared with the triple knockout (Figure 37B-E) suggesting that the metabolic network around the TCA cycle in *P. putida* is more robust than in *E. coli*.

To investigate which reactions can sustain the TCA cycle in the triple knockout, we carried out flux balance analysis (FBA) on the genome scale metabolic network of *P. putida* (iJN1411) and compared it to the metabolism subtracted of the reactions catalysed by SucCD, AceA and ScpC. In the

simulation, *ΔsucCD ΔscpC ΔaceA* showed a strong increase in the flux through the pentose phosphate pathway, which is associated with a high production of NADPH (Figure 38A). According to the simulation, this increased NADPH production balances the reduced production of NADH, and therefore ATP, from the incomplete TCA cycle through the activity transhydrogenase activity (Figure 38A). Furthermore, the simulation counterbalances the decreased production of succinate raising the flux through the Kdo 2 hexa acyl lipid A hydroxylase (LIPAH), an enzyme involved in lipopolysaccharide biosynthesis, consuming α-ketoglutarate and producing succinate (Figure 38A).

These results strongly suggest that the growth defect of the knockout strain is due to a reduced production of ATP caused by the stall of the TCA cycle. Therefore, the limiting factor for growth is ATP, and not succinate production, that can be replenished through other anaplerotic reactions. Nevertheless, *P. putida* cells grown in glucose have been reported to poorly express the transhydrogenase [329], suggesting that the distribution identified *in silico* could not be biologically relevant.

To verify the FBA results, we grew wild type and *ΔsucCD ΔscpC ΔaceA* on 1-^{13}C glucose and evaluated the mass isotopomer distributions (MIDs) of the amino acids derived from to the pentose phosphate pathway. As show in Figure 38B, there is no significant difference between the MIDs of tyrosine, serine and phenylalanine in the *ΔsucCD ΔscpC ΔaceA* strain and in the wild type. This confutes the high flux value simulated for the pentose phosphate pathway in the *ΔsucCD ΔscpC ΔaceA* and rejects the hypothesis that transhydrogenase can cope with a putative decrease in NADH and ATP synthesis (Figure 38A,B).

A

B

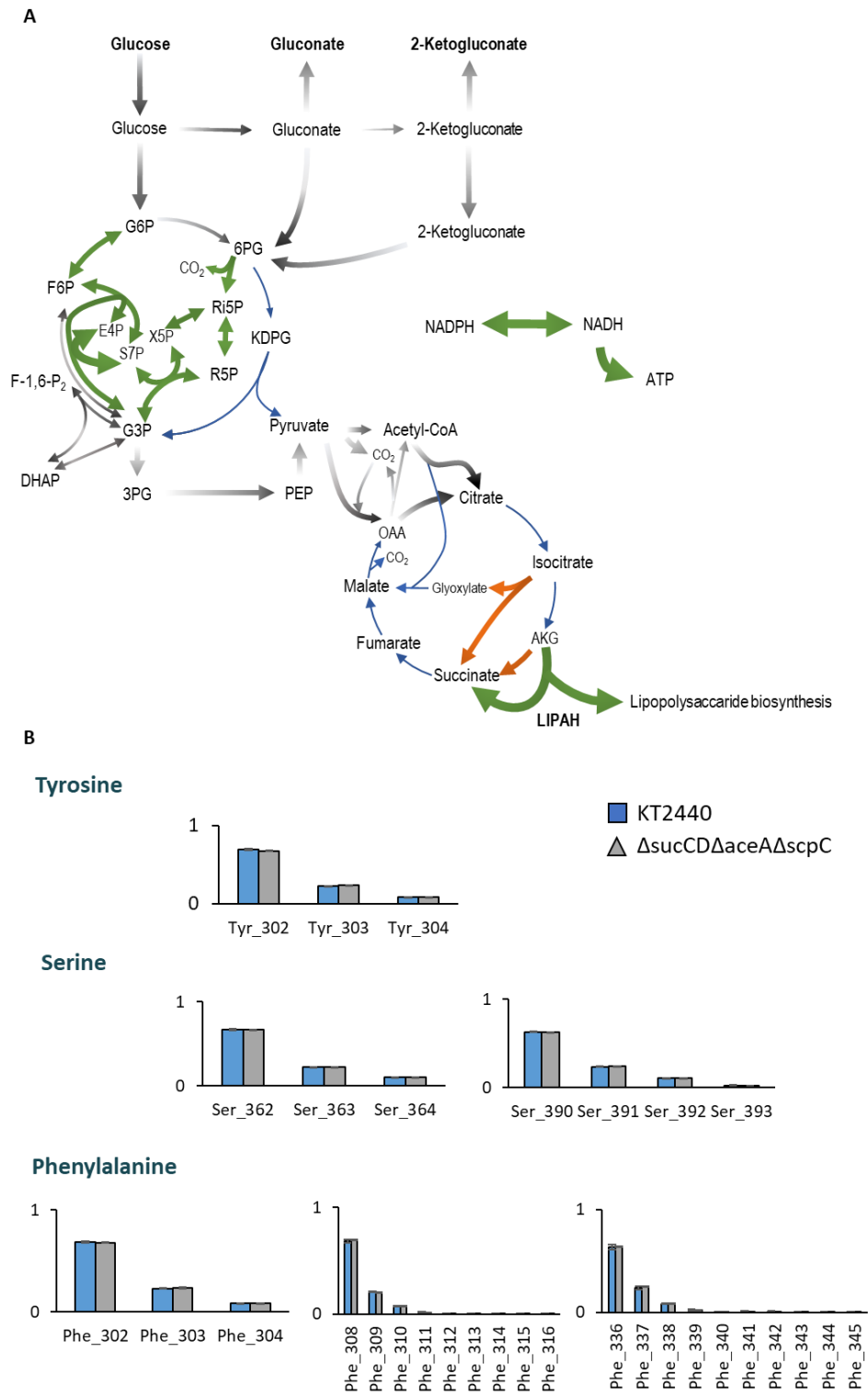**Figure 38.** Caption in the next page

Figure 38. (A) Representation of the fluxes distribution for the central metabolism of *P. putida* in the *ΔsucCD ΔscpC ΔaceA* strain. The figure shows the comparisons between metabolic fluxes calculated on *P. putida* the genome scale metabolic network (iJN1463) for the wild type and the triple knockout strain. Green and thick arrows show consistent increases in the fluxes, grey ones represent mild increase while no changes are shown by blue and thin arrows. (B) MIDs of amino acids derived from the pentose phosphate pathway. Cells have been grown in biological triplicates in minimal de Bont media supplemented with 100% 1-^{13}C Glucose.

Future perspectives

The first round of the DBTLc for SAM overproduction in *P. putida* allowed us to understand that TCA cycle in this organism is more robust than in *E. coli.* This is in line with the fact that *P. putida*, as environmental bacteria, as a higher overall robustness than the enterobacteria *E. coli*. In general, this is a pivotal point to keep in mind during the design of new engineering strategies. *E. coli* cannot be considered a model organism for any Gram-negative bacteria and pilot projects, or preliminary experiment run in this organism are not necessarily translatable to other species.

The second round of the design for coupling of SAM overproduction with the TCA cycle was based on the analysis of the connectivity in the genome scale metabolic network of *P. putida.* Using Cytoscape (version 3.8.2), we selected the secondary level of interactions between succinate and the rest of the network and calculated the stress value of each node. Here, we identified those reactions whose deletion is more probable to affect the overall connectivity of the network and, after a manual curation of the results, we defined sets of putative targets responsible for the replenishment of succinate in the *ΔsucCD ΔscpC ΔaceA* strains (Table 6). The identified targets will be tackled in groups using the CRISPR/Cas9 genome base editor technique [330] in order to rapidly screen the metabolite(s) mainly involved in the synthesis of succinate.

In such a way, we aim to obtain a strain with a decreased growth on glucose due to the disruption of the TCA cycle. This will allow us to establish the coupling between the TCA cycle and the heterologous pathway for SAM production. Furthere omics analysis will allow for the fine tuning of the metabolic fluxes through these pathways and will help the development of a *P. putida* chassis for the production of SAM-derived compounds.

α-Ketoglutarate	Succinyl-CoA	SuccinylHomoserine	Fumarate	Spared
PP_4222	PP_3952 (pcaJ)	PP_0659 (metB)	PP_2095 (pyrD)	PP_2334 (mmgF)
PP_0230 (atsK)	PP_3951 (pcaI)	PP_4594	PP_1426 (nadB)	PP_4475 (astE)
PP_2909 (csiD)	PP_3122 (atoA)	PP_2528	PP_4193 (sdhC)	PP_1525 (dapE)
PP_2423 (lpxOA)	PP_3123 (atoB)		PP_4192 (sdhD)	
PP_4570			PP_4191 (sdhA)	
PP_0213 (gabD-I)			PP_4190 (sdhB)	
PP_4422 (gabD-II)				
PP_2488 (sad-I)				

Table 6. List of targets identified analysing the topology of *P. putida* genome scale metabolic network. The targets are grouped accordingly the metabolites from which succinate is synthetised.

Discussion and

Future perspective

The present thesis shows that the knowledge and technologies develop to understand and manipulate biological systems can serve three purposes: understand the core mechanism governing the systems, ameliorate pathological conditions and engineer living organisms to produce compounds of interests.

As highlighted in the introduction, these goals must be pursued being aware that every living organism has been selected to be fit and robust [1]. The molecular mechanism governing a pathway cannot be fully understood without considering their general control strategy. Valuable therapeutic approaches must be developed having in mind that robustness and fragility are the opposite sides of the same coin. Successful engineering strategies require a deep understanding of reaction network and control solutions of the host metabolism. All these aspects are exemplified by the works presented in this thesis and highlight gaps and future directions of this research fields.

The investigation of the molecular mechanism regulating cellular metabolism is clearly lacking a system-wide understanding of the influence of metabolism on protein activity through protein-metabolite interactions (Figure 6, Chapter 1). Metabolites of the central carbon metabolism have been proved to alter the activity of enzymes and protein kinases through allosteric regulations. Anyway, the magnitude of this phenomenon, and the molecular details of all the interaction taking place in a cell are still far from being exhaustively described.

This lack of knowledge is slowing down the development of comprehensive description of the regulation of metabolic fluxes and of the crosstalk between signalling pathways [186,331]. Hence, this is affecting the

understanding of the molecular mechanism underling pathological conditions and the engineering of cells for biotechnological purposes.

Recently, Prof. Picotti and co-workers started to investigate protein conformational changes induced by interaction with metabolites in *E. coli* and *S. cerevisiae* crude extracts. Their approach is based on a partial digestion of the proteome and detection of the produced peptides by MS analysis [36]. Proteins interacting with metabolites and undergoing to conformational changes result to have an altered accessibility for protease and, therefore, a varied abundance of peptides involved in the interaction or in the conformational change [36]. This strategy allowed for the identification of novel PMIs between metabolites and enzymes of the central carbon metabolism but, more importantly, highlighted that only half of the putative interactions involved metabolic enzymes [36]. Being this the most promising approach, several others have been attempted either fishing for proteins interacting with a specific metabolite or the other way round [34]. Nevertheless, these studies focused on the interaction between metabolites and enzymatic proteins and they all required in vitro validation. Interestingly, computational approaches proved that putative regulatory PMIs can also be identified integrating omics data with kinetic models [332]. Interestingly, a study inhibiting the 1513 metabolism-related genes in *E. coli* suggests that metabolites involved in allosteric regulation present a strong variation in their concentrations when their interactors are silenced, opening to the definition of an interaction map based on genetic and metabolomics data [333].

The results presented in chapters 3 and 4 show that the use of model organisms is pivotal for the discovery of potential new therapeutical solutions. The combination of methionine supplementation and AMPK

inhibition significatively ameliorate the aggressiveness of two hepatocellular carcinoma cell lines. In the meanwhile, the *V. unguicolata* extracts proved to extend the life span of several model organism, reducing the α-synuclein toxicity in models of neurodegenerative diseases. Anyway, preclinical studies must be validated by clinical study before reaching the patients and actually bring advantage to the society. This process brings to the market approximatively the 10% of compounds that enter the trials and takes from 10 to 15 years with a cost between 1.5 to 2.0 billion USD [334]. Two key factors that strongly decrease the success rate of clinical trials are the selection of suitable patients and their enrolling in a useful time for the trial [334]. To face these issues, FDA approved the use of artificial intelligence techniques improving the selection of patients, finding patterns in omics database and literature depositary, and automating the patients monitoring [334].

Besides the use of these sophisticated correlations, new techniques blending pharmacokinetic and pharmacodynamic modelling with system biology techniques lead to the development of in-silico clinical trial (ISCT) methodologies [335]. The vision of this approach is to reduce and refine animal and human trials using patient-specific models, providing solutions for more economically and ethically sustainable trial processes [335]. Physiological models for the assessment of pro-arrhythmic cardiotoxicity proved to be suitable to replace animal experimentation [336]. Even more interestingly, an in silico artificial pancreas describing a population of 300 virtual patient has been approved by the FDA for the test of new control for the regulation of glucose level in type 1 diabetes patients [337].

These examples prove that the deep understanding of the molecular mechanism and control strategies regulating biological processes allow for

the development of reliable models useful for the development of new therapeutical solutions.

These approaches are inherently less applicable to diseases whose molecular origin is poorly understood. In these cases, phenotypic screening proved to be a good solution for the identification of first-in-class drugs through the screening of compounds library [338]. These assays consist in testing the activity of libraries of small-molecules on disease models to evaluate their effect on disease-related phenotype [338].

In the past decades, this top-down approach identified more first-in-class active compounds than target-based screening [339]. This is partly due the tackling of the diseased phenotype exploring different mechanisms of action, without preliminary hypothesis about the biological processes that require to be modulated [338]. Moreover, the observation that one drug interacts on average with six molecular target support the use of phenotypic screening in favour of target-based assays [340].

The compound-based approach is applied on a plethora of biological models such as cell lines, iPS and patient-derived primary cell lines. Microorganisms such as model yeasts or bacteria are generally less exploited in these kind of studies (except than in new antibiotic discovery), however, they may represent strategical platform for preliminary screening. Being cheaper, faster and easier to manipulate they could serve in the discarding of compounds with general toxicity, instability and those target of resistance mechanisms. Moreover, the availability of genome-scale libraries of knockout strains could help in the identification of the molecular target of the selected compound or allow for the identification of new drug to gene interactions.

Similarly to new drugs approvement, also the commercialization of biotechnological processes present a high rate of failure [341], such that only the 2% of the global commodity chemicals are obtained through bioprocesses [315]. Among the reasons for this low rate of success, there is the difficulty in scaling up promising strains from the laboratory to the industry. Strains developed in lab-scale fermenters hardly ever behave the same in big scale due to the fluctuation in the cultivation environment, genetic drift over long-term growth and differences in the general physiology of the strain [341]. To address this issue, high-throughput sequencing and omics analysis could help the characterization of producing strains, as well as the modelling of large-scale fermenters conditions can drive strains design [341].

Moreover, the economic and environmental sustainability of a biobased process can be influenced by several other aspects such as the cost of the feedstock, the supply chain, the consumption of field and waters and the competition with petrochemical processes [315]. To consider all these parameters, it has been recently proposed to combine the assessment of economic sustainability (TEA) with the assessment of environmental sustainability (LCA). This allows to identify the contribution of each factor to the general sustainability, highlighting the aspects that must be improved. Hence, to run this analysis at the initial step of the strain optimization enables to adjust the strain design to meet key characteristics, increasing the success probability of the scaled-up process [315].

Concluding, the future direction of all these branches of biological research is characterized by the integration of different type of data (by the means of computational approaches) to provide a system level interpretation of biological processes. This will require an increasing understanding of the

molecular details but considering that every component is integrated in a wider system that influence and is influenced by its functioning.

Materials and methods

Strains, cell lines and cell culture methods

Strains used in this thesis are listed in Table 7. Yeast cells were grown at 30 °C in synthetic media containing 2% and 5% glucose (Merck Life Science, Milan, Italy) or 2% ethanol (Merck Life Science, Milan, Italy), 6.7 g/L yeast nitrogen base (Formedium, Hunstanton, England), and 50 mg/L of the required amino acids (Merck Life Science, Milan, Italy). For the growth in presence of natural extracts, the latter were dissolved in the medium at a concentration of 0.2% or 0.5% and filtered through 0.22 μm filters. For shift-up experiments, cells were grown overnight in 2% ethanol. At the mid-exponential phase (cellular concentration 0.5–0.8 OD/mL), glucose was added at a final concentration of 2%, and samples were collected at different timepoints, quenched, and extracted as reported below. The ras2Δ, tpk1Δtpk2Δtpk3Δyak1Δ, and pde2Δcyr1Δyak1Δ strains, which are unable to grow on ethanol, were pre-cultured overnight in 2% glucose media and then transferred to 2% ethanol media for 2 h before the shift-up experiment.

Pseudomonas putida strains were grown at 30° C de Bont media (3.88g/L K_2HPO_4, 1.63g/L NaH_2PO_4, 2.00g/L $(NH_4)_2SO_4$, 0.1 g/L $MgCl_2·6H_2O$, 10mg/L EDTA, 2mg/L $ZnSO_4·7H_2O$, 1mg/L $CaCl_2·2H_2O$, 5 mg/L $FeSO_4·7H_2O$, 0.2mg/L $Na_2MoO_4·2H_2O$, 0.2mg/L $CuSO_4·5H_2O$, 0.4 mg/L $CoCl_2·6H_2O$, 1mg/L $MnCl_2·2H_2O$) supplemented with 20mM glucose or 26,6mM citrate or 34mM succinate as carbon source. Growth curves conducted in 96-multiwell plates were followed at OD600 in a Synergy™ MX microtiter plate reader (BioTek Instruments Inc., Winooski, VT, USA). Growth curves in shaken flask have been conducted at 200 rpm in a MaxQ™ 8000 incubator (ThermoFisher Scientific, Waltham, MA, USA).

HepG2 liver cancer cells, SW480 colorectal cancer cells, A549 lung cancer cells, and MCF7 breast cancer cells were obtained from ATCC. Huh7 liver

cancer cells were provided by the Japanese Collection of Research Bioresources (JCRB) Cell Bank.

HepG2, Huh7, SW480 and A549 cells were cultured using RPMI1640 supplemented with 10% (v/v) FBS, 2 mM L-glutamine, 100 U/mL penicillin, and 100 µg/mL streptomycin. MCF7 were cultured using EMEM/NEAA supplemented with 10% (v/v) FBS, 2 mM L-glutamine, 100 U/mL penicillin, and 100 µg/mL streptomycin. SH-SY5Y human neuroblastoma cells were cultured at in complete medium (50% HAM, 50% DMEM, 10% fetal bovine

Strain	Genotype	Source
W303 1a		OpenBiosystem
CDC25^{T1490P}	W303-1a cdc25::CDC25^{T1490P}	Peeters et al., 2017
ras2Δ	BY472 *ras2::KanMX*	This work
tpk1Δtpk2Δtpk3Δyak1Δ	*W303-1a tpk1::ADE8 tpk2::HIS3 tpk3::TRP1 yak1::LEU2 ura3-52 leu2-3,112 trp1 ade8*	Van De Velde et al., 2008
pde1Δcyr1Δyak1Δ	*W303-1a pde2::TRP1 cyr1::KanMX yak1::LEU2*	Van De Velde et al., 2008
Hxt-Null	CENPK2C MATa *MAL2-8c SUC2 hxt17 ura3-52 gal2::loxP stl1::loxP agt1::loxP ydl247w::loxP yjr160c::loxP hxt13::loxP hxt15::loxP hxt16::loxP hxt14::loxP hxt12::loxP hxt9::loxP hxt11::loxP hxt10::loxP*	Elbing et al., 2004

	hxt8::loxP hxt514::loxP *hxt2::loxP* *hxt367::loxP*	
Hxt1 only	HXT7prom-HXT1-HXT7term *ura3-52::URA3*	Elbing et al., 2004
Hxt7 *only*	HXT7prom-HXT7-HXT7term *ura3-52::URA3*	Elbing et al., 2004
Tm6*	HXT7prom-TM6(HXT1 bp1-741, HXT7 bp742-1713)-HXT7term *ura3-52::URA3*	Elbing et al., 2004
CENPK2C	*leu2-3 ura3-52 trp1-2898 his3-1 MAL2-8C SUC2 HXT17*	Elbing et al., 2004
pfk1Δpfk2Δ	CENPK2C *pfk1::KanMX pfk2::HPH*	This work
CENPK JT4	Mat*a LCR1*	Kummel et al., 2010
pfk1Δpfk2Δ	CENPK JT4 *pfk1::KanMX pfk2::HPH*	This work
pfk1Δpfk2Δ	W303-1a *pfk1::KanMX pfk2::HPH*	This work
Snf1-TAP	BY4741 SNF1-TAP *his3Δ1 leu2Δ0 met15Δ0 ura3Δ0*	OpenBiosystem
BY4742	MATα *his3Δ1 leu2Δ0 lys2Δ0 ura3Δ0*	Euroscarf
snf1Δ	BY4742 MATα *his3Δ1 leu2Δ0 lys2Δ0 ura3Δ01 snf1::HPH*	This study
atg1Δ	BY4742 MATα *his3Δ1 leu2Δ0 lys2Δ0 ura3Δ01 atg1*::KanMX	This study
ras2Δ	BY4742 MATα *his3Δ1 leu2Δ0 lys2Δ0 ura3Δ01 ras2*::KanMX	This study

tor2Δ	BY4742 *MATα his3Δ1 leu2Δ0 lys2Δ0 ura3Δ01 tor2*::KanMX	This study
wt [empty]	BY4742 MATα *his3Δ1 leu2Δ0 lys2Δ0 ura3Δ0* [pYX242]	This study
wt [αSyn]	BY4742 MATα *his3Δ1 leu2Δ0 lys2Δ0 ura3Δ0* [pYX242-SNCA]	This study

Table 7. List of yeast strains used in this thesis.

serum, 3 mM glutamine, 100 units/ml penicillin and 100 µg/ml streptomycin). Cells were maintained at 37 °C in a humidified 5% CO_2 incubator. Methionine was dissolved in water at 45 mg/mL and added at a final concentration of 1.5 mg/mL to RPMI1640 medium; in the control medium, the same amount of water was added. Compound C (Calbiochem, San Diego, CA, USA) was dissolved in DMSO and added to the medium at a final concentration of 2 µM for HepG2, SW480, A549, and MCF7 cells, and at 1.5 µM for Huh7 cells.

Wild type *Drosophila melanogaster* (Canton S) was kindly provided by Dr Daniela Grifoni (University of Bologna, Italy). Flies were maintained at constant temperature (25°C) and humidity (60%) with a 12/12 h light–dark cycle. Flies were reared on Formula 4-24 ® media (Carolina Biological, Burlington, NC, USA). The composition of this diet, as indicated by the manufacturer, is as follows: oat flour, soy flour, wheat flour, other starches, dibasic calcium phosphate, calcium carbonate, citric acid, niocinamide, riboflavin, sodium chloride, sodium iron pyrophosphate, sucrose, thiamine, mononitrate, brewer's yeast, emulsifier preservatives, mold inhibitor, food colouring. The Formula 4-24 diet requires separate application of yeast pellets (*Saccharomyces cerevisiae*) and saturation of this dry media mixture

with water. After eclosion, males and females emerged within 1-2 day were allowed to mate freely for two days before female separation into vials containing 1 g Formula 4-24 Instant Drosophila Medium (Carolina) soaked with 4 ml water containing 0.5% or 0.2% bean extract. A total of 20 flies were placed in each vial. Female flies emerging within a 2-day period were collected under FlyNap (Carolina) anaesthesia. A total of 600 fruit flies were divided into 3 groups: control group, flies supplemented with 0.2% bean extract and flies supplemented with 0.5% bean extract. Flies were transferred into vials containing fresh food every 2-3 days and the number of living flies was counted. This was repeated until all flies had died. Kaplan-Meier survival curves were generated for lifespan assessment.

Standard procedures for *C. elegans* strain maintenance were followed [342]. The strain used in this study, JZF142 [pdat-1::hαSyn; pdat-1::DsRed], was kindly provided by Prof. J. Feng (Case Western Reserve University, US) [45]. The *C. elegans* strain was grown on Nematode Growth Medium (NGM) containing agar, seeded with *E. coli* OP50 at 20°C. Lyophilized extract *from V. unguiculata* was solubilized in sterile distilled water at two dilutions, 2% or 5% w/V, and sterilized with 0.22μm filter. α-synuclein expressing animals were exposed to the following treatments: 0.2% or 0.5% of *V. unguiculata* extract, water as negative control (mock) and 3 mM valproic acid (VA) as positive control [46]. *C. elegans* animals at L4 developmental stage were transferred into 12-well plates with NGM agar containing the different conditions as quadruplicates and allowed to become adults and lay eggs. After 14 hours the adults were discarded and the synchronized F1 progeny was allowed to grow in the presence of chronic treatments. F1 animals have been transferred every 3 days on new plates with treatment, until the day

of analysis, to maintain them well fed and separated from the next generation.

Small-Interfering RNA-Mediated Gene Silencing

To silence AMPK α/α', we used RNA interference by using small-interfering RNA (siRNA). Reverse transfection was performed on HepG2 and Huh7 cells with control siRNA (control siRNA-C, Santa Cruz Biotechnology) or siAMPKα/α' (Santa Cruz Biotechnology, Heidelberg, Germany) specific oligos by using the Lipofectamine 2000 reagent (Invitrogen, Carlsbad, CA, USA). AMPKα/α' expression was detected by immunoblotting to confirm the silencing achievement.

Growth curves, CLS and MTT test

Growth curves of mammalian cells were performed plating 1.5×10^5 cells in 6 well plates, the day after the medium was changed (control medium, high methionine, Compound C or High methionine and Compound C). Cells were counted at t = 0, 48 h and 72 h.

Chronological life span of yeast strains was carried out growing cells in liquid medium until mid-late exponential phase. Cultures were then inoculated into flasks containing medium in the presence or absence of the natural extracts (0.2% or 0.5% as indicated in each experiment). Survival was assessed by propidium iodide staining (PI) at the indicated time points with the Cytoflex cytofluorimeter (Beckman Coulter) and analysed with the Cytoflex software. For some experiments, survival was also confirmed by colony-forming units (CFUs) after 2 days of incubation at 30°C on YEPDA agar plates.

Viability of mammalian cells was assessed with MTT assay optimized for the SH-SY5Y cell line. Briefly, SH-SY5Y cells were seeded into 96-well plates at a density of 10000 cells/well in fresh complete medium and grown for 24 h. Then, cells were exposed for 48 h to 5 µM α1synuclein obtained at different times of aggregation in the presence or in the absence of the *Vigna unguiculata* extract. Cells were also treated with the corresponding concentrations of extract used in the aggregation of α-synuclein and the viability was similar to that of untreated control cells. After 48 h of incubation, the culture medium was removed and cells were incubated for 1 h at 37°C in 100 µl serum-free DMEM without phenol red, containing 0.5 mg/ml MTT. Then, 100 µl of cell lysis solution (20% SDS, 50% N,N-dimethylformamide) was added to each well and samples were incubated at 37°C for 2 h to allow complete cell lysis. Absorbance values were measured using iMARK microplate reader (Bio-Rad) at 595 nm. Final absorption values were calculated by averaging each sample in triplicate after blank subtraction. Statistical analysis of the data was performed by using one-way analysis of variance (ANOVA).

Migration and clonogenic assays

Migration of mammalian cell was assessed using transwell permeable supports (Costar) with 8.0 µM filter membranes. Cells were treated with high methionine and/or Compound C for 24 h, and then serum starved for 24 h. 5×10^4 HepG2 cells and 3.5×10^4 Huh7 cells were resuspended in 100 µL of serum free medium (always in the presence or absence of high methionine and/or Compound C), plated onto each filter and 500 µL of complete medium (containing 10% FBS) were placed in the lower chamber. After 24 h, filters were washed, fixed and stained with 0.5% Coomassie brilliant blue (in

10% acetic acid, 45% methanol). Cells on the upper surface of the filters were removed with cotton swabs. Cells that had invaded to the lower surface of the filter were counted under the microscope.

For clonogenic assay a total of 2500 cells were plated in a 6 well plates, treated with high methionine and/or Compound C for 10–15 days (the medium was changed every 3–4 days). Then, colonies were fixed with 70% ethanol for 5 min, stained with 0.5% crystal violet in 10% ethanol for 15 min, finally, washed with water and manually counted.

ROS determination

Intracellular reactive oxygen species (ROS) were determined using the fluorescent probe 2',7'– dichlorofluorescein diacetate, acetyl ester (CM-H2 DCFDA; Molecular Probes), a cell-permeant indicator for ROS that becomes fluorescent upon removal of the acetate groups by cellular esterases and oxidation. SH1SY5Y cells were plated on 96-well plates at a density of 10000 cells/well and exposed for 48 h to the α1synuclein samples. Then, 10 μM DCFDA in DMEM without phenol red was added to each well. The fluorescence values at 538 nm were detected after 30 min by Fluoroscan Ascent FL (Thermo-Fisher). Cells were also treated with the corresponding concentrations of extract used in the aggregation of α-synuclein and ROS levels resulted similar to that of untreated control cells. Statistical analysis of the data was performed by using one-way analysis of variance (ANOVA).

Measurement of glucose consumption

Yeast cells in the exponential phase of growth were sampled by centrifugation, collecting the supernatants. Glucose concentration at each timepoint was measured using the D-Glucose HK/G6P DH Kit (Megazyme,

Bray, Ireland), according to the manufacturer's instructions. Glucose consumption rate (mmol/g × h) was calculated as the angular coefficient of the correlation between glucose concentration (mmol/mL) and cellular concentration, corrected for the cellular dry weight (mg/mL) and time (h).

Measurement of Drosophila body weights

Changes in body weights were used as an indicator of the food intake. Flies were fed on standard diet with and without bean extract for 30 or 45 days. For each condition (0.2% bean extract supplementation and control), five vials containing 20 flies/vial were counted. Flies in each group were anesthetized by FlyNap (Carolina) and then weighed on a balance. The mean body weights of the flies in each group were calculated.

Protein extraction, cell fractionation and immunoblotting

For protein extraction from yeast equal amounts of cells (OD) were collected and quenched using TCA 6% (Merck Life Science, Milan, Italy) and lysed in lysis buffer (6M UREA, 1% SDS, 50 mM Tris-HCl pH7.5, 5 mM EDTA). To assess the Snf1/AMPK phosphorylation state, crude extracts were obtained breaking yeast cells with acid-washed glass beads (Merck Life Science, Milan, Italy) and 10 vortex/ice cycles of 30 sec each. Crude extracts were denatured in SDS sample buffer (40% glycerol, 20% β-mercaptoethanol, 9.2% SDS, 0.25 mM Tris-HCl pH 6.8, 0.01% BBF) and heated for 5 min at 95 ∘C. Western blot analysis was conducted with anti-phosphoT172-AMPK antibody (Cell Signalling, Danvers, MA, USA), anti-His antibody (Merck Life Science, Milan, Italy), and anti-TAP antibody (Thermo Fisher Scientific, Waltham, MA, USA). Densitometric analyses were conducted with ImageJ software v1.51 (NIH, http://imagej.nih.gov/ij/, accession date 23 April 2018). The cytoplasmic-

membrane fractionation experiment was conducted using the MEM-PER kit (Thermo), following the manufacturer's instructions on yeast spheroplasts. Western blot analysis was performed using anti-Synuclein antibody (1:1000, Sigma Aldrich), anti-Pgk1 antibody (1:1000, Molecular Probes, used as loading control and cytoplasmic marker) and anti-Pma1 antibody (1:1500, Abcam, used as membrane marker).

Total extracts from mammalian cells were prepared using RIPA buffer (50 mM Tris-HCl pH 7.5, 150 mM NaCl, 0.5% sodium deoxycholate, 1% NP40, 0.1% SDS), plus 1 mM PMSF (phenylmethanesulfonylfluoride), protease inhibitor cocktail (Roche, Indianapolis, IN) and phosphatase inhibitor cocktail (Sigma-Aldrich, St. Louis, MO, USA). Protein concentration was determined using the Bio-Rad protein assay. Western blot analysis was performed using anti-AMPK antibody (Cell Signaling), anti-phosphoT172-AMPK antibody (Cell Signaling), anti-vinculin antibody (Sigma-Aldrich), anti-phospho-T389-p70 S6K (Cell Signaling, kindly provided by Evelina Gatti), anti-phospho79-Acc1 antibody (Cell Signaling), anti-Akt (Cell Signaling) anti-phosphoS473-Akt (Cell Signaling), anti-tubulin (Cell Signaling).

Snf1/AMPK immunopurification and *in vitro* dephosphorylation assay

Snf1/AMPK purification was carried out in a strain expressing Snf1-TAP. Cells were cultured in 2% complete synthetic medium and harvested by filtration after diauxic shift. Cells were lysed using ice-cold lysis buffer (50 mM Tris-HCl pH 7.5, 150 mM NaCl, 0.1% NP-40, 10% glycerol) plus 1 mM PMSF (phenylmethanesulfonylfluoride fluoride), proteases inhibitor mix (Complete EDTA free Protease Inhibitor Cocktails Tablets, Roche) and phosphatase inhibitor mix (Cocktail 2, Sigma-Aldrich), in the presence of an equal volume of acid-washed glass beads (Merck) by 20 vortex/ice cycles of

1 min each. Protein concentration was measured using Bradford protein assay (Bio-Rad).

Snf1/AMPK complex was purified from 70 mg of total protein extract using 100 µl Rabbit IgG-Agarose resin (Merck), eluting native Snf1/AMPK complex in 150 µl of TEV buffer (20 mM HEPES pH 7, 0.5 mM DTT, 150 mM NaCl) with 40 units TEV protease (Merck). 18 µl of Snf1/AMPK native complex was dephosphorylated with 1.5 µg of human PP2Cα phosphatase (SRP6062, Merck) at 37° C in assay buffer (20 mM HEPES pH 7, 0.5 mM DTT, 2 mM MgCl$_2$, 100 mM NaCl), in the absence or presence of 0.5 mM or 1 mM G6P (Merck) (final volume 45 µl). The reaction was stopped by adding SDS-sample buffer after 0, 2, 4, 6, 8 minutes. The phosphorylation of Snf1/AMPK was assayed by Western blot analysis with anti-phosphoT172-AMPK antibody (Cell Signalling) and densitometric analyses were conducted with ImageJ software (NIH, http://imagej.nih.gov/ij/).

PP2Cα phosphatase (SRP6062, Merck) activity in presence sugar phosphates was measured in 96-multiwell plate adding 1.5 µg of phosphatase, 10mM of para-nitrophenyl-phosphate (pNPP) and 0.5mM or 1mM of G6P, G1P, F16BP, T6P in assay buffer (20 mM HEPES pH 7, 0.5 mM DTT, 2 mM MgCl$_2$, 100 mM NaCl) at 37° C

Gene expression analysis in *D. melanogaster*

Total RNA was extracted from the whole bodies of either 30 days or 45 days old flies belonging to the 0.2% group by using RNeasy Mini Kit (QIAGEN GmbH, Hilden, Germany). The 0.2% supplementation has been chosen because it was the one able to significantly increase lifespan in Drosophila. All the experiments were performed in triplicate. The yield and purity of the

RNA were measured using NanoVue Spectrophotometer (GE Healthcare, Milano, Italy). Only samples with density ratios A260/A280>1.8 were used. cDNA was obtained by reverse transcribing mRNA starting from 1 µg of total RNA using iScript cDNA Synthesis Kit (BIO-RAD, Hercules, CA, USA), following the manufacturer's protocol. The subsequent polymerase chain reaction (PCR) was performed in a total volume of 10 µl containing 2.5 µl (12.5 ng) of cDNA, 5 µl SsoAdvanced Universal SYBR Green Supermix (BIO-RAD), 2 µl of dH20 RNA free and 0.5 µl (500 nM) of each primer: Sirt1, fwd: CATTATGCCGCATTTCGCCA, rev: GAAGGTGTTCACTGAGGCCA. Foxo, fwd: AGGCTGACCCACACAGATAAC, rvs: GGCTCCACAAAGTTTTCGGG. Notch, fwd: CGCTTCCTGCACAAGTGTC, rvs: GCGCAGTAGGTTTTGCCATT. HO, fwd: ATGTCAGCGAGCGAAGAAACA, rvs: TGGCTTTACGCAACTCCTTTG. Trxr, fwd: TGGATCTGCGCGACAAGAAAG, rvs: GAAGGTCTGGGCGGTGATTG. RPL32, fwd: GCCCACCGGATTCAAGAAGT, rvs: CTTGCGCTTCTTGGAGGAG. With RPL32 as reference gene.

Molecular docking

Protein structure of Snf1/AMPK heterotrimer regulatory core were retrieved from Protein Data Bank [http://www.rscb.org](PDBID 2QLV). Crystal structures were processed with Protein Preparation wizard in MAESTRO [Schrödinger Release 2020-4: Maestro, Schrödinger, LLC, New York, NY, 2020] to fill missing side chains and set proper protonation states of residues at pH 7.0 ± 0.2. Docking simulations were performed with GLIDE [Schrödinger Release 2020-4: Glide, Schrödinger, LLC, New York, NY, 2020] using the extra precision (XP) (Friesner et al., 2006) protocol without any constraint. A screening for possible interactions between G6P and Snf1 complex was carried out with SwissDock [http://www.swissdock.ch]. Grid

receptor boxes of 36 Å x 36 Å x 36 Å were generated around putative binding sites.

The whole sequences from AAKB2_HUMAN, AAKB1_RAT, SIP2_YEAST, GAL83_YEAST, and SNF1_YEAST, AAPK1_HUMAN and AAPK1_RAT entries from UniprotKB database were submitted to Clustal Omega (https://www.ebi.ac.uk/Tools/msa/clustalo/) in order to obtain a reliable multiple sequence alignment.

Only the partial alignment containing residues involved at the interface between the CBM/GBD of the β–subunit and the AMPK kinase domain were shown in Figure 13. These residues were identified by an analysis on rat AMPK complex structure (PDB ID: 4qfg) since it is the only structure available with no activators positioned at the interface. The analysis of the contact residues was performed by UCSF Chimera software, by imposing a threshold of 4 Å from the interacting partner.

Isothermal calorimetry assay

Isothermal calorimetry assays were conducted with the MicroCal PEAQ-ITC (Malvern Panalytical Ltd, Malvern UK) following the standard procedure of the manufacturer (feedback high, 20 injections) and adjusting the spacing time to better distinguish consecutives peaks. Snf1-TAP tagged was purified from yeast cells cultured in 2% glucose complete synthetic medium. Cell was loaded with 200 µl of Snf1 complex (9µM) and titrated with either 300 µM G6P) or 100 µM NADH dissolved in kinase buffer (20 mM HEPES pH 7, 0.5 mM DTT, 2 mM $MgCl_2$, 100 mM NaCl).

Chemical and proteomic characterization of the extracts

Starch content was evaluated by the enzymatic assay Total Starch AOAC Method 996.1 1 and AACC Method 76.13 (Megazyme ®, Ireland). Briefly, 50 mg of extract were suspended in 200 µl of ethanol 80% v/v and 1 ml of 2 M KOH. Samples were magnetically stirred for 20 min at 4°C. Then, 4 ml of sodium acetate pH=3.8 were added, followed by the addition of 50 µl of α-amylase (8300 U/mL) and 50 µl of amyloglucosidase (AMG, 3300 U/ml). Samples were incubated for 30 min with intermittent mixing on a vortex mixer, then centrifuged for 10 min at 3000 rpm to recover the supernatant. In order to evaluate total starch content, a reaction mixture was prepared as follows in a quartz cell: 1 ml H_2O, 25 µl of sample, 50 µl of a buffer solution pH = 7.6, 50 µl NADP+/ATP. The solution was incubated for 3 min at room temperature and then the absorbance was read at 340 nm against the blank. Then, 10 µl of a solution containing hexokinase (HK) and glucose-6-phosphate1dehydrogenase (G6PDH) was added. After an incubation of 5 min at room temperature, the absorbance was read against the blank again at 340 nm. Data are expressed as g of starch per 100 g of extract.

Amino acids were quantified through a HPLC-DAD method. A 1260 Infinity II LC System (Agilent, USA, 2018) was set up for the analysis. The calibration curve was made up using an amino acid mixed solution (Merck, Germany) in a concentration range between 0.078 mM and 1.25 mM. The column was an Agilent Poroshell HPH C18 (100 x 4.6 mm, 2.7 µm) coupled with a guard column (AdvanceBio Oligo 4.6 x 5 mm, 2.7 µm) and it was kept at 40°C. Mobile phases were: A - 10 mM Na_2HPO_4 pH=8.2 and B - Acetonitrile: Methanol: Water 45:45:10. The elution program was the following (%B): 0-0.35 min 2%, 13.4 min 57%, 13.5 min 100%, 15.7 min 100%,

15.8 min 2%, 18 min end. Flow rate was constant at 1.5 ml/min. All solvents were HPLC grade, whereas the buffer, solutions and samples were pre-filtered with a 0.22 µm filter. OPA (o-Phthaldialdehyde reagent, Merck, Germany) was chosen as derivatizing agent acting as a fluorophore. Injection volume was 10 µl. The signal used to visualize the fluorescence was set at 338 nm bandwidth 10 nm with a reference wavelength of 390 nm bandwidth 20 nm. All data were displayed and analysed on Agilent ChemStation software. Data are expressed as g of amino acids per 100 g of extract.

Total protein content was evaluated by using the Bradford assay as follows: 1 ml of 50% Coomassie-Brilliant Blue Bradford reagent (ThermoFisher, USA) was incubated at room temperature with 2 µl of extract of known concentration for a minute. Absorbance was read against blank at 595 nm and fitted on a calibration curve made up with BSA (Bovine Serum Albumin) in a range between 0 and 6 mg/ml. Data are expressed as g of protein per 100 g of extract.

Proteomics analysis

Proteomics analysis of natural extracts were conducted reducing, derivatizing and digesting the extracts with trypsin (protein: protease ratio 20:1) as described in [343], before MS/MS analysis. Peptides separation was achieved on a Thermo Easy-nLC 1000, with a linear gradient from 95% solvent A (2 % ACN, 0.1% formic acid) to 30% solvent B (80% acetonitrile, 0.1% formic acid) over 60 min, from 30 to 60% solvent B in 5 min and from 60 to 100% solvent B in 2 min at a constant flow rate of 0.25 µl/min, with a single run time of 75 min. MS data were acquired on a Thermo Q-Exactive-HF, with a data-dependent top 15 method, the survey full scan MS spectra

(300-1650 m/z) were acquired in the Orbitrap with 60000 resolution, AGC target 3e6, IT 20 ms. For HCD spectra resolution was set to 15000, AGC target 1e5, IT 80 ms; normalized collision energy 28 and isolation width of 1.2 m/z. Raw label-free MS/MS files from Thermo Xcalibur software (version 4.1) [343] were analysed using Proteome Discoverer software (version 2.2, Thermo Fisher Scientific) and searched with Sequest algorithm against the proteome of NCBI Phaseoleae (release 05/08/2019). The minimum required peptide length was set to 6 amino acids with carbamidomethylation as fixed modification, Met oxidation and Arg/Gln deamidation as variable modifications. The mass spectrometry proteomic data have been deposited to the ProteomeXchange Consortium via the PRIDE [344] partner repository with the dataset identifier PXD017716.

Shotgun Mass Spectrometry and Label Free Quantification

Four technical replicates were performed for each HepG2 sample, grown for 48 h in the presence or absence of high methionine and/or Compound C. Proteins were lysed in RapiGest 0.1% (RG, Waters Corporation, Milford, MA, USA), reduced with 13 mM DTE (30 min at 55 °C) and alkylated with 26 mM iodoacetamide (30 min at 23 °C). Protein digestion was performed using sequence-grade trypsin (Roche) for 16 h at 37 °C using a protein/trypsin ratio of 20:1. The proteolytic digested was desalted using Zip-Tip C18 (Millipore, Burlington, MA, USA) before MS analysis [345]. LC-ESI-MS/MS analysis was performed on a Dionex UltiMate 3000 HPLC System with a PicoFrit ProteoPrep C18 column (200 mm, internal diameter of 75 μM). Gradient: 2% ACN in 0.1% formic acid for 10 min, 2–4% ACN in 0.1% formic acid for 6 min, 4–30% ACN in 0.1% formic acid for 147 min, and 30–50% ACN in 0.1% formic

for 3 min, at a flow rate of 0.3 µL/min. The eluate was electrosprayed into an LTQ OrbitrapVelos (Thermo Fisher Scientific, Bremen, Germany) through a Proxeon nanoelectrospray ion source (Thermo Fisher Scientific), as reported in [343]. The LTQ-Orbitrap was operated in positive mode in data-dependent acquisition mode to automatically alternate between a full scan (*m/z* 350–2000) in the Orbitrap (at resolution 60,000, AGC target 1,000,000) and subsequent CID MS/MS in the linear ion trap of the 20 most intense peaks from full scan (normalized collision energy of 35%). Data acquisition was controlled by Xcalibur 2.0 and Tune 2.4 software (Thermo Fisher Scientific).

A database search was conducted against the Homo Sapiens Uniprot sequence database (release 6 March 2019) with MaxQuant (version 1.6.0.1) software, using the following parameters: the initial maximum allowed mass deviation of 15 ppm for monoisotopic precursor ions and 0.5 Da for MS/MS peaks, trypsin enzyme specificity, a maximum of 2 missed cleavages, carbamidomethyl cysteine as fixed modification, N-terminal acetylation, methionine oxidation, asparagine/glutamine deamidation and serine/threonine/tyrosine phosphorylation as variable modifications. Quantification was performed using the built in XIC-based label-free quantification (LFQ) algorithm using fast LFQ [346]. False protein identifications (1%) were estimated by searching MS/MS spectra against the corresponding reversed-sequence (decoy) database. Statistical analysis was performed using the Perseus software (version 1.5.5.3, **https://maxquant.net/perseus/**). Only proteins present and quantified in at least 75% of the repeats were positively identified and used for statistical analysis. An ANOVA test (cut-off at 0.05 *p*-value) was carried out to identify proteins differentially expressed among the four conditions.

Focusing on specific comparisons, proteins were considered differentially expressed if they were present only in one condition or showed significant *t*-test difference (Student's *t*-test *p* value ≤ 0.05) [347]. Bioinformatic analyses were carried out by Ingenuity® Pathway Analysis software (IPA® - QIAGEN) to cluster enriched annotation groups of Biological Processes, Pathways, and Networks within the set of identified proteins. Functional grouping was based on Fischer's exact test *p* value ≤ 0.05 (i.e., −log10 ≥ 1.3) and at least 3 counts. Comparison between the proteomic and metabolomic data was performed by IPA and by MetaboAnalyst software R3.0 [348]. Enrichment analysis aimed to evaluate whether the observed genes and metabolites in a particular pathway are significantly enriched (Fisher's exact test 0.05), while the topology analysis aimed to evaluate whether a given gene or metabolite plays an important role in a biological response, based on its position within a pathway (pathway impact).

The mass spectrometry proteomics data have been deposited to the ProteomeXchange Consortium via the PRIDE partner repository, with the dataset identifier 7MlKNZqC.

GC/MS metabolomics

Small molecule contents of natural extracts were by GC/MS. 5 mg of each sample were accurately weighed, suspended in 50 µl of 2wt% methoxylamine hydrochloride in pyridine and incubated for 90 min at 37°C. Then, 80 µl of MBDSTFA (N-methyl-N-ter-butyldimethylsilyl-trifluoroacetamide) +1% TBDMCS (tertbutyldimethylchlorosilane) were added and the samples were incubated at 60° C for 30 min. After incubation at room temperature overnight, the samples were analysed by using an ISQ™ QD Single Quadrupole GC-MS (Thermo Fisher) equipped with a VF-5ms

(30 m x 0.25 mm i.d. x 0.25 µm; Agilent Technology). Injection volume: 1 µl. Oven program: 100° C for 2 min; then 6° C/min to 280° C for 15 min; Run Time 42 min. Helium was used as the gas carrier. SS Inlet: Mode Splitless. Inlet temperature: 280° C. Flow 1.0 ml/min. MS transfer line: 270° C. Ion source: 250° C. Ionization mode: electron impact: 70 eV. Acquisition mode: full scan. To compare the composition of the extracts, for each analyte identified by GC/MS a target ion (m/z) was extracted by the TIC and the corresponding area was calculated.

Metabolites extraction for GC-MS analysis of mammalian cells was conducted quickly rinsing cells with 0.9% NaCl and quenched with 800 µL of 1:1 ice-cold methanol: water and collected by scraping. Cells were sonicated 5 s for 5 pulses at 70% power twice and then 400 µL of chloroform were added. Samples were vortexed at 4 °C for 20 min, and then centrifuged at 12,000 g for 10 min at 4 °C. The aqueous phase was collected in a glass insert for solvent evaporation in a centrifugal vacuum concentrator (Concentrator plus/ Vacufuge® plus, Eppendorf) at 30 °C for about 2.5 h. Derivatization was performed using automated sample prep WorkBench instrument (Agilent Technologies, Santa Clara, CA, USA). Dried polar metabolites were dissolved in 60 µL of 2% methoxyamine hydrochloride in pyridine (ThermoFisher) and held at 40 °C for 6 h. After the reaction, 90 µL of MSTFA (N-Methyl-N-(trimethylsilyl) trifluoroacetamid) was added, and samples were incubated at 60 °C for 1 h. Derivatized samples were analysed by GC-MS using a DB-35MS column (30 m × 0.25 mm i.d. × 0.25 µm) installed in an Agilent 7890B gas chromatograph (GC) interfaced with an Agilent 7200 Accurate-Mass Quadrupole Time-of-Flight (QTOF) mass spectrometer (MS), operating under electron impact (EI) ionization at 70 eV. Samples (1 µL) were injected in a spitless mode at 250 °C, using helium as the carrier gas at a flow rate of

1 mL/min. The GC oven temperature was held at 100 °C for 2 min and increased to 325 °C at 10 °C/min. GC/MS data processing was performed using Agilent Muss Hunter software. Relative metabolites abundance was carried out after normalization to internal standard d27 Myristic acid and cell number and statistical analyses were performed using MetaboAnalyst 4.0 [349].

13C labelling and analysis of isotopomer distributions of proteinogenic amino acids by GC-MS

Pellets were re-suspended in 200 μL of 6 M HCl and incubated at 110 °C for 16 hours to lyse the cells and hydrolyse the respective proteomes. Hydrolysed samples were then filtered on a filter plate (AcroPrep Advance 96-well Filter, 0.2 μm membrane, product ID 8019) by positive pressure and dried. Dried samples were then derivatized by adding 35 μL of pyridine (Sigma-Aldrich, cat no. 270407) and 50 μL of MBTSFA + 1% (wt/wt) TBDMSClS (Sigma-Aldrich, cat no. 375934), mixed by pipetting and incubated at 60 °C for 30 min. 75 μL of the derivatized samples were aliquoted to LC-MS vials with glass inserts for GC-MS analysis within 12h from derivatization on an Agilent 5977 GC-MS system with an Agilent DB-5ms capillary column (30m, inner diameter of 0.25 mm, film thickness of 0.25 μm, cat no. 122-5532). Samples were measured in full-scan mode, using a 1:100 split ratio, with the following gradient: start at 160 °C, hold for 1 min, ramp to 310 °C at 20 °C/min, hold for 1 min. We considered for further analysis fragments listed in [350] Table 3. Raw chromatographic data was integrated using SmartPeak [351].

LC/MS metabolomics

Metabolites extraction for LC-MS analysis of mammalian cells was conducted quickly rinsing cells with 0.9% NaCl and quenched with 500 μL ice-cold 70:30 acetonitrile-water. Plates were placed at −80 °C for 10 min, then the cells were collected by scraping. Cells were sonicated as above and then centrifuged at 12,000 g for 10 min at 4 °C. The supernatant was collected in a glass insert and dried as above. Samples were then resuspended with 150 μL of H_2O prior to analyses. LC separation was performed using an Agilent 1290 Infinity UHPLC system and an InfinityLab Poroshell 120 PFP column (2.1 × 100 mm, 2.7 μm; Agilent Technologies). Mobile phase A was water with 0.1% formic acid. Mobile phase B was acetonitrile with 0.1% formic acid. The injection volume was 15 μL and LC gradient conditions were: 0 min: 100% A; 2 min: 100% A; 4 min: 99% A; 10 min: 98% A;11 min: 70% A; 15 min: 70% A; 16 min: 100% A with 5 min of post-run. Flow rate was 0.2 mL/min, and the column temperature was 35 °C. MS detection was performed using an Agilent 6550 iFunnel Q-TOF mass spectrometer with Dual JetStream source operating in negative ionization mode. MS parameters were gas temp: 285 °C; gas flow: 14 l/min; nebulizer pressure: 45psig; sheath gas temp: 330 °C; sheath gas flow: 12 l/min; VCap: 3700 V; Fragmentor: 175 V; Skimmer: 65 V; Octopole RF: 750 V. Active reference mass correction was through a second nebulizer using masses with m/z: 112.9855 and 1033.9881 dissolved in the mobile phase 2-propanol-acetonitrile-water (70:20:10 v/v). Data were acquired from m/z 60–1050. Data analysis and isotopic natural abundance correction was performed with MassHunter ProFinder (Agilent Technologies). Relative metabolites abundance was carried out after normalization to cell number and statistical analyses were performed using MetaboAnalyst 4.0 [349].

Seahorse analysis

Absolute quantification of glucose, lactate, glutamine, and glutamate in spent media was determined enzymatically using YSI2950 bioanalyzer (YSI Incorporated, Yellow Springs, OH, USA). Mitochondrial oxygen consumption rate (OCR) and extracellular acidification rate (ECAR) were determined by using Seahorse XFe96 Analyzer (Agilent Technologies). HepG2 and Huh7 cells were seeded in Agilent Seahorse cell culture microplates at density of 2×10^4 cells/well for HepG2 or 1×10^4 cell/well for Huh7 72 h prior to the assay. A total of 24 h after seeding cells were treated with high methionine (1.5 g/L) and/or Compound C (2 µM for HepG2 and at 1.5 µM for Huh7 cells) for 48 h, and then analysed by using the Seahorse XF ATP rate assay kit (Agilent Technologies), according to manufacturer instructions. Three measurements of OCR and ECAR were taken for the baseline and after the sequential injection of mitochondrial inhibitors (1.5 µM oligomycin and 1.5 µM rotenone/antimycin A). OCR and ECAR from each well were normalized by protein content by using the Bradford assay.

Flux balance analysis

The genome-scale metabolic network reconstruction (genome-scale metabolic model, GSMM) for P. putida, iJN1411 [352], was subjected to Flux Balance Analysis (FBA) [184] within the COBRApy toolbox [353] to predict optimal metabolic flux distributions, to identify reactions contributing to a supply of succinate, and to test genetic strain designs. The growth-limiting determinants, the glucose-uptake rate, and ATP maintenance requirement were fixed at rates of 6.3 mmol gCDW h-1 and 0.92 mmol gCDW h-1, respectively (experimentally determined by [354,355], respectively). Flux distributions were visualized in Escher [356].

Fluorescence microscopy on yeast

In situ immunofluorescence was performed on formaldehyde-fixed cells and carried using α-synuclein immunostaining (1:2000, Sigma Aldrich) followed by indirect immunofluorescence using rhodamine-conjugated anti-rabbit antibody (1:1000, Pierce Chemical Co). Digital images were taken with a Nikon DS-Qi MC camera mounted on a Nikon Eclipse 600 and controlled by the NIS elements imaging software (Nikon) with an oil 100X 0.5-1.3 PlanFluor oil objective (Nikon). In vitro aggregation of α-synuclein α-synuclein was expressed in *Escherichia coli* BL21(DE3) cells transformed with the pET28b/α-synuclein plasmid. The recombinant protein was expressed and purified according to a previously described procedure [251]and further purified by RP-HPLC. The identity and purity of the eluted material were assessed by mass spectrometry. Protein samples (250 μM), filtered through a 0.22 μm pore-size filter (Millipore, Bedford, MA, USA) were incubated at 37°C in 20 mM sodium phosphate buffer, pH 7.4 up to 3 days under shaking at 900 rpm with a thermo-mixer in the absence or in the presence of extract by using molar protein/substance ratios of 1:0.5 (E0.5) and 1:1 (E1). Oligomer-enriched or fibril-enriched sample were prepared by incubating a-synuclein for 24 h or 72 h, respectively.

ThT assay

The ThT binding assay was performed according to LeVine [59], using a 25 μM ThT solution in 20 mM sodium phosphate buffer, pH 7.0. Each sample, diluted at a final concentration of 6.25 μM, was transferred into a 96-well half-area, low-binding, clear bottom (200 μl/well) and ThT fluorescence was read at the maximum intensity of fluorescence of 485 nm using a Biotek Synergy 1H plate reader; buffer fluorescence was subtracted from the

fluorescence values of all samples. In controls experiments, a significant interference of the highest concentrations of cowpea extract on ThT fluorescence was observed, so the two molar ratio protein:extract with lowest fluorescence interference were selected.

ANS assay

Samples containing aggregating a-synuclein with and without cowpea extract at 250 μM were investigated for their ability to bind 8-anilinonaphthalene-1-sulfonic acid (ANS; Sigma Aldrich, Saint Louis, MO, US). 5 μl of each sample at different times of aggregation was transferred into a 96-well half-area, low-binding, clear bottom (200 μl/well), and ANS (50 μM) fluorescence intensity was read at the binding intensity of fluorescence of 480 nm in a Biotek Synergy 1H plate reader; buffer fluorescence was subtracted from the fluorescence values of all samples. In control experiments, a significant interference of the highest concentrations of the extract on ANS binding fluorescence was observed, so we selected the two molar ratios protein:extract with the lowest fluorescence interference.

Transmission electron microscopy (TEM) imaging

5 μl aliquots of α-synuclein aggregated in the presence or the absence of cowpea extract were withdrawn at different aggregation times, loaded onto a formvar/carbon-coated 400 mesh nickel grids (Agar Scientific, Stansted, UK) and negatively stained with 2.0% (w/v) uranyl acetate (Sigma-Aldrich). The grid was air-dried and examined using a JEM 1010 transmission electron microscope at 80 kV excitation voltage.

References

1.	Kitano, H. *Foundations of systems biology*; MIT Press, 2001; ISBN 9780262112666.

2.	Kitano, H. Biological robustness. *Nat. Rev. Genet.* **2004**, *5*, 826–837, doi:10.1038/nrg1471.

3.	Gancedo, J.M. The early steps of glucose signalling in yeast. **2008**, doi:10.1111/j.1574-6976.2008.00117.x.

4.	Efeyan, A.; Comb, W.C.; Sabatini, D.M. Nutrient-sensing mechanisms and pathways. *Nature* 2015, *517*, 302–310.

5.	Peeters, K.; Van Leemputte, F.; Fischer, B.; Bonini, B.M.; Quezada, H.; Tsytlonok, M.; Haesen, D.; Vanthienen, W.; Bernardes, N.; Gonzalez-Blas, C.B.; et al. Fructose-1,6-bisphosphate couples glycolytic flux to activation of Ras. *Nat. Commun.* **2017**, *8*, doi:10.1038/s41467-017-01019-z.

6.	Zhang, C.S.; Hawley, S.A.; Zong, Y.; Li, M.; Wang, Z.; Gray, A.; Ma, T.; Cui, J.; Feng, J.W.; Zhu, M.; et al. Fructose-1,6-bisphosphate and aldolase mediate glucose sensing by AMPK. *Nature* **2017**, *548*, 112–116, doi:10.1038/nature23275.

7.	Zhang, Y.; Primavesi, L.F.; Jhurreea, D.; Andralojc, P.J.; Mitchell, R.A.C.; Powers, S.J.; Schluepmann, H.; Delatte, T.; Wingler, A.; Paul, M.J. Inhibition of SNF1-related protein kinaseI activity and regulation of metabolic pathways by trehalose-6-phosphate1[w][OA]. *Plant Physiol.* **2009**, *149*, 1860–1871, doi:10.1104/pp.108.133934.

8.	Nicastro, R.; Sardu, A.; Panchaud, N.; De Virgilio, C. The Architecture of the Rag GTPase Signaling Network. *Biomolecules* **2017**, *7*, 48, doi:10.3390/biom7030048.

9.	Saxton, R.A.; Knockenhauer, K.E.; Wolfson, R.L.; Chantranupong, L.; Pacold, M.E.; Wang, T.; Schwartz, T.U.; Sabatini, D.M. Structural basis

for leucine sensing by the Sestrin2-mTORC1 pathway. *Science (80-.).* **2016**, *351*, 53–58, doi:10.1126/science.aad2087.

10. Chantranupong, L.; Scaria, S.M.; Saxton, R.A.; Gygi, M.P.; Shen, K.; Wyant, G.A.; Wang, T.; Harper, J.W.; Gygi, S.P.; Sabatini, D.M. The CASTOR Proteins Are Arginine Sensors for the mTORC1 Pathway. *Cell* **2016**, *165*, 153–164, doi:10.1016/j.cell.2016.02.035.

11. Gu, X.; Orozco, J.M.; Saxton, R.A.; Condon, K.J.; Liu, G.Y.; Krawczyk, P.A.; Scaria, S.M.; Wade Harper, J.; Gygi, S.P.; Sabatini, D.M. SAMTOR is an S-adenosylmethionine sensor for the mTORC1 pathway. *Science (80-.).* **2017**, *358*, 813–818, doi:10.1126/science.aao3265.

12. Zhang, F.; Pracheil, T.; Thornton, J.; Liu, Z. Adenosine Triphosphate (ATP) Is a Candidate Signaling Molecule in the Mitochondria-to-Nucleus Retrograde Response Pathway. *Genes (Basel).* **2013**, *4*, 86–100, doi:10.3390/genes4010086.

13. Cole, J.T.; Kean, W.S.; Pollard, H.B.; Verma, A.; Watson, W.D. Glucose-6-phosphate reduces calcium accumulation in rat brain endoplasmic reticulum. *Front. Mol. Neurosci.* **2012**, *5*, doi:10.3389/fnmol.2012.00051.

14. Ukai, H.; Araki, Y.; Kira, S.; Oikawa, Y.; May, A.I.; Noda, T. Gtr/Ego-independent TORC1 activation is achieved through a glutamine-sensitive interaction with Pib2 on the vacuolar membrane. *PLoS Genet.* **2018**, *14*, doi:10.1371/journal.pgen.1007334.

15. Nunes, C.; Primavesi, L.F.; Patel, M.K.; Martinez-Barajas, E.; Powers, S.J.; Sagar, R.; Fevereiro, P.S.; Davis, B.G.; Paul, M.J. Inhibition of SnRK1 by metabolites: Tissue-dependent effects and cooperative inhibition by glucose 1-phosphate in combination with trehalose 6-phosphate. *Plant Physiol. Biochem.* **2013**, *63*, 89–98,

doi:10.1016/j.plaphy.2012.11.011.

16. Chakravarti, D.; LaBella, K.A.; DePinho, R.A. Telomeres: history, health, and hallmarks of aging. *Cell* **2021**, *184*, 306–322, doi:10.1016/J.CELL.2020.12.028.

17. McCormick, M.A.; Promislow, D.E.L. Recent Advances in the Systems Biology of Aging. *Antioxid. Redox Signal.* **2018**, *29*, 973–984, doi:10.1089/ARS.2017.7367.

18. Burkewitz, K.; Zhang, Y.; Mair, W.B. AMPK at the nexus of energetics and aging. *Cell Metab.* **2014**, *20*, 10–25, doi:10.1016/J.CMET.2014.03.002.

19. Sun, S.; Baryshnikova, A.; Brandt, N.; Gresham, D. Genetic interaction profiles of regulatory kinases differ between environmental conditions and cellular states. *Mol. Syst. Biol.* **2020**, *16*, e9167, doi:10.15252/MSB.20199167.

20. Tripodi, F.; Castoldi, A.; Nicastro, R.; Reghellin, V.; Lombardi, L.; Airoldi, C.; Falletta, E.; Maffioli, E.; Scarcia, P.; Palmieri, L.; et al. Methionine supplementation stimulates mitochondrial respiration. *Biochim. Biophys. Acta - Mol. Cell Res.* **2018**, *1865*, 1901–1913, doi:10.1016/J.BBAMCR.2018.09.007.

21. Lu, S.C.; Mato, J.M. S-adenosylmethionine in liver health, injury, and cancer. *Physiol. Rev.* **2012**, *92*, 1515–1542, doi:10.1152/PHYSREV.00047.2011/ASSET/IMAGES/LARGE/Z9J00412 26300008.JPEG.

22. Nielsen, J.; Keasling, J.D. Engineering Cellular Metabolism. *Cell* **2016**, *164*, 1185–1197, doi:10.1016/J.CELL.2016.02.004.

23. Volke, D.C.; Calero, P.; Nikel, P.I. Pseudomonas putida. *Trends Microbiol.* 2020, *28*, 512–513.

24. Karas Kuželički, N. S-Adenosyl Methionine in the Therapy of Depression and Other Psychiatric Disorders. *Drug Dev. Res.* **2016**, *77*, 346–356, doi:10.1002/ddr.21345.

25. Zhang, Y.; He, Y.; Zhang, N.; Gan, J.J.; Zhang, S.; Dong, Z. Combining protein and metabolic engineering strategies for biosynthesis of melatonin in Escherichia coli. *Microb. Cell Fact.* **2021**, *20*, 1–13, doi:10.1186/S12934-021-01662-8/FIGURES/6.

26. Zhao, X.Q.; Gust, B.; Heide, L. S-Adenosylmethionine (SAM) and antibiotic biosynthesis: Effect of external addition of SAM and of overexpression of SAM biosynthesis genes on novobiocin production in Streptomyces. *Arch. Microbiol.* **2010**, *192*, 289–297, doi:10.1007/S00203-010-0548-X/FIGURES/4.

27. Koirala, N.; Pandey, R.P.; Thuan, N.H.; Ghimire, G.P.; Jung, H.J.; Oh, T.J.; Sohng, J.K. Metabolic engineering of Escherichia coli for the production of isoflavonoid-4'-O-methoxides and their biological activities. *Biotechnol. Appl. Biochem.* **2019**, *66*, 484–493, doi:10.1002/BAB.1452.

28. Sudarsan, N.; Hammond, M.C.; Block, K.F.; Welz, R.; Barrick, J.E.; Roth, A.; Breaker, R.R. Tandem riboswitch architectures exhibit complex gene control functions. *Science (80-.).* **2006**, *314*, 300–304, doi:10.1126/SCIENCE.1130716/SUPPL_FILE/1130716SUDARSON_SOM.PDF.

29. Dippe, M.; Brandt, W.; Rost, H.; Porzel, A.; Schmidt, J.; Wessjohann, L.A. Rationally engineered variants of S-adenosylmethionine (SAM) synthase: Reduced product inhibition and synthesis of artificial cofactor homologues. *Chem. Commun.* **2015**, *51*, 3637–3640, doi:10.1039/c4cc08478k.

30. Friedlander, T.; Mayo, A.E.; Tlusty, T.; Alon, U. Evolution of Bow-Tie Architectures in Biology. *PLOS Comput. Biol.* **2015**, *11*, e1004055, doi:10.1371/journal.pcbi.1004055.

31. Stelling, J.; Sauer, U.; Szallasi, Z.; Doyle, F.J.; Doyle, J. Robustness of Cellular Functions. *Cell* **2004**, *118*, 675–685, doi:10.1016/j.cell.2004.09.008.

32. Busti, S.; Coccetti, P.; Alberghina, L.; Vanoni, M. Glucose Signaling-Mediated Coordination of Cell Growth and Cell Cycle in Saccharomyces Cerevisiae. *Sensors* **2010**, *10*, 6195–6240, doi:10.3390/s100606195.

33. Ewald, J.C. How yeast coordinates metabolism, growth and division. *Curr. Opin. Microbiol.* 2018, *45*, 1–7.

34. Diether, M.; Sauer, U. Towards detecting regulatory protein–metabolite interactions. *Curr. Opin. Microbiol.* 2017, *39*, 16–23.

35. Diether, M.; Nikolaev, Y.; Allain, F.H.; Sauer, U. Systematic mapping of protein-metabolite interactions in central metabolism of Escherichia coli . *Mol. Syst. Biol.* **2019**, *15*, doi:10.15252/msb.20199008.

36. Piazza, I.; Kochanowski, K.; Cappelletti, V.; Fuhrer, T.; Noor, E.; Sauer, U.; Picotti, P. A Map of Protein-Metabolite Interactions Reveals Principles of Chemical Communication. *Cell* **2018**, *172*, 358-372.e23, doi:10.1016/j.cell.2017.12.006.

37. Eisenmesser, E.Z.; Millet, O.; Labeikovsky, W.; Korzhnev, D.M.; Wolf-Watz, M.; Bosco, D.A.; Skalicky, J.J.; Kay, L.E.; Kern, D. Intrinsic dynamics of an enzyme underlies catalysis. *Nature* **2005**, *438*, 117–121, doi:10.1038/nature04105.

38. Kim, E.; Lee, S.; Jeon, A.; Choi, J.M.; Lee, H.S.; Hohng, S.; Kim, H.S. A

single-molecule dissection of ligand binding to a protein with intrinsic dynamics. *Nat. Chem. Biol.* **2013**, *9*, 313–318, doi:10.1038/nchembio.1213.

39. Boehr, D.D.; Nussinov, R.; Wright, P.E. The role of dynamic conformational ensembles in biomolecular recognition. *Nat. Chem. Biol.* 2009, *5*, 789–796.

40. Gianni, S.; Dogan, J.; Jemth, P. Distinguishing induced fit from conformational selection. *Biophys. Chem.* **2014**, *189*, 33–39, doi:10.1016/j.bpc.2014.03.003.

41. Koshland, D.E. Application of a Theory of Enzyme Specificity to Protein Synthesis. *Proc. Natl. Acad. Sci.* **1958**, *44*, 98–104, doi:10.1073/pnas.44.2.98.

42. Ma, B.; Kumar, S.; Tsai, C.-J.; Nussinov, R. Folding funnels and binding mechanisms. *Protein Eng. Des. Sel.* **1999**, *12*, 713–720, doi:10.1093/protein/12.9.713.

43. Weikl, T.R.; Paul, F. Conformational selection in protein binding and function. *Protein Sci.* 2014, *23*, 1508–1518.

44. Kirschner, K.; Eigen, M.; Bittman, R.; Voigt, B. THE BINDING OF NICOTINAMIDE-ADENINE DINUCLEOTIDE TO YEAST D-GLYCERALDEHYDE-3-PHOSPHATE DEHYDROGENASE: TEMPERATURE-JUMP RELAXATION STUDIES ON THE MECHANISM OF AN ALLOSTERIC ENZYME. *Proc. Natl. Acad. Sci.* **1966**, *56*, 1661–1667, doi:10.1073/pnas.56.6.1661.

45. Johnson, K.A. Role of induced fit in enzyme specificity: A molecular forward/reverse switch. *J. Biol. Chem.* 2008, *283*, 26297–26301.

46. Lee, G.M.; Craik, C.S. Trapping moving targets with small molecules. *Science (80-.).* 2009, *324*, 213–215.

47. Wagner, J.R.; Lee, C.T.; Durrant, J.D.; Malmstrom, R.D.; Feher, V.A.; Amaro, R.E. Emerging Computational Methods for the Rational Discovery of Allosteric Drugs. *Chem. Rev.* 2016, *116*, 6370–6390.

48. Tsai, C.-J.; Kumar, S.; Ma, B.; Nussinov, R. Folding funnels, binding funnels, and protein function. *Protein Sci.* **1999**, *8*, 1181–1190, doi:10.1110/ps.8.6.1181.

49. Alberghina, L.; Coccetti, P.; Orlandi, I. Systems biology of the cell cycle of Saccharomyces cerevisiae: From network mining to system-level properties. *Biotechnol. Adv.* 2009, *27*, 960–978.

50. Alberghina, L.; Mavelli, G.; Drovandi, G.; Palumbo, P.; Pessina, S.; Tripodi, F.; Coccetti, P.; Vanoni, M. Cell growth and cell cycle in Saccharomyces cerevisiae: Basic regulatory design and protein-protein interaction network. *Biotechnol. Adv.* **2012**, *30*, 52–72, doi:10.1016/j.biotechadv.2011.07.010.

51. Conrad, M.; Schothorst, J.; Kankipati, H.N.; Van Zeebroeck, G.; Rubio-Texeira, M.; Thevelein, J.M. Nutrient sensing and signaling in the yeast *Saccharomyces cerevisiae*. *FEMS Microbiol. Rev.* **2014**, *38*, 254–299, doi:10.1111/1574-6976.12065.

52. González, A.; Hall, M.N. Nutrient sensing and <scp>TOR</scp> signaling in yeast and mammals. *EMBO J.* **2017**, *36*, 397–408, doi:10.15252/embj.201696010.

53. Kayikci, Ö.; Nielsen, J. Glucose repression in *Saccharomyces cerevisiae*. *FEMS Yeast Res.* **2015**, *15*, fov068, doi:10.1093/femsyr/fov068.

54. Knorre, D.; Sokolov, S.; Zyrina, A.; Cell, F.S.-M.; 2016, undefined How do yeast sense mitochondrial dysfunction? *ncbi.nlm.nih.gov*.

55. Tripodi, F.; Nicastro, R.; Reghellin, V.; Coccetti, P. Post-translational

modifications on yeast carbon metabolism: Regulatory mechanisms beyond transcriptional control. *Biochim. Biophys. Acta - Gen. Subj.* 2015, *1850*, 620–627.

56. Steyfkens, F.; Zhang, Z.; Van Zeebroeck, G.; Thevelein, J.M. Multiple transceptors for macro- and micro-nutrients control diverse cellular properties through the PKA pathway in yeast: A paradigm for the rapidly expanding world of eukaryotic nutrient transceptors up to those in human cells. *Front. Pharmacol.* 2018, *9*.

57. Colombo, S.; Ma, P.; Cauwenberg, L.; … J.W.-T.E.; 1998, undefined Involvement of distinct G-proteins, Gpa2 and Ras, in glucose-and intracellular acidification-induced cAMP signalling in the yeast Saccharomyces cerevisiae. *embopress.org*.

58. Xue, Y.; Batlle, M.; Hirsch, J.P. GPR1 encodes a putative G protein-coupled receptor that associates with the Gpa2p Galpha subunit and functions in a Ras-independent pathway. *EMBO J.* **1998**, *17*, 1996–2007, doi:10.1093/emboj/17.7.1996.

59. Kataoka, T.; Powers, S.; McGill, C.; Fasano, O.; Strathern, J.; Broach, J.; Wigler, M. Genetic analysis of yeast RAS1 and RAS2 genes. *Cell* **1984**, *37*, 437–445, doi:10.1016/0092-8674(84)90374-X.

60. Jacquet, E.; Parrini, M.C.; Bernardi, A.; Martegani, E.; Parmeggiani, A. Properties of the catalytic domain of CDC25, a saccharomyces cerevisiae GDP/GTP exchange factor: Comparison of its activity on full-length and c-terminal truncated ras2 proteins. *Biochem. Biophys. Res. Commun.* **1994**, *199*, 497–503, doi:10.1006/bbrc.1994.1256.

61. Rolland, F.; de Winde, J.H.; Lemaire, K.; Boles, E.; Thevelein, J.M.; Winderickx, J. Glucose-induced cAMP signalling in yeast requires both a G-protein coupled receptor system for extracellular glucose

detection and a separable hexose kinase-dependent sensing process. *Mol. Microbiol.* **2000**, *38*, 348–358, doi:10.1046/j.1365-2958.2000.02125.x.

62. Toda, T.; Cameron, S.; Sass, P.; Zoller, M.; Scott, J.D.; McMullen, B.; Hurwitz, M.; Krebs, E.G.; Wigler, M. Cloning and characterization of BCY1, a locus encoding a regulatory subunit of the cyclic AMP-dependent protein kinase in Saccharomyces cerevisiae. *Mol. Cell. Biol.* **1987**, *7*, 1371–1377, doi:10.1128/mcb.7.4.1371.

63. Rolland, F.; Wanke, V.; Cauwenberg, L.; Ma, P.; Boles, E.; Vanoni, M.; de Winde, J.H.; Thevelein, J.M.; Winderickx, J. The role of hexose transport and phosphorylation in cAMP signalling in the yeast Saccharomyces cerevisiae. *FEMS Yeast Res.* **2001**, *1*, 33–45, doi:10.1111/j.1567-1364.2001.tb00011.x.

64. Blázquez, M.A.; Lagunas, R.; Gancedo, C.; Gancedo, J.M. Trehalose-6-phosphate, a new regulator of yeast glycolysis that inhibits hexokinases. *FEBS Lett.* **1993**, *329*, 51–54, doi:10.1016/0014-5793(93)80191-V.

65. Heinisch, J. Construction and physiological characterization of mutants disrupted in the phosphofructokinase genes of Saccharomyces cerevisiae. *Curr. Genet.* **1986**, *11*, 227–234, doi:10.1007/BF00420611.

66. Huberts, D.H.E.W.; Niebel, B.; Heinemann, M. A flux-sensing mechanism could regulate the switch between respiration and fermentation. *FEMS Yeast Res.* **2012**, *12*, 118–128, doi:10.1111/j.1567-1364.2011.00767.x.

67. Buck, J.; Sinclair, M.L.; Schapal, L.; Cann, M.J.; Levin, L.R. Cytosolic adenylyl cyclase defines a unique signaling molecule in mammals.

Proc. Natl. Acad. Sci. U. S. A. **1999**, *96*, 79–84, doi:10.1073/pnas.96.1.79.

68.   Chen, Y.; Cann, M.J.; Litvin, T.N.; Iourgenko, V.; Sinclair, M.L.; Levin, L.R.; Buck, J. Soluble adenylyl cyclase as an evolutionarily conserved bicarbonate sensor. *Science (80-.).* **2000**, *289*, 625–628, doi:10.1126/science.289.5479.625.

69.   Cann, M.J.; Hammer, A.; Zhou, J.; Kanacher, T. A defined subset of adenylyl cyclases is regulated by bicarbonate ion. *J. Biol. Chem.* **2003**, *278*, 35033–35038, doi:10.1074/jbc.M303025200.

70.   Steegborn, C.; Litvin, T.N.; Levin, L.R.; Buck, J.; Wu, H. Bicarbonate activation of adenylyl cyclase via promotion of catalytic active site closure and metal recruitment. *Nat. Struct. Mol. Biol.* **2005**, *12*, doi:10.1038/nsmb880.

71.   Saalau-Bethell, S.M.; Berdini, V.; Cleasby, A.; Congreve, M.; Coyle, J.E.; Lock, V.; Murray, C.W.; O'Brien, M.A.; Rich, S.J.; Sambrook, T.; et al. Crystal Structure of Human Soluble Adenylate Cyclase Reveals a Distinct, Highly Flexible Allosteric Bicarbonate Binding Pocket. *ChemMedChem* **2014**, *9*, 823–832, doi:10.1002/cmdc.201300480.

72.   Esposito, G.; Jaiswal, B.S.; Xie, F.; Krajnc-Franken, M.A.M.; Robben, T.J.A.A.; Strik, A.M.; Kuil, C.; Philipsen, R.L.A.; Van Duin, M.; Conti, M.; et al. Mice deficient for soluble adenylyl cyclase are infertile because of a severe sperm-motility defect. *Proc. Natl. Acad. Sci. U. S. A.* **2004**, *101*, 2993–2998, doi:10.1073/pnas.0400050101.

73.   Ramirez, C.; Hauser, A.D.; Vucic, E.A.; Bar-Sagi, D. Plasma membrane V-ATPase controls oncogenic RAS-induced macropinocytosis. *Nature* **2019**, *576*, 477–481, doi:10.1038/s41586-019-1831-x.

74.   Commisso, C.; Davidson, S.M.; Soydaner-Azeloglu, R.G.; Parker, S.J.;

Kamphorst, J.J.; Hackett, S.; Grabocka, E.; Nofal, M.; Drebin, J.A.; Thompson, C.B.; et al. Macropinocytosis of protein is an amino acid supply route in Ras-transformed cells. *Nature* **2013**, *497*, 633–637, doi:10.1038/nature12138.

75. Roelofs, J.; Van Haastert, P.J.M. Deducing the Origin of Soluble Adenylyl Cyclase, a Gene Lost in Multiple Lineages. *Mol. Biol. Evol.* **2002**, *19*, 2239–2246, doi:10.1093/oxfordjournals.molbev.a004047.

76. Klengel, T.; Liang, W.J.; Chaloupka, J.; Ruoff, C.; Schröppel, K.; Naglik, J.R.; Eckert, S.E.; Mogensen, E.G.; Haynes, K.; Tuite, M.F.; et al. Fungal adenylyl cyclase integrates CO_2 sensing with cAMP signaling and virulence. *Curr. Biol.* **2005**, *15*, 2021–2026, doi:10.1016/j.cub.2005.10.040.

77. Mogensen, E.G.; Janbon, G.; Chaloupka, J.; Steegborn, C.; Man, S.F.; Moyrand, F.; Klengel, T.; Pearson, D.S.; Geeves, M.A.; Buck, J.; et al. Cryptococcus neoformans senses CO_2 through the carbonic anhydrase Can2 and the adenylyl cyclase Cac1. *Eukaryot. Cell* **2006**, *5*, 103–111, doi:10.1128/EC.5.1.103-111.2006.

78. Jungbluth, M.; Mösch, H.U.; Taxis, C. Acetate regulation of spore formation is under the control of the Ras/cyclic AMP/protein kinase a pathway and carbon dioxide in Saccharomyces cerevisiae. *Eukaryot. Cell* **2012**, *11*, 1021–1032, doi:10.1128/EC.05240-11.

79. Ohkuni, K.; Hayashi, M.; Yamashita, I. Bicarbonate-mediated social communication stimulates meiosis and sporulation of Saccharomyces cerevisiae. *Yeast* **1998**, *14*, 623–631, doi:10.1002/(SICI)1097-0061(199805)14:7<623::AID-YEA264>3.0.CO;2-D.

80. Coccetti, P.; Nicastro, R.; Tripodi, F. Conventional and emerging roles of the energy sensor snf1/AMPK in saccharomyces cerevisiae. *Microb.*

Cell 2018, *5*, 482–494.

81. Herzig, S.; Shaw, R.J. AMPK: Guardian of metabolism and mitochondrial homeostasis. *Nat. Rev. Mol. Cell Biol.* 2018, *19*, 121–135.

82. Crepin, N.; Rolland, F. SnRK1 activation, signaling, and networking for energy homeostasis. *Curr. Opin. Plant Biol.* 2019, *51*, 29–36.

83. Carlson, M.; Osmond, B.C.; Botstein, D. MUTANTS OF YEAST DEFECTIVE IN SUCROSE UTILIZATION. *Genetics* **1981**, *98*.

84. Nicastro, R.; Tripodi, F.; Guzzi, C.; Reghellin, V.; Khoomrung, S.; Capusoni, C.; Compagno, C.; Airoldi, C.; Nielsen, J.; Alberghina, L.; et al. Enhanced amino acid utilization sustains growth of cells lacking Snf1/AMPK. *Biochim. Biophys. Acta - Mol. Cell Res.* **2015**, *1853*, 1615–1625, doi:10.1016/J.BBAMCR.2015.03.014.

85. Castermans, D.; Somers, I.; Kriel, J.; Louwet, W.; Wera, S.; Versele, M.; Janssens, V.; Thevelein, J.M. Glucose-induced posttranslational activation of protein phosphatases PP2A and PP1 in yeast. *Cell Res.* **2012**, *22*, 1058–1077, doi:10.1038/cr.2012.20.

86. Ruiz, A.; Xu, X.; Carlson, M. Roles of two protein phosphatases, Reg1-Glc7 and Sit4, and glycogen synthesis in regulation of SNF1 protein kinase. *Proc. Natl. Acad. Sci. U. S. A.* **2011**, *108*, 6349–6354, doi:10.1073/pnas.1102758108.

87. Ruiz, A.; Xu, X.; Carlson, M. Ptc1 protein phosphatase 2C contributes to glucose regulation of SNF1/AMP-activated protein kinase (AMPK) in Saccharomyces cerevisiae. *J. Biol. Chem.* **2013**, *288*, 31052–31058, doi:10.1074/jbc.M113.503763.

88. Mayer, F.V.; Heath, R.; Underwood, E.; Sanders, M.J.; Carmena, D.; McCartney, R.R.; Leiper, F.C.; Xiao, B.; Jing, C.; Walker, P.A.; et al. ADP

Regulates SNF1, the Saccharomyces cerevisiae Homolog of AMP-Activated Protein Kinase. *Cell Metab.* **2011**, *14*, 707–714, doi:10.1016/J.CMET.2011.09.009.

89. Chandrashekarappa, D.G.; McCartney, R.R.; Schmidt, M.C. Ligand binding to the AMP-activated protein kinase active site mediates protection of the activation loop from dephosphorylation. *J. Biol. Chem.* **2013**, *288*, 89–98, doi:10.1074/jbc.M112.422659.

90. Barrett, L.; Orlova, M.; Maziarz, M.; Kuchin, S. Protein Kinase A Contributes to the Negative Control of Snf1 Protein Kinase in Saccharomyces cerevisiae. **2012**, doi:10.1128/EC.05061-11.

91. Nicastro, R.; Tripodi, F.; Gaggini, M.; Castoldi, A.; Reghellin, V.; Nonnis, S.; Tedeschi, G.; Coccetti, P. Snf1 Phosphorylates Adenylate Cyclase and Negatively Regulates Protein Kinase A-dependent Transcription in Saccharomyces cerevisiae. *J. Biol. Chem.* **2015**, *290*, 24715–26, doi:10.1074/jbc.M115.658005.

92. Rubenstein, E.; McCartney, R.; … C.Z.-J. of B.; 2008, undefined Access denied: Snf1 activation loop phosphorylation is controlled by availability of the phosphorylated threonine 210 to the PP1 phosphatase. *ASBMB*.

93. Hawley, S.A.; Boudeau, J.; Reid, J.L.; Mustard, K.J.; Udd, L.; Mäkelä, T.P.; Alessi, D.R.; Hardie, D.G. Complexes between the LKB1 tumor suppressor, STRADα/β and MO25α/β are upstream kinases in the AMP-activated protein kinase cascade. *J. Biol.* **2003**, *2*, 1–16, doi:10.1186/1475-4924-2-28.

94. Hawley, S.A.; Pan, D.A.; Mustard, K.J.; Ross, L.; Bain, J.; Edelman, A.M.; Frenguelli, B.G.; Hardie, D.G. Calmodulin-dependent protein kinase kinase-β is an alternative upstream kinase for AMP-activated protein

kinase. *Cell Metab.* **2005**, *2*, 9–19, doi:10.1016/j.cmet.2005.05.009.

95. Carling, D.; Zammit, V.A.; Hardie, D.G. A common bicyclic protein kinase cascade inactivates the regulatory enzymes of fatty acid and cholesterol biosynthesis. *FEBS Lett.* **1987**, *223*, 217–222, doi:10.1016/0014-5793(87)80292-2.

96. Zong, H.; Ren, J.M.; Young, L.H.; Pypaert, M.; Mu, J.; Birnbaum, M.J.; Shulman, G.I. AMP kinase is required for mitochondrial biogenesis in skeletal muscle in response to chronic energy deprivation. *Proc. Natl. Acad. Sci. U. S. A.* **2002**, *99*, 15983–15987, doi:10.1073/pnas.252625599.

97. Suter, M.; Riek, U.; Tuerk, R.; Schlattner, U.; Wallimann, T.; Neumann, D. Dissecting the role of 5'-AMP for allosteric stimulation, activation, and deactivation of AMP-activated protein kinase. *J. Biol. Chem.* **2006**, *281*, 32207–32216, doi:10.1074/jbc.M606357200.

98. Xiao, B.; Sanders, M.J.; Underwood, E.; Heath, R.; Mayer, F. V.; Carmena, D.; Jing, C.; Walker, P.A.; Eccleston, J.F.; Haire, L.F.; et al. Structure of mammalian AMPK and its regulation by ADP. *Nature* **2011**, *472*, 230–233, doi:10.1038/nature09932.

99. Davies, S.P.; Helps, N.R.; Cohen, P.T.W.; Hardie, D.G. 5'-AMP inhibits dephosphorylation, as well as promoting phosphorylation, of the AMP-activated protein kinase. Studies using bacterially expressed human protein phosphatase-2Cα and native bovine protein phosphatase-2Ac. *FEBS Lett.* **1995**, *377*, 421–425, doi:10.1016/0014-5793(95)01368-7.

100. Li, X.; Wang, L.; Zhou, X.E.; Ke, J.; De Waal, P.W.; Gu, X.; Tan, M.H.E.; Wang, D.; Wu, D.; Xu, H.E.; et al. Structural basis of AMPK regulation by adenine nucleotides and glycogen. *Cell Res.* **2015**, *25*, 50–66,

doi:10.1038/cr.2014.150.

101.   Chen, L.; Xin, F.-J.; Wang, J.; Hu, J.; Zhang, Y.-Y.; Wan, S.; Cao, L.-S.; Lu, C.; Li, P.; Frank Yan, S.; et al. Conserved regulatory elements in AMPK. *Nature* **2013**, *498*, doi:10.1038/nature12189.

102.   Zhang, Y.L.; Guo, H.; Zhang, C.S.; Lin, S.Y.; Yin, Z.; Peng, Y.; Luo, H.; Shi, Y.; Lian, G.; Zhang, C.; et al. AMP as a low-energy charge signal autonomously initiates assembly of axin-ampk-lkb1 complex for AMPK activation. *Cell Metab.* **2013**, *18*, 546–555, doi:10.1016/j.cmet.2013.09.005.

103.   Zhang, C.S.; Jiang, B.; Li, M.; Zhu, M.; Peng, Y.; Zhang, Y.L.; Wu, Y.Q.; Li, T.Y.; Liang, Y.; Lu, Z.; et al. The lysosomal v-ATPase-ragulator complex is a common activator for AMPK and mTORC1, acting as a switch between catabolism and anabolism. *Cell Metab.* **2014**, *20*, 526–540, doi:10.1016/j.cmet.2014.06.014.

104.   Rago, F.; Saltzberg, D.; Allen, K.N.; Tolan, D.R. Enzyme Substrate Specificity Conferred by Distinct Conformational Pathways. *J. Am. Chem. Soc.* **2015**, *137*, 13876–13886, doi:10.1021/jacs.5b08149.

105.   McBride, A.; Ghilagaber, S.; Nikolaev, A.; Hardie, D.G. The Glycogen-Binding Domain on the AMPK β Subunit Allows the Kinase to Act as a Glycogen Sensor. *Cell Metab.* **2009**, *9*, 23–34, doi:10.1016/j.cmet.2008.11.008.

106.   Wiatrowski, H.A.; van Denderen, B.J.W.; Berkey, C.D.; Kemp, B.E.; Stapleton, D.; Carlson, M. Mutations in the Gal83 Glycogen-Binding Domain Activate the Snf1/Gal83 Kinase Pathway by a Glycogen-Independent Mechanism. *Mol. Cell. Biol.* **2004**, *24*, 352–361, doi:10.1128/mcb.24.1.352-361.2004.

107.   Emanuelle, S.; Hossain, M.I.; Moller, I.E.; Pedersen, H.L.; van de

Meene, A.M.L.; Doblin, M.S.; Koay, A.; Oakhill, J.S.; Scott, J.W.; Willats, W.G.T.; et al. SnRK1 from *Arabidopsis thaliana* is an atypical AMPK. *Plant J.* **2015**, *82*, 183–192, doi:10.1111/tpj.12813.

108. Broeckx, T.; Hulsmans, S.; Rolland, F. The plant energy sensor: evolutionary conservation and divergence of SnRK1 structure, regulation, and function. **2016**, doi:10.1093/jxb/erw416.

109. Baena-González, E.; Rolland, F.; Thevelein, J.M.; Sheen, J. A central integrator of transcription networks in plant stress and energy signalling. *Nature* **2007**, *448*, 938–942, doi:10.1038/nature06069.

110. Muraro, D.; Byrne, H.M.; King, J.R.; Bennett, M.J. Mathematical Modelling Plant Signalling Networks. *Math. Model. Nat. Phenom* **2013**, *8*, 5–24, doi:10.1051/mmnp/20138402.

111. Emanuelle, S.; Doblin, M.S.; Stapleton, D.I.; Bacic, A.; Gooley, P.R. Molecular Insights into the Enigmatic Metabolic Regulator, SnRK1. *Trends Plant Sci.* 2016, *21*, 341–353.

112. Zhai, Z.; Keereetaweep, J.; Liu, H.; Feil, R.; Lunn, J.E.; Shanklin, J. Trehalose 6-phosphate positively regulates fatty acid synthesis by stabilizing wrinkled1[open]. *Plant Cell* **2018**, *30*, 2616–2627, doi:10.1105/tpc.18.00521.

113. Shimobayashi, M.; Hall, M.N. Making new contacts: The mTOR network in metabolism and signalling crosstalk. *Nat. Rev. Mol. Cell Biol.* **2014**, *15*, 155–162, doi:10.1038/nrm3757.

114. Kim, E.; Goraksha-Hicks, P.; Li, L.; Neufeld, T.P.; Guan, K.L. Regulation of TORC1 by Rag GTPases in nutrient response. *Nat. Cell Biol.* **2008**, *10*, 935–945, doi:10.1038/ncb1753.

115. Binda, M.; Péli-Gulli, M.P.; Bonfils, G.; Panchaud, N.; Urban, J.; Sturgill, T.W.; Loewith, R.; De Virgilio, C. The Vam6 GEF Controls TORC1 by

Activating the EGO Complex. *Mol. Cell* **2009**, *35*, 563–573, doi:10.1016/j.molcel.2009.06.033.

116. Kim, A.; Cunningham, K.W. A LAPF/phafin1-like protein regulates TORC1 and lysosomal membrane permeabilization in response to endoplasmic reticulum membrane stress. *Mol. Biol. Cell* **2015**, *26*, 4631–4645, doi:10.1091/mbc.E15-08-0581.

117. Zhang, T.; Péli-Gulli, M.P.; Yang, H.; De Virgilio, C.; Ding, J. Ego3 functions as a homodimer to mediate the interaction between Gtr1-Gtr2 and Ego1 in the EGO complex to activate TORC1. *Structure* **2012**, *20*, 2151–2160, doi:10.1016/j.str.2012.09.019.

118. Kira, S.; Tabata, K.; Shirahama-Noda, K.; Nozoe, A.; Yoshimori, T.; Noda, T. Reciprocal conversion of Gtr1 and Gtr2 nucleotidebinding states by Npr2-Npr3 inactivates TORC1 and induces autophagy. *Autophagy* **2014**, *10*, 1565–1578, doi:10.4161/auto.29397.

119. Bonfils, G.; Jaquenoud, M.; Bontron, S.; Ostrowicz, C.; Ungermann, C.; De Virgilio, C. Leucyl-tRNA Synthetase Controls TORC1 via the EGO Complex. *Mol. Cell* **2012**, *46*, 105–110, doi:10.1016/j.molcel.2012.02.009.

120. Hohmann, S.; Thevelein, J.M. The cell division cycle gene CDC60 encodes cytosolic leucyl-tRNA synthetase in Saccharomyces cerevisiae. *Gene* **1992**, *120*, 43–49, doi:10.1016/0378-1119(92)90007-C.

121. Echols, N.; Harrison, P.; Balasubramanian, S.; Luscombe, N.M.; Bertone, P.; Zhang, Z.; Gerstein, M. *Comprehensive analysis of amino acid and nucleotide composition in eukaryotic genomes, comparing genes and pseudogenes*; 2002; Vol. 30;.

122. Ghaemmaghami, S.; Huh, W.K.; Bower, K.; Howson, R.W.; Belle, A.;

Dephoure, N.; O'Shea, E.K.; Weissman, J.S. Global analysis of protein expression in yeast. *Nature* **2003**, *425*, 737–741, doi:10.1038/nature02046.

123. Rock, F.L.; Mao, W.; Yaremchuk, A.; Tukalo, M.; Crépin, T.; Zhou, H.; Zhang, Y.K.; Hernandez, V.; Akama, T.; Baker, S.J.; et al. An antifungal agent inhibits an aminoacyl-tRNA synthetase by trapping tRNA in the editing site. *Science (80-.).* **2007**, *316*, 1759–1761, doi:10.1126/science.1142189.

124. Powis, K.; De Virgilio, C. Conserved regulators of Rag GTPases orchestrate amino acid-dependent TORC1 signaling. *Cell Discov.* 2016, *2*, 1–16.

125. Hara, K.; Yonezawa, K.; Weng, Q.P.; Kozlowski, M.T.; Belham, C.; Avruch, J. Amino acid sufficiency and mTOR regulate p70 S6 kinase and eIF-4E BP1 through a common effector mechanism. *J. Biol. Chem.* **1998**, *273*, 14484–14494, doi:10.1074/jbc.273.23.14484.

126. Menon, S.; Dibble, C.C.; Talbott, G.; Hoxhaj, G.; Valvezan, A.J.; Takahashi, H.; Cantley, L.C.; Manning, B.D. Spatial control of the TSC complex integrates insulin and nutrient regulation of mTORC1 at the lysosome. *Cell* **2014**, *156*, 771–785, doi:10.1016/j.cell.2013.11.049.

127. Sancak, Y.; Peterson, T.R.; Shaul, Y.D.; Lindquist, R.A.; Thoreen, C.C.; Bar-Peled, L.; Sabatini, D.M. The rag GTPases bind raptor and mediate amino acid signaling to mTORC1. *Science (80-.).* **2008**, *320*, 1496–1501, doi:10.1126/science.1157535.

128. Sancak, Y.; Bar-Peled, L.; Zoncu, R.; Markhard, A.L.; Nada, S.; Sabatini, D.M. Ragulator-rag complex targets mTORC1 to the lysosomal surface and is necessary for its activation by amino acids. *Cell* **2010**, *141*, 290–303, doi:10.1016/j.cell.2010.02.024.

129. Long, X.; Lin, Y.; Ortiz-Vega, S.; Yonezawa, K.; Avruch, J. Rheb binds and regulates the mTOR kinase. *Curr. Biol.* **2005**, *15*, 702–713, doi:10.1016/j.cub.2005.02.053.

130. Han, J.M.; Jeong, S.J.; Park, M.C.; Kim, G.; Kwon, N.H.; Kim, H.K.; Ha, S.H.; Ryu, S.H.; Kim, S. Leucyl-tRNA synthetase is an intracellular leucine sensor for the mTORC1-signaling pathway. *Cell* **2012**, *149*, 410–424, doi:10.1016/j.cell.2012.02.044.

131. Bar-Peled, L.; Chantranupong, L.; Cherniack, A.D.; Chen, W.W.; Ottina, K.A.; Grabiner, B.C.; Spear, E.D.; Carter, S.L.; Meyerson, M.; Sabatini, D.M. A tumor suppressor complex with GAP activity for the Rag GTPases that signal amino acid sufficiency to mTORC1. *Science (80-.).* **2013**, *340*, 1100–1106, doi:10.1126/science.1232044.

132. Wolfson, R.L.; Chantranupong, L.; Saxton, R.A.; Shen, K.; Scaria, S.M.; Cantor, J.R.; Sabatini, D.M. Sestrin2 is a leucine sensor for the mTORC1 pathway. *Science (80-.).* **2016**, *351*, 43–48, doi:10.1126/science.aab2674.

133. Saxton, R.A.; Chantranupong, L.; Knockenhauer, K.E.; Schwartz, T.U.; Sabatini, D.M. Mechanism of arginine sensing by CASTOR1 upstream of mTORC1. *Nature* **2016**, *536*, 229–233, doi:10.1038/nature19079.

134. Parsons, A.B.; Brost, R.L.; Ding, H.; Li, Z.; Zhang, C.; Sheikh, B.; Brown, G.W.; Kane, P.M.; Hughes, T.R.; Boone, C. Integration of chemical-genetic and genetic interaction data links bioactive compounds to cellular target pathways. *Nat. Biotechnol.* **2004**, *22*, 62–69, doi:10.1038/nbt919.

135. Costanzo, M.; Baryshnikova, A.; Bellay, J.; Kim, Y.; Spear, E.D.; Sevier, C.S.; Ding, H.; Koh, J.L.Y.; Toufighi, K.; Mostafavi, S.; et al. The genetic landscape of a cell. *Science (80-.).* **2010**, *327*, 425–431,

doi:10.1126/science.1180823.

136. Wang, S.; Tsun, Z.Y.; Wolfson, R.L.; Shen, K.; Wyant, G.A.; Plovanich, M.E.; Yuan, E.D.; Jones, T.D.; Chantranupong, L.; Comb, W.; et al. Lysosomal amino acid transporter SLC38A9 signals arginine sufficiency to mTORC1. *Science (80-.).* **2015**, *347*, 188–194, doi:10.1126/science.1257132.

137. Sutter, B.M.; Wu, X.; Laxman, S.; Tu, B.P. XMethionine inhibits autophagy and promotes growth by inducing the SAM-responsive methylation of PP2A. *Cell* **2013**, *154*, 403, doi:10.1016/j.cell.2013.06.041.

138. Shi, L.; Wu, Y.; Sheen, J. TOR signaling in plants: conservation and innovation. *Development* 2018, *145*.

139. Xiong, Y.; McCormack, M.; Li, L.; Hall, Q.; Xiang, C.; Sheen, J. Glucose-TOR signalling reprograms the transcriptome and activates meristems. *Nature* **2013**, *496*, 181–186, doi:10.1038/nature12030.

140. Zhang, N.; Meng, Y.; Li, X.; Zhou, Y.; Ma, L.; Fu, L.; Schwarzländer, M.; Liu, H.; Xiong, Y. Metabolite-mediated TOR signaling regulates the circadian clock in Arabidopsis. *Proc. Natl. Acad. Sci. U. S. A.* **2019**, *116*, 25395–25397, doi:10.1073/pnas.1913095116.

141. Nukarinen, E.; Ngele, T.; Pedrotti, L.; Wurzinger, B.; Mair, A.; Landgraf, R.; Börnke, F.; Hanson, J.; Teige, M.; Baena-Gonzalez, E.; et al. Quantitative phosphoproteomics reveals the role of the AMPK plant ortholog SnRK1 as a metabolic master regulator under energy deprivation. *Sci. Rep.* **2016**, *6*, 1–19, doi:10.1038/srep31697.

142. Gwinn, D.M.; Shackelford, D.B.; Egan, D.F.; Mihaylova, M.M.; Mery, A.; Vasquez, D.S.; Turk, B.E.; Shaw, R.J. AMPK Phosphorylation of Raptor Mediates a Metabolic Checkpoint. *Mol. Cell* **2008**, *30*, 214–

226, doi:10.1016/j.molcel.2008.03.003.

143. Kim, S.G.; Hoffman, G.R.; Poulogiannis, G.; Buel, G.R.; Jang, Y.J.; Lee, K.W.; Kim, B.Y.; Erikson, R.L.; Cantley, L.C.; Choo, A.Y.; et al. Metabolic Stress Controls mTORC1 Lysosomal Localization and Dimerization by Regulating the TTT-RUVBL1/2 Complex. *Mol. Cell* **2013**, *49*, 172–185, doi:10.1016/j.molcel.2012.10.003.

144. Dong, Y.; Silbermann, M.; Speiser, A.; Forieri, I.; Linster, E.; Poschet, G.; Allboje Samami, A.; Wanatabe, M.; Sticht, C.; Teleman, A.A.; et al. Sulfur availability regulates plant growth via glucose-TOR signaling. *Nat. Commun.* **2017**, *8*, doi:10.1038/s41467-017-01224-w.

145. Cao, P.; Kim, S.J.; Xing, A.; Schenck, C.A.; Liu, L.; Jiang, N.; Wang, J.; Last, R.L.; Brandizzi, F. Homeostasis of branched-chain amino acids is critical for the activity of TOR signaling in Arabidopsis. *Elife* **2019**, *8*, doi:10.7554/eLife.50747.

146. JT, P.; H, Y.S.; JP, V.D. Pyruvate Metabolism in Saccharomyces Cerevisiae. *Yeast* **1996**, *12*, doi:10.1002/(SICI)1097-0061(199612)12:16<1607::AID-YEA70>3.0.CO;2-4.

147. Jeong, S.Y.; Seol, D.W. The role of mitochondria in apoptosis. *J. Biochem. Mol. Biol.* 2008, *41*, 11–22.

148. Shadel, G.S.; Horvath, T.L. Mitochondrial ROS Signaling in Organismal Homeostasis. *Cell* 2015, *163*, 560–569.

149. Liao, X.S.; Small, W.C.; Srere, P.A.; Butow, R.A. Intramitochondrial functions regulate nonmitochondrial citrate synthase (CIT2) expression in Saccharomyces cerevisiae. *Mol. Cell. Biol.* **1991**, *11*, 38–46, doi:10.1128/mcb.11.1.38.

150. Liu, Z.; Butow, R.A. A Transcriptional Switch in the Expression of Yeast Tricarboxylic Acid Cycle Genes in Response to a Reduction or Loss of

Respiratory Function. *Mol. Cell. Biol.* **1999**, *19*, 6720–6728, doi:10.1128/mcb.19.10.6720.

151. Hallstrom, T.C.; Moye-Rowley, W.S. Multiple signals from dysfunctional mitochondria activate the pleiotropic drug resistance pathway in Saccharomyces cerevisiae. *J. Biol. Chem.* **2000**, *275*, 37347–37356, doi:10.1074/jbc.M007338200.

152. Butow, R.A.; Avadhani, N.G. Mitochondrial signaling: The retrograde response. *Mol. Cell* 2004, *14*, 1–15.

153. Upadhyay, S.; Srivastava, Y. Retrograde response by reactive oxygen/nitrogen species in plants involving different cellular organelles. *Biol. Chem.* 2019, *400*, 979–989.

154. Sekito, T.; Thornton, J.; Butow, R.A. Mitochondria-to-nuclear signaling is regulated by the subcellular localization of the transcription factors Rtg1p and Rtg3p. *Mol. Biol. Cell* **2000**, *11*, 2103–2115, doi:10.1091/mbc.11.6.2103.

155. Liu, Z.; Sekito, T.; SŠpiírek, M.; Thornton, J.; Butow, R.A. Retrograde signaling is regulated by the dynamic interaction between Rtg2p and Mks1p. *Mol. Cell* **2003**, *12*, 401–411, doi:10.1016/S1097-2765(03)00285-5.

156. Santulli, G.; Nakashima, R.; Yuan, Q.; Marks, A.R. Intracellular calcium release channels: an update. *J. Physiol.* 2017, *595*, 3041–3051.

157. Berridge, M.J. The inositol trisphosphate/calcium signaling pathway in health and disease. *Physiol. Rev.* **2016**, *96*, 1261–1296, doi:10.1152/physrev.00006.2016.

158. Clapper, D.L.; Walseth, T.F.; Dargie, P.J.; Hon Cheung Lee Pyridine nucleotide metabolites stimulate calcium release from sea urchin egg microsomes desensitized to inositol trisphosphate. *J. Biol. Chem.*

1987, *262*, 9561–9568.

159. Galione, A.; Lee, H.C.; Busa, W.B. Ca2+-induced Ca2+ release in sea urchin egg homogenates: Modulation by cyclic ADP-Ribose. *Science (80-.).* **1991**, *253*, 1143–1146, doi:10.1126/science.1909457.

160. Lee, H.C. Potentiation of calcium- and caffeine-induced calcium release by cyclic ADP-ribose. *J. Biol. Chem.* **1993**, *268*, 293–9.

161. Zheng, J.; Wenzhi, B.; Miao, L.; Hao, Y.; Zhang, X.; Yin, W.; Pan, J.; Yuan, Z.; Song, B.; Ji, G. Ca2+ release induced by cADP-ribose is mediated by FKBP12.6 proteins in mouse bladder smooth muscle. *Cell Calcium* **2010**, *47*, 449–457, doi:10.1016/j.ceca.2010.03.006.

162. Yamasaki-Mann, M.; Demuro, A.; Parker, I. cADPR stimulates SERCA activity in Xenopus oocytes. *Cell Calcium* **2009**, *45*, 293–299, doi:10.1016/j.ceca.2008.11.008.

163. Yamasaki-Mann, M.; Demuro, A.; Parker, I. Modulation of endoplasmic reticulum Ca2+ store filling by cyclic ADP-ribose promotes inositol trisphosphate (IP3)-evoked Ca 2+ signals. *J. Biol. Chem.* **2010**, *285*, 25053–25061, doi:10.1074/jbc.M109.095257.

164. Park, D.R.; Nam, T.S.; Kim, Y.W.; Lee, S.H.; Kim, U.H. CD38-cADPR-SERCA Signaling Axis Determines Skeletal Muscle Contractile Force in Response to β-Adrenergic Stimulation. *Cell. Physiol. Biochem.* **2018**, *46*, 2017–2030, doi:10.1159/000489441.

165. Lange, I.; Penner, R.; Fleig, A.; Beck, A. Synergistic regulation of endogenous TRPM2 channels by adenine dinucleotides in primary human neutrophils. *Cell Calcium* **2008**, *44*, 604–615, doi:10.1016/j.ceca.2008.05.001.

166. Wolf, B.A.; Colcaq, J.R.; Cornens, P.G.; Turk, J.; Mcdaniels, M.L. *Glucose 6-Phosphate Regulates Ca2+ Steady State in Endoplasmic*

Reticulum of Islets A POSSIBLE LINK IN GLUCOSE-INDUCED INSULIN SECRETION*; 1986; Vol. 261;.

167. Chen, P.Y.; Csutora, P.; Veyna-Burke, N.A.; Marchase, R.B. Glucose-6-phosphate and Ca2+ sequestration are mutually enhanced in microsomes from liver, brain, and heart. *Diabetes* **1998**, *47*, 874–881, doi:10.2337/diabetes.47.6.874.

168. Kockskämper, J.; Zima, A. V.; Blatter, L.A. Modulation of sarcoplasmic reticulum Ca $^{2+}$ release by glycolysis in cat atrial myocytes. *J. Physiol.* **2005**, *564*, 697–714, doi:10.1113/jphysiol.2004.078782.

169. Fukumoto, G.H.; Lamp, S.T.; Motter, C.; Bridge, J.H.B.; Garfinkel, A.; Goldhaber, J.I. Metabolic inhibition alters subcellular calcium release patterns in rat ventricular myocytes: implications for defective excitation-contraction coupling during cardiac ischemia and failure. *Circ. Res.* **2005**, *96*, 551–7, doi:10.1161/01.RES.0000159388.61313.47.

170. Cyert, M.S.; Philpott, C.C. Regulation of cation balance in Saccharomyces cerevisiae. *Genetics* **2013**, *193*, 677–713, doi:10.1534/genetics.112.147207.

171. Pittman, J.K. Vacuolar Ca2+ uptake. *Cell Calcium* 2011, *50*, 139–146.

172. Bonilla, M.; Cunningham, K.W. Calcium release and influx in yeast: TRPC and VGCC rule another kingdom. *Sci. STKE* 2002, *2002*.

173. Palmer, C.P.; Zhou, X.L.; Lin, J.; Loukin, S.H.; Kung, C.; Saimi, Y. A TRP homolog in Saccharomyces cerevisiae forms an intracellular Ca2+-permeable channel in the yeast vacuolar membrane. *Proc. Natl. Acad. Sci. U. S. A.* **2001**, *98*, 7801–7805, doi:10.1073/pnas.141036198.

174. Dürr, G.; Strayle, J.; Plemper, R.; Elbs, S.; Klee, S.K.; Catty, P.; Wolf, D.H.; Rudolph, H.K. The medial-Golgi ion pump Pmr1 supplies the

yeast secretory pathway with Ca2+ and Mn2+ required for glycosylation, sorting, and endoplasmic reticulum-Associated protein degradation. *Mol. Biol. Cell* **1998**, *9*, 1149–1162, doi:10.1091/mbc.9.5.1149.

175. Tisi, R.; Belotti, F.; Wera, S.; Winderickx, J.; Thevelein, J.M.; Martegani, E. Evidence for inositol triphosphate as a second messenger for glucose-induced calcium signalling in budding yeast. *Curr. Genet.* **2004**, *45*, 83–89, doi:10.1007/s00294-003-0465-5.

176. Busti, S.; Mapelli, V.; Tripodi, F.; Sanvito, R.; Magni, F.; Coccetti, P.; Rocchetti, M.; Nielsen, J.; Alberghina, L.; Vanoni, M. Respiratory metabolism and calorie restriction relieve persistent endoplasmic reticulum stress induced by calcium shortage in yeast. *Sci. Rep.* **2016**, *6*, doi:10.1038/srep27942.

177. Tökés-Füzesi, M.; Bedwell, D.M.; Repa, I.; Sipos, K.; Sümegi, B.; Rab, A.; Miseta, A. Hexose phosphorylation and the putative calcium channel component Mid1p are required for the hexose-induced transient elevation of cytosolic calcium response in Saccharomyces cerevisiae. *Mol. Microbiol.* **2002**, *44*, 1299–1308, doi:10.1046/j.1365-2958.2002.02956.x.

178. Tisi, R.; Baldassa, S.; Belotti, F.; Martegani, E. Phospholipase C is required for glucose-induced calcium influx in budding yeast. *FEBS Lett.* **2002**, *520*, 133–138, doi:10.1016/S0014-5793(02)02806-5.

179. Fu, L.; Miseta, A.; Hunton, D.; Marchase, R.B.; Bedwell, D.M. Loss of the major isoform of phosphoglucomutase results in altered calcium homeostasis in Saccharomyces cerevisiae. *J. Biol. Chem.* **2000**, *275*, 5431–5440, doi:10.1074/jbc.275.8.5431.

180. Aiello, D.P.; Fu, L.; Miseta, A.; Bedwell, D.M. Intracellular glucose 1-

phosphate and glucose 6-phosphate levels modulate Ca2+ homeostasis in Saccharomyces cerevisiae. *J. Biol. Chem.* **2002**, *277*, 45751–45758, doi:10.1074/jbc.M208748200.

181. Aiello, D.P.; Fu, L.; Miseta, A.; Sipos, K.; Bedwell, D.M. The Ca2+ homeostasis defects in a pgm2Δ strain of Saccharomyces cerevisiae are caused by excessive vacuolar Ca2+ uptake mediated by the Ca2+- ATPase Pmc1p. *J. Biol. Chem.* **2004**, *279*, 38495–38502, doi:10.1074/jbc.M400833200.

182. Feng, Y.; De Franceschi, G.; Kahraman, A.; Soste, M.; Melnik, A.; Boersema, P.J.; De Laureto, P.P.; Nikolaev, Y.; Oliveira, A.P.; Picotti, P. Global analysis of protein structural changes in complex proteomes. *Nat. Biotechnol.* **2014**, *32*, 1036–1044, doi:10.1038/nbt.2999.

183. Li, X.; Gianoulis, T.A.; Yip, K.Y.; Gerstein, M.; Snyder, M. Extensive in vivo metabolite-protein interactions revealed by large-scale systematic analyses. *Cell* **2010**, *143*, 639–650, doi:10.1016/j.cell.2010.09.048.

184. Orth, J.D.; Thiele, I.; Palsson, B.∅. What is flux balance analysis? *Nat. Biotechnol.* **2010**, *28*, 245–248, doi:10.1038/nbt.1614.

185. Nielsen, J. Yeast Systems Biology: Model Organism and Cell Factory. *Biotechnol. J.* **2019**, *14*, 1800421, doi:10.1002/BIOT.201800421.

186. Welkenhuysen, N.; Schnitzer, B.; Österberg, L.; Cvijovic, M. Robustness of nutrient signaling is maintained by interconnectivity between signal transduction pathways. *Front. Physiol.* **2019**, *10*, 1964, doi:10.3389/fphys.2018.01964.

187. Bozaquel-Morais, B.L.; Madeira, J.B.; Monteiro, M.-; Masuda, C.M.; Montero-Lomeli, C.A. A New Fluorescence-Based Method Identifies Protein Phosphatases Regulating Lipid Droplet Metabolism. *PLoS One*

2010, *5*, 13692, doi:10.1371/journal.pone.0013692.

188. Milanesi, R.; Coccetti, P.; Tripodi, F. The Regulatory Role of Key Metabolites in the Control of Cell Signaling. *Biomolecules* **2020**, *10*, 862, doi:10.3390/biom10060862.

189. Hong, S.P.; Leiper, F.C.; Woods, A.; Carling, D.; Carlson, M. Activation of yeast Snf1 and mammalian AMP-activated protein kinase by upstream kinases. *Proc. Natl. Acad. Sci. U. S. A.* **2003**, *100*, 8839–8843, doi:10.1073/pnas.1533136100.

190. Toda, T.; Uno, I.; Ishikawa, T.; Powers, S.; Kataoka, T.; Broek, D.; Cameron, S.; Broach, J.; Matsumoto, K.; Wigler, M. In yeast, RAS proteins are controlling elements of adenylate cyclase. *Cell* **1985**, *40*, 27–36, doi:10.1016/0092-8674(85)90305-8.

191. Wilson, W.A.; Hawley, S.A.; Hardie, D.G. Glucose repression/derepression in budding yeast: SNF1 protein kinase is activated by phosphorylation under derepressing conditions, and this correlates with a high AMP:ATP ratio. *Curr. Biol.* **1996**, *6*, 1426–1434, doi:10.1016/S0960-9822(96)00747-6.

192. Otterstedt, K.; Larsson, C.; Bill, R.M.; Ståhlberg, A.; Boles, E.; Hohmann, S.; Gustafsson, L. Switching the mode of metabolism in the yeast *Saccharomyces cerevisiae*. *EMBO Rep.* **2004**, *5*, 532–537, doi:10.1038/sj.embor.7400132.

193. Elbing, K.; Stahlberg, A.; Hohmann, S.; Gustafsson, L. Transcriptional responses to glucose at different glycolytic rates in Saccharomyces cerevisiae. *Eur. J. Biochem.* **2004**, *271*, 4855–4864, doi:10.1111/j.1432-1033.2004.04451.x.

194. Reifenberger, E.; Freidel, K.; Ciriacy, M. Identification of novel HXT genes in Saccharomyces cerevisiae reveals the impact of individual

hexose transporters on qlycolytic flux. *Mol. Microbiol.* **1995**, *16*, 157–167, doi:10.1111/j.1365-2958.1995.tb02400.x.

195. Kümmel, A.; Ewald, J.C.; Fendt, S.-M.; Jol, S.J.; Picotti, P.; Aebersold, R.; Sauer, U.; Zamboni, N.; Heinemann, M. Differential glucose repression in common yeast strains in response to HXK2 deletion. *FEMS Yeast Res.* **2010**, *10*, 322–332, doi:10.1111/j.1567-1364.2010.00609.x.

196. Peláez, R.; Herrero, P.; Moreno, F. Functional domains of yeast hexokinase 2. *Biochem. J.* **2010**, *432*, 181–190, doi:10.1042/BJ20100663.

197. Jeon, S.-M. Regulation and function of AMPK in physiology and diseases. *Exp. Mol. Med. 2016 487* **2016**, *48*, e245–e245, doi:10.1038/emm.2016.81.

198. Minokoshi, Y.; Alquier, T.; Furukawa, N.; Kim, Y.-B.; Lee, A.; Xue, B.; Mu, J.; Foufelle, F.; Ferré, P.; Birnbaum, M.J.; et al. AMP-kinase regulates food intake by responding to hormonal and nutrient signals in the hypothalamus. *Nat. 2004 4286982* **2004**, *428*, 569–574, doi:10.1038/nature02440.

199. López, M. AMPK Wars: the VMH Strikes Back, Return of the PVH. *Trends Endocrinol. Metab.* **2018**, *29*, 135–137, doi:10.1016/J.TEM.2018.01.004.

200. Stark, R.; Ashley, S.E.; Andrews, Z.B. AMPK and the neuroendocrine regulation of appetite and energy expenditure. *Mol. Cell. Endocrinol.* **2013**, *366*, 215–223, doi:10.1016/J.MCE.2012.06.012.

201. Vazirian, M.; Nabavi, S.M.; Jafari, S.; Manayi, A. Natural activators of adenosine 5'-monophosphate (AMP)-activated protein kinase (AMPK) and their pharmacological activities. *Food Chem. Toxicol.*

2018, *122*, 69–79, doi:10.1016/J.FCT.2018.09.079.

202. CL, L.; HM, R. Nutritional Modulation of AMPK-Impact upon Metabolic-Inflammation. *Int. J. Mol. Sci.* **2018**, *19*, doi:10.3390/IJMS19103092.

203. MS, K.; JY, P.; C, N.; PG, J.; JW, R.; HS, S.; JY, Y.; IS, N.; J, H.; IS, P.; et al. Anti-obesity effects of alpha-lipoic acid mediated by suppression of hypothalamic AMP-activated protein kinase. *Nat. Med.* **2004**, *10*, 727–733, doi:10.1038/NM1061.

204. MS, K.; KU, L. Role of hypothalamic 5'-AMP-activated protein kinase in the regulation of food intake and energy homeostasis. *J. Mol. Med. (Berl).* **2005**, *83*, 514–520, doi:10.1007/S00109-005-0659-Z.

205. ED, T.; F, D.; V, K.; GT, K.; AV, G.; Y, Z.; CB, C.; MB, W. alpha-lipoic acid regulates AMP-activated protein kinase and inhibits insulin secretion from beta cells. *Diabetologia* **2006**, *49*, 1587–1598, doi:10.1007/S00125-006-0265-9.

206. DeVit, M.J.; Johnston, M. The nuclear exportin Msn5 is required for nuclear export of the Mig1 glucose repressor of Saccharomyces cerevisiae. *Curr. Biol.* **1999**, *9*, 1231–1241, doi:10.1016/S0960-9822(99)80503-X.

207. Chavarría, M.; de Lorenzo, V. The imbroglio of the physiological Cra effector clarified at last. *Mol. Microbiol.* **2018**, *109*, 273–277, doi:10.1111/MMI.14080.

208. Momcilovic, M.; Iram, S.H.; Liu, Y.; Carlson, M. Roles of the glycogen-binding domain and SNF4 in glucose inhibition of SNF1 protein kinase. *J. Biol. Chem.* **2008**, *283*, 19521–19529, doi:10.1074/jbc.M803624200.

209. Amodeo, G.A.; Rudolph, M.J.; Tong, L. Crystal structure of the

heterotrimer core of Saccharomyces cerevisiae AMPK homologue SNF1. *Nature* **2007**, *449*, 492–495, doi:10.1038/nature06127.

210. Rubenstein, E.M.; McCartney, R.R.; Zhang, C.; Shokat, K.M.; Shirra, M.K.; Arndt, K.M.; Schmidt, M.C. Access denied: Snf1 activation loop phosphorylation is controlled by availability of the phosphorylated threonine 210 to the PP1 phosphatase. *J. Biol. Chem.* **2008**, *283*, 222–230, doi:10.1074/jbc.M707957200.

211. Momcilovic, M.; Carlson, M. Alterations at dispersed sites cause phosphorylation and activation of SNF1 protein kinase during growth on high glucose. *J. Biol. Chem.* **2011**, *286*, 23544–51, doi:10.1074/jbc.M111.244111.

212. Barzilai, N.; Bartke, A. Biological Approaches to Mechanistically Understand the Healthy Life Span Extension Achieved by Calorie Restriction and Modulation of Hormones. *Journals Gerontol. Ser. A* **2009**, *64A*, 187–191, doi:10.1093/GERONA/GLN061.

213. Cox, L.S.; Mattison, J.A. Increasing longevity through caloric restriction or rapamycin feeding in mammals: common mechanisms for common outcomes? *Aging Cell* **2009**, *8*, 607–613, doi:10.1111/J.1474-9726.2009.00509.X.

214. Masoro, E.J. Overview of caloric restriction and ageing. *Mech. Ageing Dev.* **2005**, *126*, 913–922, doi:10.1016/J.MAD.2005.03.012.

215. Piper, M.D.W.; Bartke, A. Diet and Aging. *Cell Metab.* **2008**, *8*, 99–104, doi:10.1016/J.CMET.2008.06.012.

216. López-Otín, C.; Galluzzi, L.; Freije, J.M.P.; Madeo, F.; Kroemer, G. Metabolic Control of Longevity. *Cell* **2016**, *166*, 802–821, doi:10.1016/J.CELL.2016.07.031.

217. Wahl, D.; Solon-Biet, S.M.; Cogger, V.C.; Fontana, L.; Simpson, S.J.; Le

Couteur, D.G.; Ribeiro, R. V. Aging, lifestyle and dementia. *Neurobiol. Dis.* **2019**, *130*, 104481, doi:10.1016/J.NBD.2019.104481.

218. Fontana, L.; Partridge, L.; Longo, V.D. Extending healthy life span-from yeast to humans. *Science (80-.).* **2010**, *328*, 321–326, doi:10.1126/SCIENCE.1172539/SUPPL_FILE/PLAYLIST.XML.

219. Longo, V.D.; Shadel, G.S.; Kaeberlein, M.; Kennedy, B. Replicative and chronological aging in saccharomyces cerevisiae. *Cell Metab.* **2012**, *16*, 18–31, doi:10.1016/J.CMET.2012.06.002/ATTACHMENT/A06F38AE-04BD-4C4D-B585-CA3863DB7C8E/MMC1.PDF.

220. Fontana, L.; Partridge, L. Promoting Health and Longevity through Diet: From Model Organisms to Humans. *Cell* **2015**, *161*, 106–118, doi:10.1016/J.CELL.2015.02.020.

221. Templeman, N.M.; Murphy, C.T. Regulation of reproduction and longevity by nutrient-sensing pathways. *J. Cell Biol.* **2018**, *217*, 93–106, doi:10.1083/JCB.201707168.

222. Dodel, R.; Csoti, I.; Ebersbach, G.; Fuchs, G.; Hahne, M.; Kuhn, W.; Oechsner, M.; Jost, W.; Reichmann, H.; Schulz, J.B. Lewy body dementia and Parkinson's disease with dementia. *J. Neurol. 2008 2555* **2008**, *255*, 39–47, doi:10.1007/S00415-008-5007-0.

223. De Rijk, M.C.; Launer, L.J.; Berger, K.; Breteler, M.M.B.; Dartigues, J.F.; Baldereschi, M.; Fratiglioni, L.; Lobo, A.; Martinez-Lage, J.; Trenkwalder, C.; et al. Prevalence of Parkinson's disease in Europe: A collaborative study of population-based cohorts. Neurologic Diseases in the Elderly Research Group. *Neurology* **2000**, *54*, S21-3.

224. Van Den Eeden, S.K.; Tanner, C.M.; Bernstein, A.L.; Fross, R.D.; Leimpeter, A.; Bloch, D.A.; Nelson, L.M. Incidence of Parkinson's

Disease: Variation by Age, Gender, and Race/Ethnicity. *Am. J. Epidemiol.* **2003**, *157*, 1015–1022, doi:10.1093/AJE/KWG068.

225. Lázaro, D.F.; Pavlou, M.A.S.; Outeiro, T.F. Cellular models as tools for the study of the role of alpha-synuclein in Parkinson's disease. *Exp. Neurol.* **2017**, *298*, 162–171, doi:10.1016/J.EXPNEUROL.2017.05.007.

226. Fruhmann, G.; Seynnaeve, D.; Zheng, J.; Ven, K.; Molenberghs, S.; Wilms, T.; Liu, B.; Winderickx, J.; Franssens, V. Yeast buddies helping to unravel the complexity of neurodegenerative disorders. *Mech. Ageing Dev.* **2017**, *161*, 288–305, doi:10.1016/J.MAD.2016.05.002.

227. Sampaio-Marques, B.; Pereira, H.; Santos, A.R.; Teixeira, A.; Ludovico, P. Caloric restriction rescues yeast cells from alpha-synuclein toxicity through autophagic control of proteostasis. *Aging (Albany. NY).* **2018**, *10*, 3821–3833, doi:10.18632/AGING.101675.

228. Sampaio-Marques, B.; Guedes, A.; Vasilevskiy, I.; Gonçalves, S.; Outeiro, T.F.; Winderickx, J.; Burhans, W.C.; Ludovico, P. α-Synuclein toxicity in yeast and human cells is caused by cell cycle re-entry and autophagy degradation of ribonucleotide reductase 1. *Aging Cell* **2019**, *18*, e12922, doi:10.1111/ACEL.12922.

229. Tenreiro, S.; Franssens, V.; Winderickx, J.; Outeiro, T.F. Yeast models of Parkinson's disease-associated molecular pathologies. *Curr. Opin. Genet. Dev.* **2017**, *44*, 74–83, doi:10.1016/J.GDE.2017.01.013.

230. Toth, M.L.; Melentijevic, I.; Shah, L.; Bhatia, A.; Lu, K.; Talwar, A.; Naji, H.; Ibanez-Ventoso, C.; Ghose, P.; Jevince, A.; et al. Neurite Sprouting and Synapse Deterioration in the Aging Caenorhabditis elegans Nervous System. *J. Neurosci.* **2012**, *32*, 8778–8790, doi:10.1523/JNEUROSCI.1494-11.2012.

231. Lakso, M.; Vartiainen, S.; Moilanen, A.M.; Sirviö, J.; Thomas, J.H.; Nass,

R.; Blakely, R.D.; Wong, G. Dopaminergic neuronal loss and motor deficits in Caenorhabditis elegans overexpressing human α-synuclein. *J. Neurochem.* **2003**, *86*, 165–172, doi:10.1046/J.1471-4159.2003.01809.X.

232. Phillips, R.D.; McWatters, K.H.; Chinnan, M.S.; Hung, Y.C.; Beuchat, L.R.; Sefa-Dedeh, S.; Sakyi-Dawson, E.; Ngoddy, P.; Nnanyelugo, D.; Enwere, J.; et al. Utilization of cowpeas for human food. *F. Crop. Res.* **2003**, *82*, 193–213, doi:10.1016/S0378-4290(03)00038-8.

233. Gonçalves, A.; Goufo, P.; Barros, A.; Domínguez-Perles, R.; Trindade, H.; Rosa, E.A.S.; Ferreira, L.; Rodrigues, M. Cowpea (Vigna unguiculata L. Walp), a renewed multipurpose crop for a more sustainable agri-food system: nutritional advantages and constraints. *J. Sci. Food Agric.* **2016**, *96*, 2941–2951, doi:10.1002/JSFA.7644.

234. Xiong, S.; Yao, X.; Li, A. Antioxidant Properties of Peptide from Cowpea Seed. *https://doi.org/10.1080/10942912.2011.582976* **2013**, *16*, 1245–1256, doi:10.1080/10942912.2011.582976.

235. Thangadurai, D. CHEMICAL COMPOSITION AND NUTRITIONAL POTENTIAL OF VIGNA UNGUICULATA SSP. CYLINDRICA (FABACEAE). *J. Food Biochem.* **2005**, *29*, 88–98, doi:10.1111/J.1745-4514.2005.00014.X.

236. Conti, M.V.; Campanaro, A.; Coccetti, P.; De Giuseppe, R.; Galimberti, A.; Labra, M.; Cena, H. Potential role of neglected and underutilized plant species in improving women's empowerment and nutrition in areas of sub-Saharan Africa. *Nutr. Rev.* **2019**, *77*, 817–828, doi:10.1093/NUTRIT/NUZ038.

237. Awika, J.M.; Duodu, K.G. Bioactive polyphenols and peptides in cowpea (Vigna unguiculata) and their health promoting properties: A

review. *J. Funct. Foods* **2017**, *38*, 686–697, doi:10.1016/J.JFF.2016.12.002.

238. Dodig, S.; Čepelak, I.; Pavić, I. Hallmarks of senescence and aging. *Biochem. Medica* **2019**, *29*, 0–0, doi:10.11613/BM.2019.030501/FULLARTICLE.

239. Beckman, K.B.; Ames, B.N. The free radical theory of aging matures. *Physiol. Rev.* **1998**, *78*, 547–581, doi:10.1152/PHYSREV.1998.78.2.547/ASSET/IMAGES/LARGE/JNP.AP 01F1.JPEG.

240. Frankel, S.; Ziafazeli, T.; Rogina, B. dSir2 and longevity in Drosophila. *Exp. Gerontol.* **2011**, *46*, 391–396, doi:10.1016/J.EXGER.2010.08.007.

241. Horvath, M.; Mihajlovic, Z.; Slaninova, V.; Perez-Gomez, R.; Moshkin, Y.; Krejci, A. The silent information regulator 1 (Sirt1) is a positive regulator of the Notch pathway in Drosophila. *Biochem. J.* **2016**, *473*, 4129–4143, doi:10.1042/BCJ20160563.

242. Alic, N.; Giannakou, M.E.; Papatheodorou, I.; Hoddinott, M.P.; Andrews, T.D.; Bolukbasi, E.; Partridge, L. Interplay of dFOXO and Two ETS-Family Transcription Factors Determines Lifespan in Drosophila melanogaster. *PLOS Genet.* **2014**, *10*, e1004619, doi:10.1371/JOURNAL.PGEN.1004619.

243. Casamenti, F.; Stefani, M. Olive polyphenols: new promising agents to combat aging-associated neurodegeneration. *https://doi.org/10.1080/14737175.2017.1245617* **2016**, *17*, 345–358, doi:10.1080/14737175.2017.1245617.

244. Modi, K.K.; Roy, A.; Brahmachari, S.; Rangasamy, S.B.; Pahan, K. Cinnamon and Its Metabolite Sodium Benzoate Attenuate the Activation of p21rac and Protect Memory and Learning in an Animal

Model of Alzheimer's Disease. *PLoS One* **2015**, *10*, e0130398, doi:10.1371/JOURNAL.PONE.0130398.

245. Liu, W.; Ma, H.; DaSilva, N.A.; Rose, K.N.; Johnson, S.L.; Zhang, L.; Wan, C.; Dain, J.A.; Seeram, N.P. Development of a neuroprotective potential algorithm for medicinal plants. *Neurochem. Int.* **2016**, *100*, 164–177, doi:10.1016/J.NEUINT.2016.09.014.

246. Malishev, R.; Shaham-Niv, S.; Nandi, S.; Kolusheva, S.; Gazit, E.; Jelinek, R. Bacoside-A, an Indian Traditional-Medicine Substance, Inhibits β-Amyloid Cytotoxicity, Fibrillation, and Membrane Interactions. *ACS Chem. Neurosci.* **2017**, *8*, 884–891, doi:10.1021/ACSCHEMNEURO.6B00438/SUPPL_FILE/CN6B00438_SI_001.PDF.

247. Rajan, K.E.; Preethi, J.; Singh, H.K. Molecular and Functional Characterization of Bacopa monniera: A Retrospective Review. *Evidence-based Complement. Altern. Med.* **2015**, *2015*, doi:10.1155/2015/945217.

248. Lobbens, E.S.; Breydo, L.; Skamris, T.; Vestergaard, B.; Jäger, A.K.; Jorgensen, L.; Uversky, V.; van de Weert, M. Mechanistic study of the inhibitory activity of Geum urbanum extract against α-Synuclein fibrillation. *Biochim. Biophys. Acta - Proteins Proteomics* **2016**, *1864*, 1160–1169, doi:10.1016/J.BBAPAP.2016.06.009.

249. Sampaio-Marques, B.; Felgueiras, C.; Silva, A.; Rodrigues, M.; Tenreiro, S.; Franssens, V.; Reichert, A.S.; Outeiro, T.F.; Winderickx, J.; Ludovico, P. SNCA (α-synuclein)-induced toxicity in yeast cells is dependent on sirtuin 2 (Sir2)-mediated mitophagy. *Autophagy* **2012**, *8*, 1494–1509, doi:10.4161/AUTO.21275/SUPPL_FILE/KAUP_A_10921275_SM0001.

ZIP.

250. Bucciantini, M.; Nosi, D.; Forzan, M.; Russo, E.; Calamai, M.; Pieri, L.; Formigli, L.; Quercioli, F.; Soria, S.; Pavone, F.; et al. Toxic effects of amyloid fibrils on cell membranes: the importance of ganglioside GM1. *FASEB J.* **2012**, *26*, 818–831, doi:10.1096/FJ.11-189381.

251. Palazzi, L.; Bruzzone, E.; Bisello, G.; Leri, M.; Stefani, M.; Bucciantini, M.; De Laureto, P.P. Oleuropein aglycone stabilizes the monomeric α-synuclein and favours the growth of non-toxic aggregates. *Sci. Reports 2018 81* **2018**, *8*, 1–17, doi:10.1038/s41598-018-26645-5.

252. Palazzi, L.; Leri, M.; Cesaro, S.; Stefani, M.; Bucciantini, M.; Polverino de Laureto, P. Insight into the molecular mechanism underlying the inhibition of α-synuclein aggregation by hydroxytyrosol. *Biochem. Pharmacol.* **2020**, *173*, 113722, doi:10.1016/J.BCP.2019.113722.

253. Cao, P.; Yuan, Y.; Pehek, E.A.; Moise, A.R.; Huang, Y.; Palczewski, K.; Feng, Z. Alpha-Synuclein Disrupted Dopamine Homeostasis Leads to Dopaminergic Neuron Degeneration in Caenorhabditis elegans. *PLoS One* **2010**, *5*, e9312, doi:10.1371/JOURNAL.PONE.0009312.

254. Kautu, B.B.; Carrasquilla, A.; Hicks, M.L.; Caldwell, K.A.; Caldwell, G.A. Valproic acid ameliorates C. elegans dopaminergic neurodegeneration with implications for ERK-MAPK signaling. *Neurosci. Lett.* **2013**, *541*, 116–119, doi:10.1016/J.NEULET.2013.02.026.

255. Jayathilake, C.; Visvanathan, R.; Deen, A.; Bangamuwage, R.; Jayawardana, B.C.; Nammi, S.; Liyanage, R. Cowpea: an overview on its nutritional facts and health benefits. *J. Sci. Food Agric.* **2018**, *98*, 4793–4806, doi:10.1002/JSFA.9074.

256. Greer, E.L.; Oskoui, P.R.; Banko, M.R.; Maniar, J.M.; Gygi, M.P.; Gygi,

S.P.; Brunet, A. The energy sensor AMP-activated protein kinase directly regulates the mammalian FOXO3 transcription factor. *J. Biol. Chem.* **2007**, *282*, 30107–30119, doi:10.1074/JBC.M705325200/ATTACHMENT/57911A3C-008D-4F71-ABE8-C9F0EA396A6F/MMC1.PDF.

257. Brunet, A.; Sweeney, L.B.; Sturgill, J.F.; Chua, K.F.; Greer, P.L.; Lin, Y.; Tran, H.; Ross, S.E.; Mostoslavsy, R.; Cohen, H.Y.; et al. Stress-Dependent Regulation of FOXO Transcription Factors by the SIRT1 Deacetylase. *Science (80-.).* **2004**, *303*, 2011–2015, doi:10.1126/SCIENCE.1094637/SUPPL_FILE/BRUNET.SOM.PDF.

258. Jiang, Y.; Yan, F.; Feng, Z.; Lazarovici, P.; Zheng, W. Signaling Network of Forkhead Family of Transcription Factors (FOXO) in Dietary Restriction. *Cells 2020, Vol. 9, Page 100* **2019**, *9*, 100, doi:10.3390/CELLS9010100.

259. Fontana, L.; Nehme, J.; Demaria, M. Caloric restriction and cellular senescence. *Mech. Ageing Dev.* **2018**, *176*, 19–23, doi:10.1016/J.MAD.2018.10.005.

260. Wrasidlo, W.; Tsigelny, I.F.; Price, D.L.; Dutta, G.; Rockenstein, E.; Schwarz, T.C.; Ledolter, K.; Bonhaus, D.; Paulino, A.; Eleuteri, S.; et al. A de novo compound targeting α-synuclein improves deficits in models of Parkinson's disease. *Brain* **2016**, *139*, 3217–3236, doi:10.1093/BRAIN/AWW238.

261. Perni, M.; Galvagnion, C.; Maltsev, A.; Meisl, G.; Müller, M.B.D.; Challa, P.K.; Kirkegaard, J.B.; Flagmeier, P.; Cohen, S.I.A.; Cascella, R.; et al. A natural product inhibits the initiation of α-synuclein aggregation & suppresses its toxicity. *Proc. Natl. Acad. Sci. U. S. A.* **2017**, *114*, E1009–E1017, doi:10.1073/PNAS.1610586114/VIDEO-4.

262. Braak, H.; De Vos, R.A.I.; Bohl, J.; Del Tredici, K. Gastric α-synuclein immunoreactive inclusions in Meissner's and Auerbach's plexuses in cases staged for Parkinson's disease-related brain pathology. *Neurosci. Lett.* **2006**, *396*, 67–72, doi:10.1016/J.NEULET.2005.11.012.

263. Shannon, K.M.; Keshavarzian, A.; Dodiya, H.B.; Jakate, S.; Kordower, J.H. Is alpha-synuclein in the colon a biomarker for premotor Parkinson's Disease? Evidence from 3 cases. *Mov. Disord.* **2012**, *27*, 716–719, doi:10.1002/MDS.25020.

264. CATONI, G.L. S-Adenosylmethionine; a new intermediate formed enzymatically from L-methionine and adenosinetriphosphate. *J. Biol. Chem.* **1953**, *204*, 403–416, doi:10.1016/s0021-9258(18)66148-4.

265. Alaminos, M.; Ramos, J.L. The methionine biosynthetic pathway from homoserine in Pseudomonas putida involves the metW, metX, metZ, metH and metE gene products. *Arch. Microbiol. 2001 1761* **2001**, *176*, 151–154, doi:10.1007/S002030100293.

266. Thomas, D.; Surdin-Kerjan, Y. *Metabolism of Sulfur Amino Acids in Saccharomyces cerevisiae*; 1992; Vol. 61;.

267. Foury, F. Human genetic diseases: a cross-talk between man and yeast. *Gene* **1997**, *195*, 1–10, doi:10.1016/S0378-1119(97)00140-6.

268. Loenen, W.A.M. S-Adenosylmethionine: jack of all trades and master of everything? *Biochem. Soc. Trans.* **2006**, *34*, 330–333, doi:10.1042/BST0340330.

269. Murín, R.; Vidomanová, E.; Kowtharapu, B.S.; Hatok, J.; Dobrota, D. Role of S-adenosylmethionine cycle in carcinogenesis R e v i e w. *Gen. Physiol. Biophys* **2017**, *36*, 513–520, doi:10.4149/gpb_2017031.

270. Halliday, N.M.; Hardie, K.R.; Williams, P.; Winzer, K.; Barrett, D.A. Quantitative liquid chromatography-tandem mass spectrometry

profiling of activated methyl cycle metabolites involved in LuxS-dependent quorum sensing in Escherichia coli. *Anal. Biochem.* **2010**, *403*, 20–29, doi:10.1016/j.ab.2010.04.021.

271. Cai, J.; Sun, W.-M.; Hwang, J.-J.; Stain, S.C.; Lu, S.C. Changes in S-adenosylmethionine synthetase in human liver cancer: Molecular characterization and significance. *Hepatology* **1996**, *24*, 1090–1097, doi:10.1002/HEP.510240519.

272. Pendleton, K.E.; Chen, B.; Liu, K.; Hunter, O. V.; Xie, Y.; Tu, B.P.; Conrad, N.K. The U6 snRNA m6A Methyltransferase METTL16 Regulates SAM Synthetase Intron Retention. *Cell* **2017**, *169*, 824-835.e14, doi:10.1016/J.CELL.2017.05.003.

273. Ogawa, T.; Tsubakiyama, R.; Kanai, M.; Koyama, T.; Fujii, T.; Iefuji, H.; Soga, T.; Kume, K.; Miyakawa, T.; Hirata, D.; et al. Stimulating S-adenosyl-l-methionine synthesis extends lifespan via activation of AMPK. *Proc. Natl. Acad. Sci. U. S. A.* **2016**, *113*, 11913–11918, doi:10.1073/pnas.1604047113.

274. Kumari, R.; Sahu, M.K.; Tripathy, A.; Uthansingh, K.; Behera, M. Hepatocellular carcinoma treatment: hurdles, advances and prospects. *https://doi.org/10.2217/hep-2018-0002* **2018**, *5*, HEP08, doi:10.2217/HEP-2018-0002.

275. He, L.; Tian, D.-A.; Li, P.-Y.; He, X.-X.; He, L.; Tian, D.-A.; Li, P.-Y.; He, X.-X. Mouse models of liver cancer: Progress and recommendations. *Oncotarget* **2015**, *6*, 23306–23322, doi:10.18632/ONCOTARGET.4202.

276. Roth, G.S.; Decaens, T. Liver immunotolerance and hepatocellular carcinoma: Patho-physiological mechanisms and therapeutic perspectives. *Eur. J. Cancer* **2017**, *87*, 101–112,

doi:10.1016/J.EJCA.2017.10.010.

277. Rimassa, L.; Danesi, R.; Pressiani, T.; Merle, P. Management of adverse events associated with tyrosine kinase inhibitors: Improving outcomes for patients with hepatocellular carcinoma. *Cancer Treat. Rev.* **2019**, *77*, 20–28, doi:10.1016/J.CTRV.2019.05.004.

278. Hardie, D.G. AMPK: positive and negative regulation, and its role in whole-body energy homeostasis. *Curr. Opin. Cell Biol.* **2015**, *33*, 1–7, doi:10.1016/J.CEB.2014.09.004.

279. Jeon, S.M.; Hay, N. The double-edged sword of AMPK signaling in cancer and its therapeutic implications. *Arch. Pharmacal Res. 2015 383* **2015**, *38*, 346–357, doi:10.1007/S12272-015-0549-Z.

280. Lee, C.W.; Wong, L.L.Y.; Tse, E.Y.T.; Liu, H.F.; Leong, V.Y.L.; Lee, J.M.F.; Hardie, D.G.; Ng, I.O.L.; Ching, Y.P. AMPK Promotes p53 Acetylation via Phosphorylation and Inactivation of SIRT1 in Liver Cancer Cells. *Cancer Res.* **2012**, *72*, 4394–4404, doi:10.1158/0008-5472.CAN-12-0429.

281. Yang, X.; Liu, Y.; Li, M.; Wu, H.; Wang, Y.; You, Y.; Li, P.; Ding, X.; Liu, C.; Gong, J. Predictive and preventive significance of AMPK activation on hepatocarcinogenesis in patients with liver cirrhosis. *Cell Death Dis. 2018 93* **2018**, *9*, 1–11, doi:10.1038/s41419-018-0308-4.

282. Zheng, L.; Yang, W.; Wu, F.; Wang, C.; Yu, L.; Tang, L.; Qiu, B.; Li, Y.; Guo, L.; Wu, M.; et al. Prognostic Significance of AMPK Activation and Therapeutic Effects of Metformin in Hepatocellular Carcinoma. *Clin. Cancer Res.* **2013**, *19*, 5372–5380, doi:10.1158/1078-0432.CCR-13-0203.

283. Podhorecka, M.; Ibanez, B.; Dmoszyńska, A. Metformin – its potential anti-cancer and anti-aging effects. *Adv. Hyg. Exp. Med.* **2017**, *71*, 170–

175, doi:10.5604/01.3001.0010.3801.

284. Jiang, X.; Tan, H.Y.; Teng, S.; Chan, Y.T.; Wang, D.; Wang, N. The Role of AMP-Activated Protein Kinase as a Potential Target of Treatment of Hepatocellular Carcinoma. *Cancers 2019, Vol. 11, Page 647* **2019**, *11*, 647, doi:10.3390/CANCERS11050647.

285. Lu, S.C.; Mato, J.M. *S* -adenosylmethionine in Liver Health, Injury, and Cancer. *Physiol. Rev.* **2012**, *92*, 1515–1542, doi:10.1152/physrev.00047.2011.

286. Ables, G.P.; Johnson, J.E. Pleiotropic responses to methionine restriction. *Exp. Gerontol.* **2017**, *94*, 83–88, doi:10.1016/J.EXGER.2017.01.012.

287. Frau, M.; Feo, F.; Pascale, R.M. Pleiotropic effects of methionine adenosyltransferases deregulation as determinants of liver cancer progression and prognosis. *J. Hepatol.* **2013**, *59*, 830–841, doi:10.1016/J.JHEP.2013.04.031/ATTACHMENT/153F823D-E86C-4643-B315-2CC4F11AF6E6/MMC2.PDF.

288. Pascale, R.M.; Feo, C.F.; Calvisi, D.F.; Feo, F. Deregulation of methionine metabolism as determinant of progression and prognosis of hepatocellular carcinoma. *Transl. Gastroenterol. Hepatol.* **2018**, *3*, doi:10.21037/TGH.2018.06.04.

289. Chaturvedi, S.; Hoffman, R.M.; Bertino, J.R. Exploiting methionine restriction for cancer treatment. *Biochem. Pharmacol.* **2018**, *154*, 170–173, doi:10.1016/J.BCP.2018.05.003.

290. Martínez-López, N.; Varela-Rey, M.; Ariz, U.; Embade, N.; Vazquez-Chantada, M.; Fernandez-Ramos, D.; Gomez-Santos, L.; Lu, S.C.; Mato, J.M.; Martinez-Chantar, M.L. S-adenosylmethionine and proliferation: new pathways, new targets. *Biochem. Soc. Trans.* **2008**, *36*, 848–852,

doi:10.1042/BST0360848.

291. Wang, Y.; Sun, Z.; Szyf, M.; Wang, Y.; Sun, Z.; Szyf, M. S-adenosyl-methionine (SAM) alters the transcriptome and methylome and specifically blocks growth and invasiveness of liver cancer cells. *Oncotarget* **2017**, *8*, 111866–111881, doi:10.18632/ONCOTARGET.22942.

292. Stoyanov, E.; Mizrahi, L.; Olam, D.; Schnitzer-Perlman, T.; Galun, E.; Goldenberg, D.S.; Stoyanov, E.; Mizrahi, L.; Olam, D.; Schnitzer-Perlman, T.; et al. Tumor-suppressive effect of S-adenosylmethionine supplementation in a murine model of inflammation-mediated hepatocarcinogenesis is dependent on treatment longevity. *Oncotarget* **2017**, *8*, 104772–104784, doi:10.18632/ONCOTARGET.18300.

293. Mato, J.M.; Cámara, J.; Paz, J.F. De; Caballería, L.; Coll, S.; Caballero, A.; García-Buey, L.; Beltrán, J.; Benita, V.; Caballería, J.; et al. S-Adenosylmethionine in alcoholic liver cirrhosis: a randomized, placebo-controlled, double-blind, multicenter clinical trial. *J. Hepatol.* **1999**, *30*, 1081–1089, doi:10.1016/S0168-8278(99)80263-3.

294. Wang, Y.; Tatham, M.H.; Schmidt-Heck, W.; Swann, C.; Singh-Dolt, K.; Meseguer-Ripolles, J.; Lucendo-Villarin, B.; Kunath, T.; Rudd, T.R.; Smith, A.J.H.; et al. Multiomics Analyses of HNF4α Protein Domain Function during Human Pluripotent Stem Cell Differentiation. *iScience* **2019**, *16*, 206–217, doi:10.1016/J.ISCI.2019.05.028/ATTACHMENT/D07D100E-CBA5-4B5A-8BD4-EBCC34904D04/MMC5.XLSX.

295. Yang, H.; Zheng, Y.; Li, T.W.H.; Peng, H.; Fernandez-Ramos, D.; Martínez-Chantar, M.L.; Rojas, A.L.; Mato, J.M.; Lu, S.C. Methionine

Adenosyltransferase 2B, HuR, and Sirtuin 1 Protein Cross-talk Impacts on the Effect of Resveratrol on Apoptosis and Growth in Liver Cancer Cells *. *J. Biol. Chem.* **2013**, *288*, 23161–23170, doi:10.1074/JBC.M113.487157.

296. Li, Y.; Wang, Y.; Wu, P. 5'-methylthioadenosine and cancer: old molecules, new understanding. *J. Cancer* **2019**, *10*, 927–936, doi:10.7150/JCA.27160.

297. Avila, M.A.; García-Trevijano, E.R.; Lu, S.C.; Corrales, F.J.; Mato, J.M. Methylthioadenosine. *Int. J. Biochem. Cell Biol.* **2004**, *36*, 2125–2130, doi:10.1016/J.BIOCEL.2003.11.016.

298. Pascale, R.M.; Simile, M.M.; Miglio, M.R.D.; Nufris, A.; Daino, L.; Seddaiu, M.A.; Rao, P.M.; Rajalakshmi, S.; Sarma, D.S.R.; Feo, F. Chemoprevention by S-adenosyl-L-methionine of rat liver carcinogenesis initiated by 1,2-dimethylhydrazine and promoted by orotic acid. *Carcinogenesis* **1995**, *16*, 427–430, doi:10.1093/CARCIN/16.2.427.

299. Hardie, D.G. Keeping the home fires burning†: AMP-activated protein kinase. *J. R. Soc. Interface* **2018**, *15*, doi:10.1098/RSIF.2017.0774.

300. Sanli, T.; Steinberg, G.R.; Singh, G.; Tsakiridis, T. AMP-activated protein kinase (AMPK) beyond metabolism. *http://dx.doi.org/10.4161/cbt.26726* **2013**, *15*, 156–169, doi:10.4161/CBT.26726.

301. Magaway, C.; Kim, E.; Jacinto, E. Targeting mTOR and Metabolism in Cancer: Lessons and Innovations. *Cells 2019, Vol. 8, Page 1584* **2019**, *8*, 1584, doi:10.3390/CELLS8121584.

302. Wu, Z.; Song, L.; Liu, S.Q.; Huang, D. Independent and Additive Effects of Glutamic Acid and Methionine on Yeast Longevity. *PLoS One* **2013**,

8, e79319, doi:10.1371/JOURNAL.PONE.0079319.

303. Troen, A.M.; French, E.E.; Roberts, J.F.; Selhub, J.; Ordovas, J.M.; Parnell, L.D.; Lai, C.Q. Lifespan modification by glucose and methionine in Drosophila melanogaster fed a chemically defined diet. *AGE 2006 291* **2006**, *29*, 29–39, doi:10.1007/S11357-006-9018-4.

304. Lee, B.C.; Kaya, A.; Ma, S.; Kim, G.; Gerashchenko, M. V.; Yim, S.H.; Hu, Z.; Harshman, L.G.; Gladyshev, V.N. Methionine restriction extends lifespan of Drosophila melanogaster under conditions of low amino-acid status. *Nat. Commun. 2014 51* **2014**, *5*, 1–12, doi:10.1038/ncomms4592.

305. Johnson, J.E.; Johnson, F.B. Methionine Restriction Activates the Retrograde Response and Confers Both Stress Tolerance and Lifespan Extension to Yeast, Mouse and Human Cells. *PLoS One* **2014**, *9*, e97729, doi:10.1371/JOURNAL.PONE.0097729.

306. Ables, G.P.; Ouattara, A.; Hampton, T.G.; Cooke, D.; Perodin, F.; Augie, I.; Orentreich, D.S. Dietary Methionine Restriction in Mice Elicits an Adaptive Cardiovascular Response to Hyperhomocysteinemia. *Sci. Reports 2015 51* **2015**, *5*, 1–10, doi:10.1038/srep08886.

307. Ouattara, A.; Cooke, D.; Gopalakrishnan, R.; Huang, T. hai; Ables, G.P. Methionine restriction alters bone morphology and affects osteoblast differentiation. *Bone Reports* **2016**, *5*, 33–42, doi:10.1016/J.BONR.2016.02.002.

308. Komninou, D.; Leutzinger, Y.; Reddy, B.S.; Richie, J.P. Methionine Restriction Inhibits Colon Carcinogenesis. *http://dx.doi.org/10.1207/s15327914nc5402_6* **2009**, *54*, 202–208, doi:10.1207/S15327914NC5402_6.

309. Sinha, R.; Cooper, T.K.; Rogers, C.J.; Sinha, I.; Turbitt, W.J.;

Calcagnotto, A.; Perrone, C.E.; Richie, J.P. Dietary methionine restriction inhibits prostatic intraepithelial neoplasia in TRAMP mice. *Prostate* **2014**, *74*, 1663–1673, doi:10.1002/PROS.22884.

310. Jeon, H.; Kim, J.H.; Lee, E.; Jang, Y.J.; Son, J.E.; Kwon, J.Y.; Lim, T.; Kim, S.; Park, J.H.Y.; Kim, J.-E.; et al. Methionine deprivation suppresses triple-negative breast cancer metastasis in vitro and in vivo. *Oncotarget* **2016**, *7*, 67223–67234, doi:10.18632/ONCOTARGET.11615.

311. Hens, J.R.; Sinha, I.; Perodin, F.; Cooper, T.; Sinha, R.; Plummer, J.; Perrone, C.E.; Orentreich, D. Methionine-restricted diet inhibits growth of MCF10AT1-derived mammary tumors by increasing cell cycle inhibitors in athymic nude mice. *BMC Cancer* **2016**, *16*, 1–13, doi:10.1186/S12885-016-2367-1/FIGURES/6.

312. Benavides, M.A.; Hu, D.; Baraoidan, M.K.; Bruno, A.; Du, P.; Lin, S.; Yang, W.; Bland, K.I.; Grizzle, W.E.; Bosland, M.C. L-methionine-induced alterations in molecular signatures in MCF-7 and LNCaP cancer cells. *J. Cancer Res. Clin. Oncol. 2010 1373* **2010**, *137*, 441–453, doi:10.1007/S00432-010-0897-5.

313. Iiboshi, Y.; Papst, P.J.; Kawasome, H.; Hosoi, H.; Abraham, R.T.; Houghton, P.J.; Terada, N. Amino Acid-dependent Control of p70s6k: INVOLVEMENT OF tRNA AMINOACYLATION IN THE REGULATION *. *J. Biol. Chem.* **1999**, *274*, 1092–1099, doi:10.1074/JBC.274.2.1092.

314. Nieto-Domínguez, M.; Nikel, P.I. Intersecting Xenobiology and Neometabolism To Bring Novel Chemistries to Life. *ChemBioChem* **2020**, *21*, 2551–2571, doi:10.1002/CBIC.202000091.

315. Ögmundarson, Ó.; Sukumara, S.; Herrgård, M.J.; Fantke, P. Combining Environmental and Economic Performance for Bioprocess

Optimization. *Trends Biotechnol.* **2020**, *38*, 1203–1214, doi:10.1016/J.TIBTECH.2020.04.011.

316. Davy, A.M.; Kildegaard, H.F.; Andersen, M.R. Cell Factory Engineering. *Cell Syst.* **2017**, *4*, 262–275, doi:10.1016/J.CELS.2017.02.010.

317. Nikel, P.I.; de Lorenzo, V. Pseudomonas putida as a functional chassis for industrial biocatalysis: From native biochemistry to trans-metabolism. *Metab. Eng.* **2018**, *50*, 142–155, doi:10.1016/J.YMBEN.2018.05.005.

318. Wong, C.L.; Dunn, N.W. Transmissible plasmid coding for the degradation of benzoate and m-toluate in Pseudomonas arvilla mt-2. *Genet. Res.* **1974**, *23*, 227–232, doi:10.1017/S0016672300014853.

319. Sánchez-Pascuala, A.; Fernández-Cabezón, L.; de Lorenzo, V.; Nikel, P.I. Functional implementation of a linear glycolysis for sugar catabolism in Pseudomonas putida. *Metab. Eng.* **2019**, *54*, 200–211, doi:10.1016/J.YMBEN.2019.04.005.

320. Pedersen, B.H.; Gurdo, N.; Johansen, H.K.; Molin, S.; Nikel, P.I.; La Rosa, R. High-throughput dilution-based growth method enables time-resolved exo-metabolomics of Pseudomonas putida and Pseudomonas aeruginosa. *Microb. Biotechnol.* **2021**, *14*, 2214–2226, doi:10.1111/1751-7915.13905.

321. Nikel, P.I.; Chavarría, M.; Fuhrer, T.; Sauer, U.; De Lorenzo, V. Pseudomonas putida KT2440 strain metabolizes glucose through a cycle formed by enzymes of the Entner-Doudoroff, embden-meyerhof-parnas, and pentose phosphate pathways. *J. Biol. Chem.* **2015**, *290*, 25920–25932, doi:10.1074/JBC.M115.687749/ATTACHMENT/F911104F-187D-4C2C-A1CB-AADC80B6966B/MMC1.ZIP.

322. Orsi, E.; Claassens, N.J.; Nikel, P.I.; Lindner, S.N. Growth-coupled selection of synthetic modules to accelerate cell factory development., doi:10.1038/s41467-021-25665-6.

323. Tripodi, F.; Badone, B.; Vescovi, M.; Milanesi, R.; Nonnis, S.; Maffioli, E.; Bonanomi, M.; Gaglio, D.; Tedeschi, G.; Coccetti, P. Methionine Supplementation Affects Metabolism and Reduces Tumor Aggressiveness in Liver Cancer Cells. *Cells* **2020**, *9*, 2491, doi:10.3390/cells9112491.

324. Bradley, J.D.; Flusser, D.; Katz, B.P.; Schumacher, H.R.; Brandt, K.D.; Chambers, M.A.; Zonay, L.J. A randomized, double blind, placebo controlled trial of intravenous loading with S-adenosylmethionine (SAM) followed by oral SAM therapy in patients with knee osteoarthritis. *J. Rheumatol.* **1994**, *21*, 905–911, doi:10.1007/s11814-009-0025-x.

325. O'Hagan, D.; Schaffrath, C.; Cobb, S.L.; Hamilton, J.T.G.; Murphy, C.D. Biosynthesis of an organofluorine molecule: A fluorinase enzyme has been discovered that catalyses carbon-fluorine bond formation. *Nature* **2002**, *416*, 279, doi:10.1038/416279a.

326. Born, T.L.; Blanchard, J.S. Enzyme-Catalyzed Acylation of Homoserine: Mechanistic Characterization of the Escherichia coli metA-Encoded Homoserine Transsuccinylase†. *Biochemistry* **1999**, *38*, 14416–14423, doi:10.1021/BI991710O.

327. Volke, D.C.; Turlin, J.; Mol, V.; Nikel, P.I. Physical decoupling of XylS/Pm regulatory elements and conditional proteolysis enable precise control of gene expression in Pseudomonas putida. *Microb. Biotechnol.* **2020**, *13*, 222–232, doi:10.1111/1751-7915.13383.

328. Theodosiou, E.; Breisch, M.; Julsing, M.K.; Falcioni, F.; Bühler, B.;

Schmid, A. An artificial TCA cycle selects for efficient α-ketoglutarate dependent hydroxylase catalysis in engineered Escherichia coli. *Biotechnol. Bioeng.* **2017**, *114*, 1511–1520, doi:10.1002/BIT.26281.

329. Nikel, P.I.; Pérez-Pantoja, D.; de Lorenzo, V. Pyridine nucleotide transhydrogenases enable redox balance of Pseudomonas putida during biodegradation of aromatic compounds. *Environ. Microbiol.* **2016**, *18*, 3565–3582, doi:10.1111/1462-2920.13434.

330. Tong, Y.; Whitford, C.M.; Robertsen, H.L.; Blin, K.; Jørgensen, T.S.; Klitgaard, A.K.; Gren, T.; Jiang, X.; Weber, T.; Lee, S.Y. Highly efficient DSB-free base editing for streptomycetes with CRISPR-BEST. *Proc. Natl. Acad. Sci. U. S. A.* **2019**, *116*, 20366–20375, doi:10.1073/PNAS.1913493116/-/DCSUPPLEMENTAL.

331. Welkenhuysen, N.; Borgqvist, J.; Backman, M.; Bendrioua, L.; Goksör, M.; Adiels, C.B.; Cvijovic, M.; Hohmann, S. Single-cell study links metabolism with nutrient signaling and reveals sources of variability. *BMC Syst. Biol.* **2017**, *11*, 1–10, doi:10.1186/s12918-017-0435-z.

332. Link, H.; Kochanowski, K.; Sauer, U. systematic identification of allosteric protein-metabolite interactions that control enzyme activity in vivo. *Nat. Biotechnol.* **2013**, *31*, doi:10.1038/nbt.2489.

333. Donati, S.; Kuntz, M.; Pahl, V.; Farke, N.; Beuter, D.; Glatter, T.; Gomes-Filho, J.V.; Randau, L.; Wang, C.Y.; Link, H. Multi-omics Analysis of CRISPRi-Knockdowns Identifies Mechanisms that Buffer Decreases of Enzymes in E. coli Metabolism. *Cell Syst.* **2021**, *12*, 56-67.e6, doi:10.1016/J.CELS.2020.10.011.

334. Harrer, S.; Shah, P.; Antony, B.; Hu, J. Special Issue: Rise of Machines in Medicine Artificial Intelligence for Clinical Trial Design. *Trends Pharmacol. Sci.* **2019**, *40*, 577–591, doi:10.1016/j.tips.2019.05.005.

335. Pappalardo, F.; Russo, G.; Tshinanu, F.M.; Viceconti, M. In silico clinical trials: concepts and early adoptions. *Brief. Bioinform.* **2019**, *20*, 1699–1708, doi:10.1093/BIB/BBY043.

336. Passini, E.; Britton, O.J.; Lu, H.R.; Rohrbacher, J.; Hermans, A.N.; Gallacher, D.J.; Greig, R.J.H.; Bueno-Orovio, A.; Rodriguez, B. Human in silico drug trials demonstrate higher accuracy than animal models in predicting clinical pro-arrhythmic cardiotoxicity. *Front. Physiol.* **2017**, *8*, 668, doi:10.3389/FPHYS.2017.00668/BIBTEX.

337. Kovatchev, B.P.; Breton, M.; Dalla Man, C.; Cobelli, C. In silico preclinical trials: A proof of concept in closed-loop control of type 1 diabetes. *J. Diabetes Sci. Technol.* **2009**, *3*, 44–55, doi:10.1177/193229680900300106.

338. Haasen, D.; Schopfer, U.; Antczak, C.; Guy, C.; Fuchs, F.; Selzer, P. How Phenotypic Screening Influenced Drug Discovery: Lessons from Five Years of Practice. *https://home.liebertpub.com/adt* **2017**, *15*, 239–246, doi:10.1089/ADT.2017.796.

339. Swinney, D.C.; Anthony, J. How were new medicines discovered? *Nat. Rev. Drug Discov. 2011 107* **2011**, *10*, 507–519, doi:10.1038/nrd3480.

340. Mestres, J.; Gregori-Puigjané, E.; Valverde, S.; Solé, R. V. The topology of drug –target interaction networks: implicit dependence on drug properties and target families. *Mol. Biosyst.* **2009**, *5*, 1051–1057, doi:10.1039/B905821B.

341. Wehrs, M.; Tanjore, D.; Eng, T.; Lievense, J.; Pray, T.R.; Mukhopadhyay, A. Engineering Robust Production Microbes for Large-Scale Cultivation. **2019**, doi:10.1016/j.tim.2019.01.006.

342. Brenner, S. THE GENETICS OF CAENORHABDITIS ELEGANS. *Genetics 1974*, *77*, 71–94, doi:10.1093/GENETICS/77.1.71.

343. Tedeschi, G.; Albani, E.; Borroni, E.M.; Parini, V.; Brucculeri, A.M.; Maffioli, E.; Negri, A.; Nonnis, S.; Maccarrone, M.; Levi-Setti, P.E. Proteomic profile of maternal-aged blastocoel fluid suggests a novel role for ubiquitin system in blastocyst quality. *J. Assist. Reprod. Genet. 2016 342* **2016**, *34*, 225–238, doi:10.1007/S10815-016-0842-X.

344. LeVine, H. [18] Quantification of β-sheet amyloid fibril structures with thioflavin T. *Methods Enzymol.* **1999**, *309*, 274–284, doi:10.1016/S0076-6879(99)09020-5.

345. Vernocchi, V.; Morselli, M.G.; Varesi, S.; Nonnis, S.; Maffioli, E.; Negri, A.; Tedeschi, G.; Luvoni, G.C. Sperm ubiquitination in epididymal feline semen. *Theriogenology* **2014**, *82*, 636–642, doi:10.1016/J.THERIOGENOLOGY.2014.06.002.

346. Migliaccio, O.; Pinsino, A.; Maffioli, E.; Smith, A.M.; Agnisola, C.; Matranga, V.; Nonnis, S.; Tedeschi, G.; Byrne, M.; Gambi, M.C.; et al. Living in future ocean acidification, physiological adaptive responses of the immune system of sea urchins resident at a CO2 vent system. *Sci. Total Environ.* **2019**, *672*, 938–950, doi:10.1016/J.SCITOTENV.2019.04.005.

347. Maffioli, E.; Schulte, C.; Nonnis, S.; Scalvini, F.G.; Piazzoni, C.; Lenardi, C.; Negri, A.; Milani, P.; Tedeschi, G. Proteomic dissection of nanotopography-sensitive mechanotransductive signaling hubs that foster neuronal differentiation in PC12 cells. *Front. Cell. Neurosci.* **2018**, *11*, 417, doi:10.3389/FNCEL.2017.00417/BIBTEX.

348. Pang, Z.; Chong, J.; Li, S.; Xia, J. MetaboAnalystR 3.0: Toward an Optimized Workflow for Global Metabolomics. *Metab. 2020, Vol. 10, Page 186* **2020**, *10*, 186, doi:10.3390/METABO10050186.

349. Chong, J.; Wishart, D.S.; Xia, J. Using MetaboAnalyst 4.0 for

Comprehensive and Integrative Metabolomics Data Analysis. *Curr. Protoc. Bioinforma.* **2019**, *68*, e86, doi:10.1002/CPBI.86.

350. Long, C.P.; Antoniewicz, M.R. High-resolution 13C metabolic flux analysis. *Nat. Protoc. 2019 1410* **2019**, *14*, 2856–2877, doi:10.1038/s41596-019-0204-0.

351. Kutuzova, S.; Colaianni, P.; Röst, H.; Sachsenberg, T.; Alka, O.; Kohlbacher, O.; Burla, B.; Torta, F.; Schrübbers, L.; Kristensen, M.; et al. SmartPeak Automates Targeted and Quantitative Metabolomics Data Processing. *Anal. Chem.* **2020**, *92*, 15968–15974, doi:10.1021/ACS.ANALCHEM.0C03421/SUPPL_FILE/AC0C03421_SI_0 04.XLSX.

352. Nogales, J.; Gudmundsson, S.; Duque, E.; Luis Ramos, J.; putida, P. Expanding the computable reactome in Pseudomonas putida reveals metabolic cycles providing robustness. 2 3 Running Head: Metabolic Robustness Cycles in., doi:10.1101/139121.

353. Ebrahim, A.; Lerman, J.A.; Palsson, B.O.; Hyduke, D.R. COBRApy: COnstraints-Based Reconstruction and Analysis for Python. *BMC Syst. Biol.* **2013**, *7*, 1–6, doi:10.1186/1752-0509-7-74/FIGURES/2.

354. Del Castillo, T.; Ramos, J.L.; Rodríguez-Herva, J.J.; Fuhrer, T.; Sauer, U.; Duque, E. Convergent peripheral pathways catalyze initial glucose catabolism in Pseudomonas putida: Genomic and flux analysis. *J. Bacteriol.* **2007**, *189*, 5142–5152, doi:10.1128/JB.00203-07/SUPPL_FILE/SUPPLEMENTARY_TABLE_1.DOC.

355. Ebert, B.E.; Kurth, F.; Grund, M.; Blank, L.M.; Schmid, A. Response of Pseudomonas putida KT2440 to increased NADH and ATP demand. *Appl. Environ. Microbiol.* **2011**, *77*, 6597–6605, doi:10.1128/AEM.05588-11/SUPPL_FILE/AEM05588-

11_TABLES4_REV.XLS.

356. King, Z.A.; Dräger, A.; Ebrahim, A.; Sonnenschein, N.; Lewis, N.E.; Palsson, B.O. Escher: A Web Application for Building, Sharing, and Embedding Data-Rich Visualizations of Biological Pathways. *PLOS Comput. Biol.* **2015**, *11*, e1004321, doi:10.1371/JOURNAL.PCBI.1004321.

Publications

The Regulatory Role of Key Metabolites in the Control of Cell Signaling

Riccardo Milanesi, Paola Coccetti * and Farida Tripodi

Department of Biotechnology and Biosciences, University of Milano-Bicocca, 20126 Milan, Italy;
r.milanesi2@campus.unimib.it (R.M.); farida.tripodi1@unimib.it (F.T.)
* Correspondence: paola.coccetti@unimib.it; Tel.: **+**39-02-6448-3521

check for
updates

Abstract: Robust biological systems are able to adapt to internal and environmental perturbations. This is ensured by a thick crosstalk between metabolism and signal transduction pathways, through which cell cycle progression, cell metabolism and growth are coordinated. Although several reports describe the control of cell signaling on metabolism (mainly through transcriptional regulation and post-translational modifications), much fewer information is available on the role of metabolism in the regulation of signal transduction. Protein-metabolite interactions (PMIs) result in the modification of the protein activity due to a conformational change associated with the binding of a small molecule. An increasing amount of evidences highlight the role of metabolites of the central metabolism in the control of the activity of key signaling proteins in different eukaryotic systems. Here we review the known PMIs between primary metabolites and proteins, through which metabolism affects signal transduction pathways controlled by the conserved kinases Snf1/AMPK, Ras/PKA and TORC1. Interestingly, PMIs influence also the mitochondrial retrograde response (RTG) and calcium signaling, clearly demonstrating that the range of this phenomenon is not limited to signaling pathways related to metabolism.

Keywords: Snf1/AMPK/SnRK1; Ras/PKA; TORC1; RTG; calcium; glucose; glycolysis; TCA; amino acids; protein-metabolite interaction

1. Introduction

The robustness of a biological system is defined as the ability to maintain its principal functionalities regardless of external and internal variations [1]. The concept of robustness could be applied at systems of different order of magnitude. This property generally arises from a specific architecture of the systems itself, that may be a cell, a metabolic pathway, a microbial community or a multicellular organism [2]. Robust systems are typically organized with a bow-tie architecture, where a lot of input signals converge on a limited number of elements, from which a large number of outputs emerge [3]. Metabolic and signaling networks show such an organization, with several metabolites and signals that converge on the central metabolism or on a limited number of signaling pathways [3].

A key aspect of every robust system is the ability to monitor the environmental conditions and adapt its functions to perturbations [4]. For example, from a system biology point of view, it is common to see the maximization of growth as the objective function of a cell. To do so, metabolism, growth and cell cycle progression must be coordinated and finely tuned to fully exploit the available nutrients [5,6]. This requires a precise crosstalk between metabolism, signal transduction pathways and cell cycle progression. Therefore, some molecular events should connect given metabolic reactions with signal transduction cascades, in order to coherently integrate a given flux distribution with the activity of regulatory proteins, such as the kinases upstream to signaling pathways. However, recent publications

support the idea that we still need more data to understand the role of specific metabolites in controlling proteins activity at a systems level [7,8].

Since the beginning of the omics era, emergent technologies have focused on the qualitative and quantitative analysis of chemically homogeneous groups of molecules, giving rise to transcriptomics, proteomics and metabolomics. Nevertheless, the interpretation of the data acquired with these approaches is not always straightforward, since the functioning of a biological system emerges by the interactions between chemically different molecules.

The molecular interaction between proteins and DNA has been systematically investigated for many years. On the contrary, the systematic study of the interaction between proteins and metabolites (PMI, protein-metabolite interaction) has started to be explored only very recently. Although recent reports suggest an important role of PMIs in the regulation of signaling [9,10], most publications still focus on the effect of the metabolites belonging to glycolysis and TCA cycle on the activity of the enzymes of the same pathways [7,8,11]. Therefore, a systematic analysis of the interaction between molecules of the central carbon metabolism and the proteins that compose the signal transduction network is still largely missing.

Here we review the known PMIs taking place between signal transduction pathways component and metabolites belonging to the central metabolism, focusing on the output that these interactions have on the activity of the key cellular pathways.

1. The Biochemistry of the Protein-Metabolite Interaction (PMI)

From a biochemical point of view, the final result of a Protein-metabolite interaction is a variation in the protein activity due to a conformational change associated with the binding of a small molecule. NMR and single-molecule spectroscopy studies revealed that proteins can undergo conformational changes both when bound and unbound to a small molecule, as a consequence of thermally activated exchanges between the higher and the lowest energy conformations [12,13]. This means that folded proteins in their basal conformation can sample the energy landscape moving towards relatively higher energy states, that are the one proposed to bind the ligands [14,15]. Because of this, an allosteric regulation due to the binding of a small molecule on its target can be explained by two different models: conformational selection and induced fit [16,17].

According to the conformational selection model, a protein complex spontaneously undergoes a conformational change moving from a basal state to an excited one, characterized by a higher energy and, for this reason, less abundant [17]. In this mechanism, the ligand binding takes place after the conformational change and results in the stabilization of the excited conformation, therefore leading to the enrichment of the bound molecular species [18,19]. On the contrary, in the induced fit model, ligand binding takes place with the basal conformation of the target before any conformational change, this results in an intermediate bound complex still in the initial conformation and characterized by a higher energy. The relaxation of this structure is achieved through the fitting of the target to the bound molecule, as recalled by the definition of this mechanism [16,20].

From a technological point of view, a deep understanding of the control mechanism of a given protein may be an important insight in order to rationally design drugs to target it. Alongside classical drugs that target the active site of a protein, nowadays research is focusing also on the development of molecules that may act as allosteric effectors [21,22]. For example, a possible way to exploit conformational selection is to develop molecules that bind to a protein in a high energy conformation and stabilize it, shifting the equilibrium away from the active conformation [21,23].

To achieve this aim, the detailed biochemistry of the regulation of the target must be understood, also considering possible allosteric interactions and conformational changes.

2. The Main Pathways of Nutrient Sensing and Cellular Signaling

Cell growth and progression through the cell cycle must be coordinated, as already reported, with the availability of nutrients [6,24,25]. In eukaryotic organisms, such as yeasts and mammals, but also

in plants, the most important nutrients are carbon and nitrogen sources, whose availability represents a positive signal for cellular proliferation. The perception of these nutrients relies mainly on three different signaling pathways, centered on three widely conserved protein kinases: PKA, AMPK and TORC1 complexes [26,27]. The activation of such pathways takes place through a molecular interaction between nutrients (more often a derived molecule) and a receptor. This gives rise to a transcriptional and post-translational response, that results in the regulation of genes and proteins required for protein translation, cell cycle progression and response to nutritional stress [28,29].

Mitochondrial dysfunction is signaled to the nucleus through the retrograde response pathway (RTG), which controls the expression of genes required for respiration and consumption of alternative carbon sources [30]. In addition, the release of cytoplasmic calcium from stores, which allows a huge variety of functions, from muscular contraction to neuronal activities in multicellular organisms, is a highly controlled mechanism.

A relevant part of the crosstalk between signal transduction and metabolism is known to take place at the plasma membrane, where nutrients perception elicits signal transduction resulting in the modification of gene expression and in the post-translational modification of key metabolic enzymes [31]. Some examples are the perception of glucose by Snf3 and Rgt2 in *Saccharomyces cerevisiae* and the perception of amino acids, ammonium, sulphate and phosphate through transceptors in the same organism (see [5,32] for a detailed description of these phenomena). Despite this, the aim of this review is to highlight the mechanism by which intracellular primary metabolites affect the activity of signaling pathways in different eukaryotic species, going beyond the classic description of signaling control on metabolism. All the pathways cited before are controlled by protein-metabolite interactions and will be extensively discussed in the present review. Interestingly, the involvement of PMIs in the control of mitochondrial retrograde response (RTG) and calcium signaling exemplify that this mechanism is not limited only to metabolism related pathways [30], but can be considered a general feature in cell signaling.

1.1. Protein-Metabolite Interactions Controlling the Ras/PKA Pathway

Glucose is the preferred carbon source for many organisms, including yeasts, but also for many healthy and unhealthy mammalian cell types. In the budding yeast *Saccharomyces cerevisiae*, glucose availability activates the cAMP mediated Ras/PKA pathway through extracellular and intracellular mechanisms [33]. The extracellular system relies on the G-protein coupled receptor Gpr1, which, once bound to glucose, interacts with Gpa2, the α-subunit of a heterotrimeric G-protein complex. This promotes Gpa1 loading with GTP and its release from the complex [34]. In parallel, intracellular perception of glucose is mediated by the monomeric GTP-binding protein Ras, encoded by the *RAS1* and *RAS2* genes that, in the presence of glucose, exchanges GDP with GTP, in a reaction catalyzed by the GEF (Guanine Nucleotide Exchange Factor) Cdc25 [35,36].

The two different mechanisms for Ras/PKA activation converge on the adenylate cyclase (AC) Cyr1, whose catalytic activity is triggered by the interaction with Ras2 and Gpa2, resulting in a strong increase of intracellular cAMP concentration. Interestingly, the Gpr1/Gpa2 pathway requires Ras pre-activation of Cyr1, with the result that the signaling of the availability of extracellular glucose is subordinated to its actual consumption into glycolysis [37]. Glucose-mediated increase in cAMP concentration results in PKA activation. This is achieved through the binding of the second messenger cAMP to Bcy1, the inhibiting subunit of PKA, inducing its dissociation from the catalytic subunits (Tpk1,2,3) [38]. Active PKA promotes fermentative growth by stimulating glycolytic flux. Accordingly, it represses processes associated with slow growth, such as mitochondrial respiration, stress responses and carbohydrate storage [5,31].

The Ras/PKA pathway is strongly influenced by the interactions between its components and metabolites, that coordinate the activation state of the kinase with the metabolic state of the cell. In fact, as shown in Figure 1, cAMP synthesis is responsive to glucose transport into the cell and its phosphorylation to glucose-6-phosphate (G6P), while it has been discovered only recently that

fructose-1,6-biphosphate (F1,6bP) is the glycolytic metabolite that actually controls Ras activity (Figure 1) [9,39].

Figure 1. Ras/PKA modulation by PMIs. F1,6bP (green boxes) activates Ras both in yeasts and in mammals, interacting with Cdc25 and hSos1, respectively. Extracellular bicarbonate (blue boxes) interacts with yeast adenylate cyclase, activating virulence promoting processes, such as filamentous growth in *C. albicans* and encapsulation in *C. neoformans*. In mammalian cells, bicarbonate activates soluble adenylate cyclase (sAC) enabling the competence of spermatozoa. Moreover, this interaction promotes cellular growth in oncogenic Ras-driven tumors. In *S. cerevisiae*, acetate oxidation to CO_2 through the TCA cycle induces sporulation of diploid cells grown in medium containing only this carbon source. Continuous arrows indicate direct activations, dashed lines indicate indirect processes.

Peeters and coworker started from the observation that yeast hexokinases (Hxk1 and Hxk2) are negatively controlled by the synthesis of trehalose, catalyzed by Tps1 starting from G6P [40]. *TPS1* deleted cells show a higher glycolytic flux and a stronger increase in Ras activation, with a higher amount of Ras-GTP than the wild type. This phenotype is reverted in cells completely impaired in the production of F1,6bP, due to the deletion of both phosphofructokinase genes, *PFK1* and *PFK2* [41].In addition, Ras activation positively correlates with F1,6bP concentration in permeabilized spheroplasts and remarkably, F1,6bP binds to the complex formed by the catalytic domain of hSOS (the human homolog of Cdc25) and H-RAS, one of the human isoforms of Ras (Figure 1) [9]. This interaction has been proposed to take place at the interface of the complex formed by Cdc25 and Ras; indeed, point mutations of Cdc25 residues involved in the binding impair F1,6bP activation of Ras [9]. These results strongly suggest that the glycolytic flux is connected to the PKA pathway by a molecular interaction between F1,6bP and the Ras/Cdc25 complex, which results in the activation of the G-protein and in the increase of cAMP concentration [9].

Furthermore, this allosteric regulation is coherent with the proposed role of F1,6bP as glycolytic flux-sensor. In fact, F1,6bP concentration positively correlates with sugar uptake rate and is associated with yeast fermentative metabolism [42]. *S. cerevisiae* supports its growth on glucose with a fermentative metabolism unless the concentration of this carbon source is very low. Since the Ras/PKA pathway responds to glucose availability and supports fermentation, its regulation by F1,6bP looks perfectly coherent with its function and gives mechanistic insights of how F1,6bP level could correlates with glycolytic flux and ethanol production.

Remarkably, as shown in Figure 1, F1,6bP have been clearly demonstrated to bind with hSos1, the mammalian Cdc25 homologue, suggesting that F1,6bP control on the Ras/PKA pathway is also conserved in higher eukaryotes [9].

As described above, cAMP production by adenylate cyclase (AC) plays a central role in the activation of PKA. Prokaryotes and vertebrates present two classes of AC, distinguished in

transmembrane (tmAC) and soluble (sAC) adenylate cyclases (as indicated also in Figure 1) [43]. tmACs represent the "classical" adenylate cyclases responsive to G-protein coupled receptors, while sACs result in being activated by bicarbonate ions, inducing a strong increase in their catalyticactivity [44,45]. Crystallographic analysis of human and of cyanobacteria *Spirulina platensis* sACs revealed similar structures and a conserved interaction with bicarbonate ions [46,47]. *S. platensis* sAC presents two different ATP binding sites, while a bicarbonate specific binding site is still undiscovered due to the difficulties in sAC co-crystallization with this ion [46]. On the contrary, in human sAC one of the putative ATP binding sites is reported to bind with bicarbonate ions too [47]. Despite this difference, bicarbonate interaction induces a conformational change in both these enzymes. For *S. platensis* sAC this leads to the onset of catalysis, due to the closure of the active site and to the exit of ATP pyrophosphate group thanks to its re-orientation towards Arg1117 [46].

In mammals, sAC is prevalently expressed in testis. Bicarbonate stimulation of sAC has been reported to be pivotal in the activation of processes involved in fertility and, indeed, its depletion results in sterile mice [48]. In addition, sAC is also expressed in other organs, such as kidney, and in the choroid plexus, and its function has recently been linked to the oncogenic Ras-dependent activation of pro-tumoral macropinocytosis [44,49]. This process has been reported to support cancer growth, gaining amino acids from the degradation of extracellular proteins [50]. Interestingly, the onset of this processdoes not require the activity of the tmAC, but that of the sAC, which is stimulated by the bicarbonate imported from the extracellular matrix by SLC4A7 transporter. In such a way, the metabolism of cancer cells expressing an oncogenic Ras results to be connected with the extracellular acidification, coupling pH homeostasis and metabolic adaptation of mutant Ras-driven tumors (as schematically shown in the right part of Figure 1) [49].

Phylogenetic studies revealed the existence of four different classes of AC and eukaryotes have been reported to express only class III AC. Both transmembrane and soluble mammalian AC belong to this class but, strikingly, no soluble AC have been found in *S. cerevisiae*, *Caenorhabditis elegans*, *Drosophila melanogaster* and plants [51]. Despite this, classical ACs from *Candida albicans* and *Cryptococcus neoformans* are activated by bicarbonate, promoting virulence associated processes such as filamentous growth and encapsulation (see the left part of Figure 1) [52,53]. This highlights that given the differences between the ACs expressed by mammals and yeasts, such enzymes can be valuable therapeutic targets for the treatment of *Candida* and *C. neoformans* infections.

The effect of bicarbonate on AC is also physiologically relevant for sporulation of diploid cells of *S. cerevisiae*. During this process, the Ras/PKA pathway needs to be finely tuned, since low PKA activity is required to trigger meiosis, and cAMP level oscillates during it [54]. An environmental condition that triggers sporulation is the availability of acetate as sole carbon source, while its concentration positively correlates with sporulation efficiency through a mechanism that require Ras/PKA. In particular, as schematized in Figure 1, acetate-dependent sporulation is triggered by bicarbonate ions produced by acetate oxidation in the TCA cycle and CO_2 hydration by the carbonic anhydrase (Figure 1) [55]. Bicarbonate interacts with the adenylate cyclase Cyr1, and the mutation of one of the lysine involved in the interaction (Cyr1K1712A) results in the loss of the modulation of the sporulation efficiency by acetate concentrations. The same phenotype is observed in Ras and PKA depleted cells and demonstrates that acetate modulation of sporulation passes through the Ras/PKA pathway and the modulation of Cyr1 activity, due to acetate oxidation and bicarbonate production [54].

All these results suggest that despite yeasts not expressing soluble adenylate cyclase, bicarbonate control of AC activity is conserved in bacteria, fungi and mammals, with fungi canonical ACs being controlled both by G-proteins and bicarbonate ions, as indicated in Figure 1.

1.1. Protein-Metabolite Interactions Controlling SNF1/AMPK/SnRK1 Pathway

As described above, glucose represents a positive signal for cell growth through the Ras/PKA pathway. Its presence is associated with a good nutritional condition which ensures enough carbon and energy to grow and proliferate [5]. However, since nutrient availability is only one of the parameters

that could influence the energy balance, all eukaryotic systems have evolved signaling pathways able to monitor the global energetic status of the cell. These pathways are centered on the protein kinases Snf1, AMPK and SnRK1, depending on the organism (yeast, mammals or plants), as better explained below [56–58].

These kinases operate as heterotrimeric complexes composed of a catalytic subunit α and two regulatory subunits, β and γ. SNF1/AMPK/SnRK1 complexes are active in low energy conditions and are tightly connected to the cellular metabolism. The key event in their regulation is the phosphorylation of the catalytic subunit at the level of a functionally conserved threonine (T210 in yeast, T172 in humans and T175 in plants) which activates these kinases and, as a consequence, energy-expensive processes are switch off [56–58].

In *S. cerevisiae*, Snf1 protein kinase was discovered in a genetic screening of mutants unable to grow on non-fermentable carbon sources [59]. Because of this, the SNF1 complex has generally been recognized as being active in low glucose conditions or in the presence of alternative carbon sources such as ethanol, glycerol and galactose. In these conditions, SNF1 activity is pivotal to rewire the yeast metabolism and to sustain cell growth with the induction of fatty acid oxidation, mitochondrial respiration and gluconeogenesis [29]. Despite this, recent reports suggest the involvement of SNF1 in the control of metabolism also under glucose repression [60,61].

While the Snf1 upstream kinases, Sak1, Tos3 and Elm1 are constitutively active (with Sak1 being the primary upstream kinase), the phosphatase activity of Reg1/Glc7 is strongly induced by availability of glucose [62]. Although Reg1-Glc7 PP1 plays the major role, also Ptc1 protein phosphatase 2C and Sit4 type 2A-related phosphatase were shown to contribute to glucose-regulated dephosphorylation of SNF1 [63,64].

A decrease in the ATP-to-ADP intracellular ratio is representative of a perturbation of the energy homeostasis and SNF1 activation state is controlled by a protein-metabolite interaction with ADP. As presented in Figure 2, the result of this interaction is the protection of the regulatory loop from phosphatase activity, with a resulting higher phosphorylation level of the threonine 210 [65]. Despite this clear evidence, the ADP-dependent protection of Snf1 phosphorylation is still controversial. At first, the protective effect was attributed to ADP binding with the Bateman (CBS) domains of the γ regulatory subunit [65], but later, an alternative model was proposed, according to which the direct binding of ADP in the catalytic site of the α subunit could promote phosphatase resistance [66].
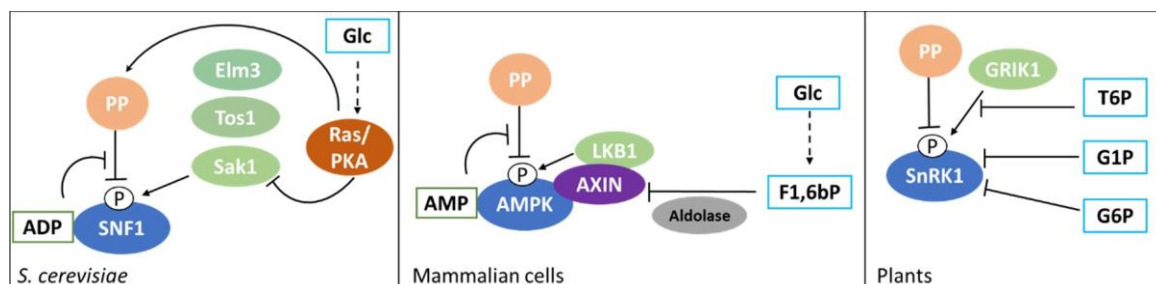
Figure 2. SNF1/AMPK/SnRK1 modulation by nucleotides (green boxes) and glucose metabolites (light blue boxes) in different species. ADP and AMP inhibit dephosphorylation of the regulatory Thr, in yeast and in mammalian cells, respectively. Glucose metabolites inhibit phosphorylation, although the specific mechanism is different in the different species. Additionally, AMPK is also controlled by glycogen through its binding with the Carbon Binding Module (CBS). See text for details. Continuous arrows indicate direct activations, dashed lines indicate indirect processes.

In addition, some data have shown that SNF1 activity negatively correlates with glucose availability and glucose-6-phosphate synthesis, although the molecular mechanism through which glucose represses SNF1 is not fully understood. It has been reported that glucose strongly increases PP1 and PP2A phosphatases activity in a PKA-dependent manner, while Sak1, the major Snf1 upstream kinase, is phosphorylated by PKA (Figure 2) [62,67]. Moreover, SNF1 complex has been reported to influence

PKA pathway by phosphorylating Cyr1 [68]. These findings suggest that Snf1 phosphorylation may be linked to glycolysis through the Ras/PKA pathway and that these kinases may be connected by a feed-back mechanism.

A different hypothesis is based on the observation that Reg1/Glc7 can dephosphorylate its target Mig1 also in low glucose conditions, suggesting that PP1 basal activity may also be sufficient to inactivate Snf1. Therefore, glucose inhibition may take place through a change in the exposure of T210, regardless the activity level of the phosphatase [69].

The SNF1 homolog AMPK plays a well conserved role in mammalian cells and, as for yeast Snf1, its activity is controlled by the phosphorylation on a regulatory Thr, T172, by the upstream kinases LKB1 and CaMKK2 [70,71]. AMPK activation reflects an energetic stress of the cell and coherently induces a downregulation of anabolism and the activation of catabolic processes, such as β-oxidation of fatty acids and mitochondrial respiration [72,73].

AMPK is activated by energy depletion sensed as a decrease in the ATP-to-AMP ratio and thanks to AMP-dependent protection of AMPK complex from phosphatase activity (Figure 2) [74,75]. It was reported that AMP interacts with the γ regulatory subunit of AMPK, similarly to what was shown for ADP on yeast SNF1 complex (Figure 2) [65,76]. The γ regulatory subunit presents four different Bateman (CBS) domains, each characterized by an AMP binding site and it has been shown that the weaker site (named site 3 by the authors) mediates AMP control of AMPK. In particular, AMP binding results in the protection from phosphatases and in the increase of the catalytic activity of the complex [75]. Interestingly, the full-length crystal structure of active AMPK shows a closed conformation in which T172 exposure to phosphatases is reduced. On the contrary, the crystal structure of unphosphorylated and inactive AMPK presents a higher exposure of T172 to the medium [77]. Strikingly, point mutations in the auto-inhibition domain of the catalytic subunit involved in the interaction with the AMP-binding site 3, abolish the AMP-induced protection from phosphatases and the increase of the catalytic activity [77,78].

In addition to this complex mechanism connecting AMPK to energy balance, it has been recently reported a connection between AMPK and the glycolytic metabolite F1,6bP, independently from the ATP-to-AMP ratio [10]. Glucose starvation has been demonstrated to increase the affinity of myristoylated AMPK for the scaffold protein AXIN, that favors AMPK-LKB1 interaction, thus promoting AMPK phosphorylation (Figure 2) [79]. This takes place on the late lysosome membrane, where a protein complex composed of Ragulator (late endosomal adaptor, MAP and mTOR activator 1 and 5) and the V-ATPase alternatively recruits mTOR, in high energy conditions, or AMPK, in low energy conditions, playing an important role in the switch from anabolism to catabolism and vice versa [80]. Remarkably, F1,6bP has been reported to promote the dissociation of the AXIN/LKB1/AMPK complex and, in keeping with that, cells lacking phosphofructokinase show a high phosphorylation of AMPK also in presence of glucose [10]. Moreover, aldolases triple knockdown causes AMPK activation regardless glucose concentration, strongly suggesting that F1,6bP effect on AMPK could be mediated by the interaction with these glycolytic enzymes (Figure 2). Aldolase split F1,6bP into glyceraldehyde-3-phosphate (G3P) and dihydroxyacetone-phosphate (DHAP) and F1,6bP binding to aldolase catalytic site is followed by a conformational change of the protein and the formation of a covalent bound between the substrate and the enzyme [81]. Strikingly, ALDOA-K230A point mutant, which is impaired in the formation of this binding, also prevents F1,6bP inhibition of AMPK and AXIN/LKB1/AMPK complex dissociation [10].

These results indicate that AMPK phosphorylation is directly controlled by glucose availability, which is sensed through changes in F1,6bP concentration, in a mechanism mediated by aldolases. This is the first clear demonstration of a regulation of AMPK activity that takes place before and independently from any variation of the energetic status of the cell, directly connecting its activity to glucose metabolism and glycolytic flux [10].

AMPK activity is also linked to glucose metabolism through the interaction with glycogen. AMPK β subunits present a glycogen binding domain (GBD), also known as carbohydrate binding module

(CBM), and its interaction with glycogen have been reported to affect AMPK activity. Single α1-6 branched glycogen molecules have been proved to act as allosteric inhibitors of AMPK, reducing its catalytic activity and preventing its phosphorylation by upstream kinases. Meanwhile, glycogen has no influence on AMPK dephosphorylation by upstream phosphatase PP2Cα and PP1 [82]. Such a control clearly suggests that AMPK, besides the perception of AMP/ATP ratio, can also monitor energy availability through the amount of reserve carbohydrates.

Interestingly, this feature of AMPK seems not to be conserved in yeast and plants. Snf1 complex β subunits Gal83 and Sip2 present a functional GBD that is involved in the control of Snf1 activity, but not through the binding of glycogen [83]; while in plants, the CBDs of the different isoform of β and βγ hybrid subunits do not show the ability to bind glycogen [84].

As concerns plants, energy homeostasis is maintained by the SnRK1 complex, the homolog of SNF1 and AMPK. Energy depleting conditions could affect photosynthesis, mitochondrial respiration or carbon allocation and activate SnRK1, that in turn, downregulates anabolic processes and promotes catabolic ones, in a very well conserved fashion [57]. SnRK1 activity is also controlled by a phosphorylation event regarding the T175 in the activation loop, and the active form of SnRK1 is represented by the canonical heterotrimeric complex composed of an α catalytic subunit and two regulatory subunits, β and γ [85].

SnRK1 phosphorylation relies on the activity of the upstream kinases GRIK1 and GRIK2, but also on a strong auto-phosphorylation activity; moreover, overexpression of the SnRK1 α subunit is sufficient to increase the catalytic activity of the complex [86]. These observations suggest that the SnRK1 complex is constitutively active, while it is repressed under energy abundance conditions. This sort of control is the reverse of those of SNF1 and AMPK complexes, but is coherent with the general feature of plant cell signaling to prefer negative regulations rather than activations [87].

We have described how yeast SNF1 and mammalian AMPK are controlled at two different levels by two different stimuli, one regarding the general energetic status of the cell, and the other responsive to glucose metabolism. Despite the structural similarities with SNF1 and AMPK, SnRK1 does not respond to changes in AMP or ADP concentration, coherently with the fact that βγ Bateman (CBS) domains present mutations in the residues involved in the binding of adenosyl-nucleotides [84,88]. On the contrary, the effect of glucose on SNF1/AMPK/SnRK1 pathway is well conserved also in plants [89].

As depicted in Figure 2, trehalose-6-phosphate (T6P), glucose-6-phosphate (G6P) and glucose-1-phosphate (G1P) can directly bind and inhibit SnRK1 [89,90]. Indeed, the availability of trehalose and sucrose signal a good nutritional state of the plant and therefore the possibility to switch on anabolic processes and growth. T6P has been reported to reduce SnRK1 catalytic activity as a non-competitive inhibitor, without affecting enzyme affinity to ATP. Furthermore, G1P influences SnRK1 enzymatic activity following the same model and, interestingly, the combination of T6P and G1P have a synergistic effect on SnRK1, opening to the hypothesis that these metabolites could bind at two different sites. On the contrary, G6P inhibits ATP binding to the catalytic domain and has a cumulative effect when combined with T6P [90]. Eventually, SnRK1 inhibition by T6P was recently reported to depend on T6P binding to KIN10, the catalytic subunit of SnRK1, affecting its interaction with the upstream kinase GRIK1, therefore reducing SnRK1 phosphorylation and enzymatic activity [91].

According to the presented evidence, we can conclude that energy homeostasis in eukaryotic cells is maintained through protein-metabolite interactions in which key metabolites transduce information to a protein-based control system, whose function is to downregulate anabolic processes and to promote catabolism.

1.1. Protein-Metabolite Interactions Controlling TOR Activity in Yeast and Mammalian Cells

Amino acids are among the nutrients that most influence the growth of eukaryotic cells. While glucose ensures energy and carbon availability, amino acids are directly connected to protein and nucleotide synthesis. The TOR pathway is deputed to amino acids perception in all eukaryotes and its

activation represents a positive signal for cellular growth; active TOR promotes anabolic processes such as protein, lipid and nucleotide synthesis and represses autophagy [92]. As for carbon, for nitrogen sources there is also a precise hierarchy in the preferred amino acids. In mammalian cells, mTORC1 is preferentially activated by leucine and arginine while glutamine is the main activator of the homolog TORC1 complex in yeast [28,93].

Amino acid sufficiency represents an essential input for TOR activation and its sensing largely relies on RAG-GTPase complexes. Amino acids stimulate the loading with GTP of RagA/B in mammalian cells and of Gtr1 in yeast, as well as the loading with GDP of RagC/D and Gtr2 in the two eukaryotic systems, promoting TOR activation [94,95]. The perception of amino acids requires their transport into the cell and Protein-metabolite interactions between key amino acids and regulator proteins upstreamof TOR.

As shown in the left part of Figure 3, in *S. cerevisiae*, glutamine and leucine activate TORC1 through Pib2 and Gtr/Ego pathways, respectively [95,96]. *PIB2* genetically interacts with *GTR1* and their double deletion leads to synthetic lethality. Moreover, the suppression of Pib2 expression in a *gtr1Δ* background completely abolishes TORC1 activation, suggesting that amino acid sufficiency in yeast is exclusively sensed through these protein complexes [96,97].
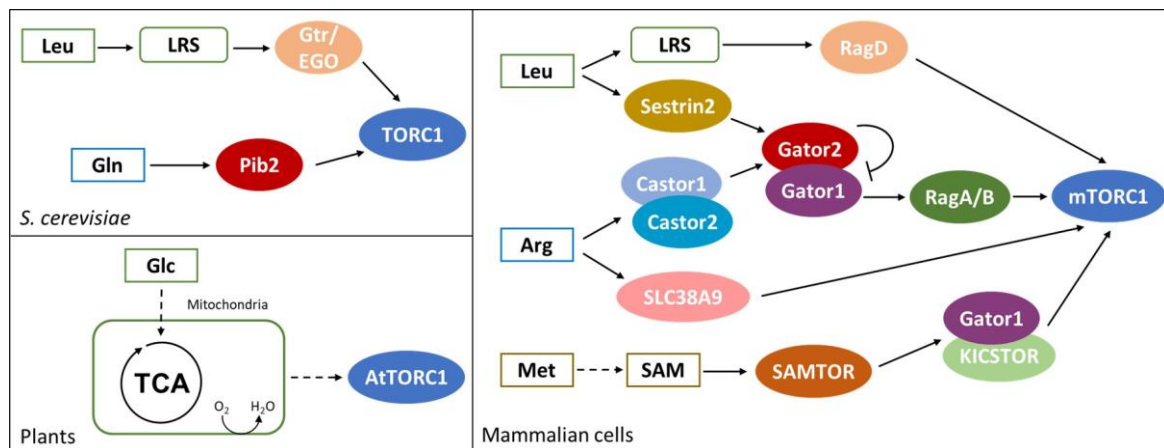
Figure 3. TOR modulation in yeast and in mammalian cells. Both in *S. cerevisiae* and in mammalian cells, leucine activates TOR through Leu-tRNA-synthase (green boxes). In addition, Gln in yeast (blue box), Arg and Met in mammalian cells (purple and orange boxes, respectively) were shown to activate TOR. Contrary to yeast and mammals, in plant cells TOR activity is controlled by glucose oxidation and mitochondrial metabolism. See text for details.

PIB2 deletion is reported to impair glutamine activation of TORC1 (Figure 3). Pib2 co-precipitates with TORC1 under amino acids sufficiency and glutamine is reported to enhance Pib2-TORC1 interaction in vitro in a dose-responsive manner. However, in vitro experiments failed to identify a direct interaction between glutamine and purified Pib2 protein; while glutamine interacts with Pib2 when incubated with cell extracts, suggesting that glutamine binding may be indirect and mediated by another Pib2 interactor [96].

The Ego complex (Ego1, Ego2, Ego3) is known to tether the Grt1/Gtr2 GTPase to the vacuole and amino acids, mainly leucine, stimulate Gtr1 loading with GTP and of Gtr2 with GDP, activating the complex [98]. In yeast, TORC1 constitutively localizes at the vacuole, forming punctate structures under amino acid starvation and diffusing all over the membrane in presence of key amino acids. Active Gtr1/Gtr2 complex strongly interacts with TORC1 and induces its activation [95,99]. As represented in Figure 3, leucine perception by the Gtr/Ego pathway relies on the leucyl-tRNA synthetase (LRS), encoded by *CDC60* [100]. Cdc60 presents both an aminoacyl-tRNA-synthetase activity and a proofreading one, functional to the control of the loading with the proper amino acid [101]. Leucine is the most abundant amino acid in proteins and its tRNA synthetase is the most expressed in yeast cells [102,103]. These

observations provide a rationale for TORC1 activation by leucine, despite the fact that it is not the preferred nitrogen source in yeast.

Cdc60 has been reported to interact with Gtr1 in the presence of leucine and treatment with the leucyl-tRNA-synthetase inhibitor 1,3-dihydro-1-hydroxy-2,1-benzoxaborole (DHBB) downregulates TORC1 activity [100]. Since DHBB is known to form an adduct at the proofreading site of the enzyme that trap it in the uncharged state, it is likely that leucine starvation may affect Cdc60-Gtr1 interaction due to an increase in tRNA^{Leu} mischarging and the activation of the proofreading activity [104,105]. Eventually, Cdc60 dissociation from Gtr1 may expose it to the interaction with a yet unknown GAP, causing GTP hydrolysis and the inactivation of the complex, leading to downregulation of TORC1 activity [100].

Pib2 and Gtr1/Gtr2 form distinct complexes with TORC1 and independently modulate its activity. Pib2, as Tor1, localizes in puncta on the vacuole under starvation and diffuses all over the vacuole membrane under amino acids sufficiency. Despite the independent functions of Pib2 and Gtr1, a strain deleted in *GTR1* shows an accumulation of both Tor1 and Pib2 puncta even in presence of amino acids, suggesting that Pib2 localization may be controlled by the Gtr1/2 complex [96]. These observation underline the fact that despite some clear evidence, further studies are required to understand the fine tuning of these two different control mechanisms in *S. cerevisiae*.

In mammalian cells, mTOR activity is controlled by both amino acid sufficiency (in particular by leucine, arginine and methionine, as shown in the right part of Figure 3) and growth factors [106,107]. Under amino acid sufficiency, the Gtr1 ortholog RagA/B is loaded with GTP and dimerizes with the Gtr2 ortholog RagC/D charged with GDP. RAG GTPases constitutively localize on the lysosome membrane and amino acids induce their interaction with the Ego ortholog Ragulator, while their interaction with Raptor recruits mTORC1 at the lysosome [108,109]. Once localized at the lysosome, mTORC1 is activated through the interaction with the GTPase RHEB, which is controlled by growth factors through the AKT pathway [107,110]. Therefore, mTORC1 is activated only when nutritional and environmental conditions are advantageous and cellular growth is both feasible and allowed.

As represented in Figure 3, the function of leucyl-tRNA-synthetase (LRS) in mediating leucine perception is conserved also in mammalian cells [111]. Amino acids and leucine availability induce LRS localization at the lysosome membrane, where it interacts with Raptor and mTORC1 complexes. Both LRS knockdown and point mutation of the leucine binding site result in a reduced activation of mTORC1 upon leucine supplementation, demonstrating that leucine availability is perceived through its binding with LRS. Leucine availability also induces the interaction of LRS with RagD; in particular, the aminoacyl-tRNA-synthetase acts as a GAP on RagD, promoting the hydrolysis of GTP to GDP and inducing the activation of mTORC1 [111].

In keeping with the fact that LRS depletion does not totally impair mTORC1 activation, leucine availability in mammalian cells is perceived also through Sestrin2 (see Figure 3), a monomeric protein sharing common folding with the carboxymucolactone decarboxylase (CMD) protein family.The C-terminal domain of Sestrin2 presents a binding pocket specific for leucine, with residues Glu451 and Arg390 interacting with leucine amine and carboxylic group, respectively. The hydrophobic base of the pocket excludes charged and polar amino acids, while large hydrophobic residues are excludedby steric clash and small one cannot form stable interactions. In addition, a lid structure completely covers leucine within the binding pocket and stabilizes the protein structure [112].

Sestrin2 is known to interact with Gator2, the inhibitor of Gator1, a protein complex acting as GAP of RagA/B. During amino acid starvation, Sestrin2 recruits Gator2 presumably promoting RagA/B GTPase activity and therefore mTORC1 inactivation. On the contrary, during amino acid sufficiency, Gator2 inhibits Gator1, promoting the loading of RagA/B with GTP and mTORC1 activation [113,114]. Leucine is reported to bind to Sestrin2 and affects Sestrin2-Gator2 interaction, while a Sestrin2 mutant impaired for the binding with Gator2 fail to activate mTORC1 in the presence of leucine [111]. Eventually, HEK-293T cells expressing a Sestrin2 mutant with a reduce affinity for leucine show a

dose-response activation of mTORC1 shifted towards a higher concentration of amino acids, clearly demonstrating that leucine-dependent activation of mTORC1 requires leucine binding to Sestrin2 [112].

As indicated in Figure 3, arginine is another amino acid known to directly affect mTORC1 activity and, also its perception, is centered on the protein Gator2 [106,115]. Amino acid starvation induces Gator2 interaction with Castor1 and Castor2, two homolog proteins presenting four small molecule binding domains (ACT) each. These proteins can combine into homo- and hetero-complexes, and their dimerization is necessary for their interaction with Gator2. Crystallographic analysis revealed that arginine binds Castor1 at the interface between ACT2 and ACT4, presumably arranging the conformation of a glycine-rich loop and therefore allowing for ACT2-ACT4 interaction [116]. I280A point mutation of Castor1 is reported to impair arginine binding with the protein, resulting in a constitutive interaction with Gator2 and in the inactivation of mTORC1, even in the presence of arginine [115,116]. According to these results, arginine availability activates mTORC1 through the inhibition of Gator1 by Gator2, that may be released from Castor1. Arginine binding is likely to induce a conformational change in Castor1 bringing to an altered exposure of key residues required for its interaction with Gator2 [116].

Interestingly, the ACT domains of Castor1 structurally resemble the allosteric regulatory domain of bacterial aspartate kinase (AK), which is known to be sensitive to leucine. Since AK is absent in metazoan and Castor1 is present only in this lineage, it is likely that arginine perception evolved starting form an already existing module, i.e., prokaryotic aspartate kinases [116]. Following this line of evidence, arginine perception could be relevant also in yeast, through the aspartate kinase Hom3. In fact, Hom3 has been reported to genetically interact with component of the EGO complex and its deletion increases rapamycin sensitivity, suggesting the involvement of Hom3 in arginine perception in yeast [117,118].

In mammalian cells, arginine perception relies also on the lysosomal transmembrane protein SLC38A9 (Figure 3). It has been reported that SLC38A9 interacts with Ragulator complex and with a RagB mutant that mimics a constitutive binding with GDP [119]. Moreover, its depletion affects mTORC1 activation by arginine availability. Since SLC38A9 presents a transport activity specific for amino acids and with a preference for arginine, it may link mTORC1 activity with arginine concentration within the lysosome [119]. Interestingly, a recent report suggests that arginine perception by Castor1 and SLC38A9 occur through independent mechanisms, but a residual mild activation of mTORC1 in cells lacking Castor1 and SLC38A9 suggests the existence of additional controls on the pathway [115].

TOR pathway in mammalian cells has been reported to be influenced also by methionine availability and, as indicated in Figure 3, through its conversation into S-Adenosylmethionine (SAM). [120]. Furthermore, SAM level can be influenced also by folate, betaine and vitamin B12, suggesting that also these molecules could indirectly influence mTORC1 activity. Methionine perception passes through a PMI between its activated form, SAM and SAMTOR, a protein presenting a class I Rossmann fold methyltransferase domain able to bind SAM [120]. This mechanism is conserved in *D. melanogaster*, which presents the SAMTOR homolog dSamtor, but not in *S. cerevisiae*, in which methionine availability is perceived through PP2A methylation and not through PMIs [121].

Differently from Sestrin2 and Castor complexes, SAMTOR negatively regulates mTORC1 interacting with Gator1 and KICSTOR, suggesting that Gator1 is inactive when bound to SAMTOR. Hence, the binding of SAM to SAMTOR results in the disruption of the SAMTOR-Gator1-KICSTOR complex, releasing Gator1 and activating mTORC1 [120].

The TOR pathway is quite conserved also in plants, even if its regulation by PMIs is much less clear. The *Arabidopsis thaliana* genome encodes functional homologs of TOR (AtTOR) and two TOR-interactors: LST8 (AtLST8-1 and AtLST8-2) and RAPTOR (AtRAPTOR1A and AtRAPTOR1B). On the contrary, no TORC2 homolog has been identified [122]. It was shown that glucose and sucrose (but not other sugars such as fructose, xylose and galactose) stimulate root growth and meristem activation in a TOR-dependent manner [123]. This glucose activation of the TOR pathway

is prevented by 2-deoxy-glucose and by inhibitors of the electron transport chain, indicating that glucose needs to pass through glycolysis and the electron transport chain to give TOR activation, as reported in Figure 3 [123]. In addition, it was recently reported that nicotinamide (vitamin B3) affects ATP level and inhibits the glucose-TOR signaling, regulating the circadian clock, meristem activation and root growth [124]. Although the precise molecular mechanism of glucose activation is still unknown, this last study suggests a link between the energetic status of the cell and TOR activity. This leads to the hypothesis that TOR activation by glucose may be mediated by the kinase SnRK1, which phosphorylates RAPTOR as in mammalian cells, where this phosphorylation has an inhibitory role [125,126]. Another proposed hypothesis is that glucose signals could be required for TORC1 dimerization [122]. In mammalian cells, the glucose/energy sensitive Tel2-Tti1-Tti2 (TTT)-RUVBL1/2 complex (which has orthologous genes in plants) is required for TORC1 dimerization and translocation to the lysosome membrane [127]. The assembly of the TTT-RUVBL1/2 complex and its interaction with TOR requires the activity of RUVBL1/2, which is repressed by respiration inhibition, therefore indirectly linking respiration and TOR activation.

In plants, TOR signaling also responds to sulfur availability. Sulfur deficiency causes a decrease in TOR activity, due to a reduction of glucose, maltose, sucrose and TCA cycle intermediates, thus indicating that sulfur shortage is sensed through the same glucose-TOR signaling described above [128].

Finally, although the major TOR activators in yeast and mammals are amino acids, no amino acid sensors have been discovered in plant genomes. In keeping with that, it was shown that TOR activity cannot be stimulates by supplying of an amino acid cocktail in plants [123]. Nevertheless, it was recently reported that mutants which accumulate branched chain amino acids (BCAA) present a higher TOR activity, which leads to an altered organization of the actin cytoskeleton and endomembranes [129]. This evidence suggests that also in plant cells, amino acids can activate the TOR pathway.

1.1. Yeast Mitochondrial Retrograde Response Is Influenced by Protein-Metabolite Interactions

Classically defined as the powerhouse of the cell, it is now clear that mitochondria functions go beyond energy production and that mitochondrial health critically define cell fate [130–132]. In mammals, yeast and plants, mitochondrial dysfunctions activate retrograde response pathways (RTGs), eliciting the transcription of nuclear genes with the aim of coping with the perturbation. In yeasts, RTG is also triggered by the shift on non-fermentable carbon sources and leads to the expression of genes involved in respiration and consumption of carbon sources alternative to glucose, but is also involved in multi-drug resistance [133–135]. As reported in Figure 4, among the different stimuli known to activate the RTG pathway in yeast there is a drop in ATP concentration, even if its level could also be influenced by non-mitochondrial processes [30]. On the contrary, in mammals and in plants, mitochondrial dysfunctions are signaled to the nucleus mainly by the alteration of mitochondrial membrane potential, followed by a strong increase in cytoplasmic calcium without involving PMIs (see [136,137], for further details).

ATP control of the RTG pathway in yeast is based on a PMI. In cells presenting healthy mitochondria (see the left part of Figure 4), the Mks1-Bmh1/2 complex prevents Rtg3 dephosphorylation and therefore its migration into the nucleus. Mitochondria dysfunctions (right part of Figure 4) induce partial dephosphorylation of the transcription factor Rtg3 and its nuclear localization in complex with Rtg1 [138]. The onset of the signaling is centered around Rtg2 that, under mitochondrial stress, binds Mks1 and promotes Rtg1-Rtg3 translocation into the nucleus [139]. Rtg2 is known to present an N-terminal ATP-binding domain similar to the Hsp70/sugar kinase/actin protein superfamily, whose activity results to be pivotal for the RTG onset [139]. It has been reported that ATP strongly impairs Rtg2 interaction with Mks1 at physiological concentrations, while a non-hydrolysable ATP homologue (adenosine 5^J-(β,γ- imido) triphosphate) has no effect on Rgt2-Mks1 interaction [140]. These results suggest that ATP must be hydrolyzed in order to induce Mks1 dissociation from Rgt2; yet, ATP interaction with the ATP-binding domain of Rtg2 has not been proved, leaving open the possibility of an indirect sensing of the ATP availability.
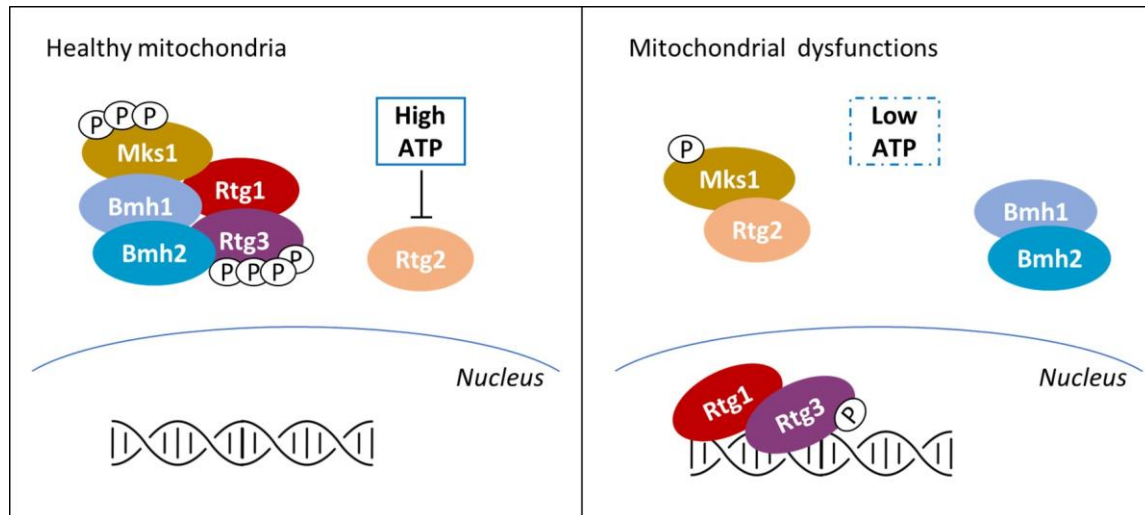
Figure 4. Regulation of the mitochondrial retrograde response in *S. cerevisiae*. In yeast cells presenting healthy mitochondria, Rtg1-Rtg3 complex is recruited to the cytosol by the Mks1-Bmh1/2 complex, with both Rtg3 and Mks1 hyper-phosphorylated. The interaction between Rgt2 and Mks1 is inhibited by ATP interaction with Rtg2 or with other components of the complex. Mitochondrial dysfunction causes a drop in ATP concentration (indicated by the dotted box), leading to Rtg2-Mks1 interaction and hypo-phosphorylated Rtg3 and Mks1. As a consequence, the nuclear localization of the Rtg1-Rtg3 complex induces the expression of RTG genes.

Strikingly, the role of ATP in controlling Mks1 activity is also reported in other yeasts, such as *Kluveromyces lactis* and *Kluveromyces waltii*, suggesting the conservation of this control mechanism among Fungi [140]. In conclusion, despite Snf1 conserved role in monitoring the energetic status of the cell, recent evidence suggest that Snf1 and RTG pathways can independently respond to ATP depletionin yeast [127].

1.1. Protein-Metabolite Interactions Controlling Calcium Release

Transient changes in the concentration of intracellular calcium are important regulators of cellular signaling in human cells. The increase of intracellular calcium can be due either to Ca^{2+} entry from the extracellular space through L-type Ca^{2+} channels and to Ca^{2+} release form the endoplasmic/sarcoplasmic reticulum (ER/SR). Two major calcium channels exist on the ER/SR, one dependent on calcium ions, the other controlled by inositol-3-phosphate (IP3). The so-called calcium-induced calcium release (CICR) is mediated by Ryanodine receptors (RyRs), homotetrameric channels, which are normally closed when the cytosolic calcium concentration is low (100–200 nM), while they are open when calcium increases up to low micromolar concentrations [141]. The other pathway of calcium release is activated by IP3 binding to IP3 receptors. Hormones, growth factors and neurotransmitters can stimulate the formation of IP3 through activation of G-protein-coupled receptors (GPCR) or tyrosine kinase associated receptors, which are associated with phospholipase C (PLC). PLC catalyzes the formation of diacylglycerol (DAG) and IP3 from phosphatidyl inositol-4,5-bisphosphate, and IP3 stimulates IP3 receptors, inducing calcium release form the endoplasmic reticulum, characterized by brief calcium transients, that can be repeated to give oscillations [142]. Instead, calcium uptake from the cytosol back into the ER/SR relies on the activity of the SERCA (sarcoendoplasmic reticulum Ca^{2+}-ATPase) pump, whose function is essential to guarantee calcium homeostasis. Calcium signaling pathway controls several different processes, among which muscle contraction, neuronal functions, gene expression, metabolism, secretion, fertilization, proliferation and defects in this pathway are associated with a wide range of pathological conditions [142].

Cyclic ADP-ribose (cADPR) is a cyclic metabolite of NAD^+, synthesized by ADP-ribosyl cyclase, and is the main known regulator of calcium release. It induces calcium release from the SR via

RyRs [143–146], it directly binds to SERCA and stimulates calcium sequestration in the SR [147–149] and can also regulate calcium influx from outside, activating the calcium influx channel TRPM2, at the cell surface [150].

In addition, as shown in Figure 5, calcium levels are also controlled by glycolysis. More than 30 years ago, it was shown that in pancreatic islets glucose-6-phosphate increased the ATP-dependent calcium content in the ER [151]. The same effect of G6P on SERCA activity was shown in other tissues [152,153], and G6P import in the ER was suggested to be required for calcium sequestration [152]. In addition, in cardiac myocytes, glycolysis is required for excitation-contraction coupling, regulating SR Ca^{2+} release and Ca^{2+} sequestration by SERCA [154,155]. Interestingly, it was shown that F6P and F1,6BP directly stimulate the open probability of RyRs, while pyruvate and lactate inhibit RyRs activity [154], suggesting that glycolysis modulates calcium release through multiple metabolites.
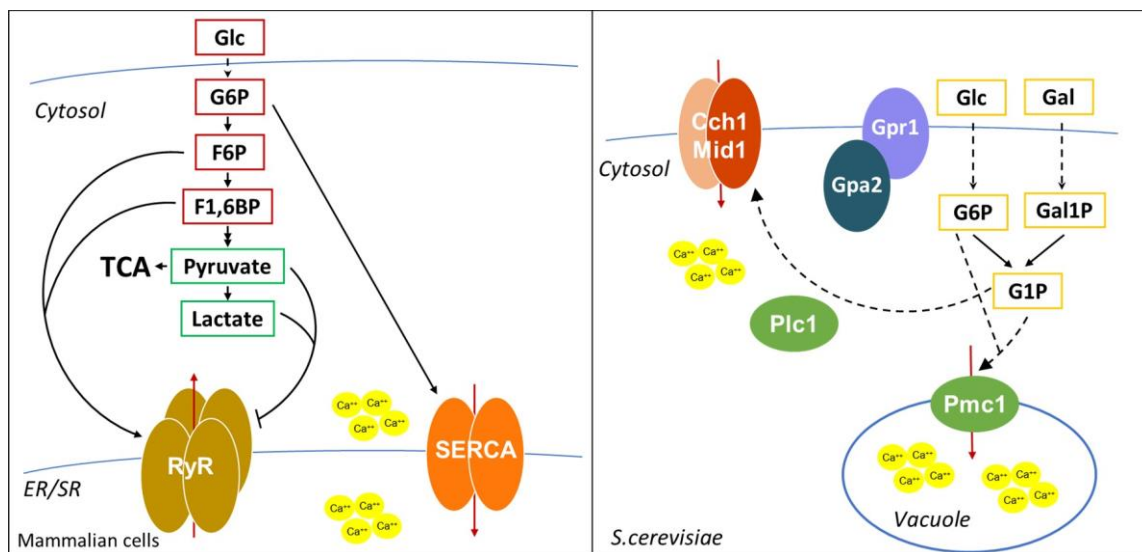
Figure 5. Overview of the effect of glycolytic intermediates on calcium accumulation into the cytoplasm. Metabolites of the upper part of glycolysis (red boxes) are reported to positively influence the activity of RyR channels and SERCA pump, regulating the oscillation of calcium concentration into the cytosol. On the contrary, metabolites of the lower part of glycolysis (green boxes) negatively regulate calcium release from ER/SR through RyR channels. In *S. cerevisiae* (dotted box) calcium import by the plasma membrane calcium channel is regulated by glucose and galactose availability through their conversion into G6P and G1P.

Calcium regulation in yeast is quite different from that in human cells. The main calcium storage organelle in yeast is the vacuole, a large organelle resembling animal lysosome, which contains more than 90% of calcium of the cell. Calcium is imported from the cytosol by the vacuolar Ca^{2+}/ATPase Pmc1 and by the H^+/Ca^{2+} antiporter Vcx1 [156–158], while Ca^{2+} efflux out of the vacuole is mediated by Yvc1 [159]. A minor, exchangeable pool of calcium is located in the ER and Golgi apparatus, where proper calcium levels are maintained by the Ca^{2+}/ATPases Spf1 and Pmr1, important for the regulation of protein folding and processing of proteins that transit through the secretory pathway [160]. Yeasts also have a calcium channel on the plasma membrane, composed by Cch1 and Mid1, responsive to intracellular Ca^{2+} storage [158]. Although *S. cerevisiae* does not have an IP3 receptor, it was shown that IP3 generation by Plc1 activation is involved in the calcium increase after glucose addition to starved cells [161].

In yeast, calcium signals are generated during mating, upon environmental stresses (such as osmotic and alkaline stress, ER stress, oxidative stress, heat shock), after glucose addition to starved-cells and during mitosis [156]. Calcium shortage was reported to affect cell cycle, cell growth, metabolism and protein folding [162,163].

Interestingly, as in mammalian cells, glucose metabolites were shown to modulate calcium levels also in *S. cerevisiae*. Glucose or galactose addition to starved cells leads to a transient calcium increase due to the opening of plasma membrane calcium channels and requires hexose transport and phosphorylation [164], but also the Gpr1/Gpa2 complex and the phospholipase C Plc1 [161,165].

Interestingly, cells lacking Pmg2, the major isoform of phosphoglucomutase that catalyzes the interconversion of G1P and G6P, present higher G1P levels when grown in galactose and show higher intracellular calcium levels [166], due to elevated Pmc1-dependent vacuolar Ca^{2+} uptake and reduced ER/Golgi Ca^{2+} accumulation [167]. Strikingly, deletion of the phosphofructokinase Pfk2 in a *pgm2Δ* strain restores the balance between G1P and G6P and restores Ca^{2+} concentration to a level comparable to that of wild type cells [168]. These data suggest that the ratio between G1P and G6P, rather than the level of each single metabolite, regulates intracellular calcium levels. However, the molecular mechanism of this regulation in still unknown, since neither G6P nor G1P are able to directly stimulate Ca^{2+} transport into the vacuole [167]. An indirect mechanism may involve the Snf3 pathway, which was shown to sense G6P levels [169] or the Gpr1/Gpa2 pathway, which has already been implicated in the calcium increase after glucose readdiction to starved cells [165].

1. Concluding Remarks

It is evident that metabolism has a strong impact on cell signaling and that the interactions between key metabolites and proteins have crucial roles in the cellular response to specific environmental and metabolic conditions. As schematically represented in Figure 6, several metabolites of the central metabolism directly participate in the regulation of different signaling pathways. Metabolites of the glycolysis modulate the SNF1/AMPK/SnRK1 pathway, as well as the PKA pathway and the calcium release mechanism. Molecules belonging to the TCA cycle regulate the retrograde response in yeast and the Ras/PKA pathway. Finally, key amino acids control the TORC1 pathway, through multiple mechanisms.

Figure 6. Overview of the Protein-metabolite interactions connecting metabolism and signal transduction pathways in different species. The central carbon metabolism influences the activity of Ras/PKA and SNF1/AMPK/SnRK1 pathways, but also the mitochondrial retrograde response, in yeast, mammals and plants (shown respectively in yellow, red and green). The availability of specific amino acids controls the activity of TOR pathway both in yeast and in mammals, while in plants its activity is influenced by mitochondrial respirations.

However, all the mechanisms reviewed here have been discovered in hypothesis-driven studies and large-scale analyses exploring protein-metabolite interactions, as well as their structural and physiological consequences on regulatory proteins, are still needed. One obvious problem is that metabolites mostly interact with metabolic enzymes, while only a small fraction is involved in interactions with signaling proteins to perform regulatory functions [170]. In addition, PMI investigation is hindered by technical problems, since different approaches are needed to study molecules with different chemical properties [7]. Several methodologies for the analysis of the interaction between proteins and small molecule have been developed in recent years (see [7] for a detailed description); however, their application has mainly been focused on the interaction between metabolites and metabolic enzymes. The dynamical nature of PMIs, the high number of interactions involving metabolic enzymes, and also the necessity of validating the binding in vitro and its effect in vivo exacerbate, if possible, the difficulties of the study of PMIs at large scale when focused on regulatory proteins.

Nevertheless, the information acquired from such studies represents actual progress for the comprehension of biological systems. For instance, a systematic analysis of in vivo PMIs in *S. cerevisiae* directed against non-polar small molecules revealed that 20% of protein kinases interact with hydrophobic metabolites [171]. Additionally, system level analysis on yeast cells shifted from glucose to ethanol revealed the requirement of the 14-3-3 protein Bmh1 for yeast growth on ethanol [148]. These examples suggest that our comprehension of the crosstalk between metabolism and cell signaling is still poor, and that the allosteric regulation of regulatory proteins by PMIs could be a common mechanism by which cell signaling could be dynamically connected to metabolism.

Author Contributions: R.M. and F.T. wrote the first draft and created all the figures. P.C. edited and completed the manuscript. All authors have read and agreed to the published version of the manuscript.

References

1. Kitano, H. Biological robustness. *Nat. Rev. Genet.* **2004**, *5*, 826–837. [CrossRef] [PubMed]
2. Kitano, H. *Foundations of Systems Biology*; MIT Press: Cambridge, MA, USA, 2001.
3. Friedlander, T.; Mayo, A.E.; Tlusty, T.; Alon, U. Evolution of Bow-Tie Architectures in Biology. *PLoS Comput. Biol.* **2015**, *11*, e1004055. [CrossRef] [PubMed]
4. Stelling, J.; Sauer, U.; Szallasi, Z.; Doyle, F.J.; Doyle, J. Robustness of Cellular Functions. *Cell* **2004**, *118*, 675–685. [CrossRef] [PubMed]
5. Busti, S.; Coccetti, P.; Alberghina, L.; Vanoni, M. Glucose signaling-mediated coordination of cell growth and cell cycle in saccharomyces cerevisiae. *Sensors* **2010**, *10*, 6195–6240. [CrossRef] [PubMed]
6. Ewald, J.C. How yeast coordinates metabolism, growth and division. *Curr. Opin. Microbiol.* **2018**, *45*, 1–7. [CrossRef] [PubMed]
7. Diether, M.; Sauer, U. Towards detecting regulatory Protein-metabolite interactions. *Curr. Opin. Microbiol.* **2017**, *39*, 16–23. [CrossRef]
8. Diether, M.; Nikolaev, Y.; Allain, F.H.; Sauer, U. Systematic mapping of protein-metabolite interactions in central metabolism of Escherichia coli. *Mol. Syst. Biol.* **2019**, *15*, e9008. [CrossRef]
9. Peeters, K.; Van Leemputte, F.; Fischer, B.; Bonini, B.M.; Quezada, H.; Tsytlonok, M.; Haesen, D.; Vanthienen, W.; Bernardes, N.; Gonzalez-Blas, C.B.; et al. Fructose-1,6-bisphosphate couples glycolytic flux to activation of Ras. *Nat. Commun.* **2017**, *8*. [CrossRef]
10. Zhang, C.S.; Hawley, S.A.; Zong, Y.; Li, M.; Wang, Z.; Gray, A.; Ma, T.; Cui, J.; Feng, J.W.; Zhu, M.; et al. Fructose-1,6-bisphosphate and aldolase mediate glucose sensing by AMPK. *Nature* **2017**, *548*, 112–116. [CrossRef]

1. Piazza, I.; Kochanowski, K.; Cappelletti, V.; Fuhrer, T.; Noor, E.; Sauer, U.; Picotti, P. A map of protein-metabolite interactions reveals principles of chemical communication. *Cell* **2018**, *172*, 358–372. [CrossRef]

2. Eisenmesser, E.Z.; Millet, O.; Labeikovsky, W.; Korzhnev, D.M.; Wolf-Watz, M.; Bosco, D.A.; Skalicky, J.J.; Kay, L.E.; Kern, D. Intrinsic dynamics of an enzyme underlies catalysis. *Nature* **2005**, *438*, 117–121. [CrossRef] [PubMed]

3. Kim, E.; Lee, S.; Jeon, A.; Choi, J.M.; Lee, H.S.; Hohng, S.; Kim, H.S. A single-molecule dissection of ligand binding to a protein with intrinsic dynamics. *Nat. Chem. Biol.* **2013**, *9*, 313–318. [CrossRef] [PubMed]

4. Boehr, D.D.; Nussinov, R.; Wright, P.E. The role of dynamic conformational ensembles in biomolecular recognition. *Nat. Chem. Biol.* **2009**, *5*, 789–796. [CrossRef] [PubMed]

5. Gianni, S.; Dogan, J.; Jemth, P. Distinguishing induced fit from conformational selection. *Biophys. Chem.* **2014**, *189*, 33–39. [CrossRef]

6. Koshland, D.E. Application of a theory of enzyme specificity to protein synthesis. *Proc. Natl. Acad. Sci. USA* **1958**, *44*, 98–104. [CrossRef]

7. Ma, B.; Kumar, S.; Tsai, C.-J.; Nussinov, R. Folding funnels and binding mechanisms. *Protein Eng. Des. Sel.* **1999**, *12*, 713–720. [CrossRef]

8. Weikl, T.R.; Paul, F. Conformational selection in protein binding and function. *Protein Sci.* **2014**, *23*, 1508–1518. [CrossRef]

9. Kirschner, K.; Eigen, M.; Bittman, R.; Voigt, B. The binding of nicotinamide-adenine dinucleotide to yeast D-glyceraldheyde-3-phosphate dehydrogenase: Temperature-jump relaxation studies on the mechanism of an allosteric enzyme. *Proc. Natl. Acad. Sci. USA* **1966**, *56*, 1661–1667. [CrossRef]

10. Johnson, K.A. Role of induced fit in enzyme specificity: A molecular forward/reverse switch. *J. Biol. Chem.* **2008**, *283*, 26297–26301. [CrossRef]

11. Lee, G.M.; Craik, C.S. Trapping moving targets with small molecules. *Science* **2009**, *324*, 213–215. [CrossRef]

12. Wagner, J.R.; Lee, C.T.; Durrant, J.D.; Malmstrom, R.D.; Feher, V.A.; Amaro, R.E. Emerging computational methods for the rational discovery of allosteric drugs. *Chem. Rev.* **2016**, *116*, 6370–6390. [CrossRef] [PubMed]

13. Tsai, C.-J.; Kumar, S.; Ma, B.; Nussinov, R. Folding funnels, binding funnels, and protein function. *Protein Sci.* **1999**, *8*, 1181–1190. [CrossRef]

14. Alberghina, L.; Coccetti, P.; Orlandi, I. Systems biology of the cell cycle of Saccharomyces cerevisiae: From network mining to system-level properties. *Biotechnol. Adv.* **2009**, *27*, 960–978. [CrossRef]

15. Alberghina, L.; Mavelli, G.; Drovandi, G.; Palumbo, P.; Pessina, S.; Tripodi, F.; Coccetti, P.; Vanoni, M. Cell growth and cell cycle in Saccharomyces cerevisiae: Basic regulatory design and protein-protein interaction network. *Biotechnol. Adv.* **2012**, *30*, 52–72. [CrossRef] [PubMed]

16. Conrad, M.; Schothorst, J.; Kankipati, H.N.; Van Zeebroeck, G.; Rubio-Texeira, M.; Thevelein, J.M. Nutrient sensing and signaling in the yeast Saccharomyces cerevisiae. *FEMS Microbiol. Rev.* **2014**, *38*, 254–299. [CrossRef] [PubMed]

17. Efeyan, A.; Comb, W.C.; Sabatini, D.M. Nutrient-sensing mechanisms and pathways. *Nature* **2015**, *517*, 302–310. [CrossRef] [PubMed]

18. González, A.; Hall, M.N. Nutrient sensing and TOR signaling in yeast and mammals. *EMBO J.* **2017**, *36*, 397–408. [CrossRef]

19. Kayikci, Ö.; Nielsen, J. Glucose repression in Saccharomyces cerevisiae. *FEMS Yeast Res.* **2015**, *15*, fov068. [CrossRef]

20. Knorre, D.; Sokolov, S.; Zyrina, A. How do yeast sense mitochondrial dysfunction? *Microb. Cell* **2016**, *3*, 532–539. [CrossRef]

21. Tripodi, F.; Nicastro, R.; Reghellin, V.; Coccetti, P. Post-translational modifications on yeast carbon metabolism: Regulatory mechanisms beyond transcriptional control. *Biochim. Biophys. Acta* **2015**, *1850*, 620–627. [CrossRef]

22. Steyfkens, F.; Zhang, Z.; Van Zeebroeck, G.; Thevelein, J.M. Multiple transceptors for macro- and micro-nutrients control diverse cellular properties through the PKA pathway in yeast: A paradigm for therapidly expanding world of eukaryotic nutrient transceptors up to those in human cells. *Front. Pharmacol.* **2018**, *9*, 191. [CrossRef] [PubMed]

1. Colombo, S.; Ma, P.; Cauwenberg, L.; Winderickx, J.; Crauwels, M.; Teunissen, A.; Nauwelaers, D.;de Winde, J.H.; Gorwa, M.; Colavizza, D.; et al. Involvement of distinct G-proteins, Gpa2 and Ras, in glucose- and intracellular acidification-induced cAMP signalling in the yeast Saccharomyces cerevisiae. *EMBO J.* **1998**, *17*, 3326–3341. [CrossRef] [PubMed]
2. Xue, Y.; Batlle, M.; Hirsch, J.P. GPR1 encodes a putative G protein-coupled receptor that associates with the Gpa2p Galpha subunit and functions in a Ras-independent pathway. *EMBO J.* **1998**, *17*, 1996–2007. [CrossRef]
3. Kataoka, T.; Powers, S.; McGill, C.; Fasano, O.; Strathern, J.; Broach, J.; Wigler, M. Genetic analysis of yeast RAS1 and RAS2 genes. *Cell* **1984**, *37*, 437–445. [CrossRef]
4. Jacquet, E.; Parrini, M.C.; Bernardi, A.; Martegani, E.; Parmeggiani, A. Properties of the catalytic domain of CDC25, a saccharomyces cerevisiae GDP/GTP exchange factor: Comparison of its activity on full-length and c-terminal truncated ras2 proteins. *Biochem. Biophys. Res. Commun.* **1994**, *199*, 497–503. [CrossRef] [PubMed]
5. Rolland, F.; de Winde, J.H.; Lemaire, K.; Boles, E.; Thevelein, J.M.; Winderickx, J. Glucose-induced cAMP signalling in yeast requires both a G-protein coupled receptor system for extracellular glucose detection and a separable hexose kinase-dependent sensing process. *Mol. Microbiol.* **2000**, *38*, 348–358. [CrossRef] [PubMed]
6. Toda, T.; Cameron, S.; Sass, P.; Zoller, M.; Scott, J.D.; McMullen, B.; Hurwitz, M.; Krebs, E.G.; Wigler, M. Cloning and characterization of BCY1, a locus encoding a regulatory subunit of the cyclic AMP-dependent protein kinase in Saccharomyces cerevisiae. *Mol. Cell. Biol.* **1987**, *7*, 1371–1377. [CrossRef]
7. Rolland, F.; Wanke, V.; Cauwenberg, L.; Ma, P.; Boles, E.; Vanoni, M.; de Winde, J.H.; Thevelein, J.M.; Winderickx, J. The role of hexose transport and phosphorylation in cAMP signalling in the yeast Saccharomyces cerevisiae. *FEMS Yeast Res.* **2001**, *1*, 33–45. [CrossRef]
8. Blázquez, M.A.; Lagunas, R.; Gancedo, C.; Gancedo, J.M. Trehalose-6-phosphate, a new regulator of yeast glycolysis that inhibits hexokinases. *FEBS Lett.* **1993**, *329*, 51–54. [CrossRef]
9. Heinisch, J. Construction and physiological characterization of mutants disrupted in the phosphofructokinase genes of Saccharomyces cerevisiae. *Curr. Genet.* **1986**, *11*, 227–234. [CrossRef]
10. Huberts, D.H.E.W.; Niebel, B.; Heinemann, M. A flux-sensing mechanism could regulate the switch between r espiration and fermentation. *FEMS Yeast Res.* **2012**, *12*, 118–128. [CrossRef]
11. Buck, J.; Sinclair, M.L.; Schapal, L.; Cann, M.J.; Levin, L.R. Cytosolic adenylyl cyclase defines a unique signaling molecule in mammals. *Proc. Natl. Acad. Sci. USA* **1999**, *96*, 79–84. [CrossRef] [PubMed]
12. Chen, Y.; Cann, M.J.; Litvin, T.N.; Iourgenko, V.; Sinclair, M.L.; Levin, L.R.; Buck, J. Soluble adenylyl cyclase as an evolutionarily conserved bicarbonate sensor. *Science* **2000**, *289*, 625–628. [CrossRef] [PubMed]
13. Cann, M.J.; Hammer, A.; Zhou, J.; Kanacher, T. A defined subset of adenylyl cyclases is regulated by bicarbonate ion. *J. Biol. Chem.* **2003**, *278*, 35033–35038. [CrossRef] [PubMed]
14. Steegborn, C.; Litvin, T.N.; Levin, L.R.; Buck, J.; Wu, H. Bicarbonate activation of adenylyl cyclase via promotion of catalytic active site closure and metal recruitment. *Nat. Struct. Mol. Biol.* **2005**, *12*, 32–37. [CrossRef]
15. Saalau-Bethell, S.M.; Berdini, V.; Cleasby, A.; Congreve, M.; Coyle, J.E.; Lock, V.; Murray, C.W.; O'Brien, M.A.; Rich, S.J.; Sambrook, T.; et al. Crystal structure of human soluble adenylate cyclase reveals a Distinct, highly flexible allosteric bicarbonate binding pocket. *Chem. Med. Chem.* **2014**, *9*, 823–832. [CrossRef]
16. Esposito, G.; Jaiswal, B.S.; Xie, F.; Krajnc-Franken, M.A.M.; Robben, T.J.A.A.; Strik, A.M.; Kuil, C.; Philipsen, R.L.A.; van Duin, M.; Conti, M.; et al. Mice deficient for soluble adenylyl cyclase are infertile because of a severe sperm-motility defect. *Proc. Natl. Acad. Sci. USA* **2004**, *101*, 2993–2998. [CrossRef]
17. Ramirez, C.; Hauser, A.D.; Vucic, E.A.; Bar-Sagi, D. Plasma membrane V-ATPase controls oncogenic RAS-induced macropinocytosis. *Nature* **2019**, *576*, 477–481. [CrossRef]
18. Commisso, C.; Davidson, S.M.; Soydaner-Azeloglu, R.G.; Parker, S.J.; Kamphorst, J.J.; Hackett, S.; Grabocka, E.; Nofal, M.; Drebin, J.A.; Thompson, C.B.; et al. Macropinocytosis of protein is an amino acid supply route in Ras-transformed cells. *Nature* **2013**, *497*, 633–637. [CrossRef]
19. Roelofs, J.; van Haastert, P.J.M. Deducing the Origin of Soluble Adenylyl Cyclase, a Gene Lost in Multiple Lineages. *Mol. Biol. Evol.* **2002**, *19*, 2239–2246. [CrossRef]
20. Klengel, T.; Liang, W.J.; Chaloupka, J.; Ruoff, C.; Schröppel, K.; Naglik, J.R.; Eckert, S.E.; Mogensen, E.G.; Haynes, K.; Tuite, M.F.; et al. Fungal adenylyl cyclase integrates CO_2 sensing with cAMP signaling and virulence. *Curr. Biol.* **2005**, *15*, 2021–2026. [CrossRef] [PubMed]

1. Mogensen, E.G.; Janbon, G.; Chaloupka, J.; Steegborn, C.; Man, S.F.; Moyrand, F.; Klengel, T.; Pearson, D.S.; Geeves, M.A.; Buck, J.; et al. Cryptococcus neoformans senses CO_2 through the carbonic anhydrase Can2 and the adenylyl cyclase Cac1. *Eukaryot. Cell* **2006**, *5*, 103–111. [CrossRef] [PubMed]

2. Jungbluth, M.; Mösch, H.U.; Taxis, C. Acetate regulation of spore formation is under the control of the Ras/cyclic AMP/protein kinase a pathway and carbon dioxide in Saccharomyces cerevisiae. *Eukaryot. Cell* **2012**, *11*, 1021–1032. [CrossRef] [PubMed]

3. Ohkuni, K.; Hayashi, M.; Yamashita, I. Bicarbonate-mediated social communication stimulates meiosis and sporulation of Saccharomyces cerevisiae. *Yeast* **1998**, *14*, 623–631. [CrossRef]

4. Coccetti, P.; Nicastro, R.; Tripodi, F. Conventional and emerging roles of the energy sensor snf1/AMPK in saccharomyces cerevisiae. *Microb. Cell* **2018**, *5*, 482–494. [CrossRef] [PubMed]

5. Herzig, S.; Shaw, R.J. AMPK: Guardian of metabolism and mitochondrial homeostasis. *Nat. Rev. Mol. Cell Biol.* **2018**, *19*, 121–135. [CrossRef]

6. Crepin, N.; Rolland, F. SnRK1 activation, signaling, and networking for energy homeostasis. *Curr. Opin. Plant Biol.* **2019**, *51*, 29–36. [CrossRef]

7. Carlson, M.; Osmond, B.C.; Botstein, D. Mutants of yeast defective in sucrose utilization. *Genetics* **1981**, *98*, 25–40.

8. Nicastro, R.; Tripodi, F.; Guzzi, C.; Reghellin, V.; Khoomrung, S.; Capusoni, C.; Compagno, C.; Airoldi, C.; Nielsen, J.; Alberghina, L.; et al. Enhanced amino acid utilization sustains growth of cells lacking Snf1/AMPK. *Biochim. Biophys. Acta* **2015**, *1853*, 1615–1625. [CrossRef]

9. Tripodi, F.; Castoldi, A.; Nicastro, R.; Reghellin, V.; Lombardi, L.; Airoldi, C.; Falletta, E.; Maffioli, E.; Scarcia, P.; Palmieri, L.; et al. Methionine supplementation stimulates mitochondrial respiration. *Biochim. Biophys. Acta* **2018**, *1865*, 1901–1913. [CrossRef]

10. Castermans, D.; Somers, I.; Kriel, J.; Louwet, W.; Wera, S.; Versele, M.; Janssens, V.; Thevelein, J.M. Glucose-induced posttranslational activation of protein phosphatases PP2A and PP1 in yeast. *Cell Res.* **2012**, *22*, 1058–1077. [CrossRef] [PubMed]

11. Ruiz, A.; Xu, X.; Carlson, M. Roles of two protein phosphatases, Reg1-Glc7 and Sit4, and glycogen synthesis in regulation of SNF1 protein kinase. *Proc. Natl. Acad. Sci. USA* **2011**, *108*, 6349–6354. [CrossRef] [PubMed]

12. Ruiz, A.; Xu, X.; Carlson, M. Ptc1 protein phosphatase 2C contributes to glucose regulation of SNF1/AMP-activated protein kinase (AMPK) in Saccharomyces cerevisiae. *J. Biol. Chem.* **2013**, *288*, 31052–31058. [CrossRef] [PubMed]

13. Mayer, F.V.; Heath, R.; Underwood, E.; Sanders, M.J.; Carmena, D.; McCartney, R.R.; Leiper, F.C.; Xiao, B.; Jing, C.; Walker, P.A.; et al. ADP Regulates SNF1, the Saccharomyces cerevisiae Homolog of AMP-Activated Protein Kinase. *Cell Metab.* **2011**, *14*, 707–714. [CrossRef] [PubMed]

14. Chandrashekarappa, D.G.; McCartney, R.R.; Schmidt, M.C. Ligand binding to the AMP-activated protein kinase active site mediates protection of the activation loop from dephosphorylation. *J. Biol. Chem.* **2013**, *288*, 89–98. [CrossRef] [PubMed]

15. Barrett, L.; Orlova, M.; Maziarz, M.; Kuchin, S. Protein Kinase A Contributes to the Negative Control of Snf1 Protein Kinase in Saccharomyces cerevisiae. *Eukaryot Cell* **2012**, *11*, 119–128. [CrossRef]

16. Nicastro, R.; Tripodi, F.; Gaggini, M.; Castoldi, A.; Reghellin, V.; Nonnis, S.; Tedeschi, G.; Coccetti, P. Snf1 Phosphorylates Adenylate Cyclase and Negatively Regulates Protein Kinase A-dependent Transcription in Saccharomyces cerevisiae. *J. Biol. Chem.* **2015**, *290*, 24715–24726. [CrossRef]

17. Rubenstein, E.M.; McCartney, R.R.; Zhang, C.; Shokat, K.M.; Shirra, M.K.; Arndt, K.M.; Schmidt, M.C. Access denied: Snf1 activation loop phosphorylation is controlled by availability of the phosphorylated threonine 210 to the PP1 phosphatase. *J. Biol. Chem.* **2008**, *283*, 222–230. [CrossRef]

18. Hawley, S.A.; Boudeau, J.; Reid, J.L.; Mustard, K.J.; Udd, L.; Mäkelä, T.P.; Alessi, D.R.; Hardie, D.G. Complexes between the LKB1 tumor suppressor, STRADα/β and MO25α/β are upstream kinases in the AMP-activated protein kinase cascade. *J. Biol.* **2003**, *2*, 1–16. [CrossRef]

19. Hawley, S.A.; Pan, D.A.; Mustard, K.J.; Ross, L.; Bain, J.; Edelman, A.M.; Frenguelli, B.G.; Hardie, D.G. Calmodulin-dependent protein kinase kinase-β is an alternative upstream kinase for AMP-activated protein kinase. *Cell Metab.* **2005**, *2*, 9–19. [CrossRef]

20. Carling, D.; Zammit, V.A.; Hardie, D.G. A common bicyclic protein kinase cascade inactivates the regulatory enzymes of fatty acid and cholesterol biosynthesis. *FEBS Lett.* **1987**, *223*, 217–222. [CrossRef]

1. Zong, H.; Ren, J.M.; Young, L.H.; Pypaert, M.; Mu, J.; Birnbaum, M.J.; Shulman, G.I. AMP kinase is required for mitochondrial biogenesis in skeletal muscle in response to chronic energy deprivation. *Proc. Natl. Acad. Sci. USA* **2002**, *99*, 15983–15987. [CrossRef] [PubMed]

2. Suter, M.; Riek, U.; Tuerk, R.; Schlattner, U.; Wallimann, T.; Neumann, D. Dissecting the role of 5^J-AMP for allosteric stimulation, activation, and deactivation of AMP-activated protein kinase. *J. Biol. Chem.* **2006**, *281*, 32207–32216. [CrossRef] [PubMed]

3. Xiao, B.; Sanders, M.J.; Underwood, E.; Heath, R.; Mayer, F.V.; Carmena, D.; Jing, C.; Walker, P.A.; Eccleston, J.F.; Haire, L.F.; et al. Structure of mammalian AMPK and its regulation by ADP. *Nature* **2011**, *472*, 230–233. [CrossRef] [PubMed]

4. Davies, S.P.; Helps, N.R.; Cohen, P.T.W.; Hardie, D.G. 5^J-AMP inhibits dephosphorylation, as well as promoting phosphorylation, of the AMP-activated protein kinase. Studies using bacterially expressed human protein phosphatase-2Cα and native bovine protein phosphatase-2Ac. *FEBS Lett.* **1995**, *377*, 421–425. [CrossRef]

5. Li, X.; Wang, L.; Zhou, X.E.; Ke, J.; De Waal, P.W.; Gu, X.; Tan, M.H.E.; Wang, D.; Wu, D.; Xu, H.E.; et al. Structural basis of AMPK regulation by adenine nucleotides and glycogen. *Cell Res.* **2015**, *25*, 50–66. [CrossRef]

6. Chen, L.; Xin, F.-J.; Wang, J.; Hu, J.; Zhang, Y.-Y.; Wan, S.; Cao, L.-S.; Lu, C.; Li, P.; Frank Yan, S.; et al. Conserved regulatory elements in AMPK. *Nature* **2013**, *498*, E8–E10. [CrossRef]

7. Zhang, Y.L.; Guo, H.; Zhang, C.S.; Lin, S.Y.; Yin, Z.; Peng, Y.; Luo, H.; Shi, Y.; Lian, G.; Zhang, C.; et al. AMP as a low-energy charge signal autonomously initiates assembly of axin-ampk-lkb1 complex for AMPK activation. *Cell Metab.* **2013**, *18*, 546–555. [CrossRef]

8. Zhang, C.S.; Jiang, B.; Li, M.; Zhu, M.; Peng, Y.; Zhang, Y.L.; Wu, Y.Q.; Li, T.Y.; Liang, Y.; Lu, Z.; et al. The lysosomal v-ATPase-ragulator complex is a common activator for AMPK and mTORC1, acting as a switch between catabolism and anabolism. *Cell Metab.* **2014**, *20*, 526–540. [CrossRef]

9. Rago, F.; Saltzberg, D.; Allen, K.N.; Tolan, D.R. Enzyme Substrate Specificity Conferred by Distinct Conformational Pathways. *J. Am. Chem. Soc.* **2015**, *137*, 13876–13886. [CrossRef]

10. McBride, A.; Ghilagaber, S.; Nikolaev, A.; Hardie, D.G. The Glycogen-Binding Domain on the AMPK β Subunit Allows the Kinase to Act as a Glycogen Sensor. *Cell Metab.* **2009**, *9*, 23–34. [CrossRef] [PubMed]

11. Wiatrowski, H.A.; van Denderen, B.J.W.; Berkey, C.D.; Kemp, B.E.; Stapleton, D.; Carlson, M. Mutations in the Gal83 Glycogen-Binding Domain Activate the Snf1/Gal83 Kinase Pathway by a Glycogen-Independent Mechanism. *Mol. Cell. Biol.* **2004**, *24*, 352–361. [CrossRef]

12. Emanuelle, S.; Hossain, M.I.; Moller, I.E.; Pedersen, H.L.; van de Meene, A.M.L.; Doblin, M.S.; Koay, A.; Oakhill, J.S.; Scott, J.W.; Willats, W.G.T.; et al. SnRK1 from Arabidopsis thaliana is an atypical AMPK. *Plant J.* **2015**, *82*, 183–192. [CrossRef] [PubMed]

13. Broeckx, T.; Hulsmans, S.; Rolland, F. The plant energy sensor: Evolutionary conservation and divergence of SnRK1 structure, regulation, and function. *J. Exp. Bot.* **2016**, *67*, 6215–6252. [CrossRef] [PubMed]

14. Baena-González, E.; Rolland, F.; Thevelein, J.M.; Sheen, J. A central integrator of transcription networks in plant stress and energy signalling. *Nature* **2007**, *448*, 938–942. [CrossRef] [PubMed]

15. Muraro, D.; Byrne, H.M.; King, J.R.; Bennett, M.J. Mathematical Modelling Plant Signalling Networks. *Math. Model. Nat. Phenom.* **2013**, *8*, 5–24. [CrossRef]

16. Emanuelle, S.; Doblin, M.S.; Stapleton, D.I.; Bacic, A.; Gooley, P.R. Molecular Insights into the Enigmatic Metabolic Regulator, SnRK1. *Trends Plant Sci.* **2016**, *21*, 341–353. [CrossRef]

17. Zhang, Y.; Primavesi, L.F.; Jhurreea, D.; Andralojc, P.J.; Mitchell, R.A.C.; Powers, S.J.; Schluepmann, H.; Delatte, T.; Wingler, A.; Paul, M.J. Inhibition of SNF1-related protein kinase1 activity and regulation of metabolic pathways by trehalose-6-phosphate1[w][OA]. *Plant Physiol.* **2009**, *149*, 1860–1871. [CrossRef]

18. Nunes, C.; Primavesi, L.F.; Patel, M.K.; Martinez-Barajas, E.; Powers, S.J.; Sagar, R.; Fevereiro, P.S.; Davis, B.G.; Paul, M.J. Inhibition of SnRK1 by metabolites: Tissue-dependent effects and cooperative inhibition by glucose 1-phosphate in combination with trehalose 6-phosphate. *Plant Physiol. Biochem.* **2013**, *63*, 89–98. [CrossRef]

19. Zhai, Z.; Keereetaweep, J.; Liu, H.; Feil, R.; Lunn, J.E.; Shanklin, J. Trehalose 6-phosphate positively regulates fatty acid synthesis by stabilizing wrinkled1[open]. *Plant Cell* **2018**, *30*, 2616–2627. [CrossRef]

20. Shimobayashi, M.; Hall, M.N. Making new contacts: The mTOR network in metabolism and signalling crosstalk. *Nat. Rev. Mol. Cell Biol.* **2014**, *15*, 155–162. [CrossRef] [PubMed]

1. Nicastro, R.; Sardu, A.; Panchaud, N.; de Virgilio, C. The Architecture of the Rag GTPase Signaling Network. *Biomolecules* **2017**, *7*, 48. [CrossRef] [PubMed]
2. Kim, E.; Goraksha-Hicks, P.; Li, L.; Neufeld, T.P.; Guan, K.L. Regulation of TORC1 by Rag GTPases in nutrient response. *Nat. Cell Biol.* **2008**, *10*, 935–945. [CrossRef] [PubMed]
3. Binda, M.; Péli-Gulli, M.P.; Bonfils, G.; Panchaud, N.; Urban, J.; Sturgill, T.W.; Loewith, R.; de Virgilio, C. The Vam6 GEF controls TORC1 by activating the EGO complex. *Mol. Cell* **2009**, *35*, 563–573. [CrossRef] [PubMed]
4. Ukai, H.; Araki, Y.; Kira, S.; Oikawa, Y.; May, A.I.; Noda, T. Gtr/Ego-independent TORC1 activation is achieved through a glutamine-sensitive interaction with Pib2 on the vacuolar membrane. *PLoS Genet.* **2018**, *14*, e1007334. [CrossRef]
5. Kim, A.; Cunningham, K.W. A LAPF/phafin1-like protein regulates TORC1 and lysosomal membrane permeabilization in response to endoplasmic reticulum membrane stress. *Mol. Biol. Cell* **2015**, *26*, 4631–4645. [CrossRef]
6. Zhang, T.; Péli-Gulli, M.P.; Yang, H.; de Virgilio, C.; Ding, J. Ego3 functions as a homodimer to mediate the interaction between Gtr1-Gtr2 and Ego1 in the EGO complex to activate TORC1. *Structure* **2012**, *20*, 2151–2160. [CrossRef]
7. Kira, S.; Tabata, K.; Shirahama-Noda, K.; Nozoe, A.; Yoshimori, T.; Noda, T. Reciprocal conversion of Gtr1 and Gtr2 nucleotidebinding states by Npr2-Npr3 inactivates TORC1 and induces autophagy. *Autophagy* **2014**, *10*, 1565–1578. [CrossRef]
8. Bonfils, G.; Jaquenoud, M.; Bontron, S.; Ostrowicz, C.; Ungermann, C.; de Virgilio, C. Leucyl-tRNA Synthetase Controls TORC1 via the EGO Complex. *Mol. Cell* **2012**, *46*, 105–110. [CrossRef]
9. Hohmann, S.; Thevelein, J.M. The cell division cycle gene CDC60 encodes cytosolic leucyl-tRNA synthetase in Saccharomyces cerevisiae. *Gene* **1992**, *120*, 43–49. [CrossRef]
10. Echols, N.; Harrison, P.; Balasubramanian, S.; Luscombe, N.M.; Bertone, P.; Zhang, Z.; Gerstein, M. Comprehensive analysis of amino acid and nucleotide composition in eukaryotic genomes, comparing genes and pseudogenes. *Nucleic Acids Res.* **2002**, *30*, 2515–2523. [CrossRef] [PubMed]
11. Ghaemmaghami, S.; Huh, W.K.; Bower, K.; Howson, R.W.; Belle, A.; Dephoure, N.; O'Shea, E.K.; Weissman, J.S. Global analysis of protein expression in yeast. *Nature* **2003**, *425*, 737–741. [CrossRef] [PubMed]
12. Rock, F.L.; Mao, W.; Yaremchuk, A.; Tukalo, M.; Crépin, T.; Zhou, H.; Zhang, Y.K.; Hernandez, V.; Akama, T.; Baker, S.J.; et al. An antifungal agent inhibits an aminoacyl-tRNA synthetase by trapping tRNA in the editing site. *Science* **2007**, *316*, 1759–1761. [CrossRef] [PubMed]
13. Powis, K.; de Virgilio, C. Conserved regulators of Rag GTPases orchestrate amino acid-dependent TORC1 signaling. *Cell Discov.* **2016**, *2*, 1–16. [CrossRef] [PubMed]
14. Hara, K.; Yonezawa, K.; Weng, Q.P.; Kozlowski, M.T.; Belham, C.; Avruch, J. Amino acid sufficiency and mTOR regulate p70 S6 kinase and eIF-4E BP1 through a common effector mechanism. *J. Biol. Chem.* **1998**, *273*, 14484–14494. [CrossRef]
15. Menon, S.; Dibble, C.C.; Talbott, G.; Hoxhaj, G.; Valvezan, A.J.; Takahashi, H.; Cantley, L.C.; Manning, B.D. Spatial control of the TSC complex integrates insulin and nutrient regulation of mTORC1 at the lysosome. *Cell* **2014**, *156*, 771–785. [CrossRef]
16. Sancak, Y.; Peterson, T.R.; Shaul, Y.D.; Lindquist, R.A.; Thoreen, C.C.; Bar-Peled, L.; Sabatini, D.M. The rag GTPases bind raptor and mediate amino acid signaling to mTORC1. *Science* **2008**, *320*, 1496–1501. [CrossRef]
17. Sancak, Y.; Bar-Peled, L.; Zoncu, R.; Markhard, A.L.; Nada, S.; Sabatini, D.M. Ragulator-rag complex targets mTORC1 to the lysosomal surface and is necessary for its activation by amino acids. *Cell* **2010**, *141*, 290–303. [CrossRef]
18. Long, X.; Lin, Y.; Ortiz-Vega, S.; Yonezawa, K.; Avruch, J. Rheb binds and regulates the mTOR kinase. *Curr. Biol.* **2005**, *15*, 702–713. [CrossRef]
19. Han, J.M.; Jeong, S.J.; Park, M.C.; Kim, G.; Kwon, N.H.; Kim, H.K.; Ha, S.H.; Ryu, S.H.; Kim, S. Leucyl-tRNA synthetase is an intracellular leucine sensor for the mTORC1-signaling pathway. *Cell* **2012**, *149*, 410–424. [CrossRef]
20. Saxton, R.A.; Knockenhauer, K.E.; Wolfson, R.L.; Chantranupong, L.; Pacold, M.E.; Wang, T.; Schwartz, T.U.; Sabatini, D.M. Structural basis for leucine sensing by the Sestrin2-mTORC1 pathway. *Science* **2016**, *351*, 53–58. [CrossRef] [PubMed]

1. Bar-Peled, L.; Chantranupong, L.; Cherniack, A.D.; Chen, W.W.; Ottina, K.A.; Grabiner, B.C.; Spear, E.D.; Carter, S.L.; Meyerson, M.; Sabatini, D.M. A tumor suppressor complex with GAP activity for the Rag GTPases that signal amino acid sufficiency to mTORC1. *Science* **2013**, *340*, 1100–1106. [CrossRef] [PubMed]
2. Wolfson, R.L.; Chantranupong, L.; Saxton, R.A.; Shen, K.; Scaria, S.M.; Cantor, J.R.; Sabatini, D.M. Sestrin2 is a leucine sensor for the mTORC1 pathway. *Science* **2016**, *351*, 43–48. [CrossRef] [PubMed]
3. Chantranupong, L.; Scaria, S.M.; Saxton, R.A.; Gygi, M.P.; Shen, K.; Wyant, G.A.; Wang, T.; Harper, J.W.; Gygi, S.P.; Sabatini, D.M. The CASTOR Proteins Are Arginine Sensors for the mTORC1 Pathway. *Cell* **2016**, *165*, 153–164. [CrossRef] [PubMed]
4. Saxton, R.A.; Chantranupong, L.; Knockenhauer, K.E.; Schwartz, T.U.; Sabatini, D.M. Mechanism of arginine sensing by CASTOR1 upstream of mTORC1. *Nature* **2016**, *536*, 229–233. [CrossRef]
5. Parsons, A.B.; Brost, R.L.; Ding, H.; Li, Z.; Zhang, C.; Sheikh, B.; Brown, G.W.; Kane, P.M.; Hughes, T.R.; Boone, C. Integration of chemical-genetic and genetic interaction data links bioactive compounds to cellular target pathways. *Nat. Biotechnol.* **2004**, *22*, 62–69. [CrossRef]
6. Costanzo, M.; Baryshnikova, A.; Bellay, J.; Kim, Y.; Spear, E.D.; Sevier, C.S.; Ding, H.; Koh, J.L.Y.; Toufighi, K.; Mostafavi, S.; et al. The genetic landscape of a cell. *Science* **2010**, *327*, 425–431. [CrossRef]
7. Wang, S.; Tsun, Z.Y.; Wolfson, R.L.; Shen, K.; Wyant, G.A.; Plovanich, M.E.; Yuan, E.D.; Jones, T.D.; Chantranupong, L.; Comb, W.; et al. Lysosomal amino acid transporter SLC38A9 signals arginine sufficiency to mTORC1. *Science* **2015**, *347*, 188–194. [CrossRef]
8. Gu, X.; Orozco, J.M.; Saxton, R.A.; Condon, K.J.; Liu, G.Y.; Krawczyk, P.A.; Scaria, S.M.; Wade Harper, J.; Gygi, S.P.; Sabatini, D.M. SAMTOR is an S-adenosylmethionine sensor for the mTORC1 pathway. *Science* **2017**, *358*, 813–818. [CrossRef]
9. Sutter, B.M.; Wu, X.; Laxman, S.; Tu, B.P.X. Methionine inhibits autophagy and promotes growth by inducing the SAM-responsive methylation of PP2A. *Cell* **2013**, *154*, 403. [CrossRef]
10. Shi, L.; Wu, Y.; Sheen, J. TOR signaling in plants: Conservation and innovation. *Development* **2018**, *145*, dev160887. [CrossRef] [PubMed]
11. Xiong, Y.; McCormack, M.; Li, L.; Hall, Q.; Xiang, C.; Sheen, J. Glucose-TOR signalling reprograms the transcriptome and activates meristems. *Nature* **2013**, *496*, 181–186. [CrossRef] [PubMed]
12. Zhang, N.; Meng, Y.; Li, X.; Zhou, Y.; Ma, L.; Fu, L.; Schwarzländer, M.; Liu, H.; Xiong, Y. Metabolite-mediated TOR signaling regulates the circadian clock in Arabidopsis. *Proc. Natl. Acad. Sci. USA* **2019**, *116*, 25395–25397. [CrossRef] [PubMed]
13. Nukarinen, E.; Ngele, T.; Pedrotti, L.; Wurzinger, B.; Mair, A.; Landgraf, R.; Börnke, F.; Hanson, J.; Teige, M.; Baena-Gonzalez, E.; et al. Quantitative phosphoproteomics reveals the role of the AMPK plant ortholog SnRK1 as a metabolic master regulator under energy deprivation. *Sci. Rep.* **2016**, *6*, 1–19. [CrossRef] [PubMed]
14. Gwinn, D.M.; Shackelford, D.B.; Egan, D.F.; Mihaylova, M.M.; Mery, A.; Vasquez, D.S.; Turk, B.E.; Shaw, R.J. AMPK phosphorylation of raptor mediates a metabolic checkpoint. *Mol. Cell* **2008**, *30*, 214–226. [CrossRef]
15. Kim, S.G.; Hoffman, G.R.; Poulogiannis, G.; Buel, G.R.; Jang, Y.J.; Lee, K.W.; Kim, B.Y.; Erikson, R.L.; Cantley, L.C.; Choo, A.Y.; et al. Metabolic stress controls mTORC1 lysosomal localization and dimerization by regulating the TTT-RUVBL1/2 complex. *Mol. Cell* **2013**, *49*, 172–185. [CrossRef]
16. Dong, Y.; Silbermann, M.; Speiser, A.; Forieri, I.; Linster, E.; Poschet, G.; Allboje Samami, A.; Wanatabe, M.; Sticht, C.; Teleman, A.A.; et al. Sulfur availability regulates plant growth via glucose-TOR signaling. *Nat. Commun.* **2017**, *8*, e1174. [CrossRef]
17. Cao, P.; Kim, S.J.; Xing, A.; Schenck, C.A.; Liu, L.; Jiang, N.; Wang, J.; Last, R.L.; Brandizzi, F. Homeostasis of branched-chain amino acids is critical for the activity of TOR signaling in Arabidopsis. *Elife* **2019**, *8*, e50747. [CrossRef]
18. Pronk, J.T.; Steensma, H.Y.; van Dijken, J.P. Pyruvate metabolism in saccharomyces cerevisiae. *Yeast* **1996**, *12*, 1607–1633. [CrossRef]
19. Jeong, S.Y.; Seol, D.W. The role of mitochondria in apoptosis. *J. Biochem. Mol. Biol.* **2008**, *41*, 11–22. [CrossRef]
20. Shadel, G.S.; Horvath, T.L. Mitochondrial ROS signaling in organismal homeostasis. *Cell* **2015**, *163*, 560–569. [CrossRef] [PubMed]
21. Liao, X.S.; Small, W.C.; Srere, P.A.; Butow, R.A. Intramitochondrial functions regulate nonmitochondrial citrate synthase (CIT2) expression in Saccharomyces cerevisiae. *Mol. Cell. Biol.* **1991**, *11*, 38–46. [CrossRef] [PubMed]

1. Liu, Z.; Butow, R.A. A Transcriptional switch in the expression of yeast tricarboxylic acid cycle genes in response to a reduction or loss of respiratory function. *Mol. Cell. Biol.* **1999**, *19*, 6720–6728. [CrossRef] [PubMed]

2. Hallstrom, T.C.; Moye-Rowley, W.S. Multiple signals from dysfunctional mitochondria activate the pleiotropic drug resistance pathway in Saccharomyces cerevisiae. *J. Biol. Chem.* **2000**, *275*, 37347–37356. [CrossRef]

3. Butow, R.A.; Avadhani, N.G. Mitochondrial signaling: The retrograde response. *Mol. Cell* **2004**, *14*, 1–15. [CrossRef]

4. Upadhyay, S.; Srivastava, Y. Retrograde response by reactive oxygen/nitrogen species in plants involving different cellular organelles. *Biol. Chem.* **2019**, *400*, 979–989. [CrossRef]

5. Sekito, T.; Thornton, J.; Butow, R.A. Mitochondria-to-nuclear signaling is regulated by the subcellular localization of the transcription factors Rtg1p and Rtg3p. *Mol. Biol. Cell* **2000**, *11*, 2103–2115. [CrossRef]

6. Liu, Z.; Sekito, T.; SŠpiírek, M.; Thornton, J.; Butow, R.A. Retrograde signaling is regulated by the dynamic interaction between Rtg2p and Mks1p. *Mol. Cell* **2003**, *12*, 401–411. [CrossRef]

7. Zhang, F.; Pracheil, T.; Thornton, J.; Liu, Z. Adenosine Triphosphate (ATP) is a candidate signaling molecule in the mitochondria-to-nucleus retrograde response pathway. *Genes (Basel)* **2013**, *4*, 86–100. [CrossRef]

8. Santulli, G.; Nakashima, R.; Yuan, Q.; Marks, A.R. Intracellular calcium release channels: An update. *J. Physiol.* **2017**, *595*, 3041–3051. [CrossRef]

9. Berridge, M.J. The inositol trisphosphate/calcium signaling pathway in health and disease. *Physiol. Rev.* **2016**, *96*, 1261–1296. [CrossRef] [PubMed]

10. Clapper, D.L.; Walseth, T.F.; Dargie, P.J.; Lee, H.C. Pyridine nucleotide metabolites stimulate calcium release from sea urchin egg microsomes desensitized to inositol trisphosphate. *J. Biol. Chem.* **1987**, *262*, 9561–9568. [PubMed]

11. Galione, A.; Lee, H.C.; Busa, W.B. Ca^{2+}-induced Ca^{2+} release in sea urchin egg homogenates: Modulation by cyclic ADP-Ribose. *Science* **1991**, *253*, 1143–1146. [CrossRef] [PubMed]

12. Lee, H.C. Potentiation of calcium- and caffeine-induced calcium release by cyclic ADP-ribose. *J. Biol. Chem.* **1993**, *268*, 293–299. [PubMed]

13. Zheng, J.; Wenzhi, B.; Miao, L.; Hao, Y.; Zhang, X.; Yin, W.; Pan, J.; Yuan, Z.; Song, B.; Ji, G. Ca^{2+} release induced by cADP-ribose is mediated by FKBP12.6 proteins in mouse bladder smooth muscle. *Cell Calcium* **2010**, *47*, 449–457. [CrossRef] [PubMed]

14. Yamasaki-Mann, M.; Demuro, A.; Parker, I. cADPR stimulates SERCA activity in Xenopus oocytes. *Cell Calcium* **2009**, *45*, 293–299. [CrossRef] [PubMed]

15. Yamasaki-Mann, M.; Demuro, A.; Parker, I. Modulation of endoplasmic reticulum Ca^{2+} store filling by cyclic ADP-ribose promotes inositol trisphosphate (IP3)-evoked Ca^{2+} signals. *J. Biol. Chem.* **2010**, *285*, 25053–25061. [CrossRef]

16. Park, D.R.; Nam, T.S.; Kim, Y.W.; Lee, S.H.; Kim, U.H. CD38-cADPR-SERCA signaling axis determines skeletal muscle contractile force in response to β-adrenergic stimulation. *Cell. Physiol. Biochem.* **2018**, *46*, 2017–2030. [CrossRef]

17. Lange, I.; Penner, R.; Fleig, A.; Beck, A. Synergistic regulation of endogenous TRPM2 channels by adenine dinucleotides in primary human neutrophils. *Cell Calcium* **2008**, *44*, 604–615. [CrossRef]

18. Wolf, B.A.; Colcaq, J.R.; Cornens, P.G.; Turk, J.; Mcdaniels, M.L. Glucose 6-Phosphate Regulates Ca^{2+} steady state in endoplasmic reticulum of islets a possible link in glucose-induced insulin secretion. *J. Biol. Chem.* **1986**, *261*, 16284–16287.

19. Chen, P.Y.; Csutora, P.; Veyna-Burke, N.A.; Marchase, R.B. Glucose-6-phosphate and Ca^{2+} sequestration are mutually enhanced in microsomes from liver, brain, and heart. *Diabetes* **1998**, *47*, 874–881. [CrossRef] [PubMed]

20. Cole, J.T.; Kean, W.S.; Pollard, H.B.; Verma, A.; Watson, W.D. Glucose-6-phosphate reduces calcium accumulation in rat brain endoplasmic reticulum. *Front. Mol. Neurosci.* **2012**, *5*, 51. [CrossRef] [PubMed]

21. Kockskämper, J.; Zima, A.V.; Blatter, L.A. Modulation of sarcoplasmic reticulum Ca 2+ release by glycolysis in cat atrial myocytes. *J. Physiol.* **2005**, *564*, 697–714. [CrossRef] [PubMed]

22. Fukumoto, G.H.; Lamp, S.T.; Motter, C.; Bridge, J.H.B.; Garfinkel, A.; Goldhaber, J.I. Metabolic inhibition alters subcellular calcium release patterns in rat ventricular myocytes: Implications for defective excitation-contraction coupling during cardiac ischemia and failure. *Circ. Res.* **2005**, *96*, 551–557. [CrossRef]

1. Cyert, M.S.; Philpott, C.C. Regulation of cation balance in Saccharomyces cerevisiae. *Genetics* **2013**, *193*, 677–713. [CrossRef] [PubMed]
2. Pittman, J.K. Vacuolar Ca^{2+} uptake. *Cell Calcium* **2011**, *50*, 139–146. [CrossRef]
3. Bonilla, M.; Cunningham, K.W. Calcium release and influx in yeast: TRPC and VGCC rule another kingdom. *Sci. STKE* **2002**, *2002*, PE17. [CrossRef]
4. Palmer, C.P.; Zhou, X.L.; Lin, J.; Loukin, S.H.; Kung, C.; Saimi, Y. A TRP homolog in Saccharomyces cerevisiae forms an intracellular Ca^{2+}-permeable channel in the yeast vacuolar membrane. *Proc. Natl. Acad. Sci. USA* **2001**, *98*, 7801–7805. [CrossRef]
5. Dürr, G.; Strayle, J.; Plemper, R.; Elbs, S.; Klee, S.K.; Catty, P.; Wolf, D.H.; Rudolph, H.K. The medial-Golgi ion pump Pmr1 supplies the yeast secretory pathway with Ca^{2+} and Mn^{2+} required for glycosylation, sorting, and endoplasmic reticulum-Associated protein degradation. *Mol. Biol. Cell* **1998**, *9*, 1149–1162. [CrossRef]
6. Tisi, R.; Belotti, F.; Wera, S.; Winderickx, J.; Thevelein, J.M.; Martegani, E. Evidence for inositol triphosphate as a second messenger for glucose-induced calcium signalling in budding yeast. *Curr. Genet.* **2004**, *45*, 83–89. [CrossRef]
7. Iida, H.; Sakaguchi, S.; Yagawa, Y.; Anraku, Y.J. Cell Cycle Control by Ca^{2+} in Saccharomyces Cerevisiae. *J. Biol. Chem.* **1990**, *265*, 16–22.
8. Busti, S.; Mapelli, V.; Tripodi, F.; Sanvito, R.; Magni, F.; Coccetti, P.; Rocchetti, M.; Nielsen, J.; Alberghina, L.; Vanoni, M. Respiratory metabolism and calorie restriction relieve persistent endoplasmic reticulum stress induced by calcium shortage in yeast. *Sci. Rep.* **2016**, *6*, 27942. [CrossRef]
9. Tökés-Füzesi, M.; Bedwell, D.M.; Repa, I.; Sipos, K.; Sümegi, B.; Rab, A.; Miseta, A. Hexose phosphorylation and the putative calcium channel component Mid1p are required for the hexose-induced transient elevation of cytosolic calcium response in Saccharomyces cerevisiae. *Mol. Microbiol.* **2002**, *44*, 1299–1308. [CrossRef]
10. Tisi, R.; Baldassa, S.; Belotti, F.; Martegani, E. Phospholipase C is required for glucose-induced calcium influx in budding yeast. *FEBS Lett.* **2002**, *520*, 133–138. [CrossRef]
11. Fu, L.; Miseta, A.; Hunton, D.; Marchase, R.B.; Bedwell, D.M. Loss of the major isoform of phosphoglucomutase results in altered calcium homeostasis in Saccharomyces cerevisiae. *J. Biol. Chem.* **2000**, *275*, 5431–5440. [CrossRef]
12. Aiello, D.P.; Fu, L.; Miseta, A.; Sipos, K.; Bedwell, D.M. The Ca^{2+} homeostasis defects in a pgm2Δ strain of Saccharomyces cerevisiae are caused by excessive vacuolar Ca^{2+} uptake mediated by the Ca^{2+}-ATPase Pmc1p. *J. Biol. Chem.* **2004**, *279*, 38495–38502. [CrossRef] [PubMed]
13. Aiello, D.P.; Fu, L.; Miseta, A.; Bedwell, D.M. Intracellular glucose 1-phosphate and glucose 6-phosphate levels modulate Ca^{2+} homeostasis in Saccharomyces cerevisiae. *J. Biol. Chem.* **2002**, *277*, 45751–45758. [CrossRef] [PubMed]
14. Dlugai, S.; Hippler, S.; Wieczorke, R.; Boles, E. Glucose-dependent and -independent signalling functions of the yeast glucose sensor Snf3. *FEBS Lett.* **2001**, *505*, 389–392. [CrossRef]
15. Feng, Y.; de Franceschi, G.; Kahraman, A.; Soste, M.; Melnik, A.; Boersema, P.J.; de Laureto, P.P.; Nikolaev, Y.; Oliveira, A.P.; Picotti, P. Global analysis of protein structural changes in complex proteomes. *Nat. Biotechnol.* **2014**, *32*, 1036–1044. [CrossRef]
16. Li, X.; Gianoulis, T.A.; Yip, K.Y.; Gerstein, M.; Snyder, M. Extensive in vivo metabolite-protein interactions revealed by large-scale systematic analyses. *Cell* **2010**, *143*, 639–650. [CrossRef]

Article

AMPK Phosphorylation Is Controlled by Glucose Transport Rate in a PKA-Independent Manner

Riccardo Milanesi, Farida Tripodi *⬤**, Jacopo Vertemara, Renata Tisi** ⬤ **and Paola Coccetti ***

Department of Biotechnology and Biosciences, University of Milano-Bicocca, 20126 Milano, Italy;
r.milanesi2@campus.unimib.it (R.M.); jacopo.vertemara@unimib.it (J.V.); renata.tisi@unimib.it (R.T.)
* Correspondence: farida.tripodi1@unimib.it (F.T.); paola.coccetti@unimib.it (P.C.);
  Tel.: +39-026-448-3521 (F.T. & P.C.)

Abstract: To achieve growth, microbial organisms must cope with stresses and adapt to the environment, exploiting the available nutrients with the highest efficiency. In *Saccharomyces cerevisiae*, Ras/PKA and Snf1/AMPK pathways regulate cellular metabolism according to the supply of glucose, alternatively supporting fermentation or mitochondrial respiration. Many reports have highlighted crosstalk between these two pathways, even without providing a comprehensive mechanism of regulation. Here, we show that glucose-dependent inactivation of Snf1/AMPK is independent from the Ras/PKA pathway. Decoupling glucose uptake rate from glucose concentration, we highlight a strong coordination between glycolytic metabolism and Snf1/AMPK, with an inverse correlation between Snf1/AMPK phosphorylation state and glucose uptake rate, regardless of glucose concentration in the medium. Despite fructose-1,6-bisphosphate (F1,6BP) being proposed as a glycolytic flux sensor, we demonstrate that glucose-6-phosphate (G6P), and not F1,6BP, is involved in the control of Snf1/AMPK phosphorylation state. Altogether, this study supports a model by which Snf1/AMPK senses glucose flux independently from PKA activity, and thanks to conversion of glucose into G6P.

Keywords: Snf1/AMPK; *Saccharomyces cerevisiae*; glucose-6-phosphate; hexose transport; protein–metabolite interaction

1. Introduction

Every living organism must adapt to challenging environments, coping with stresses and monitoring the availability of nutrients. For microbial cells, the success of this adaptation is represented by the ability to grow, such that the maximization of the growth rate is usually taken as the objective function of a cell [1]. To this aim, the fine-tuning of several cellular processes is pivotal for the coordination of metabolism, cell cycle, and growth. In this process, the crosstalk between different signaling pathways is necessary to successfully coordinate cell functions, as highlighted by the widespread bow-tie architecture of signal transduction pathways [2].

The budding yeast *Saccharomyces cerevisiae* is a powerful model for studying fundamental aspects of eukaryotic cell biology, especially connected to signal transduction and metabolism, thanks to the high degree of conservation of several key cellular processes between yeast and mammalian cells [3]. Its metabolism is characterized by the preferential aerobic fermentation of glucose, similarly to Warburg-positive transformed cells. In yeast cells, glucose availability is perceived by Snf3/Rgt2 and Gpr1/Gpa2 systems, activates the Ras/PKA pathway, and suppresses the Snf1/AMPK pathway [4]. This results in the promotion of glucose fermentation and cell growth, while stress tolerance, mitochondrial respiration, and the consumption of alternative carbon sources to glucose are repressed [5]. On the other hand, low glucose concentration is associated with the repression of the Ras/PKA pathway and the activation of Snf1/AMPK, leading to the induction of genes associated with respiration, β-oxidation, and the upregulation of stress tolerance [6].

Among the genes controlled by glucose availability, there are those required for glu- cose transport. *S. cerevisiae* possesses at least 20 different glucose transporters, all presenting a common structure with 12 transmembrane regions, and characterized by different affinity and capacity parameters [4]. Yeast specialization for glucose consumption is highlighted by its ability to dynamically adapt the expression pattern of glucose transporters according to the extracellular glucose concentration. High titration leads to the expression of low-affinity and high-capacity transporters (such as Hxt1 and Hxt3), allowing for a massive intake flux. Instead, a decrease in glucose concentration leads to the expression of high-affinity and low-capacity transporters (such as Hxt7, Htx6 and Gal2), succeeding in the passive import of glucose even at low millimolar concentrations [4].

The PKA and Snf1/AMPK pathways' opposite activations suggest the existence of a thick crosstalk between these two pathways. Indeed, Snf1/AMPK phosphorylates and inhibits Cyr1—the adenylate cyclase upstream of the PKA pathway [7]. On the other hand, PKA is known to phosphorylate and inactivate Sak1—the major activator kinase of Snf1/AMPK [8]. This feedback mechanism—by which PKA inactivates Snf1/AMPK, and vice versa, according to nutritional conditions—allows yeast cells to avoid transcriptional inconsistencies undermining cellular homeostasis. In any case, the molecular mechanism underlying this crosstalk is still missing [9].

Yeast cells selectively consume different carbon sources through respiration or fermentation. It has been shown that sugar uptake rate defines the manner of their consumption, going beyond the classical model by which yeast's metabolic fate is controlled by glucose concentration in the growth medium [10]. Moreover, fructose-1,6-bisphosphate (F1,6BP) concentration has been reported to be correlated with sugar transport rate, mirroring the glycolytic flux and potentially acting as a flux sensor [10,11]. Following this line of evidence, F1,6BP could couple the glycolytic rate with the switch between respiration and fermentation, giving rise to a flux-sensing mechanism. Several reports also suggest that the coordination of cell metabolism and signaling takes place through protein–metabolite interactions (PMIs) between key molecules of the central metabolism and proteins belonging to different signaling pathways [12]. Interestingly, F1,6BP has been reported to interact with Cdc25—the guanine nucleotide exchange factor upstream of Ras—inducing the activation of the Ras/PKA pathway [13]. This interaction connects PKA with the function of F1,6BP as a reporter of the glycolytic flux, suggesting a molecular regulatory role of the flux-sensing mechanism. Strikingly, the Ras/PKA pathway is also responsible for the activation of Reg1/Glc7—the phosphatase complex upstream of Snf1/AMPK—thus leaving open the hypothesis that Snf1/AMPK activation state may be indirectly linked to glucose metabolism through F1,6BP synthesis and PKA activation.

In keeping with this hypothesis, mammalian AMPK has recently been proven to be controlled by F1,6BP, which induces the release of AMPK from the AXIN/LKB1/AMPK complex [14]. In this process, signal transduction from glycolysis to AMPK is mediated by F1,6BP's interaction with aldolase, whose activity is essential for F1,6BP-dependent control of the AMPK activation state [14]. However, the *S. cerevisiae* ortholog of the AXIN/LKB1/AMPK complex has not been identified, suggesting a different coordination between glycolysis and Snf1/AMPK activity.

In the present paper, we investigate whether the connection between Snf1/AMPK and glycolytic metabolism is indirectly mediated by the Ras/PKA pathway. Interestingly, we demonstrate that glucose-6-phosphate (G6P), and not F1,6BP, is involved in the control of the Snf1/AMPK phosphorylation state. We also report that the Ras/PKA pathway is dispensable for the inhibition of Snf1/AMPK upon glucose replenishment. Therefore, we propose that the glycolytic flux is sensed by different signaling pathways (i.e., Snf1/AMPK and Ras/PKA) independently, and through interactions with different glycolytic metabo- lites (i.e., G6P and F1,6BP), to achieve the proper cellular response to the specific nutrient condition.

1. Results

1.1. Glucose Inhibition of Snf1/AMPK Is Independent from the Ras/PKA Pathway

The Snf1/AMPK activation state is controlled by phosphorylation of the regulatory residue Thr210—a substrate of both the upstream kinases (Sak1, Tos3, and Elm1) and the Reg1/Glc7 phosphatase [15,16]. Glucose availability promotes Snf1-T210 dephosphorylation, while growth on non-fermentable carbon sources is associated with a high level of Snf1/AMPK phosphorylation. As already reported, PKA phosphorylates Sak1, inducing a mild reduction in Snf1/AMPK phosphorylation [8]. According to another report, the activity of Snf1/AMPK upstream kinases is not influenced by glucose availability [17]. In addition, Reg1/Glc7 phosphatase is activated by glucose in a Ras/PKA-dependent manner [16]. Taken together, all of these observations prompted us to better investigate the involvement of the Ras/PKA pathway in the control of the phosphorylation state of Snf1/AMPK.

Since the Ras/PKA pathway is linked to glycolysis by F1,6BP physical interaction with Cdc25 [13], we first asked whether Snf1/AMPK phosphorylation may be indirectly influenced by this interaction. To address this issue, we carried out shift-up experiments, growing yeast cells in ethanol (a condition in which Snf1/AMPK phosphorylation is high) and then adding glucose at the final concentration of 2% (which induces a rapid Snf1/AMPK dephosphorylation). Snf1/AMPK phosphorylation rapidly decreased in the wild-type strain, becoming barely detectable 5 min after the addition of glucose (Figure 1a). The same behavior was observed in the $CDC25^{T1490P}$ mutant, known to prevent F1,6BP-dependent activation of Ras [13] (Figure 1a). To further dissect the involvement of the Ras/PKA pathway, we decided to test the effect of the lack of the Ras2 protein on Snf1/AMPK dephosphorylation, carrying out a shift-up experiment in a *ras2*Δ strain. As in the $CDC25^{T1490P}$ strain (Figure 1a), we also observed complete dephosphorylation of Snf1/AMPK after 5 min in the *ras2*Δ strain (Figure 1b), thus excluding the possibility that Snf1/AMPK could indirectly perceive the availability of glucose through F1,6BP stimulation of the Ras/PKA pathway.
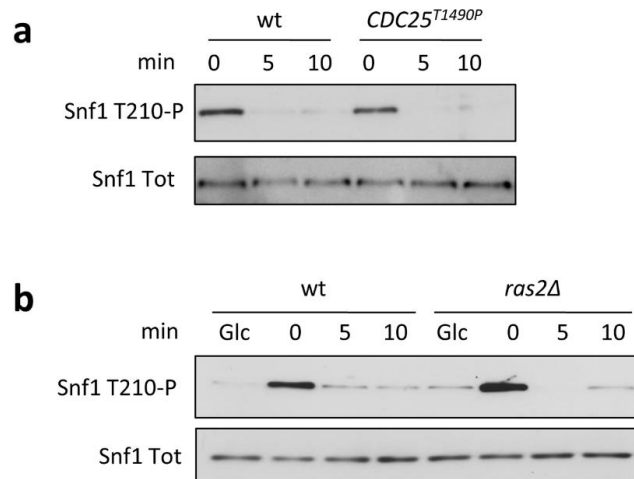
Figure 1. *Cont.*
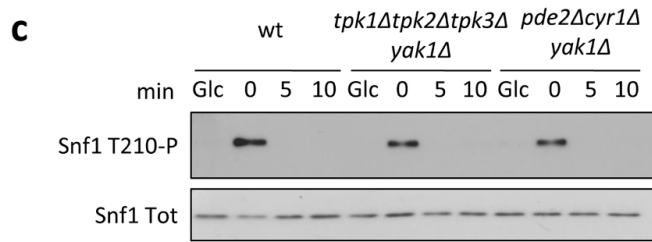
Figure 1. Snf1-T210 phosphorylation is independent from the Ras/PKA pathway. (**a**–**c**) Shift-up experiments in (**a**) wild-type and $CDC25^{T1490P}$ strains, (**b**) $ras2\Delta$ strain, and (**c**) strains lacking PKA activity ($tpk1\Delta tpk2\Delta tpk3\Delta yak1\Delta$ and $pde1\Delta cyr1\Delta yak1\Delta$). One representative Western blot analysis using anti-pAMPK antibody (to detect Snf1-T210 phosphorylation) and anti-His antibody (to detect total Snf1) is shown.

As reported previously, Ras/PKA activity is pivotal for glucose induction of PP1 and PP2A phosphatases [16]. The glucose-dependent Snf1/AMPK dephosphorylation in the $ras2\Delta$ strain shown in Figure 1b can either depend on residual Ras activity due to the presence of Ras1, still able to activate the PKA pathway [18], or be completely independent from the PKA-dependent phosphatase activation. To discern between these two possibilities, we carried out shift-up experiments in the $tpk1\Delta tpk2\Delta tpk3\Delta yak1\Delta$ strain, which completely lacks PKA activity. We also confirmed that no defect in Snf1/AMPK dephosphorylation was observed in this background (Figure 1c), thus excluding any involvement of PKA activity in Snf1/AMPK inactivation upon glucose replenishment.

Along with the glycolytic flux, the Ras/PKA pathway perceives extracellular glucose availability through the Gpr1/Gpa2 system, which integrates nutritional signals with the modulation of cell fate via cAMP synthesis and PKA activation [4]. Therefore, we cannot exclude the possibility that PKA activation triggered by extracellular glucose could influence the Snf1/AMPK phosphorylation state. To rule this out, we performed a shift-up experiment in a $pde1\Delta cyr1\Delta yak1\Delta$ strain, in which $CYR1$ deletion prevents both intracel- lular and extracellular stimulation of PKA activity. Remarkably, as in the control strain, Snf1/AMPK was completely dephosphorylated after the shift-up (Figure 1c), supporting a model by which its phosphorylation state is controlled by glucose independently from the Ras/PKA pathway, in terms of both intracellular and extracellular perception of glucose.

1.1. Snf1/AMPK Phosphorylation Is Correlated with Glucose Transport Rate

Snf1/AMPK phosphorylation has always been correlated with glucose availability. A high glucose concentration is associated with low phosphorylation of Snf1/AMPK, while high phosphorylation of Snf1/AMPK is a feature of cells grown in low glucose concentrations (lower than 0.05%) [19]. Moreover, different glucose concentrations are associated with alternative metabolic states of yeast cells. Indeed, a high glucose concentration supports fermentation, while a low one induces a respiratory metabolism.

Recently, yeast metabolism has been correlated with sugar transport rate, which induces fermentation in a high glucose flux and mitochondrial respiration in a low one [10]. Considering this change of paradigm from glucose concentration to its flux rate, we also asked whether Snf1/AMPK phosphorylation state could be controlled by glucose transport rate rather than glucose concentration in the medium.

To address this issue, we used yeast strains expressing only one type of hexose transporter under a constitutive promoter: the high-capacity low-affinity Hxt1, the high-affinity low-capacity Hxt7, or the chimeric transporter Tm6*, composed of the N-terminal of Hxt1 and the C-terminal of Hxt7 [20]. As previously reported, these strains exhibited a reduction in glucose consumption rate, with the Tm6*-expressing strain showing the lowest transport rate in both 2% and 5% glucose-containing media [21] (Figure 2a).
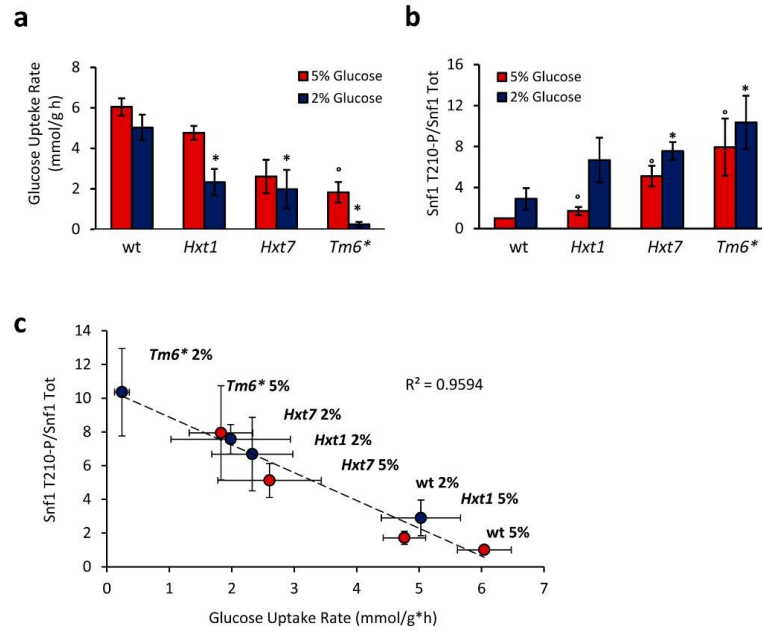
Figure 2. Snf1-T210 phosphorylation correlates with glucose transport rate. (**a**) Glucose uptake rate and (**b**) Snf1-T210 phosphorylation level measured in 2% and 5% glucose media of yeast strains expressing only Hxt1, Hxt7, or the chimeric transporter Tm6*, under a constitutive, non-glucose-responsive promoter. Mean ± standard deviation is shown ($n = 3$ for each). * $p < 0.05$ relative to wt in 2% glucose; ° $p < 0.05$ relative to wt in 5% glucose (t-test). (**c**) Linear correlation between Snf1 phosphorylation and glucose uptake rate shown in (**a**,**b**).

Interestingly, these strains also presented altered phosphorylation of Snf1/AMPK. In fact, all of the mutants showed an increased level of Snf1-T210 phosphorylation, in both 2% and 5% glucose media (conditions in which wild-type cells present a fermentative metabolism and a very low Snf1-T210 phosphorylation; Figure 2b). Altering the expression of glucose transporters, we managed to uncouple glucose transport rate from glucose concentration in the medium, observing complete independence of Snf1/AMPK phosphorylation from glucose concentration (Figure 2b). Indeed, we found an inverse correlation between Snf1/AMPK phosphorylation state and glucose consumption rate (Figure 2c), demonstrating that Snf1/AMPK activation state is not statically controlled by glucose availability, but rather dynamically regulated by transport flux.

To confirm that Snf1/AMPK activation depends on glucose transport, we carried out shift-up experiments using a strain deleted in all of the hexose transporters (*Hxt-Null*) and unable to grow on glucose due to its inability to import glucose from the medium [22]. The addition of glucose to ethanol-grown cells induced rapid and almost complete dephosphorylation of Snf1/AMPK in the wild-type strain (Figure 3a). Conversely, in the *Hxt-Null* mutant, Snf1/AMPK phosphorylation remained high after the addition of glucose, without any significant decrease until 60 min (Figure 3a). These data demonstrate that if glucose import is prevented, Snf1/AMPK dephosphorylation is completely impaired.
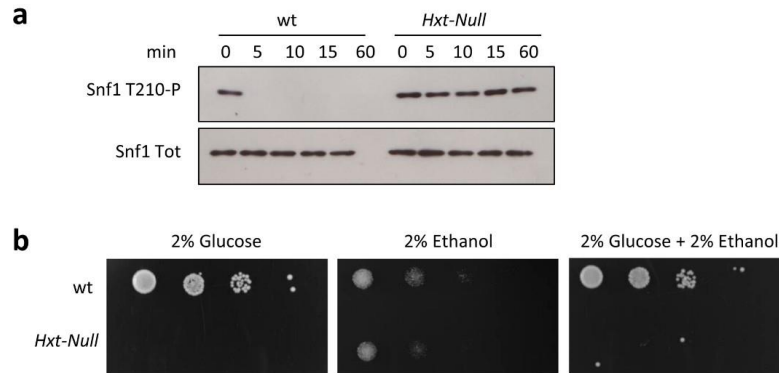
Figure 3. Snf1-T210 dephosphorylation requires glucose transport. (**a**,**b**) Shift-up experiments in wild-type and *Hxt-Null* strains. Cells were harvested after 0, 5, 10, 15, and 60 min of glucose supplementation; anti-pAMPK antibody (to detect Snf1-T210 phosphorylation) and anti-His antibody (to detect total Snf1/AMPK) were used; one representative immunoblot is shown. (**b**) Wild-type and *Hxt-Null* strains were equalized, spotted at 10-fold serial dilutions, and grown on synthetic complete plates containing 2% glucose, 2% ethanol, or 2% glucose and 2% ethanol as carbon sources.

The fact that glucose does not affect Snf1/AMPK phosphorylation in the *Hxt-Null* strain (Figure 3a) implies that the perception of extracellular glucose is not involved in the regulation of Snf1/AMPK activity. This is also consistent with the unaffected dephosphorylation of Snf1/AMPK in the *pde1Δcyr1Δyak1Δ* strain (Figure 1c), where the sensing of extracellular glucose no longer impinges on the Ras/PKA pathway [7].

Once active, Snf1/AMPK is known to alter the transcription and the activity of metabolic genes and enzymes counteracting glucose catabolite repression [23]. In agree- ment with a previous report, and despite the high level of phosphorylation of Snf1/AMPK, the *Hxt-Null* strain was unable to grow when glucose and ethanol were mixed as carbon sources [21] (Figure 3b). Furthermore, our attempt to isolate *Hxt-Null* mutants able to consume ethanol in the presence of glucose failed. These results indicate that glucose catabolite repression predominates over the consumption of alternative carbon sources to glucose, even when the Snf1/AMPK regulatory mechanism is impaired.

1.1. G6P, and Not F1,6BP, Influences Snf1/AMPK Phosphorylation

The dependency of Snf1/AMPK phosphorylation on glucose transport rate (Figure 2) is consistent with the existence of a flux-sensing mechanism that coordinates cell signaling with glycolytic rate. F1,6BP concentration has been proposed to be the core of this mecha- nism, being proportional to the glycolytic flux [11]. In addition, in mammalian cells, F1,6BP controls the stability of the AXIN/LKB1/AMPK complex, thus regulating AMPK-T172 phosphorylation [14].

As shown above, we excluded any effect of F1,6BP on the Snf1/AMPK phosphoryla- tion state mediated by the Ras/PKA pathway (Figure 1). Because of this, we wondered whether F1,6BP may affect the Snf1/AMPK activation state through other mechanisms. To address this issue, we carried out shift-up experiments in a yeast strain in which both genes encoding for phosphofructokinase (*PFK1* and *PFK2*) were deleted to prevent the synthesis of F1,6BP from glucose [24] (Figure 4a). Surprisingly, the *pfk1Δpfk2Δ* strain presented rapid and almost complete dephosphorylation of Snf1/AMPK upon the addition of glucose, as did the control strain (Figure 4b).
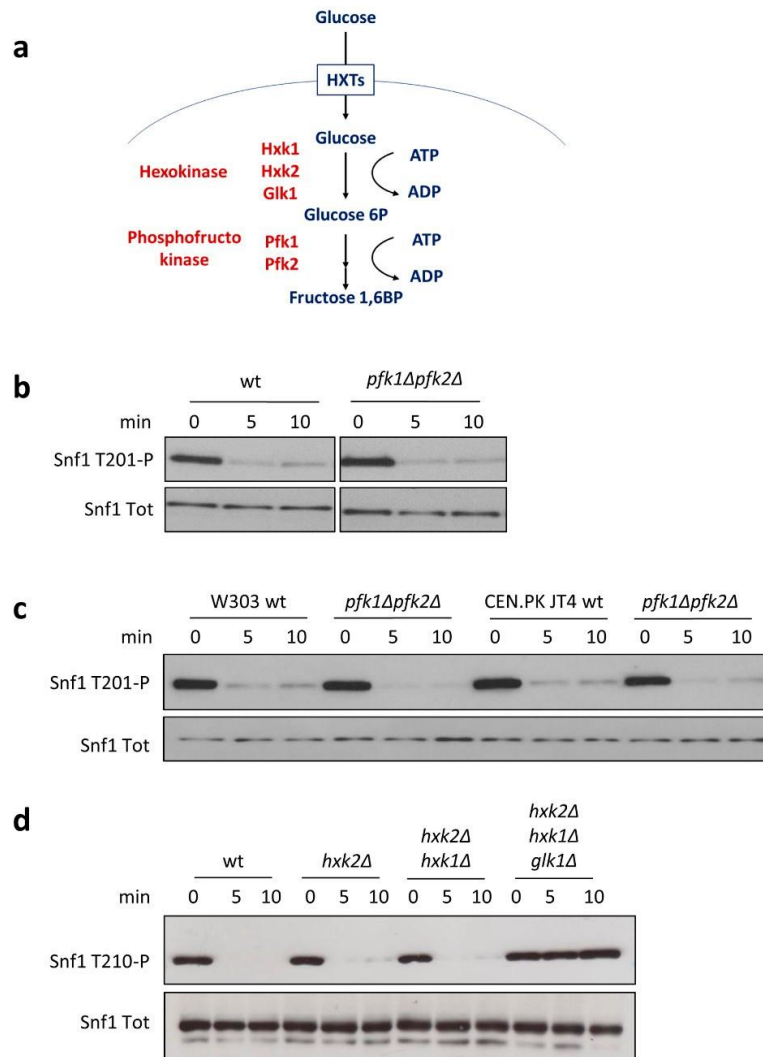
Figure 4. Snf1-T210 phosphorylation depends on G6P. (**a**) Schematic representation of the upper part of glycolysis in yeast. (**b**) Shift-up experiments in the *pfk1Δpfk2Δ* strain, with the two genes coding for phosphofructokinase deleted. (**c**) Shift-up experiments in *pfk1Δpfk2Δ* mutants in W303 and CEN.PK JT4 backgrounds. (**d**) Shift-up experiments in strains with one or more genes coding for hexokinases deleted. Anti-pAMPK antibody (to detect Snf1-T210 phosphorylation) and anti-His antibody (to detect total Snf1) were used. One representative immunoblot is shown.

Yeast strains of the CEN.PK background have been proven to carry a point mutation in the *CYR1* gene, known to influence yeast metabolism upon the deletion of glycolytic genes [25]. To completely exclude side effects due to this mutation, we also conducted shift-up experiments in the W303 and CEN.PK JT4 backgrounds, bearing the wild-type *CYR1* gene [25]. Remarkably, in both the backgrounds, we observed complete dephosphorylation of Snf1/AMPK without phosphofructokinase activity and upon the addition of glucose (Figure 4c), indicating that F1,6BP is not involved in the control of the activation state of Snf1/AMPK. Thus, despite the inverse correlation between Snf1/AMPK phosphorylation

and glucose uptake rate (Figure 2c), we failed to show a correlation between F1,6BP synthesis and Snf1/AMPK activation (Figure 4b,c).

Next, we investigated the role of hexokinases (Hxk1, Hxk2, and Glk1), given that glucose-6-phosphate (G6P) synthesis was already suggested to influence Snf1/AMPK phosphorylation state [5]. Among yeast hexokinases, Hxk2 represents the catalytically dominant form, which also has a regulatory function involved in the maintenance of glucose repression [26]. Nevertheless, Snf1/AMPK dephosphorylation in the *hkx2*Δ strain still responded to the addition of glucose, suggesting that Hxk2's regulatory function is not involved in the control of Snf1/AMPK activation (Figure 4d). Similarly to *hxk2*Δ cells, the double-deleted *hxk1*Δ*hxk2*Δ strain also showed rapid dephosphorylation of Snf1/AMPK upon the addition of glucose (Figure 4d), while only the triple-mutant *hxk1*Δ*hxk2*Δ*glk1*Δ, completely lacking hexokinase activity, resulted in a loss of Snf1/AMPK dephosphorylation (Figure 4d). These results are consistent with a recent publication showing that G6P—and not F1,6BP—concentration peaks within a few minutes after the addition of glucose [13].

Altogether, these data strongly indicate that G6P is the glycolytic intermediate that connects Snf1/AMPK phosphorylation with glucose metabolism.

1. Discussion

AMPK is a master regulator of glucose metabolism, as well as lipid metabolism, and in higher eukaryotes it plays crucial roles in several diseases, such as cancer, obesity, and diabetes [27]. Hypothalamic AMPK plays a critical role in whole-body energy homeostasis, mediating the effects of hormones and nutrients on food intake, energy expenditure, and metabolism of peripheral organs [28–31]. Indeed, AMPK activity is regulated by several compounds other than glucose, such as α-lipoic acid, leptin, insulin, ghrelin, cytokines, as well as natural compounds such as resveratrol, curcumin, epigallocatechin 3-gallate, and many others [32–34]. Among these, α-lipoic acid—a cofactor of mitochondrial enzymes with antioxidant capacity—was shown to decrease AMPK activity in the hypothalamus, leading to anti-obesity effects in different organisms [35,36]. On the other hand, α-lipoic acid was shown to increase AMPK activation in β-cells [37] and in the liver in eukaryotic systems [36].

Although AMPK modulation is much more complex in mammals, the use of model organisms to elucidate fundamental aspects of its regulation is a valuable tool to understand its activity in vivo. In particular, *Saccharomyces cerevisiae* biochemistry and genetics are extremely useful to study the crosstalk between different signaling pathways, as exemplified by this work.

S. cerevisiae has evolved its metabolism to optimally consume glucose across a wide range of concentrations. This is achieved through a complex signaling network specialized for the sensing of glucose availability and for the dynamic adaptation of cellular metabolism [5]. The Ras/PKA pathway is strongly activated by glucose availability, and its function enhances cellular proliferation as well as glucose fermentation. PKA is also known to enhance the glycolytic flux, stimulating the pyruvate kinase Cdc19 and the 6-phosphofructo2-kinase Pfk26 through phosphorylation, triggering a positive feedback loop in which glucose availability stimulates glycolysis and simultaneously inhibits gluconeogenesis [38] (Figure 5).

Meanwhile, a glucose concentration higher than 0.05% represses Snf1-T210 phosphorylation, preventing the expression of genes involved in mitochondrial respiration, oxidation of fatty acids, and the consumption of alternative carbon sources to glucose [6]. Of note, PKA is also known to positively regulate the activity of the phosphatase Reg1/Glc7, responsible for Snf1/AMPK inactivation [16] (Figure 5).
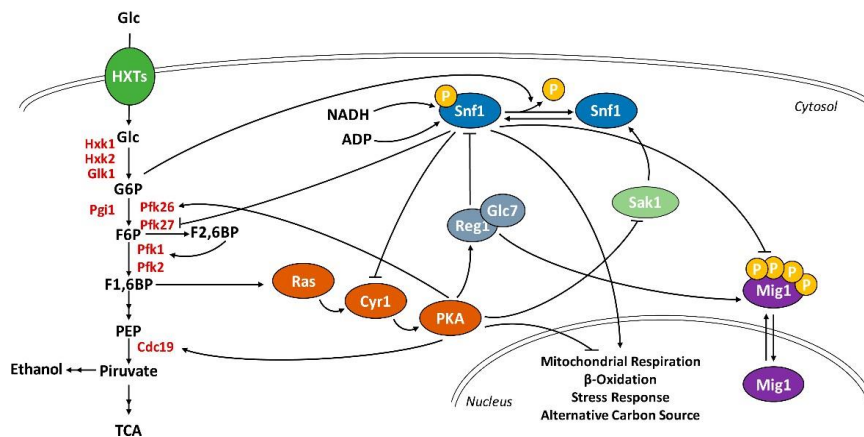
Figure 5. Schematic representation of the interactions between the glycolysis, Ras/PKA, and Snf1/AMPK pathways. F1,6BP synthesis influences Ras/PKA activity which, in turn, phosphorylates Pfk26 and Cdc19, stimulating the glycolytic flux. G6P promotes Snf1/AMPK dephosphorylation, thus inhibiting the kinase. NADH and ADP interact with Snf1/AMPK, giving rise to an interaction hub for the monitoring of cellular metabolism. Active PKA stimulates Reg1/Glc7 and reduces Sak1 activity, without influencing the Snf1/AMPK phosphorylation state, during a nutritional shift-up. In turn, phosphorylated Snf1/AMPK inhibits Cyr1 and Pfk27 activity and prevents Mig1 nuclear translocation. As a final result, PKA and Snf1/AMPK alternatively regulate the expression of genes involved in mitochondrial metabolism, stress response, and alternative carbon metabolism.

In the present work, we investigate the connection between Snf1/AMPK and Ras/PKA pathways during the onset of glucose catabolite repression (i.e., during a nutritional shift from ethanol to glucose). Our results clearly show that glucose induction of Snf1/AMPK dephosphorylation is completely independent of Ras/PKA activity, despite the dominant role of Ras/PKA in regulating yeast glucose metabolism (Figure 1).

Signaling pathways are known to be organized with a bow-tie architecture, in which several signals are independently sensed by different signaling molecules, and then converge on a limited number of downstream effectors [39]. Thus, the Ras/PKA and Snf1/AMPK pathways are independently and alternatively influenced by glycolysis during a nutritional shift-up, while their signals can integrate on downstream effectors (Figure 5). An example of this concept is shown in Figure 3: even if Snf1/AMPK is highly phosphorylated in the *Hxt-Null* strain, cells robustly persist in the preference of glucose as carbon source, suggesting that glucose fermentation still predominates over Snf1/AMPK stimulation of ethanol consumption.

Glucose control of Snf1-T210 phosphorylation has long been considered to be dependent on glucose concentration in the growth medium [19]. To maximize glucose consumption, yeast cells have also evolved a signaling pathway controlling the expression of glucose transporters, in accordance with the availability of this nutrient. This regulation results in the matching of high glucose concentrations with the expression of the high-capacity transporters, whereas high-affinity transporters are expressed when the glucose concentration is low. Thus, glucose uptake rate is inherently dependent on glucose availability [4]. However, working with yeast strains constitutively expressing only one glucose transporter (either Hxt1, Hxt7, or Tm6*), we managed to decouple glucose transport rate from glucose availability in the medium. This allowed us to depict an inverse correlation between Snf1-T210 phosphorylation state and glucose transport rate, clearly showing that the activity of this kinase is dynamically regulated by glucose transport flux (Figure 2). Our results are also in agreement with previously reported microfluidic experiments, which proved an altered nuclear localization of Mig1 in the Hxt1-only and Hxt7-only strains [40]. Mig1 is a transcriptional repressor known to inhibit the expression of genes involved in

alternative carbon metabolism. In turn, active Snf1/AMPK massively phosphorylates Mig1, promoting its Msn5-mediated export from the nucleus [41]. Moreover, the altered Mig1 nuclear localization in strains with a modified glucose transport indicates that glucose uptake rate influences the entire Snf1/AMPK pathway, alongside its downstream key metabolic effectors. Of note, a connection has recently been reported between mammalian AMPK and glycolytic metabolism [14], supporting consistent evolutionary conservation of that regulation.

As recently reviewed, protein–metabolite interactions (PMIs) are molecular events pivotal for the coordination between cellular metabolism and signal transduction [12].

F1,6BP is one of the most influential metabolites, controlling both Ras/PKA activation in yeast and AMPK phosphorylation inhibition in mammalian cells, through a mechanism mediated by aldolases [13,14]. Moreover, sugar phosphates such as G6P, G1P, and T6P inhibit SnRK1 (the plant ortholog of AMPK) [42,43], suggesting evolutionary conservation of the role of sugar phosphates in the regulation of the AMPK kinases. In keeping with that, our data show that G6P regulates Snf1/AMPK phosphorylation; indeed, mutant strains completely lacking glucose transporters or hexokinases are unresponsive to the addition of glucose (Figures 3a and 4d). However, we cannot rule out the possibility that this interaction is direct or mediated, since we did not succeed in measuring the interaction between G6P and the Snf1/AMPK complex through isothermal calorimetry analysis.

We further explored the possibility of a direct interaction by considering the carbohydrate-binding properties of Snf1/AMPK β-subunits. Thus, we performed a docking analysis with several sugar phosphates on the glycogen-binding domain (GBD) of Sip2 (from PDB ID: 2qlv) or Gal83 (modelled by homology, based on Sip2-GBD). In fact, Gal83 GBD was previously reported to be required for the glucose-dependent dephosphorylation of Snf1 [44]. Unfortunately, this approach failed to detect a binding pocket with a high affinity for G6P. Thus, we considered the hypothesis of G6P acting on GBD when bound on the active complex. The conformation of the active complex in yeast is not available, but several structures of the active mammalian AMPK were resolved where the carbon-binding motif (CBM) of the β-subunit was docked on the active kinase domain, generating a pocket that can bind to several activators [45,46]. We attempted the construction of a homology model for the yeast GBD in the same conformation, but it was evident that whereas the kinase pocket facing CBM is conserved from mammalian to yeast, neither the GBD fromSip2 nor from Gal83 shares the characteristics of the mammalian homolog interface (see Supplementary Figure S1). This raises doubts as to whether this conformation could actually exist in yeast.

The only other structure available in yeast was obtained with the truncated C-terminal portion of Snf1, and shows the Sip2-GBD docked on a completely different site, bound to Snf4 [47]. This is not compatible with the presence of the kinase domain in the active complex, as characterized for mammalian AMPK complexes. In this yeast structure, we could identify potential binding pockets for G6P, although it is still unclear whether this conformation represents an alternative physiological state for the Snf1 complex, possibly reflecting the inactive conformation of Snf1. Thus, at the moment, only our in vivo data can strongly support the dependence of the Snf1/AMPK phosphorylation state on G6P.

Therefore, metabolites of the upper part of glycolysis result in actively influencing the signaling pathways that regulate glucose metabolism in yeast, mammals, and plants [13,14,42,43]. The present work highlights that yeast Snf1/AMPK undergoes a similar regulation, with G6P being the molecule connecting the Snf1/AMPK phosphorylation state with glycolytic flux; indeed, this enables the monitoring of glucose metabolism and the coordination of fermentative and respiratory metabolism. In addition, through the interaction with ADP [48] (Figure 5), Snf1/AMPK senses the energetic status of the cell and regulates catabolic and anabolic processes to achieve energy homeostasis.

In conclusion, our observations, alongside previously reported interactions, underline the role of Snf1/AMPK as a central hub for the tuning of cellular metabolism throughprotein–metabolite interactions.

1. Materials and Methods

1.1. The Yeast Strains and Growth Conditions

The *S. cerevisiae* strains employed in this work are listed in Table S1. Cells were grown at 30 °C in synthetic media containing 2% and 5% glucose (Merck Life Science, Milan, Italy) or 2% ethanol (Merck Life Science, Milan, Italy), 6.7 g/L yeast nitrogen base (Formedium, Hunstanton, England), and 50 mg/L of the required amino acids (Merck Life Science, Milan, Italy).

For shift-up experiments, cells were grown overnight in 2% ethanol. At the mid-exponential phase (cellular concentration 0.5–0.8 OD/mL), glucose was added at a final concentration of 2%, and samples were collected at different timepoints, quenched, and extracted as reported below. The *ras2Δ*, *tpk1Δtpk2Δtpk3Δyak1Δ*, and *pde2Δcyr1Δyak1Δ* strains, which are unable to grow on ethanol, were pre-cultured overnight in 2% glucose media and then transferred to 2% ethanol media for 2 h before the shift-up experiment.

1.2. Protein Extraction, Immunoblotting, and Densitometric Analysis

To assess the Snf1/AMPK phosphorylation state, cells were quenched using 6% TCA (Merck Life Science, Milan, Italy). Then, the cells were lysed in UREA buffer (6 M UREA, 1% SDS, 50 mM Tris-HCl pH 7.5, 5 mM EDTA) in the presence of an equal volume of acid-washed glass beads (Merck Life Science, Milan, Italy) by 10 vortex/ice cycles of 30 sec each. Crude extracts were denatured in SDS sample buffer (40% glycerol, 20% β-mercaptoethanol, 9.2% SDS, 0.25 mM Tris-HCl pH 6.8, 0.01% BBF) and heated for 5 min at 95 °C.

Western blot analysis was conducted with anti-phosphoT172-AMPK antibody (Cell Signaling, Danvers, MA, USA), anti-His antibody (Merck Life Science, Milan, Italy), and anti-TAP antibody (Thermo Fisher Scientific, Waltham, MA, USA). Densitometric analyses were conducted with ImageJ software v1.51 (NIH, http://imagej.nih.gov/ij/, accession date 23 April 2018).

1.3. Glucose Consumption Rate

Cells in the exponential phase of growth were sampled by centrifugation, collecting the supernatants. Glucose concentration at each timepoint was measured using the D-Glucose HK/G6P DH Kit (Megazyme, Bray, Ireland), according to the manufacturer's instructions.

Glucose consumption rate (mmol/g ×h) was calculated as the angular coefficient of the correlation between glucose concentration (mmol/mL) and cellular concentration, corrected for the cellular dry weight (mg/mL) and time (h).

1.4. Statistical Analysis

Experiments were performed in triplicate. Results were compared by using Student's two-sided *t*-test. Differences were considered statistically significant at $p < 0.05$.

References

1. Orth, J.D.; Thiele, I.; Palsson, B. What is flux balance analysis? *Nat. Biotechnol.* **2010**, *28*, 245–248. [CrossRef]
2. Kitano, H. *Foundations of Systems Biology*; MIT Press: Cambridge, MA, USA, 2001; ISBN 9780262112666.
3. Nielsen, J. Yeast Systems Biology: Model Organism and Cell Factory. *Biotechnol. J.* **2019**, *14*, e1800421. [CrossRef] [PubMed]
4. Busti, S.; Coccetti, P.; Alberghina, L.; Vanoni, M. Glucose Signaling-Mediated Coordination of Cell Growth and Cell Cycle in *Saccharomyces cerevisiae*. *Sensors* **2010**, *10*, 6195–6240. [CrossRef] [PubMed]
5. Conrad, M.; Schothorst, J.; Kankipati, H.N.; Van Zeebroeck, G.; Rubio-Texeira, M.; Thevelein, J.M. Nutrient sensing and signaling in the yeast *Saccharomyces cerevisiae*. *FEMS Microbiol. Rev.* **2014**, *38*, 254–299. [CrossRef]
6. Coccetti, P.; Nicastro, R.; Tripodi, F. Conventional and emerging roles of the energy sensor Snf1/AMPK in *Saccharomyces cerevisiae*. *Microb. Cell* **2018**, *5*, 482–494. [CrossRef] [PubMed]
7. Nicastro, R.; Tripodi, F.; Gaggini, M.; Castoldi, A.; Reghellin, V.; Nonnis, S.; Tedeschi, G.; Coccetti, P. Snf1 Phosphorylates Adenylate Cyclase and Negatively Regulates Protein Kinase A-dependent Transcription in *Saccharomyces cerevisiae*. *J. Biol. Chem.* **2015**, *290*, 24715–24726. [CrossRef]
8. Barrett, L.; Orlova, M.; Maziarz, M.; Kuchin, S. Protein Kinase a Contributes to the Negative Control of Snf1 Protein Kinase in *Saccharomyces cerevisiae*. *Eukaryot. Cell* **2011**, *11*, 119–128. [CrossRef]
9. Welkenhuysen, N.; Schnitzer, B.; Österberg, L.; Cvijovic, M. Robustness of Nutrient Signaling Is Maintained by Interconnectivity Between Signal Transduction Pathways. *Front. Physiol.* **2019**, *9*, 1964. [CrossRef] [PubMed]
10. Huberts, D.H.E.W.; Niebel, B.; Heinemann, M. A flux-sensing mechanism could regulate the switch between respiration and fermentation. *FEMS Yeast Res.* **2011**, *12*, 118–128. [CrossRef] [PubMed]
11. Bozaquel-Morais, B.L.; Madeira, J.B.; Maya-Monteiro, C.M.; Masuda, C.A.; Montero-Lomelí, M. A New Fluorescence-Based Method Identifies Protein Phosphatases Regulating Lipid Droplet Metabolism. *PLoS ONE* **2010**, *5*, e13692. [CrossRef] [PubMed]
12. Milanesi, R.; Coccetti, P.; Tripodi, F. The Regulatory Role of Key Metabolites in the Control of Cell Signaling. *Biomolecules* **2020**, *10*, 862. [CrossRef]
13. Peeters, K.; Van Leemputte, F.; Fischer, B.; Bonini, B.M.; Quezada, H.; Tsytlonok, M.; Haesen, D.; Vanthienen, W.; Bernardes, N.; Gonzalez-Blas, C.B.; et al. Fructose-1,6-bisphosphate couples glycolytic flux to activation of Ras. *Nat. Commun.* **2017**, *8*, 1–15. [CrossRef] [PubMed]
14. Zhang, C.-S.; Hawley, S.A.; Zong, Y.; Li, M.; Wang, Z.; Gray, A.; Ma, T.; Cui, J.; Feng, J.-W.; Zhu, M.; et al. Fructose-1,6-bisphosphate and aldolase mediate glucose sensing by AMPK. *Nature* **2017**, *548*, 112–116. [CrossRef]
15. Hong, S.-P.; Leiper, F.; Woods, A.; Carling, D.; Carlson, M. Activation of yeast Snf1 and mammalian AMP-activated protein kinase by upstream kinases. *Proc. Natl. Acad. Sci. USA* **2003**, *100*, 8839–8843. [CrossRef]
16. Castermans, D.; Somers, I.; Kriel, J.; Louwet, W.; Wera, S.; Versele, M.; Janssens, V.; Thevelein, J.M. Glucose-induced posttranslational activation of protein phosphatases PP2A and PP1 in yeast. *Cell Res.* **2012**, *22*, 1058–1077. [CrossRef]
17. Rubenstein, E.M.; McCartney, R.R.; Zhang, C.; Shokat, K.M.; Shirra, M.K.; Arndt, K.M.; Schmidt, M.C. Access Denied: Snf1 Activation Loop Phosphorylation Is Controlled by Availability of the Phosphorylated Threonine 210 to the PP1 Phosphatase. *J. Biol. Chem.* **2008**, *283*, 222–230. [CrossRef] [PubMed]
18. Toda, T.; Uno, I.; Ishikawa, T.; Powers, S.; Kataoka, T.; Broek, D.; Cameron, S.; Broach, J.; Matsumoto, K.; Wigler, M. In yeast, RAS proteins are controlling elements of adenylate cyclase. *Cell* **1985**, *40*, 27–36. [CrossRef]
19. Wilson, W.; Hawley, S.A.; Hardie, D. Glucose repression/derepression in budding yeast: SNF1 protein kinase is activated by phosphorylation under derepressing conditions, and this correlates with a high AMP:ATP ratio. *Curr. Biol.* **1996**, *6*, 1426–1434. [CrossRef]
20. Otterstedt, K.; Larsson, C.; Bill, R.; Ståhlberg, A.; Boles, E.; Hohmann, S.; Gustafsson, L. Switching the mode of metabolism in the yeast *Saccharomyces cerevisiae*. *EMBO Rep.* **2004**, *5*, 532–537. [CrossRef]
21. Elbing, K.; Ståhlberg, A.; Hohmann, S.; Gustafsson, L. Transcriptional responses to glucose at different glycolytic rates in *Saccharomyces cerevisiae*. *JBIC J. Biol. Inorg. Chem.* **2004**, *271*, 4855–4864. [CrossRef]
22. Reifenberger, E.; Freidel, K.; Ciriacy, M. Identification of novel HXT genes in *Saccharomyces cerevisiae* reveals the impact of individual hexose transporters on qlycolytic flux. *Mol. Microbiol.* **1995**, *16*, 157–167. [CrossRef]
23. Kayikci, Ö.; Nielsen, J. Glucose repression in *Saccharomyces cerevisiae*. *FEMS Yeast Res.* **2015**, *15*, fov068. [CrossRef]
24. Heinisch, J. Construction and physiological characterization of mutants disrupted in the phosphofructokinase genes of *Saccharomyces cerevisiae*. *Curr. Genet.* **1986**, *11*, 227–234. [CrossRef]

1. Kümmel, A.; Ewald, J.C.; Fendt, S.-M.; Jol, S.J.; Picotti, P.; Aebersold, R.; Sauer, U.; Zamboni, N.; Heinemann, M. Differential glucose repression in common yeast strains in response to HXK2 deletion. *FEMS Yeast Res.* **2010**, *10*, 322–332. [CrossRef] [PubMed]
2. Peláez, R.; Herrero, P.; Moreno, F. Functional domains of yeast hexokinase. *Biochem. J.* **2010**, *432*, 181–190. [CrossRef] [PubMed]
3. Jeon, S.-M. Regulation and function of AMPK in physiology and diseases. *Exp. Mol. Med.* **2016**, *48*, e245. [CrossRef] [PubMed]
4. Minokoshi, Y.; Alquier, T.; Furukawa, N.; Kim, Y.-B.; Lee, A.; Xue, B.; Mu, J.; Foufelle, F.; Ferre, P.; Birnbaum, M.; et al. AMP-kinase regulates food intake by responding to hormonal and nutrient signals in the hypothalamus. *Nature* **2004**, *428*, 569–574. [CrossRef]
5. López, M. AMPK Wars: The VMH Strikes Back, Return of the PVH. *Trends Endocrinol. Metab.* **2018**, *29*, 135–137. [CrossRef]
6. Stark, R.; Ashley, S.E.; Andrews, Z.B. AMPK and the neuroendocrine regulation of appetite and energy expenditure. *Mol. Cell. Endocrinol.* **2013**, *366*, 215–223. [CrossRef]
7. Lamberigts, C.; Wang, Y.; Dierckx, T.; Buys, N.; Everaert, N.; Buyse, J. The influence of thyroid state on hypothalamic AMP-activated protein kinase pathways in broilers. *Gen. Comp. Endocrinol.* **2021**, *311*, 113838. [CrossRef]
8. Vazirian, M.; Nabavi, S.M.; Jafari, S.; Manayi, A. Natural activators of adenosine 5′-monophosphate (AMP)-activated protein kinase (AMPK) and their pharmacological activities. *Food Chem. Toxicol.* **2018**, *122*, 69–79. [CrossRef]
9. Lyons, C.L.; Roche, H.M. Nutritional Modulation of AMPK-Impact upon Metabolic-Inflammation. *Int. J. Mol. Sci.* **2018**, *19*, 3092. [CrossRef] [PubMed]
10. Kim, M.S.; Lee, K.U. Role of hypothalamic 5′-AMP-activated protein kinase in the regulation of food intake and energy homeostasis. *J. Mol. Med.* **2005**, *83*, 514–520. [CrossRef]
11. Kim, M.-S.; Park, J.-Y.; Namkoong, C.; Jang, P.-G.; Ryu, J.-W.; Song, H.-S.; Yun, J.-Y.; Nam-Goong, I.S.; Ha, J.; Park, I.-S.; et al. Anti-obesity effects of α-lipoic acid mediated by suppression of hypothalamic AMP-activated protein kinase. *Nat. Med.* **2004**, *10*, 727–733. [CrossRef] [PubMed]
12. Wang, Y.; Everaert, N.; Song, Z.; Decuypere, E.; Vermeulen, D.; Buyse, J. Alpha-lipoic acid impairs body weight gain of young broiler chicks via modulating peripheral AMPK. *Comp. Biochem. Physiol. Part A Mol. Integr. Physiol.* **2017**, *211*, 34–40. [CrossRef]
13. Targonsky, E.D.; Dai, F.; Koshkin, V.; Karaman, G.T.; Gyulkhandanyan, A.V.; Zhang, Y.; Chan, C.B.; Wheeler, M.B. α-Lipoic acid regulates AMP-activated protein kinase and inhibits insulin secretion from beta cells. *Diabetologia* **2006**, *49*, 1587–1598. [CrossRef] [PubMed]
14. Tripodi, F.; Nicastro, R.; Reghellin, V.; Coccetti, P. Post-translational modifications on yeast carbon metabolism: Regulatory mechanisms beyond transcriptional control. *Biochim. Biophys. Acta (BBA) Gen. Subj.* **2015**, *1850*, 620–627. [CrossRef]
15. Kitano, H. Biological robustness. *Nat. Rev. Genet.* **2004**, *5*, 826–837. [CrossRef]
16. Welkenhuysen, N.; Borgqvist, J.; Backman, M.; Bendrioua, L.; Goksör, M.; Adiels, C.B.; Cvijovic, M.; Hohmann, S. Single-cell study links metabolism with nutrient signaling and reveals sources of variability. *BMC Syst. Biol.* **2017**, *11*, 1–10. [CrossRef] [PubMed]
17. DeVit, M.J.; Johnston, M. The nuclear exportin Msn5 is required for nuclear export of the Mig1 glucose repressor of *Saccharomyces cerevisiae*. *Curr. Biol.* **1999**, *9*, 1231–1241. [CrossRef]
18. Zhang, Y.; Primavesi, L.; Jhurreea, D.; Andralojc, P.J.; Mitchell, R.; Powers, S.J.; Schluepmann, H.; Delatte, T.; Wingler, A.; Paul, M.J. Inhibition of SNF1-Related Protein Kinase1 Activity and Regulation of Metabolic Pathways by Trehalose-6-Phosphate. *Plant. Physiol.* **2009**, *149*, 1860–1871. [CrossRef] [PubMed]
19. Nunes, C.; Primavesi, L.; Patel, M.K.; Martinez-Barajas, E.; Powers, S.J.; Sagar, R.; Fevereiro, P.; Davis, B.G.; Paul, M.J. Inhibition of SnRK1 by metabolites: Tissue-dependent effects and cooperative inhibition by glucose 1-phosphate in combination with trehalose 6-phosphate. *Plant. Physiol. Biochem.* **2013**, *63*, 89–98. [CrossRef]
20. Momcilovic, M.; Iram, S.; Liu, Y.; Carlson, M. Roles of the Glycogen-binding Domain and Snf4 in Glucose Inhibition of SNF1 Protein Kinase. *J. Biol. Chem.* **2008**, *283*, 19521–19529. [CrossRef]
21. Xiao, B.; Sanders, M.J.; Underwood, E.; Heath, R.; Mayer, F.V.; Carmena, D.; Jing, C.; Walker, P.A.; Eccleston, J.F.; Haire, L.F.; et al. Structure of mammalian AMPK and its regulation by ADP. *Nature* **2011**, *472*, 230–233. [CrossRef] [PubMed]
22. Li, X.; Wang, L.; Zhou, X.E.; Ke, J.; de Waal, P.; Gu, X.; Tan, M.H.E.; Wang, D.; Wu, D.; Xu, H.E.; et al. Structural basis of AMPK regulation by adenine nucleotides and glycogen. *Cell Res.* **2014**, *25*, 50–66. [CrossRef]
23. Amodeo, G.A.; Rudolph, M.J.; Tong, L. Crystal structure of the heterotrimer core of *Saccharomyces cerevisiae* AMPK homologue SNF. *Nature* **2007**, *449*, 492–495. [CrossRef] [PubMed]
24. Mayer, F.V.; Heath, R.; Underwood, E.; Sanders, M.J.; Carmena, D.; McCartney, R.R.; Leiper, F.; Xiao, B.; Jing, C.; Walker, P.A.; et al. ADP Regulates SNF1, the *Saccharomyces cerevisiae* Homolog of AMP-Activated Protein Kinase. *Cell Metab.* **2011**, *14*, 707–714. [CrossRef]

Protective effect of *Vigna unguiculata* extract against aging and neurodegeneration

Farida Tripodi[1], Linda Lombardi[1], Lorenzo Guzzetti[1], Davide Panzeri[1], Riccardo Milanesi[1], Manuela Leri[2,3], Monica Bucciantini[2], Cristina Angeloni[4], Daniela Beghelli[5], Silvana Hrelia[6], Giada Onorato[7], Elia Di Schiavi[7], Ermelinda Falletta[8], Simona Nonnis[9], Gabriella Tedeschi[9], Massimo Labra[1], Paola Coccetti[1]

[1]Department of Biotechnology and Biosciences, University of Milano-Bicocca, Milano, Italy
[2]Department of Experimental and Clinical Biomedical Sciences, University of Firenze, Firenze, Italy
[3]Department of Neuroscience, Psychology, Drug Research and Child Health, University of Firenze, Firenze, Italy
[4]School of Pharmacy, University of Camerino, Camerino, Italy
[5]School of Biosciences and Veterinary Medicine, University of Camerino, Camerino, Italy
[6]Department for Life Quality Studies, Alma Mater Studiorum, University of Bologna, Rimini, Italy
[7]Institute of Biosciences and BioResources (IBBR), CNR, Naples, Italy
[8]Department of Chemistry, University of Milano, Milano, Italy
[9]Department of Veterinary Medicine (DIMEVET), University of Milano, Milano, Italy

Correspondence to: Paola Coccetti; **email:** paola.coccetti@unimib.it

ABSTRACT

Aging and age-related neurodegeneration are among the major challenges in modern medicine because of the progressive increase in the number of elderly in the world population. Nutrition, which has important long- term consequences for health, is an important way to prevent diseases and achieve healthy aging. The beneficial effects of *Vigna unguiculata* on metabolic disorders have been widely documented. Here, we show that an aqueous extract of *V. unguiculata* beans delays senescence both in *Saccharomyces cerevisiae* and *Drosophila melanogaster*, in a Snf1/AMPK-dependent manner. Consistently, an increased expression of FOXO, SIRT1, NOTCH and heme oxygenase (HO) genes, already known to be required for the longevity extension in *D. melanogaster*, is also shown. Preventing α-synuclein self-assembly is one of the most promising approaches for the treatment of Parkinson's disease (PD), for which aging is a risk factor. *In vitro* aggregation of α-synuclein, its toxicity and membrane localization in yeast and neuroblastoma cells are strongly decreased in the presence of bean extract. In a *Caenorhabditis elegans* model of PD, *V. unguiculata* extract substantially reduces the number of the age-dependent degeneration of the cephalic dopaminergic neurons. Our findings support the role of *V. unguiculata* beans as a functional food in age-related disorders.

age-related disorders [5, 7]. Thus, there is an increasing interest in nutrition as a way both to prevent diseases and to reach healthy aging.

Much of the current knowledge on the molecular mechanisms of aging comes from lifespan studies on short-lived model organisms, such as the budding yeast *Saccharomyces cerevisiae*, *Drosophila melanogaster* and *Caenorhabditis elegans* [8]. Specifically, AMPK (AMP-activated protein kinase), IGF (insulin-like growth factor) and TORC1 (target of rapamycin kinase complex 1) signaling pathways play key functions in regulating aging [9–11].

Neurodegenerative diseases, characterized by aberrant aggregates of the presynaptic protein α-synuclein, are collectively referred to as synucleinopathies, the second most common group of neurodegenerative diseases [12–14]. One of the most common synucleinopathies is Parkinson's disease (PD) and autosomal dominant forms of PD have been linked to mutations in α- synuclein. In PD patients, neurodegeneration is found predominantly in dopaminergic neurons. Despite the advances in the study of these pathologies, the detailed molecular mechanism of neuronal degeneration is still largely unknown. Several studies underline the relevant role of cellular models for a better understanding of the molecular regulation of human pathologies [15]. As such, budding yeast has been extensively employed in models of synucleinopathies [16–19]. In addition, an age-related degeneration of dopaminergic neurons has been shown in wild-type *C. elegans* [20]. Interestingly, neuronal and dendritic loss are accelerated and more severe when human α-synuclein is expressed in dopaminergic neurons in *C. elegans* [21].

Vigna unguiculata (L.) Walp. or cowpea is the most relevant *Vigna* species for human food. It is cultivated in tropical and subtropical zones of the world, including Africa, Asia, Latin America and also in some Mediterranean countries [22, 23]. Cowpea seeds are a good source of proteins, which mainly consist of globulins (vicilins or 7S globulins) and, to a lesser extent, albumins, glutelins and prolamins [24]. From a nutritional point of view, there is a high ratio of essential-to-non-essential amino acids, which is over 50%, suggesting the potential capacity of cowpea to cover human nutritional requirements [25, 26]. Moreover, bioactive peptides with antioxidant activity are successfully obtained from enzymatic proteolysis of cowpea proteins, indicating also its potentiality as a functional food [24]. In comparison with other legumes, cowpea has a low-fat content with high level of unsaturated fatty acids and is also characterized by a high proportion of carbohydrates (mainly dietary fibers and resistant starch) [24]. Apart from the relevant

source of essential macronutrients, cowpea also constitutes an interesting source of micronutrients [27].

All these features, together with the presence of minerals (calcium, iron and zinc) and phytochemicals, such as phenolic compounds, are attracting the attention of consumers and researchers, also because of its beneficial properties for health, including anti-diabetic, anti-cancer, anti-hyperlipidemic, anti-inflammatory and anti-hypertensive properties [28].

The aim of the present study is to investigate whether *V. unguiculata* also has anti-aging and neuroprotective effects, exploiting different model organisms to address complementary aspects. We show that an aqueous extract from *V. unguiculata* beans increases lifespan in yeast cells, being dependent on Snf1/AMPK (sucrose- non-fermenting/AMP-activated protein kinase) and Ras/PKA (Rat sarcoma/protein kinase A) pathways. Its pro-longevity feature is also confirmed on the multicellular organism *D. melanogaster*, which is consistent with the increased expression of AMPK-dependent genes associated with fly lifespan extension. Cowpea extract is able to significantly reduce the aggregation of α-synuclein *in vitro* and to attenuate its toxicity both in yeast and neuroblastoma cells. Remarkably, in a nematode model expressing human α-synuclein, the age-dependent degeneration of the dopaminergic neurons is strongly reduced under chronic treatments with *V. unguiculata* extract.

RESULTS

Vigna unguiculata extract extends lifespan in yeast cells

Considering the nutritional properties and positive effects for health of *Vigna unguiculata* [28], we investigated the composition of aqueous bean extracts from *V. unguiculata* in comparison with those obtained from *Cajanus cajan* L. and *Phaseolus vulgaris* L., originating from the Arusha area in Tanzania. *V. unguiculata* extract was characterized by a higher starch amount and less proteins compared to the extracts obtained from the other pulses, while the percentage of total amino acids was comparable among species (Figure 1A–1C). We also confirmed that cowpea seeds are a good source of amino acids (included the essential ones), as well as of unsaturated fatty acids (more abundant in comparison with the other two beans), confirming its nutritionally desirable features (Supplementary Tables 1, 2) [24].

To explore if these differences could have an impact on the longevity of yeast cells, exponentially growing cells were treated with 0.2% of the extracts from *V.*

unguiculata, *C. cajan* or *P. vulgaris* beans and chronological lifespan was monitored by measuring the viability of the cultures throughout time. Although all theextracts increased longevity of yeast cells, the highest response was evident in the presence of *V. unguiculata* one, with a mean lifespan increasing from 3 days to about

9.5 days (Figure 1D, Table 1). On the basis of the aboveresults, we decided to continue our analysis by using onlythe cowpea extract. A strong dose-response effect on yeast longevity was observed by increasing the concentration of *V. unguiculata* extract in the culture (from 0.2% to 0.5%), since it was able to extend the mean lifespan up to 16 days at the higher concentration (Figure 1E, Table 1). Its anti-aging properties were evident also when the extract was added to "aged" cells,

i.e. after they had already entered the stationary phase (Figure 1F). Remarkably, cowpea extract not originatingfrom Arusha maintained the same effect, letting us to suppose that the origin of the beans has no relevant impact on its anti-aging features (data not shown).

Cell growth was then monitored in the presence of the highest concentration of the extract. Although the growth rate in the presence of 0.5% extract showed onlya minor increase in exponential phase, the final biomassof the population was more than doubled in comparison with the control (Figure 1G). On the other hand, the consumption of glucose in the media during theexponential phase of growth was strongly reduced (more than 50%), suggesting that the presence of either starch or proteins induced a decrease of glucose uptake from the medium (Figure 1H). However, the lower glucose consumption in the presence of the extract have no effect on the experimental determination of CLS, which starts after carbon source exhaustion.

Importantly, the anti-aging effect of the extract was synergistic with caloric restriction, one of the most effective non-genetic interventions known to promote lifespan extension in several model organisms [10] (Supplementary Figure 1). Overall, the data presented indicate that cowpea aqueous extract extends chronological aging in yeast cells.

To increase our knowledge on the composition of *V. unguiculata* extract we performed a proteomic analysis. Interestingly, we identified 174 proteins with a molecular weight ranging from 200 to less than 20 kDa, of which 10% are oxidoreductase, 12% are stress response proteins while 25% are still uncharacterized (Figure 2A, 2B).

The signaling pathways connected to longevity regulation are well known in yeast. Among them, the Snf1/AMPK (sucrose-non fermenting/AMP-activatedprotein kinase) and the autophagic pathways are anti-

aging pathways, while the Ras2/PKA (Rat sarcoma/protein kinase A) and the TORC1 (target of rapamycin complex 1) pathways are pro-aging ones [8, 9, 29]. To identify through which of them the cowpea extract extended yeast chronological lifespan, we tested its effect on mutants bearing deletion in one of the aforementioned pathways (*snf1Δ*, *atg1Δ*, *ras2Δ*, *tor1Δ*) (Figure 2C–2F, Table 2). The anti-aging effect of 0.2% cowpea extract was still evident in *tor1Δ* and *atg1Δ* strains (Figure 2C, 2E, Table 2), while it was strongly reduced in *ras2Δ* and *snf1Δ* mutants (Figure 2D, 2F, Table 2), indicating that the Ras/PKA and the Snf1/AMPK pathways are involved in mediating theanti-aging effect of cowpea extract in yeast cells.

### *Vigna unguiculata* extract supplementation extends lifespan in *Drosophila melanogaster*

To investigate the pro-longevity effect of the cowpea extract also in a multicellular organism, female CantonS flies were lifelong supplemented with 0.2% or 0.5%

V. unguiculata extract. A significant marked increase in mean lifespan was observed in flies supplemented with 0.2% bean extract in respect to controls (40.09±1.08 days *vs* 31.82±0.86 days; 25.99% increase), while mean lifespan of flies supplemented with 0.5% bean extract was comparable to that of control flies (Figure 3A). These data are only partially in agreement with the results obtained in yeast cells, where the 0.5% cowpea supplementation was more effective than the 0.2% one. Nevertheless, considering only the survivorship data obtained after a 3 weeks supplementation, a higher survival of flies supplemented with 0.5% in respect to both 0.2% supplement and control was observed (Supplementary Figure 2A, 2B).

To verify whether the increase of the mean lifespan in the presence of 0.2% extract was due to bean extract supplementation itself and not to CR induced by bean extract off-flavor, the body weights of flies were recorded at 30 and 45 days. No differences in fly body weights were observed, suggesting an equal food uptakein control and supplemented groups (Figure 3B).

To better clarify, at a molecular level, the positive effectof 0.2% cowpea extract supplementation on *D. melanogaster* lifespan, the expression of genes involvedin preserving cellular homeostasis and longevity was investigated. Flies were supplemented with cowpea extract for 30 or 45 days and the expression of genes involved in aging-related signaling pathways (SIRT1 - sirtuin 1-, FOXO -Forkhead box O- and NOTCH) and antioxidant defense systems (HO - heme oxygenase and TRXR - thioredoxin reductase) were measured (Figure 3C–3F). Oxidative stress has been recognized to

play a key role in aging [30]. The oxidative stress theory of aging speculates that the functional losses typical of elderly are associated with the accumulation of structural impairments caused by the oxidative damage to macromolecules [31]. HO expression was significantly up-regulated by cowpea extract supplementation after both 30 and 45 days (Figure 3C), while TRXR was not influenced at all (data not shown), suggesting that *V. unguiculata* extract partially modulates the endogenous antioxidant defense system.

SIRT1, a member of the class III NAD$^+$-dependent histone deacetylases (HDACs) has been implicated in the extension of longevity in *D. melanogaster* [32]. SIRT1 expression was significantly up-regulated in flies supplemented with cowpea extract after both 30 and 45 days (Figure 3D). Remarkably, also NOTCH expression increased at both time points (Figure 3E), in accordance with findings showing that SIRT1 is a positive modulator of NOTCH [33]. FOXO is a fundamental transcriptional regulator of the insulin pathway modulating growth and proliferation and its increase has been associated with extension of flies lifespan [34]. Although FOXO expression after 30 days of supplementation with *V. unguiculata* was the same as in control flies, cowpea extract triggered a significant up- regulation of FOXO expression at 45 days (Figure 3F). In agreement with the gene expression, the level of FoxO and Sirt1 proteins increased in flies supplemented with cowpea extract (Figure 3G–3I).
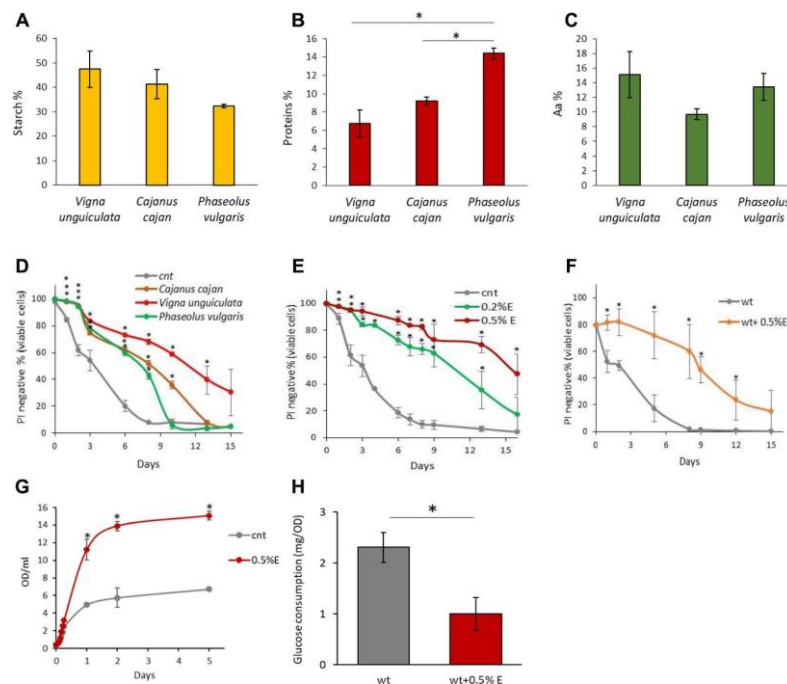
Figure 1. Chemical properties of bean extracts. (**A**) Starch content, (**B**) protein content and (**C**) amino acid content in *V. unguiculata*, *C. cajan* and *P. vulgaris* extracts. *p<0.05. (**D**) CLS of yeast cells grown in the absence or presence of 0.2% *V. unguiculata*, *C. cajan* and *P. vulgaris* extracts. *p<0.05 relative to control cells. (**E**) CLS of yeast cells grown in SD medium containing 2% glucose in the absence or presence of 0.2% or 0.5% *V. unguiculata* extract, added in exponential phase of growth. *p<0.05 relative to control cells. (**F**) CLS of yeast cells grown in SD medium containing 2% glucose in the absence or presence of 0.5% *V. unguiculata* extract, added to cells in stationary phase (and not in exponential phase, as in the other experiments). *p<0.05 relative to control cells. (**G**) Growth curves of yeast cells grown in SD medium containing 2% glucose in the absence or presence of 0.5% extract *V. unguiculata*. *p<0.05 relative to control cells. (**H**) Glucose consumption (mg/OD) of yeast cells grown in SD medium in the absence or presence of 0.5% *V. unguiculata* extract, measured on growth media sample at multiple time points during exponential phase of growth (0.2-2.5 OD/ml). *p<0.05 relative to control cells.

Table 1. Mean and maximal lifespan of wt cells grown in the presence of the indicated extracts.

	lifespan (days)	
wt strain	**mean**	**maximal**
cnt (no extract)	3.05 ± 0.42	9.46 ± 1.47
0.2% *P. vulgaris*	6.42 ± 0.12	11.72 ± 0.05
0.2% *C. cajan*	7.74 ± 0.30	13.53 ± 0.32
0.2% *V. unguiculata*	9.55 ± 0.49	18.55 ± 0.64
0.5% *V. unguiculata*	16.03 ± 3.01	>20
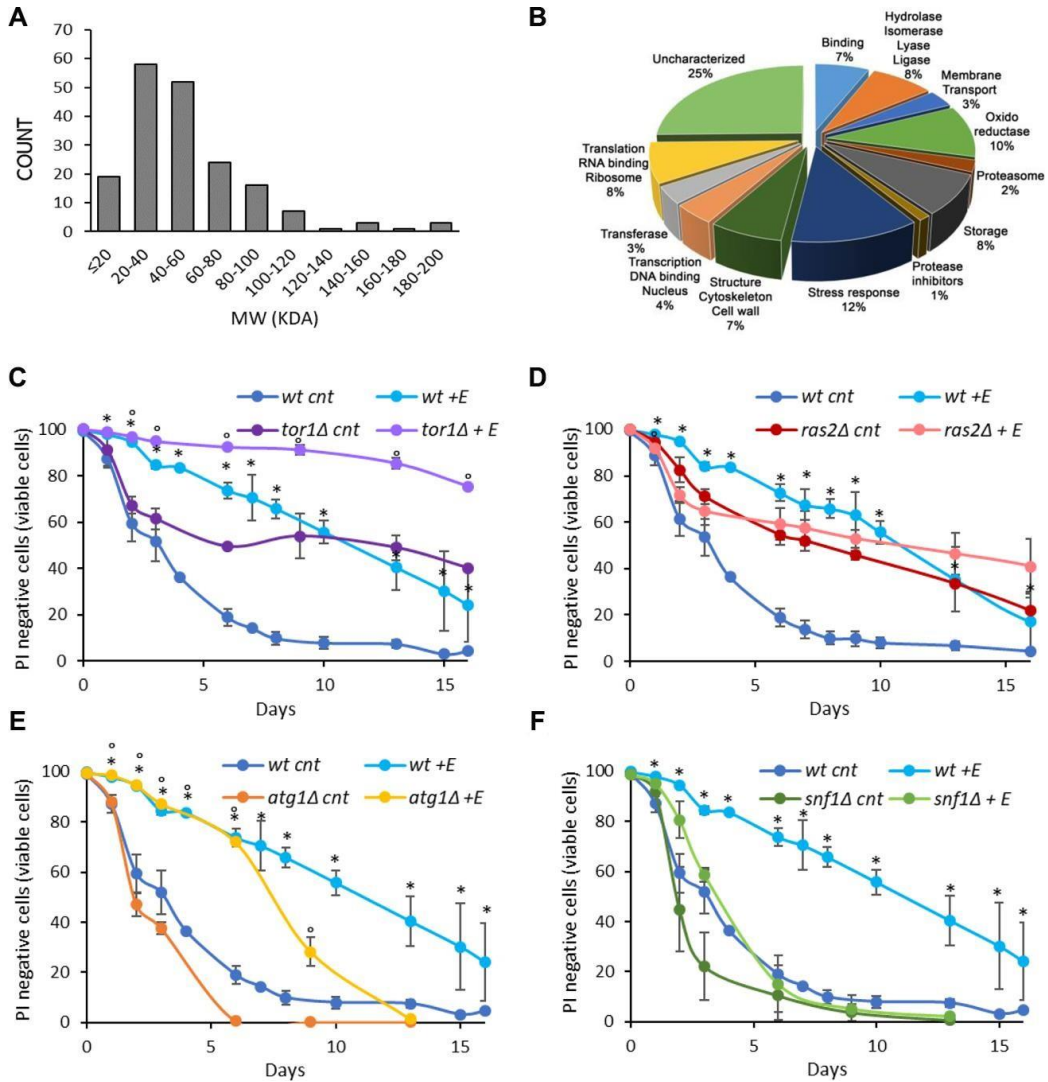
Figure 2. Cowpea extract extends yeast lifespan. (**A**, **B**) Analysis of *V. unguiculata* extract by mass spectrometry using a shotgun proteomic approach to identify all the proteins present in the sample. (A) MW distribution and (B) classification of the proteins identified. The data have been deposited to the ProteomeXchange Consortium via the PRIDE partner repository with the dataset identifier PXD017716. (**C**–**F**)CLS of wt and (**C**) *tor1Δ*, (**D**) *ras2Δ*, (**E**) *atg1Δ*, (**F**) *snf1Δ* cells, grown in SD medium containing 2% glucose in the absence or presence of 0.2%
V. unguiculata extract. *p<0.05 relative to untreated wt cells, °p<0.05 relative to untreated mutant cells. Curves of wt untreated cells and treated with the extract were repeated in **C**–**F**.

Table 2. Mean and maximal lifespan of mutant strains grown in the presence of 0.2% *V. unguiculata* extract. Data of wt cells were repeated for clarity.

	lifespan (days)			
	mean		maximal	
strain	cnt	0.2% E	cnt	0.2% E
wt	3.05 ± 0.42	9.55 ± 0.49	9.46 ± 1.47	18.55 ± 0.64
ras2Δ	7.48 ± 0.40	10.48 ± 4.98	18.95 ± 1.34	>20
tor1Δ	5.87 ± 0.23	>20	18.5 ± 0.14	>20
atg1Δ	2.22 ± 0.10	7.35 ± 0.21	4.95 ± 0.21	11.45 ± 0.78
snf1Δ	2.0 ± 0.42	3.35 ± 0.21	4.8 ± 2.40	7.2 ± 1.56

Thus, the aging-related signaling pathways of SIRT1, FOXO and NOTCH are involved in mediating the effect of cowpea extract in fruit flies.

Vigna unguiculata extract reduces both α-synuclein toxicity and aggregation *in vitro*

Extensive literature reports the fibrillation-inhibiting effects of plant extracts, including those consumed as part of a healthy diet [35, 36] and others found in traditional medicine [37–40].

α-Synuclein is a presynaptic protein associated with the pathophysiology of synucleinopathies, including Parkinson's disease [12–14], and budding yeast has been extensively employed in models of synucleinopathies [16]. Thus, the effect of *V.unguiculata* extract on the longevity of yeast cells over-
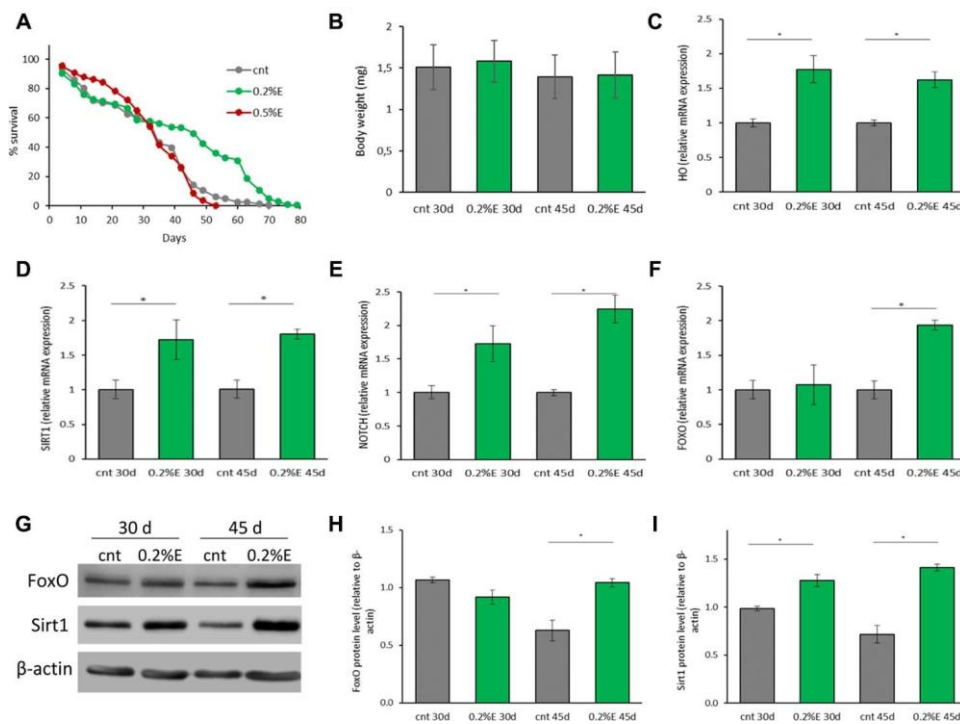
Figure 3. Cowpea extract extends *D. melanogaster* lifespan. (**A**) Survivorship of adult female *D. melanogaster*. Flies were supplemented with 0.2% and 0.5% bean extract lifelong. (**B**) Body weights of *D. melanogaster* supplemented with 0.2% bean extract. Flies were supplemented with 0.2% bean extract for 30 or 45 days. (**C–F**) Expression of genes related to longevity and oxidative stress. Flies were supplemented with 0.2% cowpea extract for 30 or 45 days. Total RNA was isolated and the mRNA levels of HO (**C**), SIRT1 (**D**), NOTCH (**E**), FOXO (**F**) were quantified using RT-PCR. (**G**) Western analysis using anti-FoxO and anti-Sirt1 antibodies on proteins extracts from flies supplemented with 0.2% cowpea extract for 30 or 45 days. (**H–I**) Densitometric analysis of FoxO and Sirt1 proteins. *p<0.05 with respect to the corresponding controls.

expressing the human α-synuclein [41] was evaluated. Interestingly, the addition of cowpea extract to exponentially growing cells strongly reduced the toxic effects of α-synuclein with a significant marked increase in mean lifespan (11.19 ± 2.18 days *vs* 2.22 ±

0.31 days; 404% increase) (Figure 4A, Table 3). Although α-synuclein protein was still present 3 days after the treatment (Supplementary Figure 3), it was lesslocalized to the plasma membrane, as shown by immunofluorescence analysis (Figure 4B, 4C) and cell fractionation (Figure 4D). These data suggest that a different localization of α-synuclein, rather than its protein clearance, could be responsible for the reduced toxicity in the presence of the bean extract.

The process of α-synuclein fibrillation was then investigated *in vitro* at two different concentrations of cowpea extract. The increase of ThT and ANS fluorescence emission intensity was used to quantifyfibrils formation and conformational change of the protein with or without cowpea extract (Figure 4E, 4F). The presence of *V. unguiculata* extract led to a significant concentration-independent decrease of ThT fluorescence in the α-synuclein aggregation solution,with an increase of the lag time and a decrease of both β-sheet growth rate and final equilibrium levels (Figure 4E). In agreement with a nucleation-dependentpolymerization model, α-synuclein exhibited a sigmoidal binding without cowpea extract (Figure 4E).

These evidences suggest that *V. unguiculata* extract significantly altered the amyloid aggregation pattern of α-synuclein. Moreover, the ANS binding fluorescence data indicate that the cowpea extract might increase the formation of α-synuclein species with minor solventexposure of hydrophobic clusters, or it might decrease the binding of ANS to α-synuclein surfaces (Figure 4F).The morphology of α-synuclein aggregates was alsostudied by TEM analysis. After 24 h of aggregation, the protein, either alone or in the presence of cowpea extract, existed as globular micelle-like and prefibrillar assemblies (Figure 4G). After 72 h of aggregation in theabsence of the extract, α-synuclein samples were mostlymature fibrils. Remarkably, the presence of cowpea extract enriched the samples with short fibrils covered by densely packed globular clusters (Figure 4G).Overall, these findings are consistent with an inhibitory effect of *V. unguiculata* extract on the formation ofamyloid fibrils.

It has been reported that cytotoxicity of amyloidogenic species largely depends on their biophysical surface properties, which influences their reactivity with thecellular plasma membrane [42–44]. To assess α-synuclein toxicity, we performed MTT assays on the human neuroblastoma SH-SY5Y cell line exposed for

48 h to extracellular α-synuclein aggregates pre-formed *in vitro* in the absence or in the presence of cowpea extract. Coherently, α-synuclein obtained without extract supplementation exhibited the highest cytotoxicity: oligomers (Ol) and fibrils (Fib) showed about 70% and 50% viability, respectively (Figure 5A). In cells incubated with α-synuclein aggregates formed in the presence of the extract, toxicity was reduced and cell viability was about 83% with oligomers (Ol/E0.5) and 86% with fibrils (Fib/E0.5) increasing up to 100% and 95% at the highest concentration of the extract (Figure 5A). Accordingly, ROS level significantly decreased in cells exposed to oligomers and fibrils formed in the presence of cowpea extract (Figure 5B).

These data suggest that in the presence of *V. unguiculata* extract, α-synuclein aggregation is redirected into non-toxic aggregate species.

To further explore the potential mechanism for the protective effect of the cowpea extract, the interactionof α-synuclein aggregates with the plasma membrane ofneuroblastoma cells was monitored by confocal microscopy. As previously reported [43, 44], a large number of α-synuclein oligomers or fibrils (stained in red) were bound to the cell membrane (stained in green)(Figure 5C). When cells were exposed to α-synuclein aggregates formed in the presence of cowpea extracts, the binding of both oligomers and fibrils to the cellular membranes was drastically reduced (Figure 5C).

In conclusion, these data show that the presence of cowpea extract during α-synuclein aggregation decreasesthe ability of the resulting aggregates to bind the plasmamembrane and to raise ROS production and cytotoxicity.

Vigna unguiculata extract reduces α-synuclein induced neurodegeneration in *Caenorhabditis elegans*

In order to evaluate the neuroprotective effects of cowpea extract on a multicellular organism, we turned to the nematode *C. elegans*. The expression of human α-synuclein in *C. elegans* causes the age-dependent degeneration and death of the four cephalic dopaminergic neurons (CEP), a phenotype which can be easily scored using a red fluorescent marker expressed only in those neurons [45]. Consistent with previous reports, we observed an age-related decline in the number of fluorescent dopaminergic neurons expressing human α-synuclein (Supplementary Figure 4). Thus, we investigated the effects of *V. unguiculata* extract both at 0.2% and 0.5%, in 6-day adult animals (Figure 6A, 6B). While in mock treated animals a mean of 3 out of 4 CEP neurons died, in animals exposed to *V. unguiculata* extracts
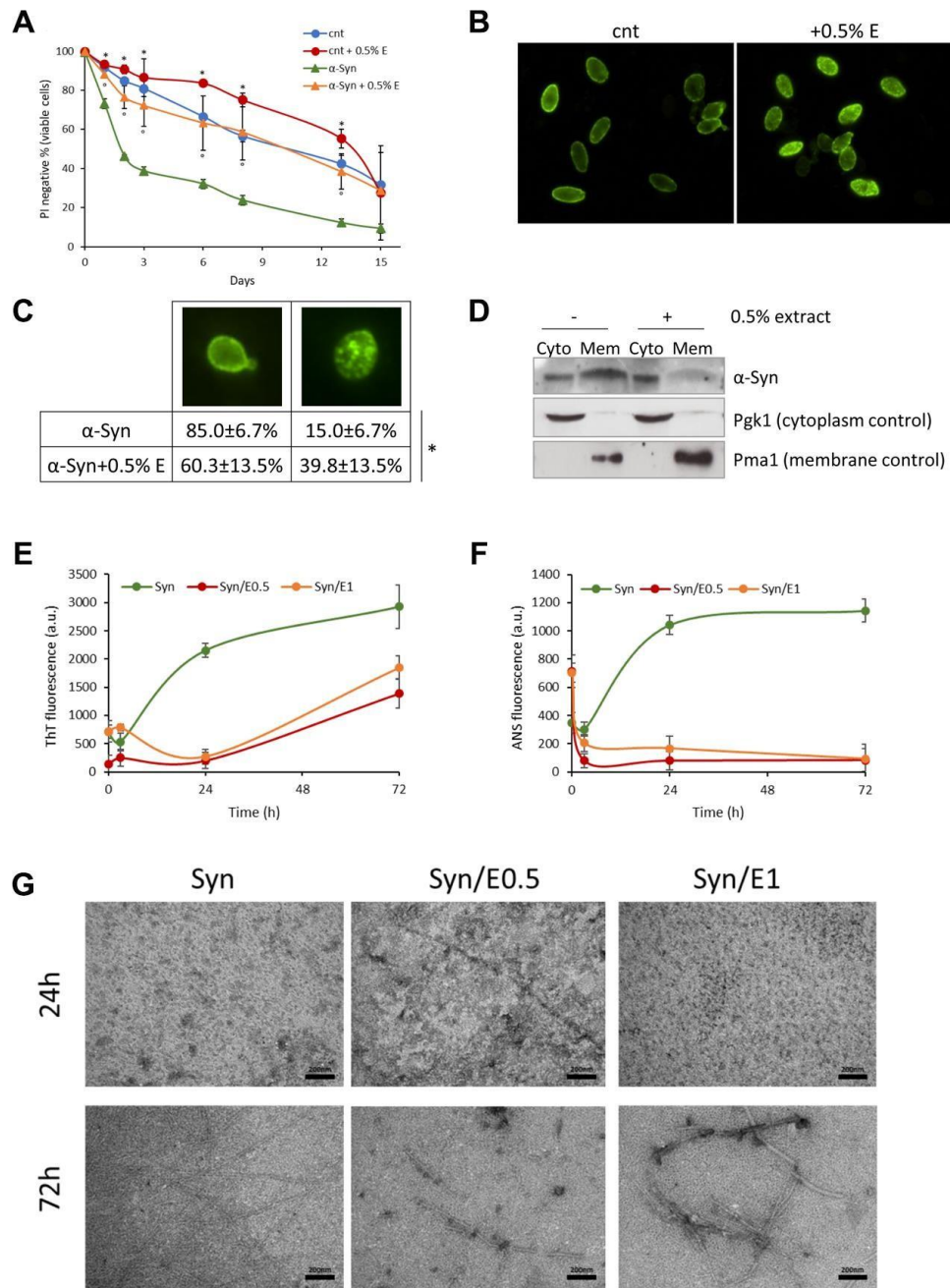
Figure 4. Cowpea extract reduces α-synuclein toxicity and aggregation. (**A**) CLS of yeast cells bearing pYX242 empty vector or pYX242-SNCA plasmid grown in SD medium containing 2% glucose in the absence or presence of 0.5% *V. unguiculata* extract. *p<0.05 relative to untreated cells bearing the empty vector, °p<0.05 relative to untreated α-synuclein expressing cells. (**B**, **C**) Immunofluorescence showing localization of α-synuclein in cells untreated or treated for 1 day with 0.5% *V. unguiculata* extract. The percentage of cells with α- synuclein localized in the cellular membrane is shown in (**C**). *p<0.05. (**D**) Western analysis using anti-α-synuclein antibody on cytolpasmic and membrane fractions isolated from wt [pYX242-SNCA] cells after 1-day treatment with 0.5% *V. unguiculata* extract. Pgk1 was used as cytoplasmic marker, Pma1 as membrane marker. (**E**, **F**) α-synuclein aggregation process followed by ThT fluorescence (**E**) and ANS binding (**F**) assays. (**G**) TEM pictures taken from α-synuclein aggregation mixture after 24 h and 72 h of incubation in the absence or in the presence of cowpea extract at molar ratio protein:extract 1:0.5 (E0.5) and 1:1 (E1); scale bars are shown.

Table 3. Mean and maximal lifespan of yeast cells bearing pYX242 empty vector or pYX242-SNCA plasmid grown inthe absence or presence of 0.5% *V. unguiculata* extract.

	lifespan (days)			
	mean		maximal	
strain	cnt	0.5% E	cnt	0.5% E
[pYX242]	9.96 ± 0.49	13.3 ± 1.13	>15	>15
[pYX242-SNCA]	2.22 ± 0.31	11.19 ± 2.18	14.21 ± 1.06	>15

there was a partial rescue of neurodegeneration, with 2 neurons dying in 0.2% extract and only 1 in 0.5%. A similar effect was observed in animals treated with 3 mM valproic acid (positive control) [46].

Our results indicate that *V. unguiculata* extract protects CEP dopaminergic neurons from degeneration in a *C. elegans* model of α-synuclein toxicity, in a dose- dependent manner.

DISCUSSION

Cowpea is considered as a source of health-promoting compounds, with a low fat and high protein content, as well as dietary fibers, phenolic compounds and minerals. Consumption of cowpea is associated with reduced risk of gastrointestinal disorders, cardiovasculardiseases, hypercholesterolemia, obesity, diabetes and several types of cancer [47]. We now add new
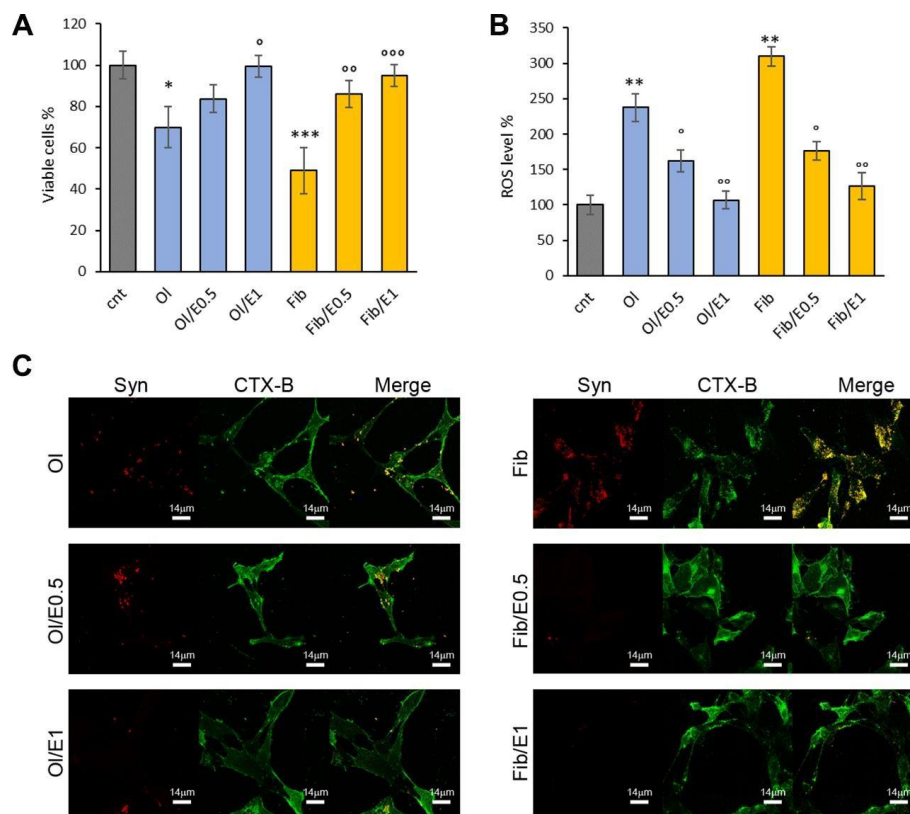
Figure 5. *V. unguiculata* extract reduces α-synuclein toxicity in neuroblastoma cells. (**A**, **B**) SH-SY5Y cells were grown for 48 h in the absence (cnt) or presence of 5 μM α-synuclein solution obtained after 24 h (oligomers, Ol) and 72 h (fibrills, Fib) of aggregation, withoutor with extract at molar ratio protein:extract 1:0.5 (E0.5) and 1:1 (E1). (**A**) Cell viability assessed by MTT assay and (**B**) ROS level evaluated by DCFDA fluorescence intensity assays. *$p<0.05$; **$p<0.01$; ***$p<0.001$ *vs* untreated cells. °$p<0.05$; °°$p<0.01$ *vs* treated cells with α-synuclein aggregates oligomeric (Ol) and fibrillar (Fib) grown without extract. (**C**) Z-projection of SH-SY5Y cell images by α-synuclein immunostaining (red) and CTX-B plasma membrane staining (green). Scale bars are shown.

important health benefits of cowpea beans, *i.e.* theiranti-aging and neuroprotective effects. Indeed, we showthat *V. unguiculata* extract extends lifespan, in two different eukaryotic models, such as budding yeast and fruit flies (Figures 1, 3). The extension of longevity requires Snf1/AMPK pathway in yeast (Figure 2F) and induces the upregulation of two downstream proteins of the AMPK pathway, such as FOXO and SIRT1 in *Drosophila* (Figure 3) [48–50]. Strikingly, it has been reported that AMPK and SIRT1 are downregulated withaging and their pharmacological activation is necessary to increase longevity [5].

The anti-senescence properties of cowpea extract are strongly additive with caloric restriction (SupplementaryFigure 1), the most effective non-genetic intervention delaying senescence [51], suggesting that *V. unguiculata*beans could display their best effect in terms of aging delay in a proper dietary regimen.

The strong neuroprotective features of cowpea extract are conserved in evolutionary distant eukaryotic

systems. Indeed, *V. unguiculata* extract decreases α-synuclein toxicity in both yeast and neuroblastoma cells, as well as in a *C. elegans* PD model by partially rescuing the degeneration of cephalic dopaminergic neurons (Figure 6).

The anti-aggregation properties of cowpea on α- synuclein is clearly evident (Figure 4E–4G). Along similar lines, the extract decreases the localization of α- synuclein to cell membrane both in the yeast model, in which α-synuclein is intracellularly expressed (Figure 4A–4D), and in neuroblastoma cells, where α-synuclein is added to the medium (Figure 5), also in keeping with the minor solvent exposure of hydrophobic clusters detected by ANS on amyloid assemblies (Figure 4F). These results suggest that *V. unguiculata* extract decreases the neurotoxicity caused by the intracellular accumulation of α-synuclein aggregates and the cellular damage induced by oligomeric aggregates interacting with the cell membrane by displacing the toxic protein from the lipidic bilayer. Our data are in accordance withrecent results showing that inhibition of α-synuclein
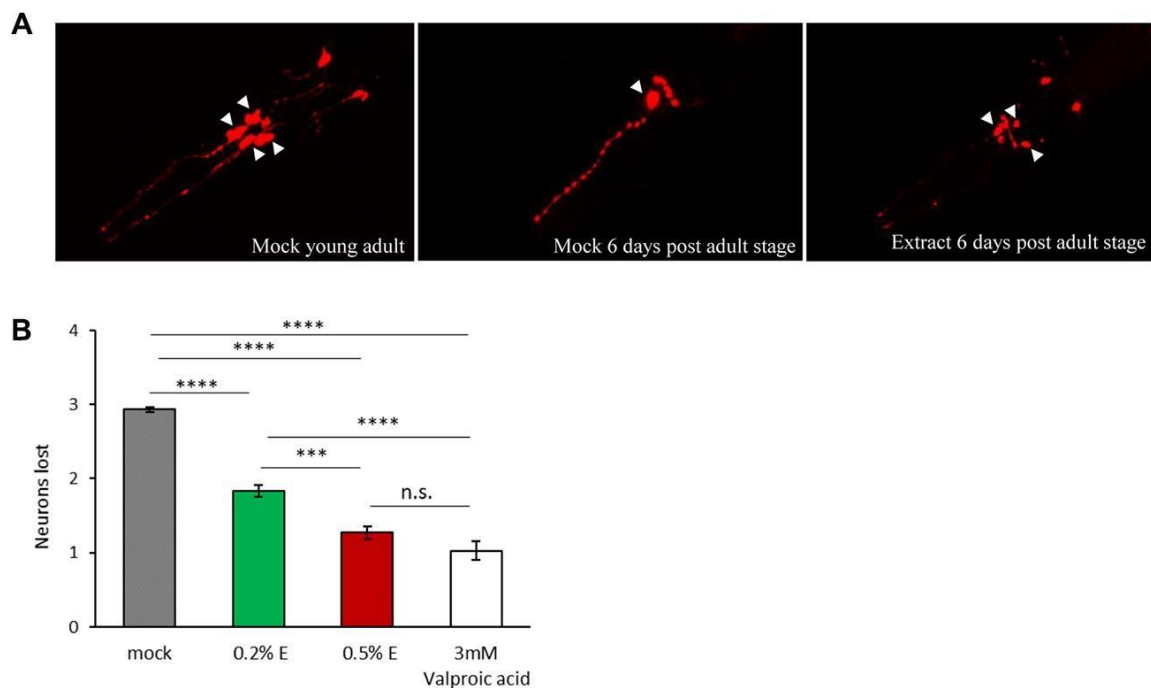
Figure 6. *V. unguiculata* extract is neuroprotective in a dose-dependent manner in a *C. elegans* model of α-synuclein toxicity.
(**A**) The four CEP neurons (indicated by arrowheads), expressing DsRed and human α-synuclein, are viable and with a wild type morphology in young adult animals cultivated in mock conditions (left panel); only one neuron is visible and viable after 6 days from adult stage cultivated in mock conditions (central panel); 0.5% *V. unguiculata* extract partially rescued the neurodegeneration after 6 days from adult stage (right panel). Anterior is to the left. (**B**) Quantification of dopaminergic neuron loss in human α-synuclein expressing animals grown with 0.2% and 0.5% of *V. unguiculata* extract. ***p<0.001, ****p<0.0001. The number of animals scored with mock is 95, with 0.2% extract is 103, with 0.5% extract is 94 and with 3 mM valproic acid 92.

binding to membranes reduces the toxicity of the protein both in worms and in mice [52, 53].

The aqueous extract of cowpea beans contains starch, amino acids, as well as several different proteins and peptides (Figures 1A–1C, 2A, 2B), while it is probably very poor in phenolic compounds. Although abundance of starch and proteins is generally considered negative from an aging point of view [10], the protection against senescence and neurodegeneration might be the result of a synergistic effect of different elements. Indeed, the nutrient combination of the extract rather than a single component might be responsible for the metabolic reprogramming, which leads to the longevity phenotype.

Although the identity of the active components in the extract remains to be investigated, the extractionprocess strongly mimics the way in which these beans are consumed. Therefore, the anti-aging and neuro- protecting compounds are likely to be conserved during the cooking process. Remarkably, it has been reported that cooking legumes in water increases the insoluble fiber content, protein quality and digestibility, although with a reduction of the content of vitamins and minerals[47]. Therefore, the use of cowpea beans should beencouraged and eventually the identification of the bioactive compounds could lead to the development of specific dietary supplements to support healthy aging and to delay neurodegeneration.

Any dietary intervention that has the potential of delaying the progression of age-related diseases could improve the quality of life of the aging population, inducing also an important impact on the economic implications of elderly on the society. Thus, *V. unguiculata* consumption in the global food chain is encouraging since our study suggests that cowpea beanssupplementation can prevent age-related disorders.

Although data on bioactive compounds from cowpea are still poor, some reports indicate components like peptides may contribute to health benefits derived from cowpea [28]. Remarkably, several proteins identified byproteomic analysis are still uncharacterized (Figure 2A, 2B). We believe that additional work is necessary to discover the bioactive compounds in cowpea and their interactions to efficiently exploit them in foods, such as snacks and breakfast cereals by targeting benefits to immune function and health gut. Indeed, interesting data show that progression of PD has been frequently associated with dysbiosis of gut microbiota [54, 55].

In conclusion, considering the role of functional food in the management of age-related diseases, we strongly support the intake of *V. unguiculata* beans to reduce
senescence, neuroinflammation and the extent of neurodegeneration.

MATERIALS AND METHODS

Extract preparation

V. unguiculata, *C. cajan* and *P. vulgaris* seeds were purchased from two markets (Kilombero and Arusha Central Market) in Arusha, Tanzania (3°22'0.01"S, 36°40'59.99"E). Seeds of each species were boiled for 1h and left cool down for the subsequent hour. The treatment was performed to mimic the condition of consumption, as described in [56]. Then, seeds were incubated at 50°C overnight till dryness and grinded to obtain a fine powder. 2 g of seed dry powder were suspended in 50 ml of ultrapure MilliQ water. Then, pulses were extracted through a magnetic stirrer at 500 rpm for 5 minutes and centrifuged at 5000 g for 30 min. Supernatant was recovered and freeze-dried.

Chemical and proteomic characterization of the extracts

Starch content
Starch content was evaluated by the enzymatic assay Total Starch AOAC Method 996.1 1 and AACC Method 76.13 (Megazyme ®, Ireland). Briefly, 50 mg of extract were suspended in 200 µl of ethanol 80% v/v and 1 ml of 2 M KOH. Samples were magnetically stirred for 20 min at 4°C. Then, 4 ml of sodium acetate pH=3.8 were added, followed by the addition of 50 µl of α-amylase (8300 U/mL) and 50 µl of amyloglucosidase (AMG, 3300 U/ml). Samples were incubated for 30 min with intermittent mixing on a vortex mixer, then centrifuged for 10 min at 3000 rpm to recover the supernatant. In order to evaluate total starch content, a reaction mixture was prepared as follows in a quartz cell: 1 ml H_2O, 25 µl of sample, 50 µl of a buffer solution pH = 7.6, 50 µl NADP+/ATP. The solution was incubated for 3 min at room temperature and then the absorbance was read at 340 nm against the blank. Then, 10 µl of a solution containing hexokinase (HK) and glucose-6-phosphate- dehydrogenase (G6PDH) was added. After an incubation of 5 min at room temperature, the absorbance was read against the blank again at 340 nm. Data are expressed as g of starch per 100 g of extract.

Amino acids content
Amino acids were quantified through a HPLC-DADmethod. A 1260 Infinity II LC System (Agilent, USA, 2018) was set up for the analysis. The calibration curve was made up using an amino acid mixed solution (Merck, Germany) in a concentration range between
0.078 mM and 1.25 mM. The column was an Agilent

Poroshell HPH C18 (100 x 4.6 mm, 2.7 µm) coupled with a guard column (AdvanceBio Oligo 4.6 x 5 mm, 2.7 µm) and it was kept at 40°C. Mobile phases were: A
- 10 mM Na$_2$HPO$_4$ pH=8.2 and B -
Acetonitrile:Methanol:Water 45:45:10. The elution program was the following (%B): 0-0.35 min 2%, 13.4 min 57%, 13.5 min 100%, 15.7 min 100%, 15.8 min 2%, 18 min end. Flow rate was constant at 1.5 ml/min. All solvents were HPLC grade, whereas the buffer, solutions and samples were pre-filtered with a 0.22 µm filter. OPA (o-Phthaldialdehyde reagent, Merck, Germany) was chosen as derivatizing agent acting as a fluorophore. Injection volume was 10 µl. The signal used to visualize the fluorescence was set at 338 nm bandwidth 10 nm with a reference wavelength of 390 nm bandwidth 20 nm. All data were displayed and analyzed on Agilent ChemStation software. Data are expressed as g of amino acids per 100 g of extract.

Proteins content
Total protein content was evaluated by using the Bradford assay as follows: 1 ml of 50% Coomassie- Brilliant Blue Bradford reagent (ThermoFisher, USA) was incubated at room temperature with 2 µl of extract of known concentration for a minute. Absorbance was read against blank at 595 nm and fitted on a calibration curve made up with BSA (Bovine Serum Albumin) in a range between 0 and 6 mg/ml. Data are expressed as g of protein per 100 g of extract.

GC/MS analysis
Before the GC/MS analyses all samples were subjected to a derivatization process, as described below. About 5 mg of each sample were accurately weighed, suspended in 50 µl of 2wt% methoxylamine hydrochloride in pyridine and incubated for 90 min at 37°C. Then, 80 µl of MBDSTFA (N-methyl-N-ter-butyldimethylsilyl- trifluoroacetamide)+1% TBDMCS (tert-butyldimethylchlorosilane) were added and the samples were incubated at 60° C for 30 min. After incubation at room temperature overnight, the samples were analyzed by using a ISQ™ QD Single Quadrupole GC-MS (Thermo Fisher) equipped with a VF-5ms (30 m x 0.25 mm i.d. x 0.25 µm; Agilent Technology). Injection volume: 1 µl. Oven program: 100° C for 2 min; then 6° C/min to 280° C for 15 min; Run Time 42 min. Helium was used as the gas carrier. SS Inlet: Mode Splitless. Inlet temperature: 280° C. Flow 1.0 ml/min. MS transfer line: 270° C. Ion source: 250° C. Ionization mode: electron impact: 70 eV. Acquisition mode: full scan. In order to compare the composition of the extracts, for each analyte identified by GC/MS a target ion (m/z) was extracted by the TIC and the corresponding area was calculated. Supplementary Table 2 reports for each analyte the corresponding target ion used.

Proteomic analysis
The extract was reduced, derivatized and digested with trypsin (protein: protease ratio 20:1) as described in [57] before MS/MS analysis.

Peptides separation was achieved on a Thermo Easy- nLC 1000, with a linear gradient from 95% solvent A (2 % ACN, 0.1% formic acid) to 30% solvent B (80% acetonitrile, 0.1% formic acid) over 60 min, from 30 to 60% solvent B in 5 min and from 60 to 100% solvent B in 2 min at a constant flow rate of 0.25 µl/min, with a single run time of 75 min. MS data were acquired on a Thermo Q-Exactive-HF, with a data-dependent top 15 method, the survey full scan MS spectra (300-1650 m/z) were acquired in the Orbitrap with 60000 resolution, AGC target 3e6, IT 20 ms. For HCD spectra resolution was set to 15000, AGC target 1e5, IT 80 ms; normalized collision energy 28 and isolation width of
1.2 m/z.

Raw label-free MS/MS files from Thermo Xcalibur software (version 4.1) [57] were analyzed using Proteome Discoverer software (version 2.2, Thermo Fisher Scientific) and searched with Sequest algorithm against the proteome of NCBI Phaseoleae (release 05/08/2019). The minimum required peptide length was set to 6 amino acids with carbamidomethylation as fixed modification, Met oxidation and Arg/Gln deamidation as variable modifications.

The mass spectrometry proteomic data have been deposited to the ProteomeXchange Consortium via the PRIDE [58] partner repository with the dataset identifier PXD017716.

Yeast methods

Yeast strains and media
The yeast strains used in this paper are listed in Supplementary Table 3. Cells were grown at 30°C in minimal medium containing 2% glucose as a carbon source and 0.67% yeast nitrogen base without amino acids, supplemented with 50 mg/l of required amino acids and bases for which the strains were auxotrophic. The natural extracts were dissolved in the medium at a concentration of 0.2% or 0.5% and filtered through 0.22µm filters.

Chronological lifespan experiments (CLS)
Cell cultures were grown in liquid medium until mid- late exponential phase and then inoculated into flasks containing medium in the presence or absence of the natural extracts (0.2% or 0.5% as indicated in each experiment). Survival was assessed by propidium iodide staining (PI) at the indicated time points with the Cytoflex cytofluorimeter (Beckman Coulter) and

analyzed with the Cytoflex software. For some experiments, survival was also confirmed by colony- forming units (CFUs) after 2 days of incubation at 30°C on YEPDA agar plates.

Protein extraction, cell fractionation and immunoblotting

Equal amounts of cells were collected and quenched using TCA 6% and lysed in lysis buffer (6M UREA, 1% SDS, 50 mM Tris-HCl pH7.5, 5 mM EDTA). The
cytoplasmic-membrane fractionation experiment was conducted using the MEM-PER kit (Thermo), following the manufacturer's instructions on yeast spheroplasts. Western blot analysis was performed using anti- Synuclein antibody (1:1000, Sigma Aldrich), anti-Pgk1 antibody (1:1000, Molecular Probes, used as loading control and cytoplasmic marker) and anti-Pma1 antibody (1:1500, Abcam, used as membrane marker).

Glucose consumption assay

Extracellular levels of glucose were evaluated on growth media of wt cells exponentially growing in the absence or presence of 0.5% cowpea extract, using the Megazyme D-glucose-HK assay kit, following the manufacturer's instructions, using an EnSight Plate Reader (Perkin Elmer).

Fluorescence microscopy on yeast

In situ immunofluorescence was performed on formaldehyde-fixed cells and carried using α-synuclein immunostaining (1:2000, Sigma Aldrich) followed by indirect immunofluorescence using rhodamine- conjugated anti-rabbit antibody (1:1000, Pierce Chemical Co). Digital images were taken with a Nikon DS-Qi MC camera mounted on a Nikon Eclipse 600 and controlled by the NIS elements imaging software (Nikon) with an oil 100X 0.5-1.3 PlanFluor oil objective (Nikon).

In vitro aggregation of α-synuclein

α-synuclein was expressed in *Escherichia coli* BL21(DE3) cells transformed with the pET28b/α- synuclein plasmid. The recombinant protein was expressed and purified according to a previously described procedure [43] and further purified by RP- HPLC. The identity and purity of the eluted material were assessed by mass spectrometry**.** Protein samples (250 μM), filtered through a 0.22 μm pore-size filter (Millipore, Bedford, MA, USA) were incubated at 37°C in 20 mM sodium phosphate buffer, pH 7.4 up to 3 days under shaking at 900 rpm with a thermo-mixer in the absence or in the presence of extract by using molar protein/substance ratios of 1:0.5 (E0.5) and 1:1 (E1). Oligomer-enriched or fibril-enriched sample were prepared by incubating a-synuclein for 24 h or 72 h, respectively.

ThT assay

The ThT binding assay was performed according to LeVine [59], using a 25 μM ThT solution in 20 mM sodium phosphate buffer, pH 7.0. Each sample, diluted at a final concentration of 6.25 μM, was transferred into a 96-well half-area, low-binding, clear bottom (200 μl/well) and ThT fluorescence was read at the maximum intensity of fluorescence of 485 nm using a Biotek Synergy 1H plate reader; buffer fluorescence was subtracted from the fluorescence values of all samples. In controls experiments, a significant interference of the highest concentrations of cowpea extract on ThT fluorescence was observed, so the two molar ratio protein:extract with lowest fluorescence interference were selected (Supplementary Figure 5).

ANS assay

Samples containing aggregating a-synuclein with and without cowpea extract at 250 μM were investigated for their ability to bind 8-anilinonaphthalene-1-sulfonic acid (ANS; Sigma Aldrich, Saint Louis, MO, US). 5 μl of each samples at different times of aggregation was transferred into a 96-well half-area, low-binding, clear bottom (200 μl/well), and ANS (50 μM) fluorescence intensity was read at the binding intensity of fluorescence of 480 nm in a Biotek Synergy 1H plate reader; buffer fluorescence was subtracted from the fluorescence values of all samples. In control experiments, a significant interference of the highest concentrations of the extract on ANS binding fluorescence was observed, so we selected the two molar ratios protein:extract with the lowest fluorescence interference (Supplementary Figure 5).

Transmission electron microscopy (TEM) imaging

5 μl aliquots of α-synuclein aggregated in the presence or in the absence of cowpea extract were withdrawn at different aggregation times, loaded onto a formvar/carbon-coated 400 mesh nickel grids (Agar Scientific, Stansted, UK) and negatively stained with 2.0% (w/v) uranyl acetate (Sigma-Aldrich). The grid was air-dried and examined using a JEM 1010 transmission electron microscope at 80 kV excitation voltage.

Cell culture methods

Cell culture

SH-SY5Y human neuroblastoma cells were cultured at 37 °C in complete medium (50% HAM, 50% DMEM, 10% fetal bovine serum, 3 mM glutamine, 100 units/ml penicillin and 100 μg/ml streptomycin), in a humidified, 5% CO_2 incubator.

MTT assay

Cell viability was assessed by the MTT assay optimized for the SH-SY5Y cell line. Briefly, SH-SY5Y cells

were seeded into 96-well plates at a density of 10000 cells/well in fresh complete medium and grown for 24 h. Then, cells were exposed for 48 h to 5 μM α- synuclein obtained at different times of aggregation in the presence or in the absence of the *Vigna unguiculata* extract. Cells were also treated with the corresponding concentrations of extract used in the aggregation of α- synuclein and the viability resulted similar to that of untreated control cells. After 48 h of incubation, the culture medium was removed and cells were incubated for 1 h at 37°C in 100 μl serum-free DMEM without phenol red, containing 0.5 mg/ml MTT. Then, 100 μl of cell lysis solution (20% SDS, 50% N,N-dimethylformamide) was added to each well andsamples were incubated at 37°C for 2 h to allow complete cell lysis. Absorbance values were measured using iMARK microplate reader (Bio-Rad) at 595 nm. Final absorption values were calculated by averaging each sample in triplicate after blank subtraction. Statistical analysis of the data was performed by using one-way analysis of variance (ANOVA).

ROS determination

Intracellular reactive oxygen species (ROS) were determined using the fluorescent probe 2',7'– dichlorofluorescein diacetate, acetyl ester (CM-H2 DCFDA; Molecular Probes), a cell-permeant indicator for ROS that becomes fluorescent upon removal of the acetate groups by cellular esterases and oxidation. SH- SY5Y cells were plated on 96-well plates at a density of10000 cells/well and exposed for 48 h to the α- synuclein samples. Then, 10 μM DCFDA in DMEM without phenol red was added to each well. The fluorescence values at 538 nm were detected after 30 min by Fluoroscan Ascent FL (Thermo-Fisher). Cells were also treated with the corresponding concentrations of extract used in the aggregation of α-synuclein and ROS levels resulted similar to that of untreated control cells. Statistical analysis of the data was performed by using one-way analysis of variance (ANOVA).

Confocal imaging

Subconfluent SH-SY5Y cells grown on glass coverslips were exposed for 48 h to 5 μM (monomer concentration) α-synuclein aggregates grown in the presence or in the absence of cowpea extract at differentmolar ratios (1:0.5, E0.5; 1:1, E1). Cell membrane labelling was performed by incubating the cells with 10 ng/ml Alexa Fluor 488-conjugated CTX-B (Cholera toxin B-subunit) in cold complete medium for 30 min atroom temperature. Then, cells were fixed in 2.0% buffered paraformaldehyde for 6 min and permeabilizedby treatment with a 1:1 acetone/ethanol solution for 4 min at room temperature, washed with PBS and blockedwith PBS containing 0.5% BSA and 0.2% gelatin. Afterincubation for 1 h at room temperature with rabbit anti-

synuclein polyclonal antibody (1:600 in blocking solution), the cells were washed with PBS for 30 min under stirring and then incubated with Alexa Fluor 568- conjugated anti-rabbit secondary antibody (MolecularProbes) diluted 1:100 in PBS. Finally, cells were washed twice in PBS and once in distilled water toremove non-specifically bound antibodies. Digital images were taken with a confocal Leica TCS SP8 scanning microscope (Leica, Mannheim, Ge) equipped with a HeNe/Ar laser source for fluorescence measurements. The observations were performed usinga Leica HC PL Apo CS2 X63 oil immersion objective.

Drosophila melanogaster **methods**

Fly husbandry and supplementation and longevityassay

Wild type *Drosophila melanogaster* (Canton S) was kindly provided by Dr Daniela Grifoni (University of Bologna, Italy). Flies were maintained at constant temperature (25°C) and humidity (60%) with a 12/12 h light–dark cycle. Flies were reared on Formula 4-24 ® media (Carolina Biological, Burlington, NC, USA). Thecomposition of this diet, as indicated by the manufacturer, is as follows: oat flour, soy flour, wheat flour, other starches, dibasic calcium phosphate, calcium carbonate, citric acid, niocinamide, riboflavin, sodium chloride, sodium iron pyrophosphate, sucrose, thiamine, mononitrate, brewer's yeast, emulsifierpreservatives, mold inhibitor, food coloring. The Formula 4-24 diet requires separate application of yeast pellets (*Saccharomyces cerevisiae*) and saturation of this dry media mixture with water. After eclosion, malesand females emerged within 1-2 day were allowed to mate freely for two days before female separation into vials containing 1 g Formula 4-24 Instant Drosophila Medium (Carolina) soaked with 4 ml water containing 0.5% or 0.2% bean extract. A total of 20 flies were placed in each vial.

Female flies emerging within a 2-day period were collected under FlyNap (Carolina) anaesthesia. A totalof 600 fruit flies were divided into 3 groups: control group, flies supplemented with 0.2% bean extract and flies supplemented with 0.5% bean extract. Flies were transferred into vials containing fresh food every 2-3 days and the number of living flies was counted. This was repeated until all flies had died. Kaplan- Meier survival curves were generated for lifespan assessment.

Measurement of Drosophila body weights

Changes in body weights were used as an indicator of the food intake. Flies were fed on standard diet with andwithout bean extract for 30 or 45 days. For each condition (0.2% bean extract supplementation and

control), five vials containing 20 flies/vial were counted.

Flies in each group were anesthetized by FlyNap (Carolina) and then weighed on a balance. The mean body weights of the flies in each group were calculated.

Gene expression analysis
Total RNA was extracted from the whole bodies of either30 days or 45 days old flies belonging to the 0.2% groupby using RNeasy Mini Kit (QIAGEN GmbH, Hilden, Germany). The 0.2% supplementation has been chosen because it was the one able to significantly increase lifespan in *Drosophila*. All the experiments were performed in triplicate. The yield and purity of the RNAwere measured using NanoVue Spectrophotometer (GE Healthcare, Milano, Italy). Only samples with density ratios A260/A280>1.8 were used. cDNA was obtained byreverse transcribing mRNA starting from 1 μg of total RNA using iScript cDNA Synthesis Kit (BIO-RAD, Hercules, CA, USA), following the manufacturer's protocol. The subsequent polymerase chain reaction (PCR) was performed in a total volume of 10 μl containing 2.5 μl (12.5 ng) of cDNA, 5 μl SsoAdvancedUniversal SYBR Green Supermix (BIO-RAD), 2 μl of dH20 RNA free and 0.5 μl (500 nM) of each primer. Theprimers used are reported in Supplementary Table 4 andRPL32 was used as reference gene.

Protein extraction and immunoblotting
Proteins were isolated from the whole bodies of either 30-or 45-day old flies. Proteins were homogenized using lysis buffer (7 M urea, 2 M thiourea, 4% CHAPS, 60 mMdithiothreitol (DTT), 0.002% bromophenol blue) andcentrifuged at 12000 g at 4 °C for 5 min. The supernatantwas collected and mixed with Sample Buffer, Laemmli 2× Concentrate (Sigma Aldrich). Proteins were then loaded onto 4-20% SDS-PAGE gels followed by transfer onto nitrocellulose membranes and immunoblotted with appropriate antibodies. Anti-Sirt1 (1:1000; Cell SignalingTechnology, Beverly, MA), anti-dFoxO (1:1000, Covalab, Villeurbanne, France) and anti-β-actin (1:2000,Invitrogen Carlsbad, CA, USA) antibodies were used as primary antibodies. The HRP-conjugated anti-mouse IgG and anti-rabbit IgG antibodies were employed as the secondary antibodies (1:10000; Cell SignalingTechnology). Targeted proteins were visualized using Clarity[TM] Western ECL Substrate (BIO-RAD). Densitometric analysis of specific immunolabeled bands was performed using ImageJ software.

Statistical analysis
Each experiment was performed at least three times, and all values are represented as means ± SD. One-way ANOVA was used to compare differences among groups followed by Dunnett's (Prism 5; GraphPad

Software, San Diego, CA). Values of p<0.05 were considered statistically significant. Survival curves wereprepared by Kaplan-Meier survival analysis and analyzed using the OASIS2 software [60].

Caenorhabditis elegans methods

C. elegans strains and treatment with *V. unguiculata*extract
Standard procedures for *C. elegans* strain maintenance were followed [61]. The strain used in this study, JZF142 [*pdat-1::hαSyn; pdat-1::DsRed*], was kindly provided by Prof. J. Feng (Case Western Reserve University, US) [45]. The *C. elegans* strain was grown on Nematode Growth Medium (NGM) containing agar, seeded with *E.coli* OP50 at 20°C. Lyophilized extract from *V. unguiculata* was solubilized in sterile distilled water at two dilutions, 2% or 5% w/V, and sterilized with 0.22μm filter. α-synuclein expressing animals wereexposed to the following treatments: 0.2% or 0.5% of *V.unguiculata* extract, water as negative control (mock) and 3 mM valproic acid (VA) as positive control [46]. *C. elegans* animals at L4 developmental stage were transferred into 12-well plates with NGM agar containing the different conditions as quadruplicates and allowed to become adults and lay eggs. After 14 hours the adults were discarded and the synchronized F1 progeny was allowed to grow in the presence of chronic treatments. F1 animals have been transferred every 3 days on new plates with treatment, until the day of analysis, to maintain them well fed and separated from the next generation.

The morphology of the four cephalic dopaminergic neurons (CEP neurons) in the F1 treated animals was scored at 6 days post adult stage. The neurodegeneration analysis was performed also on untreated animals at young adult and at 6 days post- adult stage. Animals were mounted and anesthetizedwith 0.01% tetramisole hydrochloride on 4% agar pads. The neurodegeneration analysis was performed using Zeiss Axioskop microscope (Carl Zeiss). All imageswere obtained using a Leica SP2 confocal laserscanning microscope (Leica). The spectra used for imaging DsRed were: λ excitation=543 nm and λ emission=580-630 nm. GraphPad Prism software was used for statistical analysis. The statistical significance was determined using Mann Whitney test or One-way ANOVA with Kruskal–Wallis post-test. Data are reported as averages of multiple observations ± SEM.

AUTHOR CONTRIBUTIONS

on *V. unguiculata* extract. F.T., L.L., R.M. performed experiments in yeast cells. M.L. performed *in vitro* assays on α-synuclein and experiments on neuroblastoma cells. D.B. performed experiments in
D. melanogaster. G.O. performed experiments in *C. elegans*. M.B. conceived and provided materials for the experiments and participated to manuscriptpreparation. C.A., D.B. and S.H. designed experiments in *D. melanogaster* and participated to manuscript preparation. E.D.S. designed experiments in *C.elegans* and participated to manuscript preparation.
M.L. got founding and participated to manuscript preparation. P.C. and F.T. designed experiments in yeast cells and wrote the paper. P.C. coordinated the project.

CONFLICTS OF INTEREST

The authors have declared no conflicts of interest.

REFERENCES

1. Barzilai N, Bartke A. Biological approaches tomechanistically understand the healthy life spanextension achieved by calorie restriction andmodulation of hormones. J Gerontol A Biol Sci Med Sci.2009; 64:187–91. https://doi.org/10.1093/gerona/gln061 PMID:19228789

2. Cox LS, Mattison JA. Increasing longevity through caloric restriction or rapamycin feeding in mammals: common mechanisms for common outcomes? Aging Cell. 2009; 8:607–13. https://doi.org/10.1111/j.1474-9726.2009.00509.x PMID:19678809

3. Masoro EJ. Overview of caloric restriction and ageing.Mech Ageing Dev. 2005; 126:913–22. https://doi.org/10.1016/j.mad.2005.03.012 PMID:15885745

4. Piper MD, Bartke A. Diet and aging. Cell Metab. 2008;8:99–104. https://doi.org/10.1016/j.cmet.2008.06.012 PMID:18680711

5. López-Otín C, Galluzzi L, Freije JM, Madeo F, Kroemer G.Metabolic control of longevity. Cell. 2016; 166:802–21. https://doi.org/10.1016/j.cell.2016.07.031 PMID:27518560

6. Mirzaei H, Suarez JA, Longo VD. Protein and aminoacid restriction, aging and disease: from yeast tohumans. Trends Endocrinol Metab. 2014; 25:558–66. https://doi.org/10.1016/j.tem.2014.07.002 PMID:25153840

7. Wahl D, Solon-Biet SM, Cogger VC, Fontana L, SimpsonSJ, Le Couteur DG, Ribeiro RV. Aging, lifestyle anddementia. Neurobiol Dis. 2019; 130:104481. https://doi.org/10.1016/j.nbd.2019.104481 PMID:31136814

8. Fontana L, Partridge L, Longo VD. Extending healthy life span—from yeast to humans. Science. 2010; 328:321–26. https://doi.org/10.1126/science.1172539 PMID:20395504

9. Longo VD, Shadel GS, Kaeberlein M, Kennedy B.Replicative and chronological aging in saccharomycescerevisiae. Cell Metab. 2012; 16:18–31. https://doi.org/10.1016/j.cmet.2012.06.002 PMID:22768836

10. Fontana L, Partridge L. Promoting health and longevitythrough diet: from model organisms to humans. Cell. 2015; 161:106–18.

https://doi.org/10.1016/j.cell.2015.02.020 PMID:25815989

1. Templeman NM, Murphy CT. Regulation ofreproduction and longevity by nutrient-sensingpathways. J Cell Biol. 2018; 217:93–106. https://doi.org/10.1083/jcb.201707168 PMID:29074705

2. Dodel R, Csoti I, Ebersbach G, Fuchs G, Hahne M, KuhnW, Oechsner M, Jost W, Reichmann H, Schulz JB. Lewybody dementia and Parkinson's disease with dementia.J Neurol. 2008 (Suppl 5); 255:39–47. https://doi.org/10.1007/s00415-008-5007-0 PMID:18787881

3. de Rijk MC, Launer LJ, Berger K, Breteler MM, Dartigues JF, Baldereschi M, Fratiglioni L, Lobo A, Martinez-Lage J, Trenkwalder C, Hofman A. Prevalence of Parkinson's disease in Europe: a collaborative study of population-based cohorts. Neurologic diseases in the elderly research group. Neurology. 2000; 54:S21–23. PMID:10854357

4. Van Den Eeden SK, Tanner CM, Bernstein AL, Fross RD,Leimpeter A, Bloch DA, Nelson LM. Incidence ofParkinson's disease: variation by age, gender, andrace/ethnicity. Am J Epidemiol. 2003; 157:1015–22. https://doi.org/10.1093/aje/kwg068 PMID:12777365

5. Lázaro DF, Pavlou MA, Outeiro TF. Cellular models astools for the study of the role of alpha-synuclein inParkinson's disease. Exp Neurol. 2017; 298:162–71. https://doi.org/10.1016/j.expneurol.2017.05.007 PMID:28526239

6. Fruhmann G, Seynnaeve D, Zheng J, Ven K,Molenberghs S, Wilms T, Liu B, Winderickx J, Franssens V. Yeast buddies helping to unravel the complexity ofneurodegenerative disorders. Mech Ageing Dev. 2017;161:288–305. https://doi.org/10.1016/j.mad.2016.05.002 PMID:27181083

7. Sampaio-Marques B, Pereira H, Santos AR, Teixeira A,Ludovico P. Caloric restriction rescues yeast cells fromalpha-synuclein toxicity through autophagic control ofproteostasis. Aging (Albany NY). 2018; 10:3821–33. https://doi.org/10.18632/aging.101675 PMID:30530923

8. Sampaio-Marques B, Guedes A, Vasilevskiy I, Gonçalves S, Outeiro TF, Winderickx J, Burhans WC, Ludovico P. A-synuclein toxicity in yeast and human cells is caused by cell cycle re-entry and autophagy degradation of ribonucleotide reductase 1. Aging Cell.2019; 18:e12922. https://doi.org/10.1111/acel.12922 PMID:30977294

1. Tenreiro S, Franssens V, Winderickx J, Outeiro TF. Yeastmodels of Parkinson's disease-associated molecular pathologies. Curr Opin Genet Dev. 2017; 44:74–83. https://doi.org/10.1016/j.gde.2017.01.013 PMID:28232272

2. Toth ML, Melentijevic I, Shah L, Bhatia A, Lu K, TalwarA, Naji H, Ibanez-Ventoso C, Ghose P, Jevince A, Xue J,Herndon LA, Bhanot G, et al. Neurite sprouting andsynapse deterioration in the aging caenorhabditiselegans nervous system. J Neurosci. 2012; 32:8778–90. https://doi.org/10.1523/JNEUROSCI.1494-11.2012 PMID:22745480

3. Lakso M, Vartiainen S, Moilanen AM, Sirviö J, ThomasJH, Nass R, Blakely RD, Wong G. Dopaminergicneuronal loss and motor deficits in caenorhabditiselegans overexpressing human alpha-synuclein. JNeurochem. 2003; 86:165–72. https://doi.org/10.1046/j.1471-4159.2003.01809.x PMID:12807436

4. Domínguez-Perles R, Carnide V, Marques G, de CastroI, de Matos M, Carvalho M, Rosa E. Relevance, constraints and perspectives of cowpea crops in the Mediterranean Basin. Legum Perspect. 2015; 10:40–2.

5. Phillips RD, McWatters KH, Chinnan MS, Hung YC,Beuchat LR, Sefa-Dedeh S, Sakyi-Dawson E, Ngoddy P,Nnanyelugo D, Enwere J, Komey NS, Liu K, Mensa-Wilmot Y, et al. Utilization of cowpeas for human food.Field Crops Res. 2003; 82:193–213. https://doi.org/10.1016/S0378-4290(03)00038-8

6. Gonçalves A, Goufo P, Barros A, Domínguez-Perles R,Trindade H, Rosa EA, Ferreira L, Rodrigues M. Cowpea(vigna unguiculata L. Walp), a renewed multipurposecrop for a more sustainable agri-food system:nutritional advantages and constraints. J Sci FoodAgric. 2016; 96:2941–51. https://doi.org/10.1002/jsfa.7644 PMID:26804459

7. Xiong S, Yao X, Li A. Antioxidant Properties of Peptide from Cowpea Seed. Int J Food Prop. 2013; 16:1245–56. https://doi.org/10.1080/10942912.2011.582976

8. Thangadurai D. Chemical composition and nutritionalpotential of vigna unguiculata ssp. Cylindrica(fabaceae). J Food Biochem. 2005; 29:88–98. https://doi.org/10.1111/j.1745-4514.2005.00014.x

9. Conti MV, Campanaro A, Coccetti P, De Giuseppe R,Galimberti A, Labra M, Cena H. Potential role ofneglected and underutilized plant species in improvingwomen's empowerment and nutrition in areas of sub-Saharan Africa. Nutr Rev. 2019: 77:817-28. https://doi.org/10.1093/nutrit/nuz038 PMID:31313806

10. Awika JM, Duodu KG. Bioactive polyphenols andpeptides in cowpea (Vigna unguiculata) and their

health promoting properties: A review. J Funct Foods.2017; 38:686–97. https://doi.org/10.1016/j.jff.2016.12.002

1. Coccetti P, Nicastro R, Tripodi F. Conventional andemerging roles of the energy sensor Snf1/AMPK in*Saccharomyces cerevisiae*. Microb Cell. 2018; 5:482–94. https://doi.org/10.15698/mic2018.11.655 PMID:30483520

2. Dodig S, Čepelak I, Pavić I. Hallmarks of senescence andaging. Biochem Med (Zagreb). 2019; 29:030501. https://doi.org/10.11613/BM.2019.030501 PMID:31379458

3. Beckman KB, Ames BN. The free radical theory of agingmatures. Physiol Rev. 1998; 78:547–81. https://doi.org/10.1152/physrev.1998.78.2.547 PMID:9562038

4. Frankel S, Ziafazeli T, Rogina B. dSir2 and longevity indrosophila. Exp Gerontol. 2011; 46:391–96. https://doi.org/10.1016/j.exger.2010.08.007 PMID:20728527

5. Horvath M, Mihajlovic Z, Slaninova V, Perez-Gomez R,Moshkin Y, Krejci A. The silent information regulator 1(Sirt1) is a positive regulator of the notch pathway indrosophila. Biochem J. 2016; 473:4129–43. https://doi.org/10.1042/BCJ20160563 PMID:27623778

6. Alic N, Giannakou ME, Papatheodorou I, HoddinottMP, Andrews TD, Bolukbasi E, Partridge L. Interplay ofdFOXO and two ETS-family transcription factorsdetermines lifespan in drosophila melanogaster. PLoSGenet. 2014; 10:e1004619. https://doi.org/10.1371/journal.pgen.1004619 PMID:25232726

7. Casamenti F, Stefani M. Olive polyphenols: newpromising agents to combat aging-associated neurodegeneration. Expert Rev Neurother. 2017;17:345–58. https://doi.org/10.1080/14737175.2017.1245617 PMID:27762153

8. Modi KK, Roy A, Brahmachari S, Rangasamy SB, Pahan K. Cinnamon and its metabolite sodium benzoateattenuate the activation of p21rac and protectmemory and learning in an animal model ofAlzheimer's disease. PLoS One. 2015; 10:e0130398. https://doi.org/10.1371/journal.pone.0130398 PMID:26102198

9. Liu W, Ma H, DaSilva NA, Rose KN, Johnson SL, Zhang L,Wan C, Dain JA, Seeram NP. Development of aneuroprotective potential algorithm for medicinalplants. Neurochem Int. 2016; 100:164–77. https://doi.org/10.1016/j.neuint.2016.09.014 PMID:27693453

1. Malishev R, Shaham-Niv S, Nandi S, Kolusheva S, GazitE, Jelinek R. bacoside-A, an Indian traditional-medicine substance, inhibits β-amyloid cytotoxicity, fibrillation,and membrane interactions. ACS Chem Neurosci.2017; 8:884–91. https://doi.org/10.1021/acschemneuro.6b00438 PMID:28094495

2. Rajan KE, Preethi J, Singh HK. Molecular and functionalcharacterization of bacopa monniera: a retrospective review. Evid Based Complement Alternat Med. 2015; 2015:945217. https://doi.org/10.1155/2015/945217 PMID:26413131

3. Lobbens ES, Breydo L, Skamris T, Vestergaard B, JägerAK, Jorgensen L, Uversky V, van de Weert M.Mechanistic study of the inhibitory activity of geumurbanum extract against α-synuclein fibrillation.Biochim Biophys Acta. 2016; 1864:1160–69. https://doi.org/10.1016/j.bbapap.2016.06.009 PMID:27353564

4. Sampaio-Marques B, Felgueiras C, Silva A, RodriguesM, Tenreiro S, Franssens V, Reichert AS, Outeiro TF, Winderickx J, Ludovico P. SNCA (α-synuclein)-inducedtoxicity in yeast cells is dependent on sirtuin 2 (Sir2)-mediated mitophagy. Autophagy. 2012; 8:1494–509. https://doi.org/10.4161/auto.21275 PMID:22914317

5. Bucciantini M, Nosi D, Forzan M, Russo E, Calamai M,Pieri L, Formigli L, Quercioli F, Soria S, Pavone F,Savistchenko J, Melki R, Stefani M. Toxic effects ofamyloid fibrils on cell membranes: the importance ofganglioside GM1. FASEB J. 2012; 26:818–31. https://doi.org/10.1096/fj.11-189381 PMID:22071505

6. Palazzi L, Bruzzone E, Bisello G, Leri M, Stefani M, Bucciantini M, Polverino de Laureto P. Oleuropein aglycone stabilizes the monomeric α-synuclein andfavours the growth of non-toxic aggregates. Sci Rep. 2018; 8:8337. https://doi.org/10.1038/s41598-018-26645-5 PMID:29844450

7. Palazzi L, Leri M, Cesaro S, Stefani M, Bucciantini M,Polverino de Laureto P. Insight into the molecularmechanism underlying the inhibition of α-synucleinaggregation by hydroxytyrosol. Biochem Pharmacol.2020; 173:113722. https://doi.org/10.1016/j.bcp.2019.113722 PMID:31756328

8. Cao P, Yuan Y, Pehek EA, Moise AR, Huang Y,Palczewski K, Feng Z. Alpha-synuclein disrupteddopamine homeostasis leads to dopaminergic neurondegeneration in caenorhabditis elegans. PLoS One.2010; 5:e9312. https://doi.org/10.1371/journal.pone.0009312 PMID:20174477

1. Kautu BB, Carrasquilla A, Hicks ML, Caldwell KA, Caldwell GA. Valproic acid ameliorates C. Elegans dopaminergic neurodegeneration with implications for ERK-MAPK signaling. Neurosci Lett. 2013; 541:116–19. https://doi.org/10.1016/j.neulet.2013.02.026 PMID:23485787

2. Jayathilake C, Visvanathan R, Deen A, Bangamuwage R, Jayawardana BC, Nammi S, Liyanage R. Cowpea: an overview on its nutritional facts and health benefits. J Sci Food Agric. 2018; 98:4793–806. https://doi.org/10.1002/jsfa.9074 PMID:29656381

3. Greer EL, Oskoui PR, Banko MR, Maniar JM, Gygi MP, Gygi SP, Brunet A. The energy sensor AMP-activated protein kinase directly regulates the mammalian FOXO3 transcription factor. J Biol Chem. 2007; 282:30107–19. https://doi.org/10.1074/jbc.M705325200 PMID:17711846

4. Brunet A, Sweeney LB, Sturgill JF, Chua KF, Greer PL, Lin Y, Tran H, Ross SE, Mostoslavsky R, Cohen HY, Hu LS, Cheng HL, Jedrychowski MP, et al. Stress-dependent regulation of FOXO transcription factors by the SIRT1 deacetylase. Science. 2004; 303:2011–15. https://doi.org/10.1126/science.1094637 PMID:14976264

5. Jiang Y, Yan F, Feng Z, Lazarovici P, Zheng W. Signaling network of forkhead family of transcription factors (FOXO) in dietary restriction. Cells. 2019; 9:100. https://doi.org/10.3390/cells9010100 PMID:31906091

6. Fontana L, Nehme J, Demaria M. Caloric restriction and cellular senescence. Mech Ageing Dev. 2018; 176: 19–23. https://doi.org/10.1016/j.mad.2018.10.005 PMID:30395873

7. Wrasidlo W, Tsigelny IF, Price DL, Dutta G, Rockenstein E, Schwarz TC, Ledolter K, Bonhaus D, Paulino A, Eleuteri S, Skjevik ÅA, Kouznetsova VL, Spencer B, et al. A de novo compound targeting α-synuclein improves deficits in models of Parkinson's disease. Brain. 2016; 139:3217–36. https://doi.org/10.1093/brain/aww238 PMID:27679481

8. Perni M, Galvagnion C, Maltsev A, Meisl G, Müller MB, Challa PK, Kirkegaard JB, Flagmeier P, Cohen SI, Cascella R, Chen SW, Limbocker R, Sormanni P, et al. A natural product inhibits the initiation of α-synuclein aggregation and suppresses its toxicity. Proc Natl Acad Sci USA. 2017; 114:E1009–17. https://doi.org/10.1073/pnas.1610586114 PMID:28096355

9. Braak H, de Vos RA, Bohl J, Del Tredici K. Gastric alpha-synuclein immunoreactive inclusions in Meissner's and Auerbach's plexuses in cases staged for Parkinson's disease-related brain pathology. Neurosci Lett. 2006; 396:67–72. https://doi.org/10.1016/j.neulet.2005.11.012 PMID:16330147

1. Shannon KM, Keshavarzian A, Dodiya HB, Jakate S, Kordower JH. Is alpha-synuclein in the colon a biomarker for premotor Parkinson's disease? evidence from 3 cases. Mov Disord. 2012; 27:716–19. https://doi.org/10.1002/mds.25020 PMID:22550057

2. Guzzetti L, Fiorini A, Panzeri D, Tommasi N, Grassi F, Taskin E, Misci C, Puglisi E, Tabaglio V, Galimberti A, Labra M. Sustainability perspectives of Vigna unguiculata L. Walp. Cultivation under no tillage and water stress conditions. Plants (Basel). 2019; 9:48. https://doi.org/10.3390/plants9010048 PMID:31905903

3. Tedeschi G, Albani E, Borroni EM, Parini V, Brucculeri AM, Maffioli E, Negri A, Nonnis S, Maccarone M, Levi-Setti PE. Proteomic profile of maternal-aged blastocoel fluid suggests a novel role for ubiquitin system in blastocyst quality. J Assist Reprod Genet. 2017; 34:225–38. https://doi.org/10.1007/s10815-016-0842-x PMID:27924460

4. Vizcaíno JA, Csordas A, del-Toro N, Dianes JA, Griss J, Lavidas I, Mayer G, Perez-Riverol Y, Reisinger F, Ternent T, Xu QW, Wang R, Hermjakob H. 2016 update of the PRIDE database and its related tools. Nucleic Acids Res. 2016; 44:D447–56. https://doi.org/10.1093/nar/gkv1145 PMID:26527722

5. LeVine H 3rd. Quantification of beta-sheet amyloid fibril structures with thioflavin T. Methods Enzymol. 1999; 309:274–84. https://doi.org/10.1016/s0076-6879(99)09020-5 PMID:10507030

6. Yang JS, Nam HJ, Seo M, Han SK, Choi Y, Nam HG, Lee SJ, Kim S. OASIS: online application for the survival analysis of lifespan assays performed in aging research. PLoS One. 2011; 6:e23525. https://doi.org/10.1371/journal.pone.0023525 PMID:21858155

7. Brenner S. The genetics of Caenorhabditis elegans. Genetics. 1974; 77:71–94. PMID:4366476
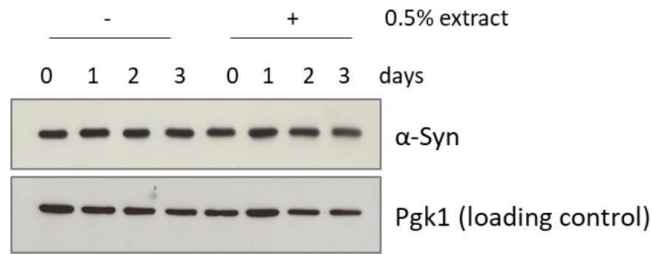
Supplementary Figures
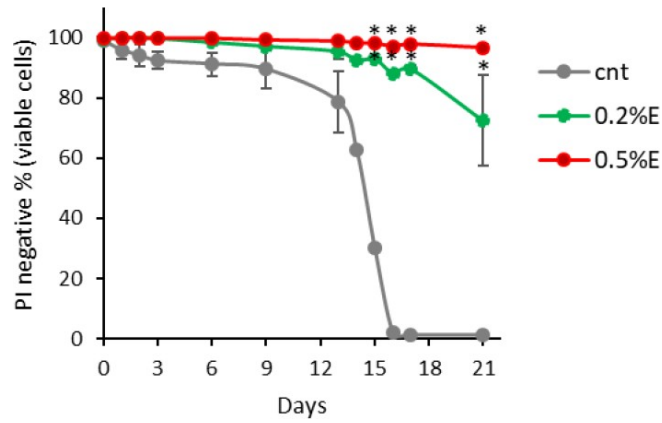
Supplementary Figure 1. The effect of cowpea extract is synergistic with caloric restriction. CLS of yeast wt cells grown in SD medium containing 0.5% glucose in the absence or presence of 0.2% or 0.5% extract of *Vigna unguiculata*. *p<0.05 relative to control cells.
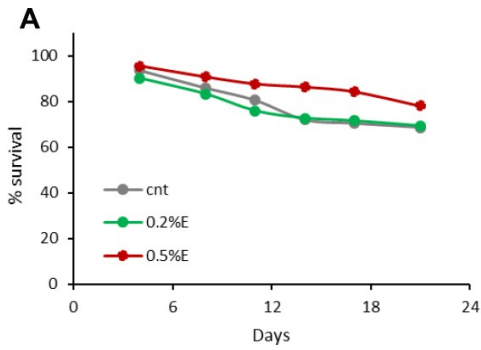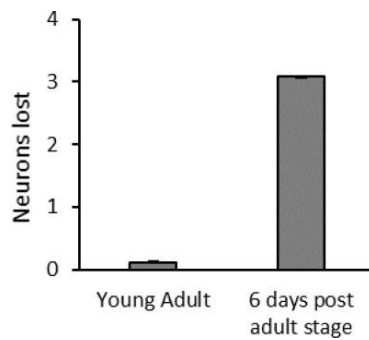

| Condition	P-value
CTRL_F v.s. 0.5% bean_F	0.0032
CTRL_F v.s. 0.2% bean_F	0.9985
0.5% bean_F v.s. 0.2% bean_F	0.0032

Supplementary Figure 2. Survivorship of adult female *D. melanogaster*. (**A**) Flies have been supplemented with 0.2 and 0.5% cowpea extract lifelong. Data are presented as percentage survival of flies as function of time (in days). (**B**) Analysis of the survivorship data with log-rank test using the online application for the survival analysis of life-span assays OASIS.

Supplementary Figure 3. α-synuclein level is unchanged but it is differently localized in the presence of cowpea extract in yeast cells. Western blot analysis is using anti-synuclein antibody in wt [pYX242-SNCA] cells after 5h, 1 day, 2 days, 3 days treatment with 0.5% *V. unguiculata* extract. Pgk1 was used as loading control.

Supplementary Figure 4. α-synuclein causes age-related dopaminergic neurons lost in *C.elegans*. Number of nonvisible CEP dopaminergic neurons in human α-synuclein expressing strain. In a wild type strain four CEP neurons expressing DsRed are always visible (not shown). In young adults almost no neurodegeneration is visible, while 6 days after adult stage a mean of 3 neurons is lost (p<0.0001 Mann- Whitney non parametric test). Error bars represent the SEM for two independent experiments. The number of young adult animals scored is 100, while after 6 days post adult stage is 91.
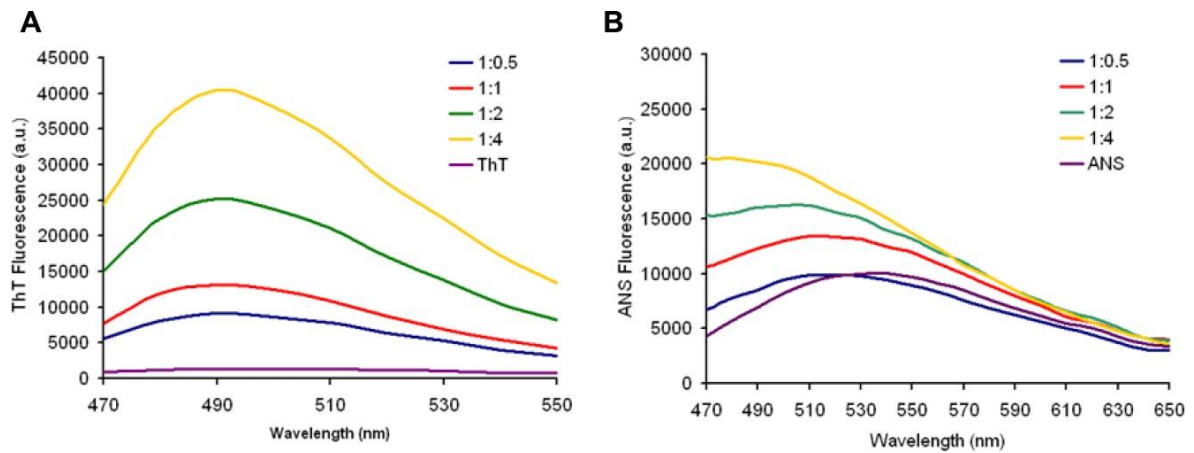
Supplementary Figure 5. Extract interferences on ThT and ANS fluorescence.

Supplementary Tables

Supplementary Table 1. Metabolite content in extracts of *P. vulgaris*, *C. cajan* and *V. unguiculata*, analysed byGC/MS. Relative amounts of each metabolite are referred to *Phaseolus vulgaris* content, which was set to 1.

	Phaseolus vulgaris	*Cajanus cajan*	*Vigna unguiculata*
aa and bases			
glycine	1.00	1.07	2.66
L-leucine	1.00	0.49	2.90
L-threonine	1.00	0.00	10.74
L-alanine	1.00	0.80	2.72
L-proline	1.00	34.35	3.94
L-asparagine	1.00	0.63	52.44
L-aspartic acid	1.00	1.55	1.05
hypoxanthine	absent	absent	present
D-pyroglutamic acid	1.00	3.93	3.17
methylthiouracil	1.00	1.11	2.40
glycolysis/fermentation and TCA			
citric acid	1.00	1.90	2.25
malic acid	1.00	0.11	0.17
lactic acid	1.00	0.98	4.60
fatty acids			
glycerol	1.00	0.71	3.28
linolealidic acid	1.00	5.33	8.41
linolenic acid	1.000	0.162	2.663
stearic acid	1.000	0.968	1.342
palmitic acid	1.000	0.779	1.209
other organic acids			
D-pipecolic acid	1.00	0.78	absent
2-pentenedioic acid	1.00	1.34	1.14
2-thiobarbituric acid	1.00	0.66	0.29
L-dihydroorotic acid	1.00	0.62	0.84
glycolic acid	1.00	1.13	1.01
D-pipecoli acid	1.00	0.69	0.00
hydracrylic acid	1.00	6.98	1.05
butenoic acid	1.00	2.46	9.71
2-pyrrolidinone-5-carboxylic acid	1.00	1.18	0.43
others			
methyl-amino acetate	1.000	0.013	0.218
acetamide	1.000	0.577	18.533
triazol-3-amine	1.000	0.910	2.026
maltol	1.000	1.291	1.125
2-mercaptophenol	1.000	1.108	1.276
urea	1.000	very low	3.444

Supplementary Table 2. Identified analytes by GC/MSand target ion used to measure the peak area.

Analytes	Target ion (m/z)
glycine	246
L-leucine	200
L-threonine	404
L-alanine	232
L-proline	184
L-asparagine	417
L-aspartic acid	418
hypoxanthine	307
D-pyroglutamic acid	300
methylthiouracil	313
Citric acid	459
Malic acid	419
DL-glyceraldehyde	115
Lactic acid	261
glycerol	377
Linolealidic acid	337
Linolenic acid	335
Stearic acid	341
Palmitic acid	313
D-pipecolic acid	186
2-pentendioic acid	315
2-thiobarbituric acid	429
L-dihydroorotic acid	443
Glycoli acid	247
2-pipecoli acid	186
Hydroacrylic acid	261
Butenoic acid	289
2-butenoic acid	273
2-pyrrolidinone-5-carboxylic acid	186
Methyl-amino-acetate	146
acetamide	116
Triazol-3-amine	213
maltol	183
2-mercaptophenol	297
urea	231

Supplementary Table 3. Yeast strains used in this study.

Strain	Genotype	Source
wt	*BY4742 MATα his3Δ1 leu2Δ0 lys2Δ0 ura3Δ0*	Euroscarf
snf1Δ	*BY4742 MATα his3Δ1 leu2Δ0 lys2Δ0 ura3Δ01 snf1::HPH*	This study
atg1Δ	*BY4742 MATα his3Δ1 leu2Δ0 lys2Δ0 ura3Δ01 atg1::KanMX*	This study
ras2Δ	*BY4742 MATα his3Δ1 leu2Δ0 lys2Δ0 ura3Δ01 ras2::KanMX*	This study
tor2Δ	*BY4742 MATα his3Δ1 leu2Δ0 lys2Δ0 ura3Δ01 tor2::KanMX*	This study
wt [empty]	*BY4742 MATα his3Δ1 leu2Δ0 lys2Δ0 ura3Δ0 [pYX242]*	This study
wt [αSyn]	*BY4742 MATα his3Δ1 leu2Δ0 lys2Δ0 ura3Δ0 [pYX242-SNCA]*	This study

Supplementary Table 4. List of primers for real-time PCR.

Gene	5'-Forward-3'	5'-Reverse-3'
Sirt1	CATTATGCCGCATTTCGCCA	GAAGGTGTTCACTGAGGCCA
Foxo	AGGCTGACCCACACAGATAAC	GGCTCCACAAAGTTTTCGGG
Notch	CGCTTCCTGCACAAGTGTC	GCGCAGTAGGTTTTGCCATT
HO	ATGTCAGCGAGCGAAGAAACA	TGGCTTTACGCAACTCCTTTG
Trxr	TGGATCTGCGCGACAAGAAAG	GAAGGTCTGGGCGGTGATTG
RPL32	GCCCACCGGATTCAAGAAGT	CTTGCGCTTCTTGGAGGAGA

Methionine Supplementation Affects Metabolism and Reduces Tumor Aggressiveness in Liver Cancer Cells

Farida Tripodi [1,*], Beatrice Badone [1], Marta Vescovi [1], Riccardo Milanesi [1], Simona Nonnis [2,3], Elisa Maffioli [2], Marcella Bonanomi [1,4], Daniela Gaglio [4,5], Gabriella Tedeschi [2,3] and Paola Coccetti [1,*]

[1] Department of Biotechnology and Biosciences, University of Milano-Bicocca, 20126 Milan, Italy; beatrice.badone@unimib.it (B.B.); m.vescovi2@campus.unimib.it (M.V.); r.milanesi2@campus.unimib.it (R.M.); marcella.bonanomi@unimib.it (M.B.)

[2] DIMEVET–Department of Veterinary Medicine, University of Milano, 20133 Milan, Italy; simona.nonnis@unimi.it (S.N.); elisa.maffioli@unimi.it (E.M.); gabriella.tedeschi@unimi.it (G.T.)

[3] CRC "Innovation for Well-Being and Environment (IWE)", University of Milano, 20133 Milan, Italy

[4] SYSBIO.ISBE.IT, Centre of Systems Biology, 20126 Milan, Italy; daniela.gaglio@ibfm.cnr.it

[5] Institute of Molecular Bioimaging and Physiology (IBFM), National Research Council (CNR), Segrate, 20090 Milan, Italy

* Correspondence: farida.tripodi1@unimib.it (F.T.); paola.coccetti@unimib.it (P.C.); Tel.: +39-02-6448-3513/21 (F.T. & P.C.)

check for updates

Abstract: Liver cancer is one of the most common cancer worldwide with a high mortality. Methionine is an essential amino acid required for normal development and cell growth, is mainly metabolized in the liver, and its role as an anti-cancer supplement is still controversial. Here, we evaluate the effects of methionine supplementation in liver cancer cells. An integrative proteomic and metabolomic analysis indicates a rewiring of the central carbon metabolism, with an upregulation of the tricarboxylic acid (TCA) cycle and mitochondrial adenosine triphosphate (ATP) production in the presence of high methionine and AMP-activated protein kinase (AMPK) inhibition. Methionine supplementation also reduces growth rate in liver cancer cells and induces the activation of both the AMPK and mTOR pathways. Interestingly, in high methionine concentration, inhibition of AMPK strongly impairs cell growth, cell migration, and colony formation, indicating the main role of AMPK in the control of liver cancer phenotypes. Therefore, regulation of methionine in the diet combined with AMPK inhibition could reduce liver cancer progression.

Keywords: AMPK; TCA cycle; migration; growth; proteomics; metabolomics; HCC

1. Introduction

Liver cancer is the second leading cause of cancer-related death worldwide. Hepatocellular carcinoma (HCC) is the most common form of primary liver cancer and is associated with chronic liver damage, which can be caused by viral infections, such as hepatitis B virus (HBV) and hepatitis C virus (HCV) infection or by alcoholic liver diseases and non-alcoholic steatohepatitis (NASH). Potentially curative treatments for very early/early stage HCC patients include surgical resection, liver transplantation and percutaneous ablation. At an advanced/late stage surgery is no longer applicable, and the currently available therapies are effective only in small groups of patients [1–3]. Very few therapeutic options, with unsatisfactory antitumor effects and toxicity, are nowadays available, thus, prognosis remains very poor. In 2007 Sorafenib was the first VEGFR TKI (vascular endothelial growth factor receptor

(VEGFR)-tyrosine kinase inhibitor (TKI)) to be approved in advanced HCC, and it is used as standard treatment for patients who have no/mild cirrhosis. However, it gives a significant, but moderate improvement in median overall survival [4]. More recently, other drugs against HCC have been approved, such as Regorafenib, Lenvatinib, and Cabozantinib [4].

AMP-activated protein kinase (AMPK) is a heterotrimeric Ser/Thr protein kinase, highly conserved from yeast to humans. It functions as a sensor of the cellular energy status: in response to metabolic stress AMPK is activated by phosphorylation on a conserved threonine residue (T172), resulting in the upregulation of adenosine triphosphate (ATP)-producing pathways (catabolism) and in the downregulation of ATP-consuming pathways (anabolism), in order to restore energy homeostasis [5]. Downregulation of AMPK in several tumor tissues has been associated with the loss of control in tumorigenesis, cell cycle progression, proliferation and survival, invasion and metastasis, cancer metabolism, and drug resistance. However, its role in carcinogenesis is still controversial, being now considered a double-edged sword that can have either pro-tumor or anti-tumor functions depending on cellular and metabolic demand [6]. The catalytic AMPK-α2 subunit is frequently under-expressed in human HCC cells and inactivation of AMPK promotes hepato-carcinogenesis [7]. It was also found that patients with cirrhosis that present low AMPK phosphorylation had a significant higher incidence of HCC than patients with high phospho-AMPK levels [8]. In addition, low phospho-AMPK staining is correlated with aggressive clinicopathologic features and poor prognosis in patients with HCC [9]. For these reasons, the activation of AMPK in patients with liver cancer has been proposed as a clinical target. Metformin, the widely used anti-diabetics drug, is the most commonly used activator of AMPK, with well-documented pharmacokinetic and safety profiles [10]. However, clinical evaluation of metformin effectiveness alone, or in combination with Sorafenib, has given no clear results yet [11].

Liver is the organ where 50% of methionine metabolism and where 85% of all transmethylation reactions take place [12]. Methionine is an essential amino-acid, particularly abundant in animal food and seafood, but also in nuts, seeds, and cereals, while it is less abundant in fruits and vegetables [13]. In the liver, methionine is converted into S-adenosyl-methionine (SAM), an important cofactor for transmethylation reactions [14]. SAM is also involved in the trans-sulfuration pathway, particularly active in the liver to give cysteine biosynthesis, the rate-limiting precursor for glutathione (GSH) synthesis. SAM is also required for the synthesis of polyamines, small positively charged molecules involved in transcription, translation, cell growth, and death [15].

Methionine restriction is associated with the increase of lifespan in different models (yeast, *Drosophila*, human fibroblasts, rodents [13]) and to the inhibition of cell growth in different cancer cells, such as sarcoma, melanoma, prostate carcinoma, colorectal cancer cells in vitro, as well as in animal models [16].

In general, a different regulation should be assumed in liver cancer cells, considering the peculiar role of the liver in both the synthesis and in the degradation of methionine. SAM is synthesized by methionine adenosyl-transferase (MAT), encoded by two genes (MAT1A and MAT2A). MAT1A is expressed in adult differentiated liver, while MAT2A is expressed in extrahepatic tissues and fetal liver. Liver carcinogenesis is associated to a switch between MAT1A and MAT2A, with a consequent less efficient methionine metabolism, that enhances the capacity of hepatocytes and hepatoma cells to utilize nutrients for anabolic processes to support growth [17]. In addition, MAT1A and GNMT (glycine N-methyltransferase) knockout mice, with very low and very high SAM levels, respectively, spontaneously develop HCC, further supporting the crucial role of methionine-cycle homeostasis for this organ [12,18].

Strikingly, it was recently published that SAM supplementation inhibits liver cancer cell invasion in vitro [19] and decreases liver cancer formation in a mouse model [20]. Additionally, a quite old clinical trial on patients with alcoholic cirrhosis and less severe hepatic dysfunction demonstrated the beneficial role of SAM treatment, by increasing GSH levels and decreasing the probability of liver transplantation and death [21].

Thus, since methionine/SAM administration in liver seems to have an opposite role than in other cancer types, more studies are necessary to support a therapeutic role of methionine or SAM supplementation in patients.

Here, we investigate the effect of methionine supplementation in liver cancer cells in vitro, to explore the possibility that alterations in methionine dietary consumption could help treatment of liver cancer.

2. Materials and Methods

2.1. Cell Cultures

HepG2 liver cancer cells [22], SW480 colorectal cancer cells [23], A549 lung cancer cells [24], and MCF7 breast cancer cells [25] were obtained from ATCC. Huh7 liver cancer cells were provided by the Japanese Collection of Research Bioresources (JCRB) Cell Bank [26].

HepG2, Huh7, SW480 and A549 cells were cultured using RPMI1640 supplemented with 10% (*v/v*) FBS, 2 mM L-glutamine, 100 U/mL penicillin, and 100 µg/mL streptomycin. MCF7 were cultured using EMEM/NEAA supplemented with 10% (*v/v*) FBS, 2 mM L-glutamine, 100 U/mL penicillin, and 100 µg/mL streptomycin. Cells were maintained at 37 °C in a humidified 5% CO_2 incubator. Methionine was dissolved in water at 45 mg/mL and added at a final concentration of 1.5 mg/mL to RPMI1640 medium; in the control medium, the same amount of water was added. Compound C (Calbiochem, San Diego, CA, USA) was dissolved in DMSO and added to the medium at a final concentration of 2 µM for HepG2, SW480, A549, and MCF7 cells, and at 1.5 µM for Huh7 cells.

2.2. Growth Curves

1.5×10^5 cells were plated in 6 well plates, the day after the medium was changed (control medium, high methionine, Compound C or High methionine and Compound C). Cells were counted at $t = 0$, 48 h and 72 h.

2.3. Migration Assay

Cell migration was assessed using transwell permeable supports (Costar) with 8.0 µm filter membranes. Cells were treated with high methionine and/or Compound C for 24 h, and then serum starved for 24 h. 5×10^4 HepG2 cells and 3.5×10^4 Huh7 cells were resuspended in 100 µL of serum free medium (always in the presence or absence of high methionine and/or Compound C), plated onto each filter and 500 µL of complete medium (containing 10% FBS) were placed in the lower chamber. After 24 h, filters were washed, fixed and stained with 0.5% Coomassie brilliant blue (in 10% acetic acid, 45% methanol). Cells on the upper surface of the filters were removed with cotton swabs. Cells that had invaded to the lower surface of the filter were counted under the microscope.

2.4. Clonogenic Assay

A total of 2500 cells were plated in a 6 well plates, treated with high methionine and/or Compound C for 10–15 days (the medium was changed every 3–4 days). Then, colonies were fixed with 70% ethanol for 5 min, stained with 0.5% crystal violet in 10% ethanol for 15 min, finally, washed with water and manually counted.

2.5. Total Protein Extraction and Western Blot

Total cell extracts were prepared using RIPA buffer (50 mM Tris-HCl pH 7.5, 150 mM NaCl, 0.5% sodium deoxycholate, 1% NP40, 0.1% SDS), plus 1 mM PMSF (phenylmethanesulfonylfluoride), protease inhibitor cocktail (Roche, Indianapolis, IN) and phosphatase inhibitor cocktail (Sigma-Aldrich, St. Louis, MO, USA). Protein concentration was determined using the Bio-Rad protein assay. Western blot analysis was performed using anti-AMPK antibody (Cell Signaling), anti-phosphoT172-AMPK antibody (Cell Signaling), anti-vinculin antibody (Sigma-Aldrich), anti-phospho-T389-p70 S6K (Cell Signaling,

kindly provided by Evelina Gatti), anti-phospho79-Acc1 antibody (Cell Signaling), anti-Akt (Cell Signaling) anti-phosphoS473-Akt (Cell Signaling), anti-tubulin (Cell Signaling).

2.6. Small-Interfering RNA-Mediated Gene Silencing

To silence AMPK α/α', we used RNA interference by using small-interfering RNA (siRNA). Reverse transfection was performed on HepG2 and Huh7 cells with control siRNA (control siRNA-C, Santa Cruz Biotechnology) or siAMPKα/α' (Santa Cruz Biotechnology, Heidelberg, Germany) specific oligos by using the Lipofectamine 2000 reagent (Invitrogen, Carlsbad, CA, USA). AMPKα/α' expression was detected by immunoblotting to confirm the silencing achievement.

2.7. Shotgun Mass Spectrometry and Label Free Quantification

Four technical replicates were performed for each HepG2 sample, grown for 48 h in the presence or absence of high methionine and/or Compound C. Proteins were lysed in RapiGest 0.1% (RG, Waters Corporation, Milford, MA, USA), reduced with 13 mM DTE (30 min at 55 °C) and alkylated with 26 mM iodoacetamide (30 min at 23 °C). Protein digestion was performed using sequence-grade trypsin (Roche) for 16 h at 37 °C using a protein/trypsin ratio of 20:1. The proteolytic digested was desalted using Zip-Tip C18 (Millipore, Burlington, MA, USA) before MS analysis [27]. LC-ESI-MS/MS analysis was performed on a Dionex UltiMate 3000 HPLC System with a PicoFrit ProteoPrep C18 column (200 mm, internal diameter of 75 μm). Gradient: 2% ACN in 0.1% formic acid for 10 min, 2–4% ACN in 0.1% formic acid for 6 min, 4–30% ACN in 0.1% formic acid for 147 min, and 30–50% ACN in 0.1% formic for 3 min, at a flow rate of 0.3 μL/min. The eluate was electrosprayed into an LTQ OrbitrapVelos (Thermo Fisher Scientific, Bremen, Germany) through a Proxeon nanoelectrospray ion source (Thermo Fisher Scientific), as reported in [28]. The LTQ-Orbitrap was operated in positive mode in data-dependent acquisition mode to automatically alternate between a full scan (*m/z* 350–2000) in the Orbitrap (at resolution 60,000, AGC target 1,000,000) and subsequent CID MS/MS in the linear ion trap of the 20 most intense peaks from full scan (normalized collision energy of 35%). Data acquisition was controlled by Xcalibur 2.0 and Tune 2.4 software (Thermo Fisher Scientific).

A database search was conducted against the Homo Sapiens Uniprot sequence database (release 6 March 2019) with MaxQuant (version 1.6.0.1) software, using the following parameters: the initial maximum allowed mass deviation of 15 ppm for monoisotopic precursor ions and 0.5 Da for MS/MS peaks, trypsin enzyme specificity, a maximum of 2 missed cleavages, carbamidomethyl cysteine as fixed modification, N-terminal acetylation, methionine oxidation, asparagine/glutamine deamidation and serine/threonine/tyrosine phosphorylation as variable modifications. Quantification was performed using the built in XIC-based label-free quantification (LFQ) algorithm using fast LFQ [29]. False protein identifications (1%) were estimated by searching MS/MS spectra against the corresponding reversed-sequence (decoy) database. Statistical analysis was performed using the Perseus software (version 1.5.5.3, https://maxquant.net/perseus/). Only proteins present and quantified in at least 75% of the repeats were positively identified and used for statistical analysis. An ANOVA test (cut-off at 0.05 *p*-value) was carried out to identify proteins differentially expressed among the four conditions. Focusing on specific comparisons, proteins were considered differentially expressed if they were present only in one condition or showed significant *t*-test difference (Student's *t*-test *p* value ≤ 0.05) [30]. Bioinformatic analyses were carried out by Ingenuity® Pathway Analysis software (IPA® - QIAGEN) to cluster enriched annotation groups of Biological Processes, Pathways, and Networks within the set of identified proteins. Functional grouping was based on Fischer's exact test *p* value ≤ 0.05 (i.e., −log10 ≥ 1.3) and at least 3 counts. Comparison between the proteomic and metabolomic data was performed by IPA and by MetaboAnalyst software R3.0 [31]. Enrichment analysis aimed to evaluate whether the observed genes and metabolites in a particular pathway are significantly enriched (Fisher's exact test 0.05), while the topology analysis aimed to evaluate whether a given gene or metabolite plays an important role in a biological response, based on its position within a pathway (pathway impact).

The mass spectrometry proteomics data have been deposited to the ProteomeXchange Consortium via the PRIDE partner repository, with the dataset identifier 7MlKNZqC.

2.8. Chemicals for Metabolomics Analysis

All chemicals and solvents used for extraction buffer and for liquid chromatography were LC-MS Chromasolv purity grade. Acetonitrile, methanol, 2-Propanol, and water was purchased from Honeywell, while chloroform and formic acid were purchased from Sigma-Aldrich.

2.9. Metabolites Extraction for GC-MS Analysis

Cells were quickly rinsed with 0.9% NaCl and quenched with 800 μL of 1:1 ice-cold methanol:water and collected by scraping. Cells were sonicated 5 s for 5 pulses at 70% power twice and then 400 μL of chloroform were added. Samples were vortexed at 4 °C for 20 min, and then centrifuged at 12,000 g for 10 min at 4 °C. The aqueous phase was collected in a glass insert for solvent evaporation in a centrifugal vacuum concentrator (Concentrator plus/ Vacufuge® plus, Eppendorf) at 30 °C for about 2.5 h.

2.10. Metabolites Extraction for LC-MS Analysis

Cells were quickly rinsed with 0.9% NaCl and quenched with 500 μL ice-cold 70:30 acetonitrile-water. Plates were placed at −80 °C for 10 min, then the cells were collected by scraping. Cells were sonicated as above and then centrifuged at 12,000 g for 10 min at 4 °C. The supernatant was collected in a glass insert and dried as above. Samples were then resuspended with 150 μL of H_2O prior to analyses.

2.11. GC-MS Metabolic Profiling

Derivatization was performed using automated sample prep WorkBench instrument (Agilent Technologies, Santa Clara, CA, USA). Dried polar metabolites were dissolved in 60 μL of 2% methoxyamine hydrochloride in pyridine (ThermoFisher) and held at 40 °C for 6 h. After the reaction, 90 μL of MSTFA (N-Methyl-N-(trimethylsilyl) trifluoroacetamid) was added, and samples were incubated at 60 °C for 1 h. Derivatized samples were analyzed by GC-MS using a DB-35MS column (30 m × 0.25 mm i.d. × 0.25 μm) installed in an Agilent 7890B gas chromatograph (GC) interfaced with an Agilent 7200 Accurate-Mass Quadrupole Time-of-Flight (QTOF) mass spectrometer (MS), operating under electron impact (EI) ionization at 70 eV. Samples (1 μL) were injected in a splitless mode at 250 °C, using helium as the carrier gas at a flow rate of 1 mL/min. The GC oven temperature was held at 100 °C for 2 min and increased to 325 °C at 10 °C/min. GC/MS data processing was performed using Agilent Muss Hunter software. Relative metabolites abundance was carried out after normalization to internal standard d27 Myristic acid and cell number and statistical analyses were performed using MetaboAnalyst 4.0 [32].

2.12. LC-MS Metabolic Profiling

LC separation was performed using an Agilent 1290 Infinity UHPLC system and an InfinityLab Poroshell 120 PFP column (2.1 × 100 mm, 2.7 μm; Agilent Technologies). Mobile phase A was water with 0.1% formic acid. Mobile phase B was acetonitrile with 0.1% formic acid. The injection volume was 15 μL and LC gradient conditions were: 0 min: 100% A; 2 min: 100% A; 4 min: 99% A; 10 min: 98% A;11 min: 70% A; 15 min: 70% A; 16 min: 100% A with 5 min of post-run. Flow rate was 0.2 mL/min, and the column temperature was 35 °C. MS detection was performed using an Agilent 6550 iFunnel Q-TOF mass spectrometer with Dual JetStream source operating in negative ionization mode. MS parameters were: gas temp: 285 °C; gas flow: 14 l/min; nebulizer pressure: 45psig; sheath gas temp: 330 °C; sheath gas flow: 12 l/min; VCap: 3700 V; Fragmentor: 175 V; Skimmer: 65 V; Octopole RF: 750 V. Active reference mass correction was through a second nebulizer using masses with *m/z*: 112.9855 and 1033.9881 dissolved in the mobile phase 2-propanol-acetonitrile-water (70:20:10 *v/v*). Data were acquired from *m/z* 60–1050. Data analysis and isotopic natural abundance correction

was performed with MassHunter ProFinder (Agilent Technologies). Relative metabolites abundance was carried out after normalization to cell number and statistical analyses were performed using MetaboAnalyst 4.0 [32].

2.13. Metabolites Quantification in the Media Samples

Absolute quantification of glucose, lactate, glutamine, and glutamate in spent media was determined enzymatically using YSI2950 bioanalyzer (YSI Incorporated, Yellow Springs, OH, USA).

2.14. Bioenergetics by Seahorse Technology

Mitochondrial oxygen consumption rate (OCR) and extracellular acidification rate (ECAR) were determined by using Seahorse XFe96 Analyzer (Agilent Technologies). HepG2 and Huh7 cells were seeded in Agilent Seahorse cell culture microplates at density of 2×10^4 cells/well for HepG2 or 1×10^4 cell/well for Huh7 72 h prior to the assay. A total of 24 h after seeding cells were treated with high methionine (1.5 g/L) and/or Compound C (2 µM for HepG2 and at 1.5 µM for Huh7 cells) for 48 h, and then analyzed by using the Seahorse XF ATP rate assay kit (Agilent Technologies), according to manufacturer instructions. Three measurements of OCR and ECAR were taken for the baseline and after the sequential injection of mitochondrial inhibitors (1.5 µM oligomycin and 1.5 µM rotenone/antimycin A). OCR and ECAR from each well were normalized by protein content by using the Bradford assay.

3. Results

3.1. High Methionine and Compound C Induce Proteomic Changes

We recently published findings that methionine activates AMPK and increases mitochondrial metabolism and respiration in the model organism *Saccharomyces cerevisiae*, especially in cells lacking Snf1/AMPK activity [33].

To investigate whether this is a conserved mechanism triggered by methionine, we explored the effect of high methionine concentrations in liver cancer cells, in the presence or absence of Compound C, which mimics AMPK inhibition. We performed a proteomic analysis on HepG2 cells grown for 48 h (CTR), in the presence of Compound C (CTRCC), in the presence of high methionine (MET), and in double treated cells (METCC) by a quantitative shotgun label free strategy. The comparison of the four data sets by an ANOVA test (*p*-value 0.05) showed proteins exclusively expressed in each condition, as well as 717 proteins common to all data sets, among which, 46 were statistically different. IPA analysis carried out on these proteins to find possible interactions highlighted that 25 out of 46 proteins differentially expressed belonged to a network classified as: cancer, protein synthesis, RNA damage and repair (Figure 1A). The upstream regulator analysis, based on prior knowledge of expected effects between transcriptional regulators and their target genes in IPA, suggested that two transcription regulators were probably involved, hepatocyte nuclear factor 1 (HNF1A, *p*-value 0.0005) and hepatocyte nuclear factor 4 (HNF4A, *p*-value 0.001) (Figure 1B), which target 6/46 and 12/46 of the proteins differentially expressed, respectively. This result suggests that the presence of methionine and Compound C significantly affects transcription, in keeping with Wang and coworkers who reported an impact on methionine metabolism by HNF4A [34].

Specific analyses were then carried out by comparing MET vs. CTR, METCC vs. MET, CTRCC vs. CTR. A summary of the results obtained is reported in Figure 3, while Table S2–S4 report the list of the proteins differentially expressed (either increased or decreased), or exclusively expressed in one condition in the three comparisons. The corresponding volcano plots are shown in Figure 1C.
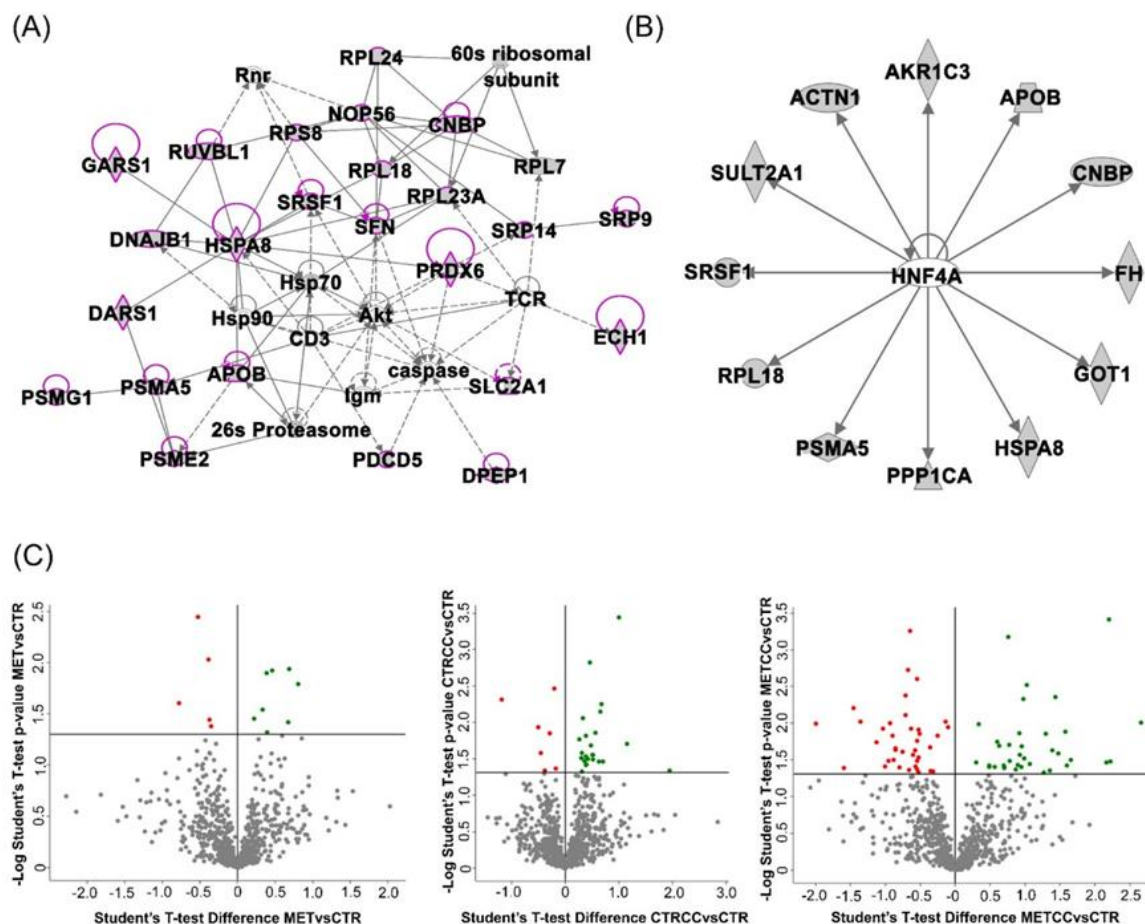
Figure 1. Bioinformatic analysis of the proteomic data of HepG2 cells grown for 48 h (CTR), in the presence of Compound C (CTRCC), high methionine (MET) and high methionine and Compound C (METCC). (**A**) Ingenuity® Pathway Analysis (IPA) analysis carried out on the 46 proteins common to all data sets, whose expression is statistically different, highlighted that 25 out of 46 proteins differentially expressed belong to a network classified as: cancer, protein synthesis, RNA damage and repair. These proteins are shown in magenta among all the proteins belonging to the pathway. Each protein is reported with the corresponding IPA symbol. (**B**) The upstream regulator analysis, based on prior knowledge of expected effects between transcriptional regulators and their target genes in IPA, shows hepatocyte nuclear factor 4 (HNF4A) (*p*-value 0.001) which target 12/46 of the proteins differentially expressed. (**C**) Volcano plots of the comparison MET versus CTR, METCC versus MET, CTRCC versus CTR. In green: proteins upregulated; in red: proteins downregulated; in grey: proteins that are not statistically different (Student's *t*-test *p*-value = 0.05).

These proteins were further analyzed to find possible enrichment in GO Biological Processes (Figure 2) and pathways (Figure 3), in the comparison between control and treatments with high methionine or/and Compound C. Differentially expressed proteins mainly belonged to the classes of metabolic processes, mitochondrion, and mitochondrial dysfunction, translation, RNA and protein processing and response to oxidative stress. As shown in Figure 2A,B and in Table S1, the expression of proteins related to oxidation-reduction events were altered, either up or downregulated, indicating a general impact on these processes in the presence of methionine and/or Compound C compared to the control. Many proteins involved in mitochondrial respiratory chain were upregulated by the double treatment with high methionine and Compound C. In particular, high methionine induced an increase of proteins involved in the mitochondrial electron transport and in complex I assembly, while Compound C treatment mainly increased the level of tricarboxylic acid (TCA) cycle and lipid metabolic processes (Figure 2A).

(A)

(B)
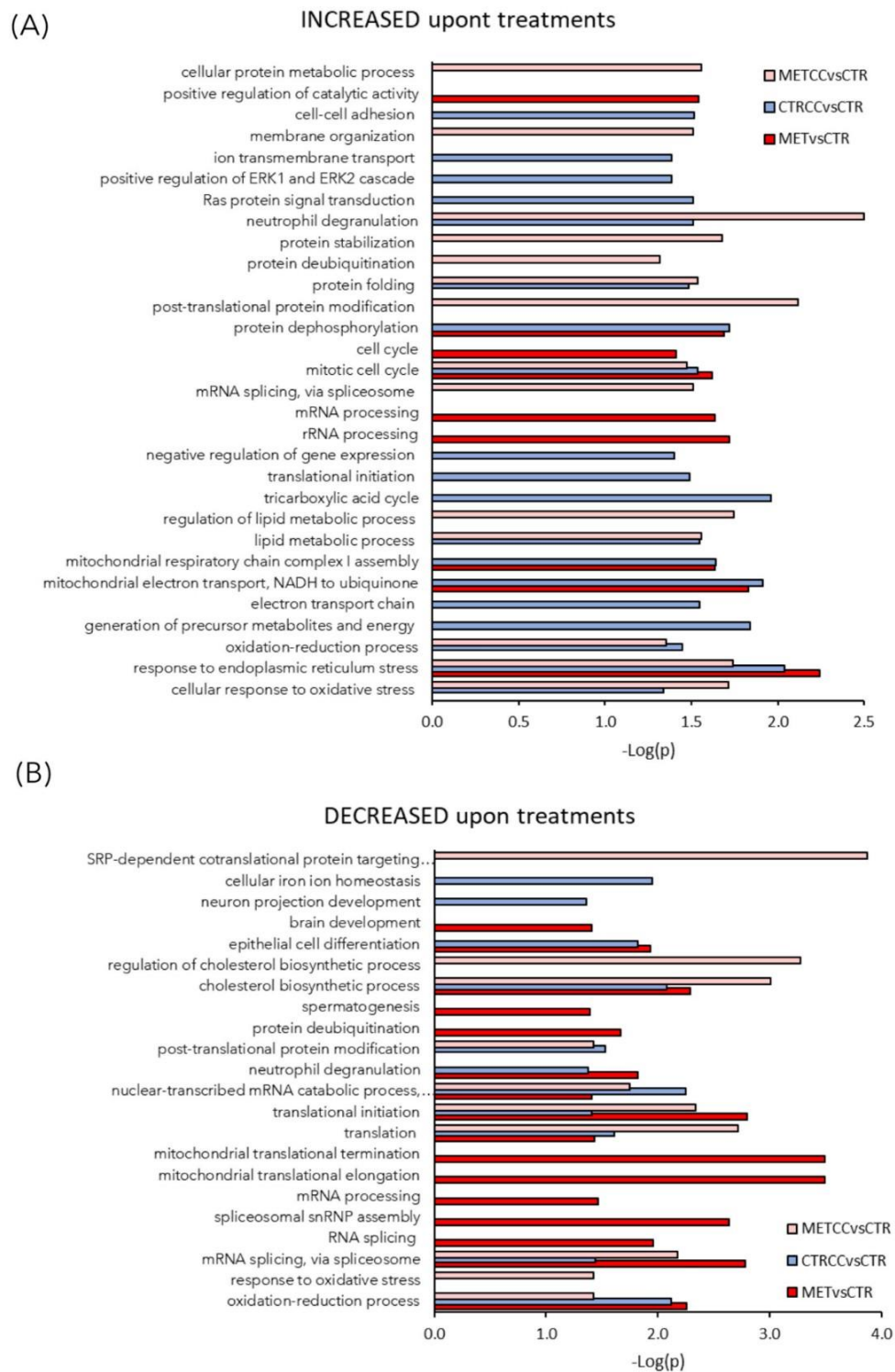
Figure 2. High methionine and Compound C induce proteomic changes. (A–C) Functional analysis of the proteins differentially expressed in the comparison MET versus CTR, METCC versus MET, CTRCC versus CTR. Proteins were considered differentially expressed if they were present only in one condition or showed significant *t*-test difference (Student's *t*-test *p* value = 0.05). (**A**) GO Biological Processes increased in the three comparison (**B**) GO Biological Processes decreased in the three comparison. Functional grouping was based on Fischer's exact test *p*-value ≤ 0.05 (i.e., −log10 ≥ 1.3) and at least three counts. In each comparison, the terms increased or decreased refer to proteins up or downregulated upon treatments.

Canonical Pathways	METvsCTR	METCCvsCTR	CTRCCvsCTR
Mitochondrial Dysfunction	5.06	6.17	7.07
Oxidative Phosphorylation	2.40	4.14	5.39
TCA Cycle II (Eukaryotic)	0.69	2.26	2.81
Production of Nitric Oxide and Reactive Oxygen Species in Macrophages	2.39	2.19	2.37
NRF2-mediated Oxidative Stress Response	1.08	3.65	1.07
Sirtuin Signaling Pathway	3.41	5.34	5.77
EIF2 Signaling	4.47	5.37	4.45
Regulation of eIF4 and p70S6K Signaling	4.55	1.31	3.59
Protein Ubiquitination Pathway	1.76	5.31	0.72
HIPPO signaling	1.10	3.07	2.90
mTOR Signaling	3.75	0.95	2.18
Breast Cancer Regulation by Stathmin1	2.28	1.50	3.03
Clathrin-mediated Endocytosis Signaling	1.04	2.83	2.35
Integrin Signaling	1.54	1.44	2.94
Superpathway of Cholesterol Biosynthesis	1.94	2.20	1.93
FXR/RXR Activation	0.77	3.75	1.41
D-myo-inositol (3,4,5,6)-tetrakisphosphate Biosynthesis	2.08	0.88	2.89
D-myo-inositol (1,4,5,6)-Tetrakisphosphate Biosynthesis	2.08	0.88	2.89
ERK/MAPK Signaling	1.04	1.57	3.13
3-phosphoinositide Degradation	1.94	0.80	2.72

Figure 3. Bioinformatic analysis of the proteomic data on HepG2 cells grown for 48 h (CTR), in the presence of Compound C (CTRCC), high methionine (MET) and high methionine and Compound C (METCC). The analysis was carried out by IPA on the proteins differentially expressed among the comparison MET versus CTR, METCC versus CTR and CTRCC versus CTR. Proteins were considered differentially expressed if they were present only in one condition or showed significant *t*-test difference (Student's *t*-test *p*-value 0.05). Functional grouping was based on Fischer's exact test *p* value ≤ 0.05 and at least three counts. The colored bars are a visual representation of the corresponding –log *p*-value reported abreast.

Methionine and Compound C presence upregulated proteins involved in the cellular response to oxidative stress, manly at the endoplasmic reticulum level (Figure 2A, Figure 3), while Compound C alone induced the expression of proteins involved in membrane organization, transmembrane transport, and cell–cell adhesion (Figure 2A).

Interestingly, methionine and Compound C altered sirtuin signaling pathway (Figure 3). This pathway is a master regulator of several cellular processes and known to both extend lifespan and regulate spontaneous tumor development. It is well known that S-adenosyl-methionine, sirtuin, and mTOR pathway are strictly related [35]. In keeping with these data and with results reported above, the proteomic analysis suggested that mTOR signaling was altered mainly in response to increased methionine in the medium (Figure 3).

Among the processes more altered in HepG2 cells treated with methionine and Compound C, RNA processing and mitochondrial translation were downregulated mainly by methionine, while Compound C had more impact on general translation (Figure 2B). Overall, the double treatment with high methionine and Compound C induced a decrease in the level of ribosomal proteins RPS9, RPL23A, RPL34, mitochondrial ribosomal proteins MRPL37, MRPS18C, and translational initiation factors, such as EIF1 and EIF3M, as well as proteins of the SRP (signal-recognition-particle) co-translational process (SRP14, SSR3, SRP9), suggesting a general reduction of translation in this condition (Table S4).

3.2. High Methionine and Compound C Induce a Metabolic Rewiring

Since methionine supplementation induced deep changes of proteins associated with cellular metabolism, we further investigated this feature by performing metabolomics analysis in cells grown with high methionine and/or Compound C. Extracellular metabolites were analyzed by YSI biochemical analyzer. In HepG2 cells, only the double treatment (high methionine and Compound C) showed an increase of glucose and glutamine consumption, with a proportional increase in lactate and glutamate secretion (Figure 4A). However, no changes in extracellular metabolites were observed in

Huh7 cells in any condition. This difference could be due to the lower growth rate of Huh7 cells, or to their higher basal metabolism compared to HepG2 cells; indeed, their basal glucose uptake and their lactate secretion were three times higher than those of HepG2 cells (Figure 4A,B).
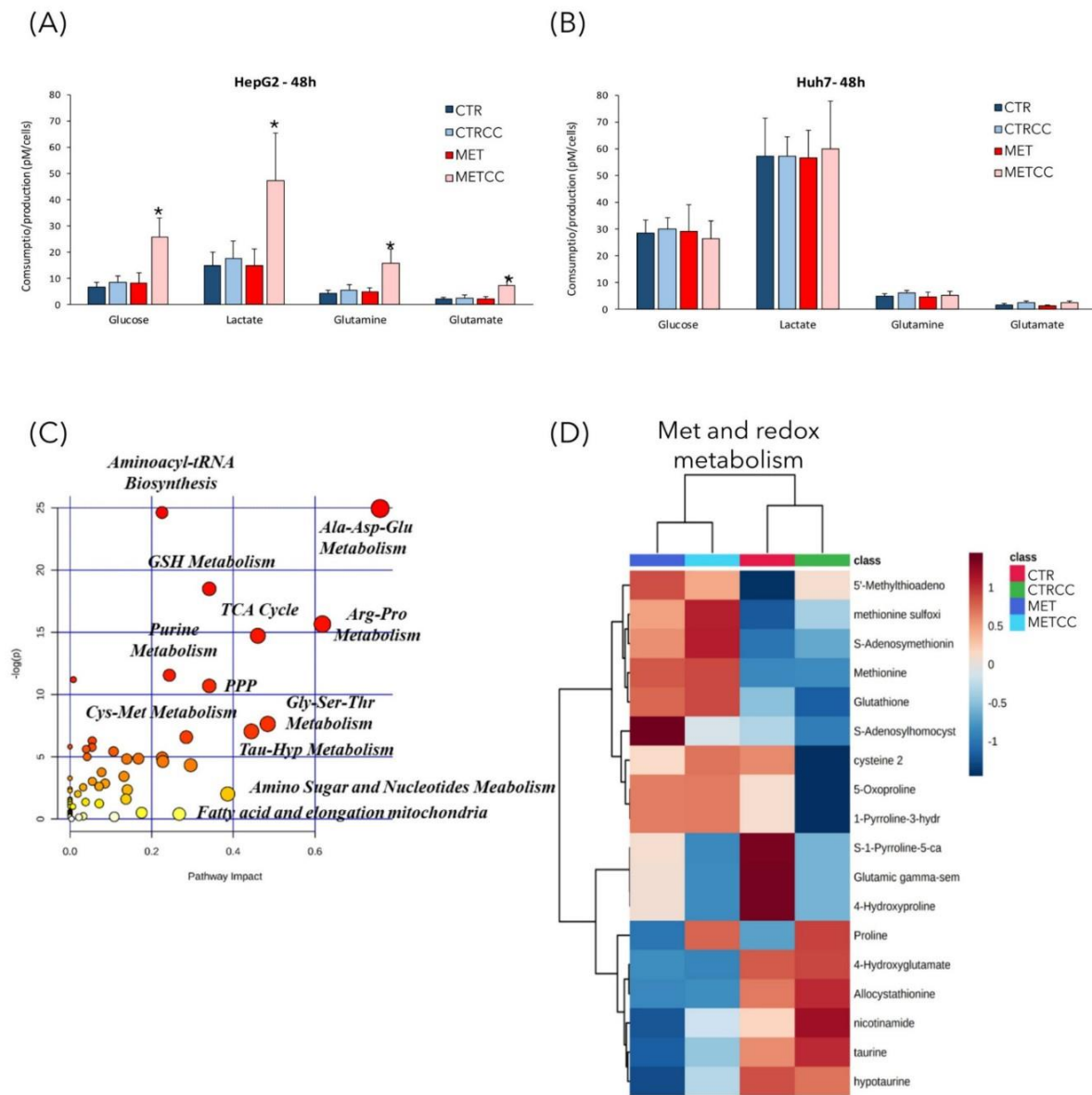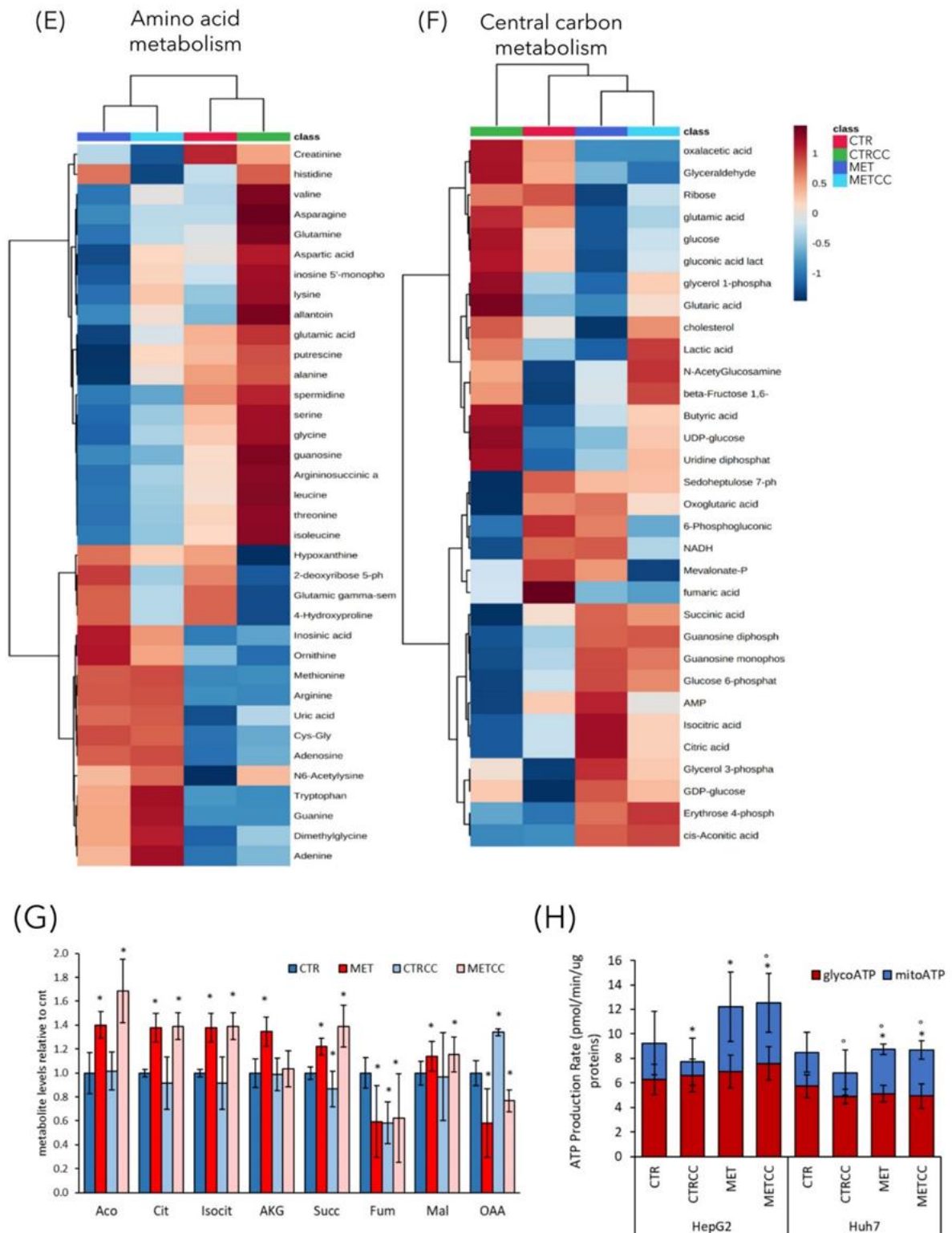

Figure 4. *Cont.*

Figure 4. High methionine and Compound C affect cellular metabolism. (**A,B**) HepG2 (**A**) and Huh7 (**B**) cells were grown for 48 h in regular medium or in the presence of high methionine and/or Compound C.

Media from three biological replicates were collected to measure glucose and glutamine consumption, lactate, and glutamate secretion. (**C**–**F**) HepG2 cells were grown for 48 h in regular medium (CTR), or in the presence of high methionine and/or Compound C. Metabolomics analysis was performed by GC/MS and LC/MS on five biological replicates, each analyzed in technical duplicate. (**C**) Metabolic pathways mostly affected in this analysis. The metabolic pathway analysis was performed using the MetaboAnalyst 4.0 tool. The metabolic pathways are represented as circles. Color intensity (white-to-red) and size of each circle reflects increasing statistical significance, based on the *p*-value [−log(P)] from the pathway enrichment analysis, and pathway impact value derived from the pathway topology analysis, respectively. (**D**–**F**) Hierarchical clustering heatmaps from one-way ANOVA analysis of differential metabolites belonging to (**D**) methionine and redox metabolism, (**E**) amino acid metabolism, (**F**) central carbon metabolism. The heatmaps were obtained using the MetaboAnalyst 4.0 tool. The color code scale indicates the normalized metabolite abundance. (**G**) Histogram of the level of metabolites of the TCA cycle in the four conditions in HepG2 cells, measured in the metabolomics analysis. The level of each metabolite in the control was set to 1. * $p < 0.05$ compared to control. (**H**) Seahorse adenosine triphosphate (ATP) rate assay analysis in HepG2 and Huh7 cells, grown for 48 h in regular medium or in the presence of high methionine and/or Compound C. * $p < 0.05$ for mitoATP compared to control, $p < 0.05$ for glycoATP compared to control.

We then measured relative abundance of intracellular metabolites in HepG2 cells treated for 48 h with high methionine and/or Compound C, by an untargeted metabolomic GC/MS and LC/MS analysis. This analysis revealed a strong metabolic change due to high methionine, but also to Compound C addition (Supplementary Figure S1, Figure 4C). The most affected pathways were those related to amino acids metabolism, like Cys-Met (as expected upon methionine supplementation), Ala-Asp-Glu, Arg-Pro, and Gly-Ser-Thr (Figure 4C), but also those related to aminoacyl-tRNA biosynthesis, coherently with the downregulation of translation associated proteins (Figure 2B). In addition, alterations in the pathways of glutathione metabolism (which is directly associated to methionine metabolism), of the sulfur-containing molecules taurine and hypotaurine, in the pathways of purine and nucleotide metabolism and of fatty acid metabolism were identified (Figure 4C). As expected, methionine supplementation in the medium (either in the presence or absence of Compound C) increased the intracellular level of methionine, but also of its derived metabolites, such as S-adenosyl-methionine and S-adenosyl-homocysteine, which are part of the methionine cycle (Figure 4D). In addition, high methionine treatment induced an increase of cysteine, which can derive from homocysteine and serine, through conversion to cystathionine, and of glutathione, which is synthesized from Cys, Glu, and Gly. In high methionine condition there was also an increase of two direct methionine derivatives, the regulatory metabolite methylthioadenosine (MTA) and the toxic compound methionine sulfoxide (Figure 4D). Remarkably, the MTA level negatively correlates with growth potential in the liver [36,37]. In fact, it has been reported that MTA decreases after partial hepatectomy, when the replicative response of hepatocytes is higher [38], and MTA administration in vitro reduces liver cell growth [39]. Furthermore, MTA inhibits the synthesis of polyamines [36], whose level is correlated with proliferation and which were indeed decreased in high methionine condition (see spermidine and putrescine, Figure 4E). On the contrary, the MTA derivatives adenine and adenosine increased in high methionine condition (Figure 4E). High methionine also induced an increase of metabolites related to the urea cycle, such as arginine, ornithine, uric acid (Figure 4E), which was probably increased to convert excess nitrogen (given by the high methionine supplied in the medium) into urea.

3.3. High Methionine and Compound C Increase Mitochondrial Functionality
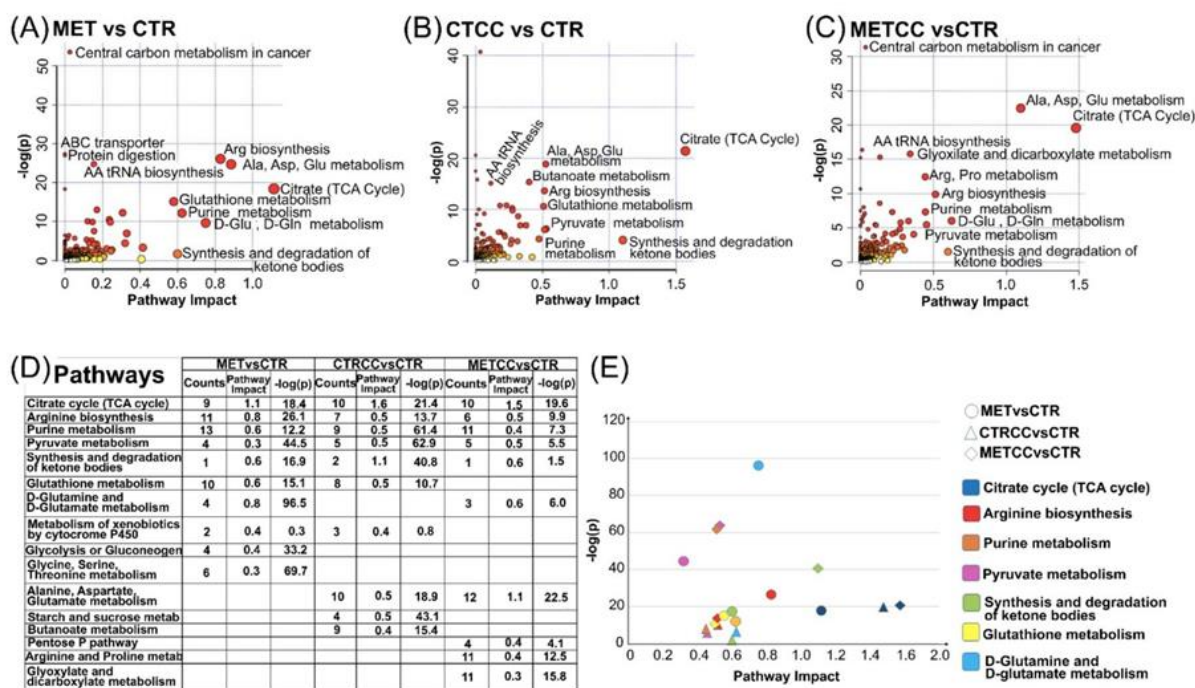
The metabolomics analysis revealed also that many metabolites of the TCA cycle were modulated by high methionine, with higher levels of cis-aconitate, citrate, isocitrate, α-ketoglutarate, succinate and malate and lower levels of fumarate and oxaloacetate compared to the control (Figure 4F,G).

Since the metabolomics and proteomics data suggested an increase of the TCA cycle, we measured the rate of ATP production from glycolysis and from mitochondrial respiration in HepG2 and Huh7

cells, through Agilent Seahorse technology (Figure 4H). Although the amount of ATP deriving from glycolysis was only slightly altered by treatments, cells grown in high methionine condition (with or without Compound C) produced a higher fraction of ATP through mitochondrial respiration (Figure 4H). The increase of mitochondrial-derived ATP was clearly evident in HepG2 cells and it was also confirmed, albeit with a lower increase, in Huh7 cells.

According to systems biology, the phenotype of a cell results from the interaction of several component, in which the emergent behavior is wider than the sum of their parts [40]. As a result of this, we decided to integrate the results from metabolomic and proteomic analysis, using the IPA and MetaboAnalyst softwares.

This integration better highlighted that TCA cycle was one of the most affected process in all three comparisons (MET versus CTR, CTRCC versus CTR, METCC versus CTR) (Figure 5A–C). However, as reported in Figure 5D,E, focusing on the first 10 more significant pathways in terms of enrichment (*p*-values) and topology (pathway impact) in the three comparisons, the integration analysis suggested that citrate and TCA cycle were more affected by the presence of Compound C than methionine, which, in turn, had a major impact on amino acid metabolism, especially of those amino acids directly linked to the nitrogen cycle, such as Arg, Gln, and Glu. In keeping with the effect on TCA cycle, pyruvate metabolism and the synthesis and degradation of ketone bodies prevailed in the presence of Compound C if compared to the supplementation of methionine (Figure 5D,E).


Pathways	METvsCTR			CTRCCvsCTR			METCCvsCTR		
	Counts	Pathway Impact	-log(p)	Counts	Pathway Impact	-log(p)	Counts	Pathway Impact	-log(p)
Citrate cycle (TCA cycle)	9	1.1	18.4	10	1.6	21.4	10	1.5	19.6
Arginine biosynthesis	11	0.8	26.1	7	0.5	13.7	6	0.5	9.9
Purine metabolism	13	0.6	12.2	9	0.5	61.4	11	0.4	7.3
Pyruvate metabolism	4	0.3	44.5	5	0.5	62.9	5	0.5	5.5
Synthesis and degradation of ketone bodies	1	0.6	16.9	2	1.1	40.8	1	0.6	1.5
Glutathione metabolism	10	0.6	15.1	8	0.5	10.7			
D-Glutamine and D-Glutamate metabolism	4	0.8	96.5				3	0.6	6.0
Metabolism of xenobiotics by cytocrome P450	2	0.4	0.3	3	0.4	0.8			
Glycolysis or Gluconeogen	4	0.4	33.2						
Glycine, Serine, Threonine metabolism	6	0.3	69.7						
Alanine, Aspartate, Glutamate metabolism				10	0.5	18.9	12	1.1	22.5
Starch and sucrose metab				4	0.5	43.1			
Butanoate metabolism				9	0.4	15.4			
Pentose P pathway							4	0.4	4.1
Arginine and Proline metab							11	0.4	12.5
Glyoxylate and dicarboxylate metabolism							11	0.3	15.8

Figure 5. Integration of metabolomics and proteomics analysis. (**A**) Metabolic and proteomic pathways mostly affected in MET versus CTR. (**B**) Metabolic and Proteomic pathways mostly affected in CTRCC versus CTR. (**C**) Metabolic and Proteomic pathways mostly affected in METCC versus CTR. The scatter plots show a summary of the joint evidence from enrichment analysis (*p*-values) and topology analysis (pathway impact). Dots size and color (white to red) are proportional to the numbers of genes and compounds present in a pathway. (**E**) List of the 10 more significant pathways in each of the three comparisons. (**E**) Scatter plot of the common pathways among the list shown in (**D**).

Strikingly, the pentose phosphate pathway, Arg/Pro metabolism, glyoxylate, and dicarboxylate metabolism were altered only upon double treatment (Figure 5D). In addition, glutathione metabolism and metabolism of xenobiotics, which were affected by single treatments, were no more altered upon double treatment (Figure 5D). These results indicate that the combination of Compound C and high

methionine does not result in a simple synergistic effect of the single treatments, but rather leads to the emergence of new features in liver cancer cell metabolism.

3.4. High Methionine Activates AMPK and mTOR Pathways

Since we previously reported that methionine can activate Snf1/AMPK in budding yeast, we then investigated the effect of methionine supplementation in liver cancer cells. AMPK showed a dose-dependent activation after 24 h in HepG2 cells (Figure 6A), detectable as increased phosphorylation on T172, as well as increased phosphorylation of Acc1-S79, the main target of AMPK, often used as reporter of its activity. It is known that AMPK activation is mainly due to an energy reduction [41], although it can also be activated without any ATP decrease [42]. Since data presented above (Figure 4H) indicate that ATP level did not decreased, but rather increased after methionine treatment, we can speculate that AMPK activation was not a result of energy deficiency.
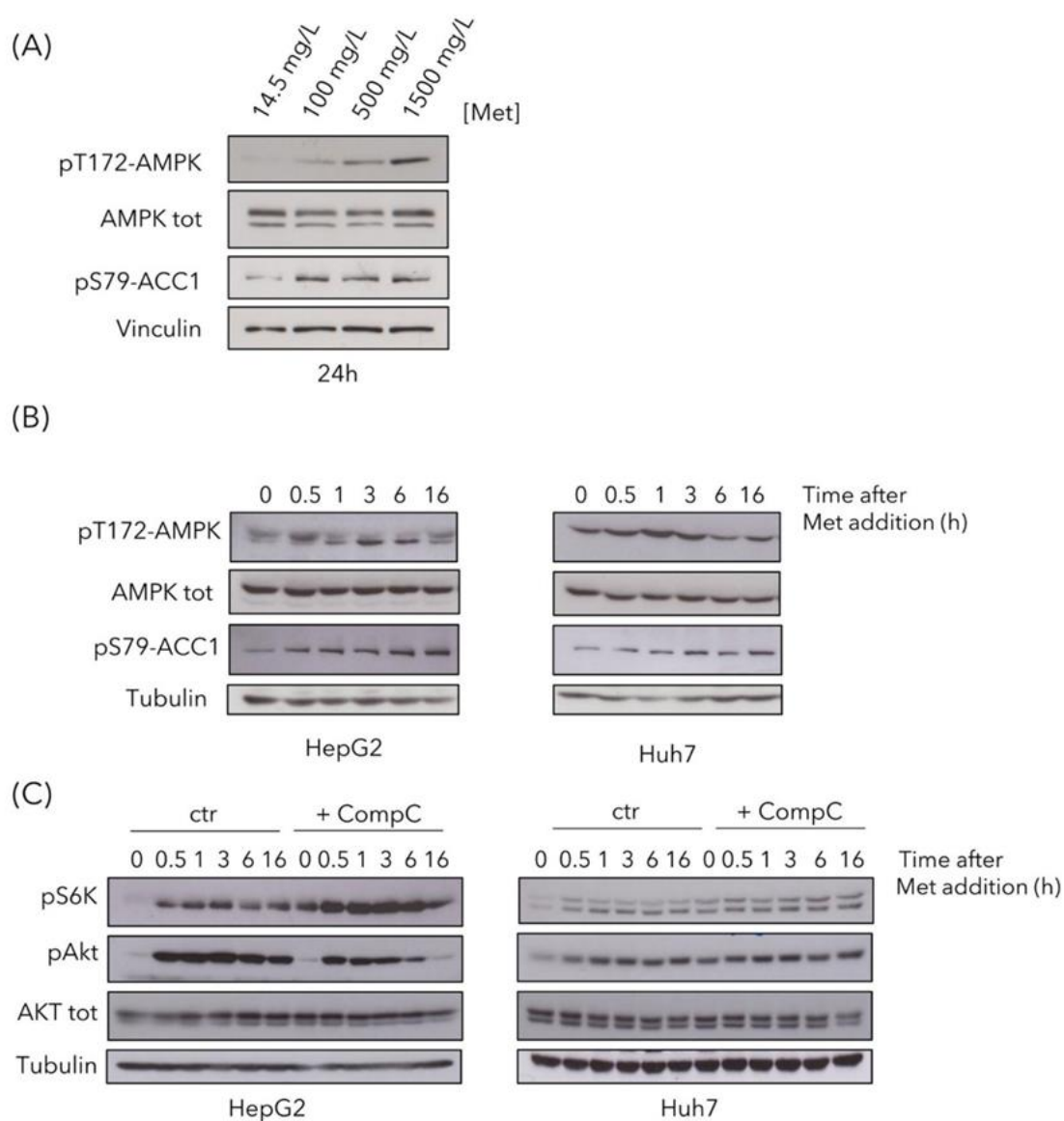
Figure 6. High methionine activates AMK-activated protein kinase (AMPK), mTOR and Akt pathways. (**A**) HepG2 were treated with methionine for 24 h and AMPK activation state was assayed by Western analysis, using the pT172-AMPK antibody (against pT172 in the activation loop) and using the anti-pS79-Acc1 antibody (against the target site of AMPK on Acc1).

An anti-AMPK total antibody and an anti-vinculin antibody were used as controls. (**B**) HepG2 and Huh7cells were gown in control medium and 1.5 g/L methionine was added to the cultures at time 0. Samples were collected at the indicated time points to evaluate AMPK activation, using an anti-pT172-AMPK antibody and an anti-pS79-Acc1 antibody. An anti-AMPK total antibody and an anti-tubulin antibody were used as controls. (**C**) HepG2 and Huh7 cells were gown for 48 h in the absence or presence of Compound C. Then 1.5 g/L methionine was added to the cultures, and samples were collected at the indicated time points to evaluate mTOR activation, using anti-pS6K antibody and Akt activation using anti-pS473-Akt antibody. Anti-Akt total antibody and anti-tubulin antibody were used as controls.

To better investigate AMPK activation, we performed time-course experiments in both HepG2 and Huh7 cell lines. A total of 1.5 g/L of methionine was added to cells growing in regular medium and phosphorylation of AMPK-T172 and of Acc1-S79 were detected by Western blot analysis (Figure 6B). AMPK phosphorylation, as well as the phosphorylation of its target Acc1, increased in both cell lines, with a peak at 0.5 h and 1 h after methionine addition, for HepG2 and Huh7 respectively (Figure 6B).

Since amino acids can activate mTOR, the master regulator of cell growth [43] and, since mTOR involvement was suggested by our proteomics analysis (Figure 3), we investigated the activation of the mTOR pathway. mTOR was activated in response to high methionine in the medium, as observed by increased pS6K phosphorylation (Figure 6C), in keeping with previously reported data [44], both in HepG2 and in Huh7 cells. Phosphorylation increased after 30-min treatment, remaining high until 16 h (Figure 6C). This increase was more evident in cells pre-treated with Compound C, in which the release of mTOR inhibition by AMPK resulted in a higher pS6K phosphorylation, both at time 0 and in response to high methionine (Figure 6C). High methionine also induced activation of the Akt pathway, involved in cell proliferation and survival [45], in both cell lines, although in HepG2 cells, it was less persistent over time when AMPK was inhibited (Figure 6C).

3.5. High Methionine Reduces Cancer Associated Phenotypes

We previously showed that, in yeast cells, methionine induced a slow-down of growth rate, especially in cells lacking Snf1/AMPK activity [33]. The increase of methionine concentration in the medium (up to 1.5 g/L, versus 15 mg/L in regular medium) induced a slight slow-down of growth rate both in HepG2 and in Huh7 cell lines (Figure 7A,B). Inhibition of AMPK with Compound C slightly reduced growth rate in both cell lines, but drastically impaired growth when combined with high methionine in the medium (Figure 7A,B). These results suggest that the effect of methionine on cellular proliferation is a conserved feature that deserves further investigation.

In addition to a higher proliferation, one of the most relevant features of cancer cells is their ability to migrate and to form colonies from single cells, to give metastasis [46]. To analyze the effect of methionine on cell migration, we used Boyden chambers and migration of serum starved cells was assessed in the presence or absence of high methionine concentration and/or Compound C. Cell migration through the membrane of the transwell was significantly impaired in high methionine in both cell lines, even more when AMPK was inhibited (Figure 7C,D).

We then tested the ability of single cells to form colonies in the presence of high methionine and/or inhibition of AMPK. As shown in Figure 7E,F, colony formation was reduced by high methionine supplementation, especially in the presence of Compound C (Figure 7E,F).

Altogether, our results suggest that high methionine supplementation inhibits cancer associated phenotypes, especially in combination with AMPK inhibition.
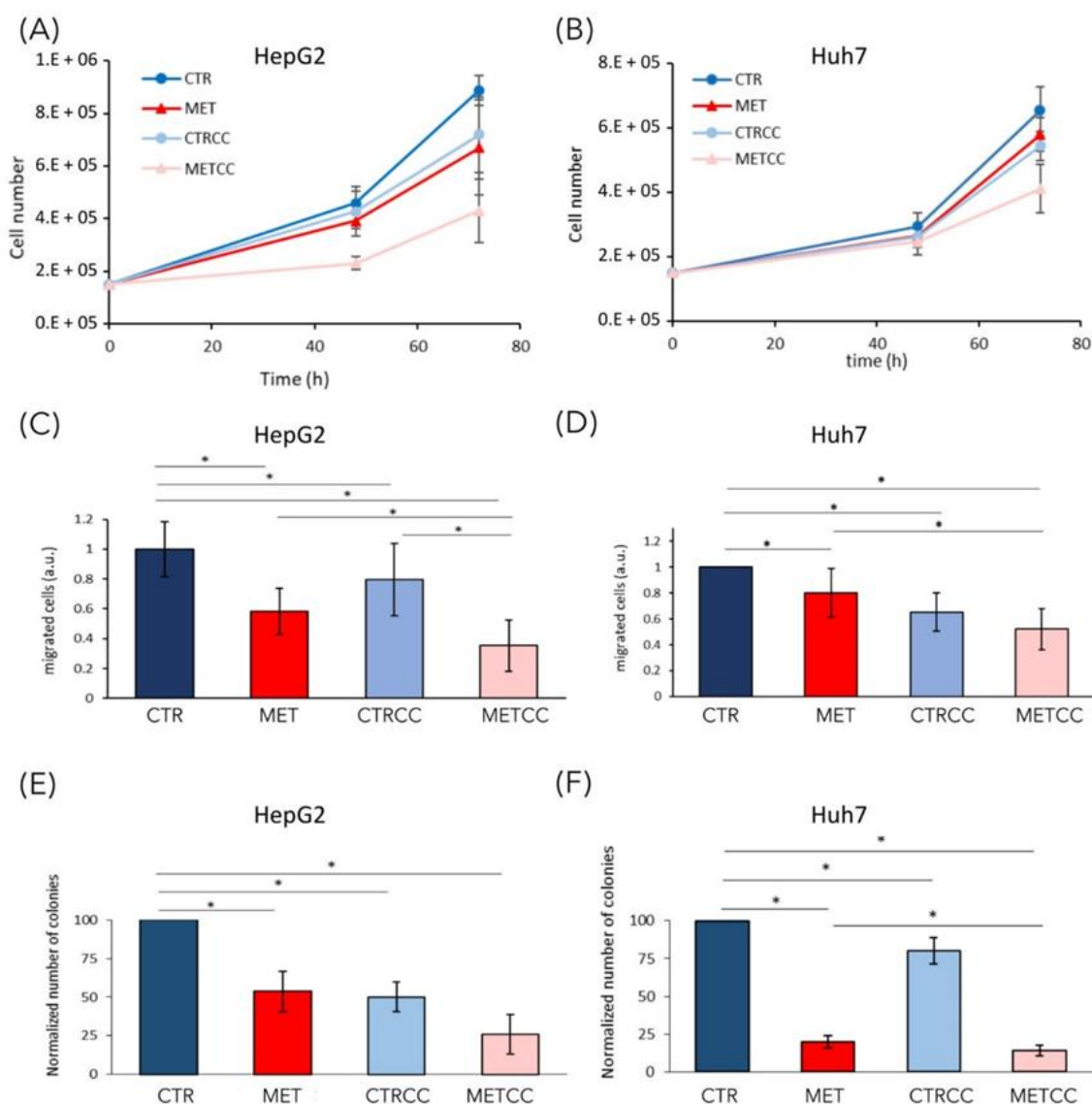
Figure 7. High methionine and Compound C inhibit cancer phenotypes. (**A,B**) Cell growth of (**A**) HepG2 and (**B**) Huh7 was monitored until 72 h in regular medium (CTR) or in the presence of 1.5 g/L methionine (MET) and/or Compound C to obtain partial AMPK inactivation (2 µM Compound C for HepG2 and 1.5 µM for Huh7). The experiments were performed at least in triplicate. (**C,D**) HepG2 or Huh7 were grown for 24 h in regular medium (CTR), or in the presence of high methionine and/or Compound C. Then they were starved for 24 h in the same medium without serum and migration was evaluated with a transwell assay for 24 h. (**E,F**) Colony formation assay of HepG2 or Huh7 grown in regular medium or in the presence of high methionine and/or Compound C. Experiments were performed in triplicate. * $p < 0.05$.

3.6. The Effect of High Methionine and Compound C is Specific for Liver Cancer Cells

Although Compound C has been extensively used to inhibit AMPK activity, it may also inhibit other kinases. To discern whether the effect of Compound C on growth inhibition in high methionine condition was specifically due to AMPK inhibition, we silenced the expression of AMPKα/α′ subunits in HepG2 and Huh7 cells and tested their growth in the presence of high methionine in the medium (Figure 8A,B). We found that cells with siAMPKα/α′ showed a reduced growth at 72 h in the presence of high methionine, thus, confirming that high methionine had a negative effect on growth when AMPK activity was low (either due to chemical inhibition or to reduction of the catalytic subunit).

These data confirm that the effect of Compound C on growth rate was mediated by AMPK inhibition, and not by non-specific effects of the compound.
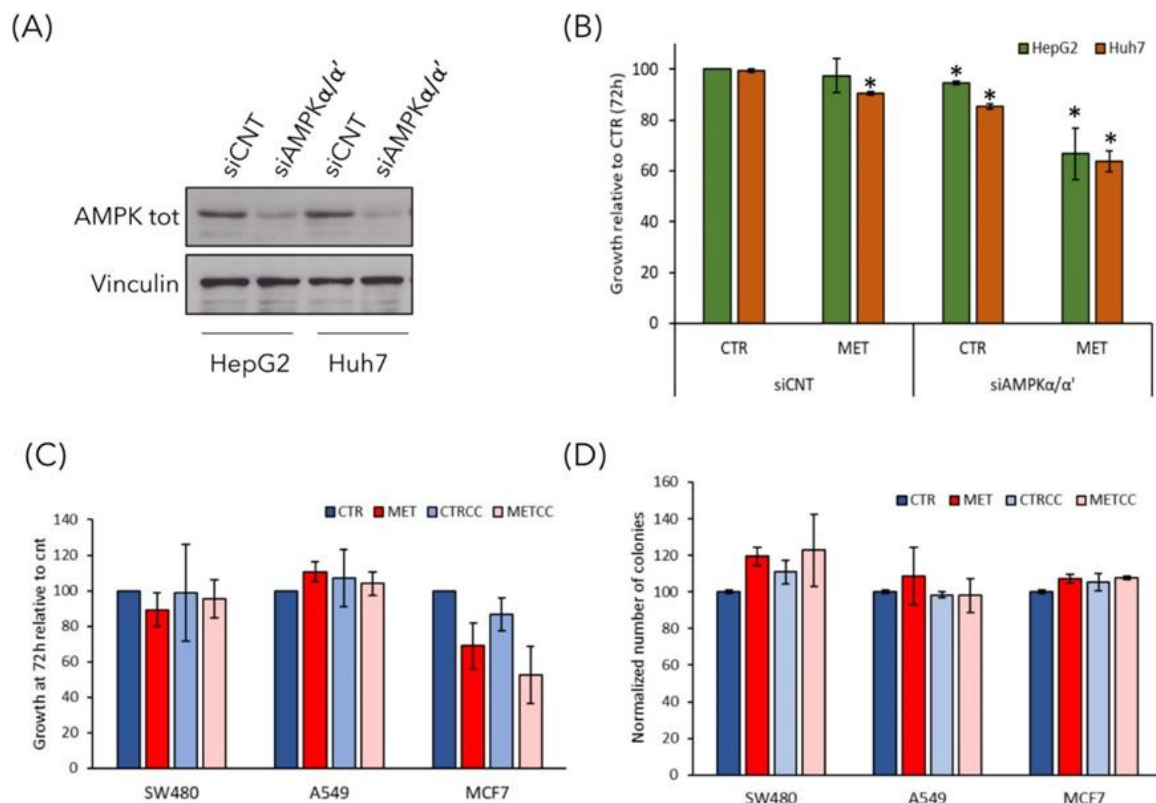
Figure 8. The effect of high methionine and AMPK inhibition is specific for liver cancer cells. (**A**,**B**) Gene knockdown for AMPKα/α′ in HepG2 and Huh7 cells was achieved by siRNA. (**A**) The level of endogenous AMPKα/α′ protein was detected by immunoblot by using anti-AMPK total antibody. anti-tubulin antibody was used as loading control. (**B**) Cell growth of HepG2 and Huh7 cells transfected with siCNT or siAMPKα/α′ was monitored for 72 h in regular medium (CTR) or in the presence of 1.5 g/L methionine (MET). Cell growth is expressed as a ratio on the growth in control medium. * $p < 0.05$ compared with siCNT cells. (**C**) Cell growth of SW480 colorectal cancer cells, A549 lung cancer cells, and MCF7 breast cancer cells was monitored until 72 h in regular medium (CTR) or in the presence of 1.5 g/L methionine (MET) and/or 2 µM Compound C. Cell growth is expressed as a ratio on the growth in control medium. (**D**) Colony formation assay of SW480, A549, and MCF7 cells grown in regular medium (CTR) or in the presence of high methionine and/or 2 µM Compound C.

Finally, to analyze whether the effect of high methionine and AMPK inhibition was specific for liver cancer cells or could be observed also on other cancer cell types, we performed the growth assay and the clonogenic assay on three cell lines deriving from different tumors: SW480 colorectal cancer cells, A549 lung cancer cells and MCF7 breast cancer cells. High methionine and/or Compound C had no effect on the growth of SW480 and A549 cells, while high methionine slightly reduced the growth of breast MCF7 cells also in combination with AMPK inhibition (Figure 8C). However, the ability of forming colonies from single cells was not impaired in none of the cell lines tested (Figure 8D), although in MCF7 cells high methionine induced the formation of smaller colonies (not shown).

Thus, we can assume that the effect of this treatment on cancer associated phenotypes is specific for liver cancer cells.

4. Discussion

The role of methionine has been long investigated in many different fields [13]. Indeed, it is well known that methionine restriction extends lifespan in different model systems, from budding yeast to

Drosophila melanogaster, *Caenorhabditis elegans*, and mammalian cells [47–50]. Methionine restriction also affects the cardiovascular system [51] and bone development [52].

On the contrary, the relationship between methionine and human cancers progression is still very ambiguous, most probably because it is cancer specific. Different studies showed that methionine restriction delays cancer progression. This was reported for instance in colon and prostate cancer animal models [53,54], as well as in breast cancer in vitro and in vivo [55,56]. On the contrary, other reports indicate that methionine supplementation induces cell-cycle arrest and transcriptional alterations in breast and prostate cancer cells [57,58].

It was reported that S-adenosyl-methionine (SAM) supplementation inhibits liver cancer cell invasion in vitro [19], by inducing changes in the methylation state of DNA, that lead to downregulation of genes involved in growth and metastasis, already known to be upregulated in liver cancer cells. In addition, in a rat model of hepatocarcinogenesis [59], as well as in a mouse model for inflammation-mediated HCC [20], SAM administration exerted a chemopreventive effect on HCC development. However, although a short-term treatment with SAM showed positive effects in the mouse model, a long-term administration did not affect tumor growth and hepatocyte proliferation [20]. Here, we explored the combination of methionine administration (the precursor of SAM) and AMPK inhibition in vitro. AMPK is a dual role kinase, being either anti- or pro-tumorigenic depending on the context, on the stage of tumor development and on the cancer type [6]. We showed that, in liver cancer cells, high methionine concentration in the medium reduces cell growth inhibits colony formation and cell migration in two different liver cancer cell lines (Figure 7) and, remarkably, these phenotypes were increased when high methionine was combined with AMPK inhibition (Figures 7 and 8). This is perfectly in line with what we observed in budding yeast, where growth rate reduction due to methionine in the medium was largely dependent on the presence of an active Snf1/AMPK pathway [33]. Moreover, methionine induces an activation of Snf1/AMPK in *S. cerevisiae*, as we observe in liver cancer cells (Figure 6), highlighting that AMPK involvement in the response to methionine is a conserved feature in eukaryotic systems. An intriguing aspect of methionine response is the activation of the mTOR pathway (Figure 6), which is coherent with the reported effect of SAM (the first metabolite of methionine) on mTOR activation through SAM-sensor upstream of mTOR1 (SAMTOR) [44]. However, the intracellular level of most amino acids was downregulated in cells grown in high methionine (Figure 4), and this probably leads to the observed downregulation of proteins involved in translation and tRNA synthesis (Figures 1, 2, 4 and 5) and to the reduction of growth rate (Figure 7). This condition—active mTOR with reduced translational capacity—reminds the condition of cycloheximide treatment, in which mTOR phosphorylates pS6K [60] although growth is impaired, thus, producing the effect of a counter circuit in the cell.

High methionine has also a strong effect on metabolome and proteome remodeling, as also reported in yeast cells [33], especially when combined with Compound C. In fact, reduction of intracellular amino acid levels and alterations in metabolites of the TCA cycle were found in both yeast and liver cancer cells. Interestingly, the observed increase of proteins and metabolites of the TCA cycle could be a direct consequence of methionine metabolism to homocysteine, which can be then converted to α-keto-butyrate and enter the mitochondria. However, in yeast cells, the effect of methionine on mitochondrial functionality was much more evident, probably due to the fact that yeast cells have a fermentative metabolism in the presence of glucose. On the contrary, in human cells, which have a mixed respirative and fermentative metabolism, the effect on mitochondria better emerges by integrating metabolomics and proteomics data. These results, together with the reduction of polyamine levels (which are associated to growth rate), could explain at least in part the observed reduction of cancer phenotypes.

Why does methionine metabolism have this anti-tumor role on liver cancer cell lines, contrary to other cancer cells? It should be noted that methionine metabolism in the liver is very peculiar, since the liver is the organ where most of the methionine is converted to S-adenosyl-methionine and where only the gene MAT1A is expressed. Therefore, most of the observed effects could be due to this

liver-specific metabolism, although we cannot exclude the possibility that methionine could carry out also other functions more related to protein synthesis. In fact, Mato and Lu suggest that liver cancer cells, in contrast to normal non-proliferating, differentiated hepatocytes, tend to utilize methionine mainly for protein synthesis [17].

An interesting translational application of our results could be to directly increase methionine uptake through the diet, both in animal models and in human patients. Methionine should easily reach the liver, since it is the physiological organ where it is metabolized. It should have no side effect on normal hepatocytes, since SAM was shown to have negligible effects on primary untransformed liver cells [19]. Therefore, further investigations should explore the possibility that alterations in methionine dietary consumption, in combination with pharmacological treatments, could have clinically relevant outcomes in liver cancer patients.

Supplementary Materials: The following are available online at http://www.mdpi.com/2073-4409/9/11/2491/s1, Table S1:Summary of the proteomic results comparing MET versus CTR, METCC versus MET, CTRCC versus CTR; Table S2: Proteins differentially expressed the comparison MET versus CTR; Table S3: Proteins differentially expressed the comparison CTRCC versus CTR; Table S4: Proteins differentially expressed the comparison METCC versus CTR; Figure S1: Hierarchical clustering heatmap from One-way ANOVA analysis of the entire set of metabolites differentially expressed.

References

1.   Kumari, R.; Sahu, M.K.; Tripathy, A.; Uthansingh, K.; Behera, M. Hepatocellular carcinoma treatment: Hurdles, advances and prospects. *Hepatic Oncol.* **2018**, *5*, HEP08. [CrossRef] [PubMed]

2.   He, L.; Tian, D.-A.; Li, P.-Y.; He, X.-X. Mouse models of liver cancer: Progress and recommendations. *Oncotarget* **2015**, *6*, 23306–23322. [CrossRef] [PubMed]

3.   Roth, G.S.; Decaens, T. Liver immunotolerance and hepatocellular carcinoma: Patho-physiological mechanisms and therapeutic perspectives. *Eur. J. Cancer* **2017**, *87*, 101–112. [CrossRef]

4.   Rimassa, L.; Danesi, R.; Pressiani, T.; Merle, P. Management of adverse events associated with tyrosine kinase inhibitors: Improving outcomes for patients with hepatocellular carcinoma. *Cancer Treat. Rev.* **2019**, *77*, 20–28. [CrossRef]

5.   Hardie, D.G. AMPK: Positive and negative regulation, and its role in whole-body energy homeostasis. *Curr. Opin. Cell Biol.* **2015**, *33*, 1–7. [CrossRef] [PubMed]

6.   Jeon, S.M.; Hay, N. The double-edged sword of AMPK signaling in cancer and its therapeutic implications. *Arch. Pharm. Res.* **2015**, *38*, 346–357. [CrossRef]

7.   Lee, C.-W.; Wong, L.L.-Y.; Tse, E.Y.-T.; Liu, H.-F.; Leong, V.Y.-L.; Lee, J.M.-F.; Hardie, D.G.; Ng, I.O.-L.; Ching, Y.-P. AMPK promotes p53 acetylation via phosphorylation and inactivation of SIRT1 in liver cancer cells. *Cancer Res.* **2012**, *72*, 4394–4404. [CrossRef]

8.   Yang, X.; Liu, Y.; Li, M.; Wu, H.; Wang, Y.; You, Y.; Li, P.; Ding, X.; Liu, C.; Gong, J. Predictive and preventive significance of AMPK activation on hepatocarcinogenesis in patients with liver cirrhosis. *Cell Death Dis.* **2018**, *9*, 264. [CrossRef]

9. Zheng, L.; Yang, W.; Wu, F.; Wang, C.; Yu, L.; Tang, L.; Qiu, B.; Li, Y.; Guo, L.; Wu, M.; et al. Prognostic significance of AMPK activation and therapeutic effects of metformin in hepatocellular carcinoma. *Clin. Cancer Res.* **2013**, *19*, 5372–5380. [CrossRef]

10. Podhorecka, M.; Ibanez, B.; Dmoszyńska, A. Metformin-its potential anti-cancer and anti-aging effects. *Postep. Hig. Med. Dosw.* **2017**, *71*, 170–175. [CrossRef]

11. Jiang, X.; Tan, H.Y.; Teng, S.; Chan, Y.T.; Wang, D.; Wang, N. The role of AMP-activated protein kinase as a potential target of treatment of hepatocellular carcinoma. *Cancers* **2019**, *11*. [CrossRef] [PubMed]

12. Lu, S.C.; Mato, J.M. S-adenosylmethionine in liver health, injury, and cancer. *Physiol. Rev.* **2012**, *92*, 1515–1542. [CrossRef] [PubMed]

13. Ables, G.P.; Johnson, J.E. Pleiotropic responses to methionine restriction. *Exp. Gerontol.* **2017**, *94*, 83–88. [CrossRef] [PubMed]

14. Frau, M.; Feo, F.; Pascale, R.M. Pleiotropic effects of methionine adenosyltransferases deregulation as determinants of liver cancer progression and prognosis. *J. Hepatol.* **2013**, *59*, 830–841. [CrossRef] [PubMed]

15. Pascale, R.M.; Feo, C.F.; Calvisi, D.F.; Feo, F. Deregulation of methionine metabolism as determinant of progression and prognosis of hepatocellular carcinoma. *Transl. Gastroenterol. Hepatol.* **2018**, *3*, 36. [CrossRef]

16. Chaturvedi, S.; Hoffman, R.M.; Bertino, J.R. Exploiting methionine restriction for cancer treatment. *Biochem. Pharmacol.* **2018**, *154*, 170–173. [CrossRef]

17. Mato, J.M.; Lu, S.C. The Hepatocarcinogenic Effect of Methionine and Choline Deficient Diets: An Adaptation to the Warburg Effect? *Alcohol Clin. Exp. Res.* **2011**, *35*, 811–814. [CrossRef]

18. Martínez-López, N.; Varela-Rey, M.; Ariz, U.; Embade, N.; Vazquez-Chantada, M.; Fernandez-Ramos, D.; Gomez-Santos, L.; Lu, S.C.; Mato, J.M.; Martinez-Chantar, M.L. S-adenosylmethionine and proliferation: New pathways, new targets. *Biochem. Soc. Trans.* **2008**, *36*, 848–852. [CrossRef]

19. Wang, Y.; Sun, Z.S.; Szyf, M. S-adenosyl-methionine (SAM) alters the transcriptome and methylome and specifically blocks growth and invasiveness of liver cancer cells. *Oncotarget* **2017**, *8*, 111866–111881. [CrossRef]

20. Stoyanov, E.; Mizrahi, L.; Olam, D.; Schnitzer-Perlman, T.; Galun, E.; Goldenberg, D.S. Tumor-suppressive effect of S-adenosylmethionine supplementation in a murine model of inflammation-mediated hepatocarcinogenesis is dependent on treatment longevity. *Oncotarget* **2017**, *8*, 104772–104784. [CrossRef]

21. Mato, J.M.; Cámara, J.; De Paz, J.F.; Caballería, L.; Coll, S.; Caballero, A.; García-Buey, L.; Beltrán, J.; Benita, V.; Caballería, J.; et al. S-Adenosylmethionine in alcoholic liver cirrhosis: A randomized, placebo-controlled, double-blind, multicenter clinical trial. *J. Hepatol.* **1999**, *30*, 1081–1089. [CrossRef]

22. LGC Website. Available online: https://www.lgcstandards-atcc.org/en/Products/All/HB-8065.aspx (accessed on 16 November 2020).

23. LGC Website. Available online: https://www.lgcstandards-atcc.org/products/all/CCL-228.aspx (accessed on 16 November 2020).

24. LGC Website. Available online: https://www.lgcstandards-atcc.org/products/all/CCL-185.aspx (accessed on 16 November 2020).

25. LGC Website. Available online: https://www.lgcstandards-atcc.org/products/all/HTB-22.aspx (accessed on 16 November 2020).

26. JCRB Cell Bank Website. Available online: https://cellbank.nibiohn.go.jp/~{}cellbank/en/search_res_det.cgi?ID=385 (accessed on 16 November 2020).

27. Vernocchi, V.; Morselli, M.G.; Varesi, S.; Nonnis, S.; Maffioli, E.; Negri, A.; Tedeschi, G.; Luvoni, G.C. Sperm ubiquitination in epididymal feline semen. *Theriogenology* **2014**, *82*, 636–642. [CrossRef] [PubMed]

28. Tedeschi, G.; Albani, E.; Borroni, E.M.; Parini, V.; Brucculeri, A.M.; Maffioli, E.; Negri, A.; Nonnis, S.; Maccarrone, M.; Levi-Setti, P.E. Proteomic profile of maternal-aged blastocoel fluid suggests a novel role for ubiquitin system in blastocyst quality. *J. Assist. Reprod. Genet.* **2017**, *34*, 225–238. [CrossRef] [PubMed]

29. Migliaccio, O.; Pinsino, A.; Maffioli, E.; Smith, A.M.; Agnisola, C.; Matranga, V.; Nonnis, S.; Tedeschi, G.; Byrne, M.; Gambi, M.C.; et al. Living in future ocean acidification, physiological adaptive responses of the immune system of sea urchins resident at a CO_2 vent system. *Sci. Total Environ.* **2019**, *672*, 938–950. [CrossRef] [PubMed]

30. Maffioli, E.; Schulte, C.; Nonnis, S.; Scalvini, F.G.; Piazzoni, C.; Lenardi, C.; Negri, A.; Milani, P.; Tedeschi, G. Proteomic dissection of nanotopography-sensitive mechanotransductive signaling hubs that foster neuronal differentiation in PC12 cells. *Front. Cell. Neurosci.* **2018**, *11*, 417. [CrossRef] [PubMed]

31. Pang, Z.; Chong, J.; Li, S.; Xia, J. Metaboanalystr 3.0: Toward an optimized workflow for global metabolomics. *Metabolites* **2020**, *10*, 186. [CrossRef]

32. Chong, J.; Wishart, D.S.; Xia, J. Using MetaboAnalyst 4.0 for Comprehensive and Integrative Metabolomics Data Analysis. *Curr. Protoc. Bioinform.* **2019**, *68*. [CrossRef]

33. Tripodi, F.; Castoldi, A.; Nicastro, R.; Reghellin, V.; Lombardi, L.; Airoldi, C.; Falletta, E.; Maffioli, E.; Scarcia, P.; Palmieri, L.; et al. Methionine supplementation stimulates mitochondrial respiration. *Biochim. Biophys. Acta Mol. Cell Res.* **2018**, *1865*, 1901–1913. [CrossRef]

34. Wang, Y.; Tatham, M.H.; Schmidt-Heck, W.; Swann, C.; Singh-Dolt, K.; Meseguer-Ripolles, J.; Lucendo-Villarin, B.; Kunath, T.; Rudd, T.R.; Smith, A.J.H.; et al. Multiomics Analyses of HNF4α Protein Domain Function during Human Pluripotent Stem Cell Differentiation. *iScience* **2019**, *16*, 206–217. [CrossRef]

35. Yang, H.; Zheng, Y.; Li, T.W.H.; Peng, H.; Fernandez-Ramos, D.; Martínez-Chantar, M.L.; Rojas, A.L.; Mato, J.M.; Lu, S.C. Methionine adenosyltransferase 2B, HuR, and sirtuin 1 protein cross-talk impacts on the effect of resveratrol on apoptosis and growth in liver cancer cells. *J. Biol. Chem.* **2013**, *288*, 23161–23170. [CrossRef]

36. Li, Y.; Wang, Y.; Wu, P. 5′-methylthioadenosine and cancer: Old molecules, new understanding. *J. Cancer* **2019**, *10*, 927–936. [CrossRef] [PubMed]

37. Avila, M.A.; García-Trevijano, E.R.; Lu, S.C.; Corrales, F.J.; Mato, J.M. Methylthioadenosine. *Int. J. Biochem. Cell Biol.* **2004**, *36*, 2125–2130. [CrossRef] [PubMed]

38. Ferioli, M.E.; Scalabrino, G. Persistently Decreased Hepatic Levels of 5′-deoxy-5′-methylthioadenosine During Regeneration of and Chemical Carcinogenesis in Rat Liver—PubMed. Available online: https://pubmed.ncbi.nlm.nih.gov/3458957/?from_single_result=Ferioli+%26+Scalabrino%2C+1986+mta+liver (accessed on 29 March 2020).

39. Pascale, R.M.; Simile, M.M.; De Miglio, M.R.; Feo, F. Chemoprevention of hepatocarcinogenesis: S-adenosyl-L-methionine. In *Alcohol*; Elsevier: Amsterdam, The Netherlands, 2002; Volume 27, pp. 193–198.

40. Alberghina, L.; Coccetti, P.; Orlandi, I. Systems biology of the cell cycle of Saccharomyces cerevisiae: From network mining to system-level properties. *Biotechnol. Adv.* **2009**, *27*, 960–978. [CrossRef]

41. Hardie, D.G. Keeping the home fires burning: AMP-activated protein kinase. *J. R. Soc. Interface* **2018**, *15*, 20170774. [CrossRef] [PubMed]

42. Sanli, T.; Steinberg, G.R.; Singh, G.; Tsakiridis, T. AMP-activated protein kinase (AMPK) beyond metabolism: A novel genomic stress sensor participating in the DNA damage response pathway. *Cancer Biol. Ther.* **2014**, *15*, 156–169. [CrossRef]

43. Magaway, C.; Kim, E.; Jacinto, E. Targeting mTOR and Metabolism in Cancer: Lessons and Innovations. *Cells* **2019**, *8*, 1584. [CrossRef]

44. Gu, X.; Orozco, J.M.; Saxton, R.A.; Condon, K.J.; Liu, G.Y.; Krawczyk, P.A.; Scaria, S.M.; Wade Harper, J.; Gygi, S.P.; Sabatini, D.M. SAMTOR is an S-adenosylmethionine sensor for the mTORC1 pathway. *Science* **2017**, *358*, 813–818. [CrossRef]

45. Nitulescu, G.M.; Van De Venter, M.; Nitulescu, G.; Ungurianu, A.; Juzenas, P.; Peng, Q.; Olaru, O.T.; Grădinaru, D.; Tsatsakis, A.; Tsoukalas, D.; et al. The Akt pathway in oncology therapy and beyond (Review). *Int. J. Oncol.* **2018**, *53*, 2319–2331. [CrossRef]

46. Fouad, Y.A.; Aanei, C. Revisiting the hallmarks of cancer. *Am. J. Cancer Res.* **2017**, *7*, 1016–1036.

47. Wu, Z.; Song, L.; Liu, S.Q.; Huang, D. Independent and additive effects of glutamic acid and methionine on yeast longevity. *PLoS ONE* **2013**, *8*, e79319. [CrossRef]

48. Troen, A.M.; French, E.E.; Roberts, J.F.; Selhub, J.; Ordovas, J.M.; Parnell, L.D.; Lai, C.Q. Lifespan modification by glucose and methionine in Drosophila melanogaster fed a chemically defined diet. *Age* **2007**, *29*, 29–39. [CrossRef] [PubMed]

49. Lee, B.C.; Kaya, A.; Ma, S.; Kim, G.; Gerashchenko, M.V.; Yim, S.H.; Hu, Z.; Harshman, L.G.; Gladyshev, V.N. Methionine restriction extends lifespan of Drosophila melanogaster under conditions of low amino-acid status. *Nat. Commun.* **2014**, *5*, 3592. [CrossRef] [PubMed]

50. Johnson, J.E.; Johnson, F.B. Methionine restriction activates the retrograde response and confers both stress tolerance and lifespan extension to yeast, mouse and human cells. *PLoS ONE* **2014**, *9*, e97729. [CrossRef] [PubMed]

51. Ables, G.P.; Ouattara, A.; Hampton, T.G.; Cooke, D.; Perodin, F.; Augie, I.; Orentreich, D.S. Dietary methionine restriction in mice elicits an adaptive cardiovascular response to hyperhomocysteinemia. *Sci. Rep.* **2015**, *5*, 1–10. [CrossRef] [PubMed]

52. Ouattara, A.; Cooke, D.; Gopalakrishnan, R.; Huang, T.-h.; Ables, G.P. Methionine restriction alters bone morphology and affects osteoblast differentiation. *Bone Rep.* **2016**, *5*, 33–42. [CrossRef]

53. Komninou, D.; Leutzinger, Y.; Reddy, B.S.; Richie, J.P. Methionine restriction inhibits colon carcinogenesis. *Nutr. Cancer* **2006**, *54*, 202–208. [CrossRef]

54. Sinha, R.; Cooper, T.K.; Rogers, C.J.; Sinha, I.; Turbitt, W.J.; Calcagnotto, A.; Perrone, C.E.; Richie, J.P. Dietary methionine restriction inhibits prostatic intraepithelial neoplasia in TRAMP mice. *Prostate* **2014**, *74*, 1663–1673. [CrossRef]

55. Jeon, H.; Kim, J.H.; Lee, E.; Jang, Y.J.; Son, J.E.; Kwon, J.Y.; Lim, T.-g.; Kim, S.; Yoon Park, J.H.; Kim, J.E.; et al. Methionine deprivation suppresses triple-negative breast cancer metastasis in vitro and in vivo. *Oncotarget* **2016**, *7*, 67223–67234. [CrossRef]

56. Hens, J.R.; Sinha, I.; Perodin, F.; Cooper, T.; Sinha, R.; Plummer, J.; Perrone, C.E.; Orentreich, D. Methionine-restricted diet inhibits growth of MCF10AT1-derived mammary tumors by increasing cell cycle inhibitors in athymic nude mice. *BMC Cancer* **2016**, *16*, 349. [CrossRef]

57. Benavides, M.A.; Hagen, K.L.; Fang, W.; Du, P.; Lin, S.; Moyer, M.P.; Yang, W.; Bland, K.I.; Grizzle, W.E.; Bosland, M.C. Suppression by L-methionine of cell cycle progression in LNCaP and MCF-7 cells but not benign cells. *Anticancer Res.* **2010**, *30*, 1881–1885.

58. Benavides, M.A.; Hu, D.; Baraoidan, M.K.; Bruno, A.; Du, P.; Lin, S.; Yang, W.; Bland, K.I.; Grizzle, W.E.; Bosland, M.C. L-methionine-induced alterations in molecular signatures in MCF-7 and LNCaP cancer cells. *J. Cancer Res. Clin. Oncol.* **2011**, *137*, 441–453. [CrossRef] [PubMed]

59. Pascale, R.M.; Simile, M.M.; De Miglio, M.R.; Nufris, A.; Daino, L.; Seddaiu, M.A.; Rao, P.M.; Rajalakshmi, S.; Sarma, D.S.; Feo, F. Chemoprevention by S-adenosyl-L-methionine of rat liver carcinogenesis initiated by 1,2-dimethylhydrazine and promoted by orotic acid. *Carcinogenesis* **1995**, *16*, 427–430. [CrossRef] [PubMed]

60. Iiboshi, Y.; Papst, P.J.; Kawasome, H.; Hosoi, H.; Abraham, R.T.; Houghton, P.J.; Terada, N. Amino acid-dependent control of p70(s6k). Involvement of tRNA aminoacylation in the regulation. *J. Biol. Chem.* **1999**, *274*, 1092–1099. [CrossRef] [PubMed]